

# Synthesis and Spectroscopic Characterization of Metalloporphyrins and Porphyrins and their Applications

By

SRUTI MONDAL  
CHEM11201604029

National Institute of Science Education and Research  
(NISER), Bhubaneswar

*A thesis submitted to the  
Board of Studies in Chemical Sciences  
In partial fulfillment of requirements  
for the Degree of*

DOCTOR OF PHILOSOPHY  
*Of*  
HOMI BHABHA NATIONAL INSTITUTE



June, 2022

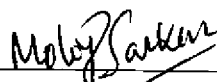
# Homi Bhabha National Institute<sup>1</sup>

## Recommendations of the Viva Voce Committee

As members of the Viva Voce Committee, we certify that we have read the dissertation prepared by **Ms. Sruti Mondal** entitled "**Synthesis and Spectroscopic Characterization of Metalloporphyrins and Porphyrins and their Applications**" and recommend that it may be accepted as fulfilling the thesis requirement for the award of Degree of Doctor of Philosophy.

Chairman -

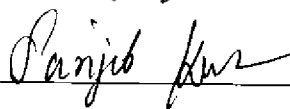
**Dr. Moloy Sarkar**



Date: 17.10.22

Guide / Convener -

**Dr. Sanjib Kar**

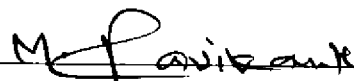


Date: 17/10/22

Co-guide -

Examiner -

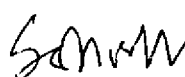
**Prof. M. Ravikanth**



Date: 17/10/22

Member 1-

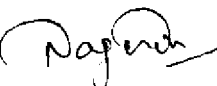
**Dr. Subhadip Ghosh**



Date: 17/10/22

Member 2-

**Dr. Nagendra K. Sharma**



Date: 17.10.22

Member 3-

**Dr. Shantanu Pal**



Date: 17/10/22

Final approval and acceptance of this thesis is contingent upon the candidate's submission of the final copies of the thesis to HBNI.

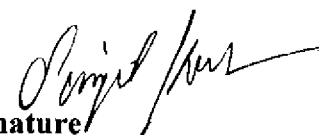
I/We hereby certify that I/we have read this thesis prepared under my/our direction and recommend that it may be accepted as fulfilling the thesis requirement.

Date: 17/10/2022

Place: BBSR

Signature Co-guide (if any)

Signature  
Guide



<sup>1</sup> This page is to be included only for final submission after successful completion of viva voce.

## STATEMENT BY AUTHOR

This dissertation has been submitted in partial fulfillment of requirements for an advanced degree at Homi Bhabha National Institute (HBNI) and is deposited in the Library to be made available to borrowers under rules of the HBNI.

Brief quotations from this dissertation are allowable without special permission, provided that accurate acknowledgement of source is made. Requests for permission for extended quotation from or reproduction of this manuscript in whole or in part may be granted by the Competent Authority of HBNI when in his or her judgment the proposed use of the material is in the interests of scholarship. In all other instances, however, permission must be obtained from the author.

*Sruti Mondal*

**Sruti Mondal**

## DECLARATION

I, hereby declare that the investigation presented in the thesis has been carried out by me.

The work is original and has not been submitted earlier as a whole or in part for a degree / diploma at this or any other Institution / University.

*Sruti Mondal*  
**Sruti Mondal**

## LIST OF PUBLICATIONS

### Journals

1. #**Sruti Mondal**, Kasturi Sahu, Bratati Patra, Subhrakant Jena, Himansu S. Biswal\*, Sanjib Kar\* *Dalton Trans.*, **2020**, *49*, 1424–1432. A new synthesis of porphyrins *via* a putative *trans*-manganese(IV)-dihydroxide intermediate.
2. #**Sruti Mondal**, Tanmoy Pain, Kasturi Sahu, Sanjib Kar\* *ACS Omega*, **2021**, *6*, 22922–22936. Large-Scale Green Synthesis of Porphyrins.
3. #**Sruti Mondal**, Antara Garai, Pratyush Kumar Naik, Jogesh Kumar Adha, Sanjib Kar\* *Inorg. Chim. Acta*, **2020**, *501*, 119300. Synthesis and characterization of antimony(V)-oxo corrole complexes.
4. **Sruti Mondal**, Pratyush Kumar Naik, Jogesh Kumar Adha, Sanjib Kar\* *Coord. Chem. Rev.*, **2019**, *400*, 213043. Synthesis, characterization, and reactivities of high valent metal–corrole (M= Cr, Mn, and Fe) complexes.
5. Kasturi Sahu, **Sruti Mondal**, Shaikh M. Mobin, Sanjib Kar\* *J. Org. Chem.*, **2021**, *86*, 3324–3333. Photocatalytic C–H Thiocyanation of Corroles: Development of Near-Infrared (NIR) Emissive Dyes.
6. Kasturi Sahu, **Sruti Mondal**, Bratati Patra, Tanmoy Pain, Sajal Kumar Patra, Carsten Dosche\*, Sanjib Kar\* *Nanoscale Adv.*, **2020**, *2*, 166-170. Regioselective thiocyanation of corroles and the synthesis of gold nanoparticle–corrole assemblies.
7. Tanmoy Pain, **Sruti Mondal**, Subhrakant Jena, Dwaipayan D. Gupta, Himansu S. Biswal\*, Sanjib Kar\* *ACS Omega*, **2022**, *7*, 28138–28147. Synthesis, Characterization, and the N Atom Transfer Reactivity of a Nitridochromium(V) Complex Stabilized by a Corrolato Ligand

8. Bratati Patra, Sebastian Sobottka, **Sruti Mondal**, Biprajit Sarkar\*, Sanjib Kar\* *Chem. Commun.*, **2018**, 54, 9945-9948. Metal coordination induced ring contraction of porphyrin derivatives.
9. Sajal Kumar Patra, Kasturi Sahu, Bratati Patra, **Sruti Mondal**, Sanjib Kar\* *Eur. J. Org. Chem.* **2018**, 6764–6767. An N, N'-Bridged Corrole: First Example of a N<sup>21</sup>,N<sup>22</sup>-Methylene Bridged Corrole Derivative.
10. Sajal Kumar Patra, Kasturi Sahu, Bratati Patra, Dipak Kumar Sahoo, **Sruti Mondal**, Payel Mukherjee, Himansu S. Biswal\*, Sanjib Kar\* *Green Chem.*, **2017**, 19, 5772–5776. Synthesis of urea derivatives via reductive carbon dioxide fixation into contracted porphyrin analogues.
11. Antara Garai, Marco Villa, Marianna Marchini, Sajal K. Patra, Tanmoy Pain, **Sruti Mondal**, Paola Ceroni,\* Sanjib Kar\* *Eur. J. Inorg. Chem.*, **2021**, 4089–4095 Synthesis, Structure, Photophysics, and Singlet Oxygen Sensitization by a Platinum(II) Complex of *Meso*-Tetra-Acenaphthyl Porphyrin.
12. **#Sruti Mondal**, Tanmoy Pain, Astam Mandal, Debabrata Maiti\* and Sanjib Kar\*. The Reaction of NOBF<sub>4</sub> with the Sb(III)-corroles: Oxidative addition of Fluoride at the Antimony and Regioselective Nitration of Corrole. (*manuscript under revision*)
13. **Sruti Mondal**, Dilruba Hasina, Tapobrata Som, Carsten Dosche\*, and Sanjib Kar\*. Making Graphene-type Material via Polymerization of Porphyrin. ChemRxiv. Cambridge: Cambridge Open Engage; 2020. DOI: 10.26434/chemrxiv.13041785.v1

#### Book Chapters

14. #Bratati Patra<sup>†</sup>, **Sruti Mondal**<sup>†</sup>, Sanjib Kar\* In *Encyclopedia of Inorganic and Bioinorganic Chemistry*; Scott, R. A., Storr, T., Eds.; John Wiley & Sons, Ltd.:

Chichester, U.K., 2020. DOI: 10.1002/ 9781119951438.eibc2729. Corroles.<sup>(†</sup>  
Equally contributed)

15. Bratati Patra, **Sruti Mondal**, Sanjib Kar\* In book: *Reference Module in Chemistry, Molecular Sciences and Chemical Engineering; Comprehensive Coordination Chemistry III (Third Edition)*, 2021, 446-477. Coordination Chemistry of Chromium in Oxidation States+ 4, + 5 and+ 6.

<sup>#</sup>Pertaining to the thesis

*Sruti Mondal*  
**Sruti Mondal**

## CONFERENCES

1. Fixation of CO<sub>2</sub> from ammonium carbonate into contracted porphyrin analogues and the synthesis of *N*<sup>21</sup>, *N*<sup>22</sup>-carbamide-corrole derivatives: **Sruti Mondal**, Sajal Kumar Patra, Kasturi Sahu, Sanjib Kar\* "National Bioorganic Chemistry Conference (NBCC)" held at National Institute of Science Education and Research (NISER) on 22-24<sup>th</sup> December-2018. (**Poster Presentation**)
2. Fixation of CO<sub>2</sub> from ammonium carbonate into contracted porphyrin analogues and the synthesis of *N*<sup>21</sup>, *N*<sup>22</sup>-carbamide-corrole derivatives. **Sruti Mondal**, Sanjib Kar\*. National Conference on Advances in Materials Chemistry and Applications (AMCA – 2019) held at Utkal University during February 23-24, 2019. (**Oral talk**)
3. A New Synthesis of Porphyrin *via* a Putative *trans*-manganese(IV)-dihydroxide Intermediate **Sruti Mondal**, Sanjib Kar\*. 1<sup>st</sup> International Conference on Recent Developments in Organic and Applied Chemistry-2020 (RDOAC-2020) held on 6-7<sup>th</sup> July, 2020 organized by Department of Chemistry, SAS, KIIT-Deemed to be University, Bhubaneswar, Odisha, India (a virtual meeting, via zoom) (**Oral talk**)
4. Synthesis and Characterization of Antimony(V)-Oxo Corrole Complexes. **Sruti Mondal**, Sanjib Kar\*. National Seminar on "Recent Advances in Materials Chemistry (RAMC-2021)" held at Utkal university during 8-9<sup>th</sup> March, 2021. (**Poster Presentation**)
5. Attended international conference on Materials for the Millennium-MATCON 2021 organized by Department of Applied Chemistry, Cochin University of Science and Technology during 15-19<sup>th</sup> March.
6. Attended ACS on campus at NISER Bhubaneswar held on 23<sup>rd</sup> July 2018

*Sruti Mondal*  
**Sruti Mondal**



**Dedicated to....**

**My Family**

## ACKNOWLEDGEMENTS

*I am sincerely grateful to the Almighty God for his graces, enormous blessings and guidance throughout my life.*

*I would like to express my sincere gratitude and respect to my supervisor, **Dr. Sanjib Kar**, Associate Professor, NISER, for his excellent guidance, patience, encouragement, kind-heartedness, and constant motivation. I am highly motivated by his optimistic approach, exceptional scientific efforts, and research knowledge.*

*I would like to thank **Prof. Sudhakar Panda**, Director, NISER, and **Prof. V. Chandrasekhar** and **Prof. T. K. Chandrashekar**, Ex-Director, NISER, for helping us with all the laboratory and instrumental facilities. I also would like to acknowledge NISER for providing fellowship.*

*I owe my sincere gratitude to my thesis monitoring committee members, **Prof. Moloy Sarkar**, **Prof. Subhadip Ghosh**, **Prof. N. K. Sharma**, **Prof. Shantanu Pal**, and **Prof. Abdur Rahaman**, for their immense help and support throughout my research time. I am also extremely grateful to the chairperson, **Prof. Bidraha Bagh**, **Dr. A. Kumar**, and **Dr. P. Pandey** for their valuable suggestions and support.*

*I express my deepest gratitude to my collaborators, **Prof. H. S. Biswal**, **Prof. D. Maiti**, **Prof. T. Som**, **Dr. C. Dosche**, and **Prof. P. Ceroni**, for helping me explore and expand various aspects of my research.*

*I am extremely grateful to **Dr. Mriganka**, **Mr. Deepak**, **Mr. Sanjaya**, **Mr. Prakash**, **Mr. Amit**, and **Mrs. Anuradha**, NISER, for the technical assistance and performing characterization of my compounds.*

*I owe my sincere gratitude to all my school teachers, graduation teachers and post-graduation professors.*

*I would also like to thank my friends, seniors, and juniors, especially **Sagarika** and **Syamasrit** for an enjoyable and memorable stay at NISER. I am thankful to my labmates, **Tanmoy**, **Sajal da**, **Bratati di**, **Subhajit**, **Kasturi**, **Panisha**, and **Manisha** for their help and support.*

*I wish to thank my loving **parents** and my **elder sister** for their never-ending support, care, unconditional love, and affection which is the key strength of all my accomplishments in my life.*

**Sruti Mondal**

## **Contents**

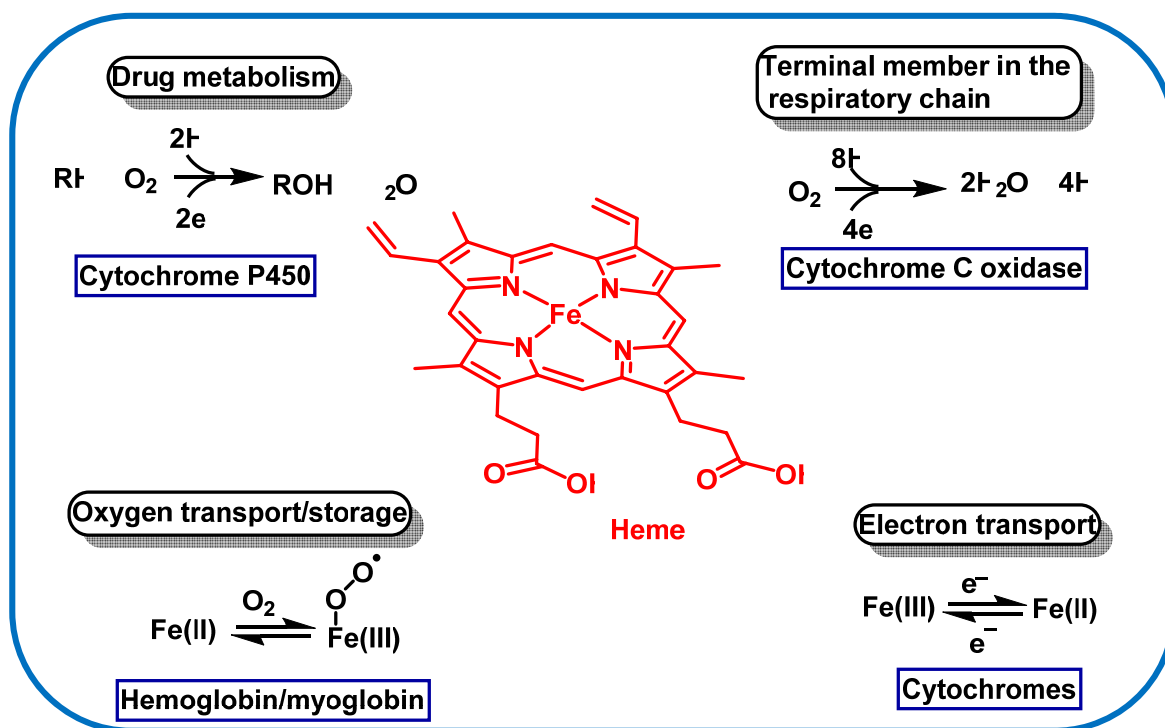
	<b>Pages</b>
<b>Synopsis</b>	xi
<b>List of Tables</b>	xx
<b>List of Schemes</b>	xxi
<b>List of Figures</b>	xxiii
<b>Glossary of Acronyms</b>	xxxii
<b>Chapter 1</b>	1
<b>Chapter 2</b>	46
<b>Chapter 3</b>	85
<b>Chapter 4</b>	117
<b>Chapter 5</b>	180

# SYNOPSIS

## 1. Introduction

In nature, porphyrins are widely abundant, and it plays a pivotal role in various biological systems. Porphyrins are often referred to as the “Pigments of Life” due to its intense colour which arises from a highly conjugated  $\pi$  system.<sup>1</sup> Porphyrins<sup>2</sup> and metallated porphyrins are present in various aromatic heterocyclic and different macrocyclic derivatives such as heme, (iron porphyrin), (found in hemoglobins, myoglobins, catalases, cytochromes, and peroxidases etc), chlorophylls, bacteriochlorophylls etc.

Porphyrins<sup>2</sup> have huge biological applications such as transportation of  $O_2$  in hemoglobin and storage of  $O_2$  in myoglobins, transportation and collection of light energy in antennae species, dioxygen reduction in oxidases, electron transfer in cytochromes, conversion of solar energy to chemical energy in photosynthetic reaction centers, and a large number of other enzymatic reactions (peroxidases, catalases, methylreductases, cytochrome P450, etc.)(Figure 1).



**Figure 1** An overview of heme activity.

Synthetic porphyrinoid derivatives and their metallated derivatives shows unique chemical, physical and biological properties due to which it has attracted lots of interest in different interdisciplinary research fields such as supramolecular building blocks, molecular electronics, photodynamic therapy.

Vitamin B<sub>12</sub>,<sup>3</sup> commonly known as cobalamin, plays a vital role in metabolism process. The molecular structure of vitamin B<sub>12</sub> resembles with the heterocyclic compound, corrin.<sup>4-6</sup> This corrin moiety has an amazing resemblance with the porphyrin ring. But unlike porphyrin rings, corrin lacks one of the carbon atoms which is involved in the linkage of two subsequent pyrrole moieties. On the other hand, the fully aromatic derivative of this corrin ring is known as corroles. Corrole is a tetrapyrrolic macrocyclic system which resembles with the central corrin moiety of vitamin B<sub>12</sub>. This term ‘corrole’ was suggested by Johnson and Price because of its resemblance with the central corrin moiety of vitamin B<sub>12</sub>.<sup>7</sup> Corrole has an aromatic 18 $\pi$ –electron system which resembles with porphyrin.<sup>8-10</sup> Therefore, the corrole macrocycle is considered as the intermediate between corrin and porphyrin macrocycle. Corroles behave as trianionic ligand whereas porphyrins are dianionic and corrin rings are monoanionic in nature. The inner-core of corrole macrocycle is comprised of three amino nitrogen and one imino nitrogen. Various types of metallocorroles have also been explored throughout the years due to their different kinds of applications in several fields.

This thesis contains some new methodologies for the synthesis of porphyrins. This thesis also contains some of the underexplored areas of metallocorrole chemistry. Synthesis of *meso*-substituted *trans*-A<sub>2</sub>B<sub>2</sub> porphyrins and A<sub>4</sub>-porphyrins *via* two-step methodology is discussed here which is different from previously reported other methodologies in many aspects and most importantly, it can be easily performed in the gram scale synthesis of porphyrins. Additionally, synthesis of various antimony-corrole

complexes, including corrolato-antimony(III) complexes, (corrolato)(oxo)antimony(V) complexes and [*trans*-difluoro(3,17-dinitro–corrolato)antimony (V)] complexes have also been explored. The luminescent properties of all these complexes are reported and its application in photocatalytic oxygenation reactions have also been discussed here. This thesis contains five chapters and the summary of all the chapters are as follows:

## **2. Chapters**

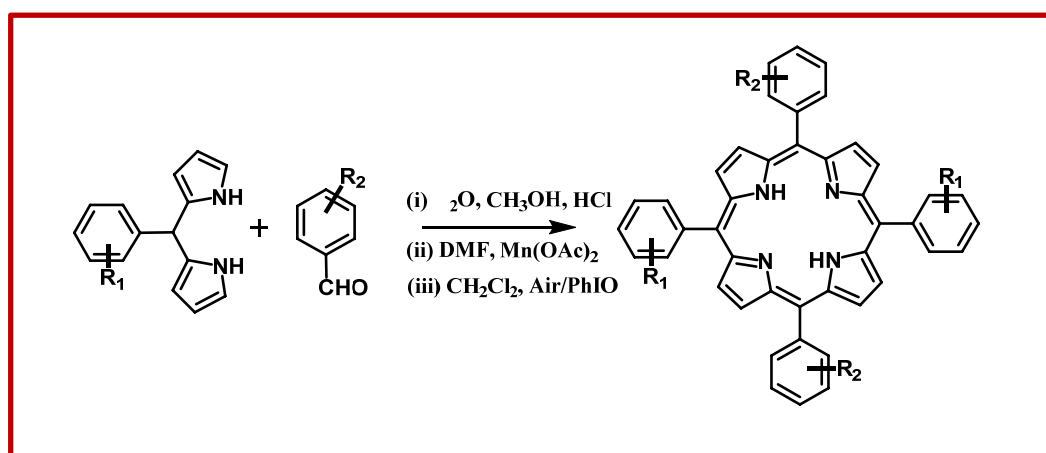
### **Chapter 1: Introduction: Evolution of Porphyrins and Corroles**

In this chapter, the importance of porphyrinoids, mainly, porphyrins and corroles are discussed which have various applications in biological science as well as materials science. The main focus of this chapter was regarding the origin, properties, various synthetic methodologies and the significant importance and applications of porphyrins as well as corrole macrocycles. The fascinating coordination chemistry of porphyrinoids, mainly, corrole including the metallocorrole complexes, properties, spectral characterization and their applications in different fields such as sensing, mainly CO sensing, dye sensitised solar cells (DSSCs), medicinal chemistry, catalysis are also thoroughly discussed. Also, the fascinating coordination chemistry of porphyrin complexes, properties, and their applications in different fields such as in organic solar cells, functional devices, also in porphyrin based polymers, porphyrin-based nanoparticles (NPs), dye sensitised solar cells (DSSCs), and medicinal chemistry are discussed extensively.

### **Chapter 2: A new synthesis of porphyrin via a putative *trans*-manganese(IV)-dihydroxide intermediate**

In this chapter, a new method for the synthesis of meso-substituted porphyrins was developed. In two-step methodology, the first step involves the condensation of

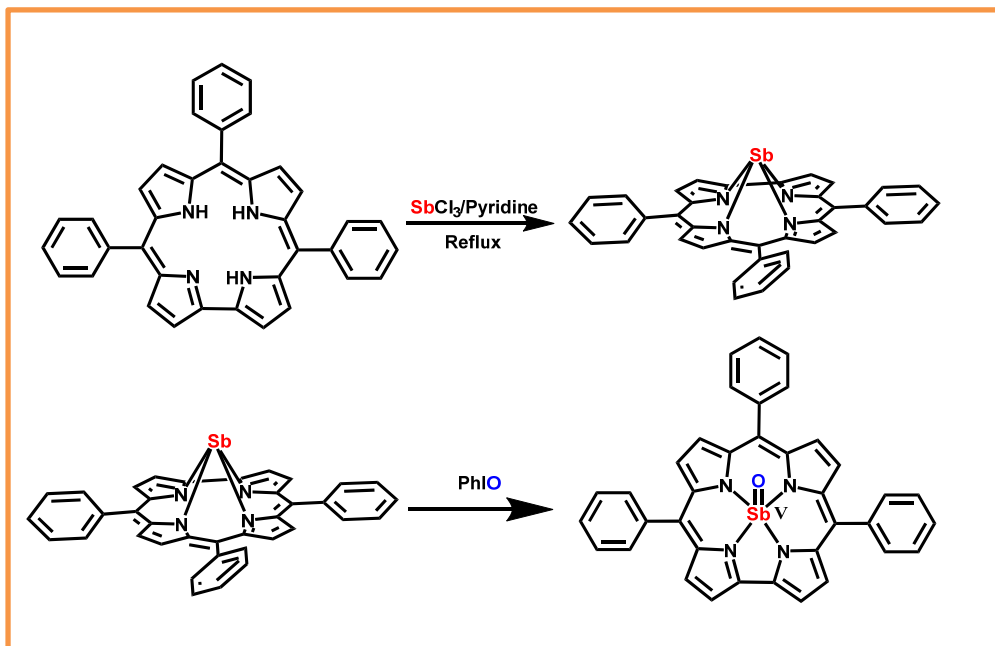
pyrrole/ dipyrromethane with aldehyde in water-methanol mixture in acidic conditions. The second step employs a manganese induced cyclization followed by oxidation via PhIO/O<sub>2</sub>. This methodology has been useful for the synthesis of wide range of trans-A<sub>2</sub>B<sub>2</sub> porphyrin and also symmetric porphyrins in moderate to good yields. A detailed investigation of the manganese induced cyclization reaction has allowed us to characterize a Mn- porphyrinogen complex. A series of analytical, spectroscopic techniques and DFT calculations has led us to the conclusion that these putative intermediate species are *trans*-manganese(IV)-dihydroxide complexes. EPR and magnetic susceptibility measurements helped us to assign the oxidation state of the manganese complexes in the native state. The question of *trans*-manganese(IV)-dihydroxide as the true intermediates for these porphyrin synthesis has been authenticated via *in-situ* UV-Vis experiments. This new methodology is certainly different from previously reported other methodologies in many aspects and most importantly, these reactions can be easily performed in the gram scale synthesis of porphyrins.





### **Chapter 3: Synthesis and characterization of Antimony(V)–oxo corrole complexes**

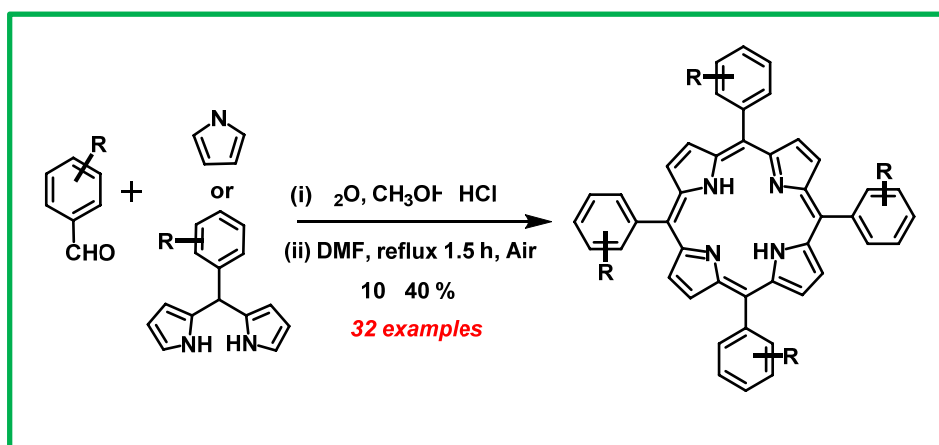
In this chapter, we have presented the synthesis of four new antimony-corrole complexes, including two corrolato-antimony(III) complexes and two (corrolato)(oxo)antimony(V) complexes and characterized them by a series of spectroscopic techniques. All the four antimony complexes, including two corrolato-antimony(III) complexes and two (corrolato)(oxo)antimony(V) complexes were diamagnetic in nature as was evident from their “normal” chemical shifts. For one of the structurally characterized corrolato-antimony(III) complexes, we have obtained two different conformers in two different solvents with slightly different bond lengths and angles.  $\text{Sb}^{\text{III}}$  corroles were dome shaped and the deviation of  $\text{Sb}^{\text{III}}$  ion with respect to the plane consisting four pyrrolic nitrogen atoms was  $\sim 0.963\text{--}0.966\text{\AA}$ . The two corrolato-antimony(III) complexes exhibited splitted Soret bands in the range of 440–462 nm due to the low symmetric nature of these molecules. The two (corrolato)(oxo)antimony(V) complexes exhibited single Soret bands in the range of 408–413 nm. All the four antimony complexes displayed weak emission in the range of 630–650 nm and a shoulder at 690–710 nm in  $\text{CH}_2\text{Cl}_2$ . These emission bands were assigned as fluorescence bands due to the observation of smaller Stokes shift in reference to the lowest energy Q-type bands. The luminescent properties of  $\text{Sb}^{\text{III}}$  corroles and  $\text{Sb}^{\text{V}}=\text{O}$  corroles were also reported herein and this paves the way for the future utilization of these class of molecules in various photocatalytic oxygen atom transfer reactions.



#### Chapter 4: Large Scale Green Synthesis of Porphyrins

In this chapter, synthesis of symmetric A<sub>4</sub>-porphyrins from aromatic aldehydes possessing a variety of substituents having the highest yield of 29%, and the [2+2] synthesis of *trans*-A<sub>2</sub>B<sub>2</sub>-porphyrins from dipyrromethanes bearing different substituents having the highest yield of 40% have been reported. The first step involves the condensation of pyrrole and aldehyde in an H<sub>2</sub>O-MeOH mixture using HCl. The obtained precipitate from the first step was dissolved in reagent grade DMF and refluxed for 1.5 h, and followed by stirring overnight in the air at room temperature. Subsequent purification through column chromatography or crystallization resulted in the formation of pure porphyrins. Advantageously, this methodology does not need any expensive chemicals like DDQ, chloranil, etc., as an oxidizing agent. This reaction also does not require a large volume of dry chlorinated solvents. Contrary to the reported methodologies, which are mostly ineffective in the gram-scale production of porphyrins, the present method perfectly caters to the need for gram-scale production of porphyrins. In essence, the present methodology represents the easiest and cheapest synthesis of porphyrin on a large scale for getting a reproducible yield of 10-40% having high purity.

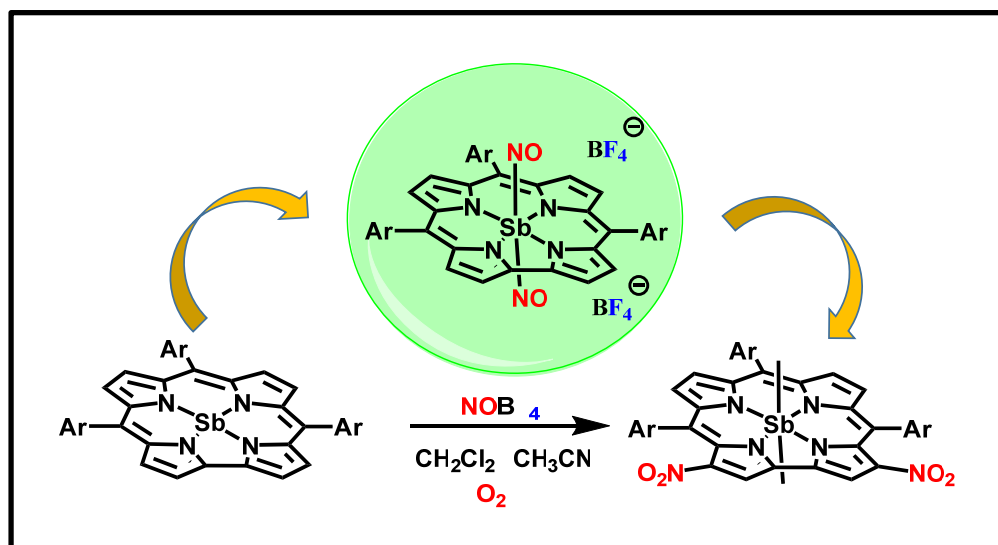
The synthesis of *trans*-A<sub>2</sub>B<sub>2</sub>-porphyrins from dipyrromethanes was also scrambling free. In a few of the examples, even column chromatography was also not necessary. A simple crystallization technique was sufficient enough to generate the desired porphyrins in good yields. The present synthetic approach thus opened up an avenue for the synthesis of a wide range of symmetric-A<sub>4</sub> and *trans*-A<sub>2</sub>B<sub>2</sub> –porphyrins on a large scale, which will further widen the practical applications of these important classes of molecules.



## Chapter 5: The Reaction of NOBF<sub>4</sub> with the Sb(III)-corroles: Oxidative addition of Fluoride at the Antimony and Regioselective Nitration of Corroles

In this chapter, corrolato Sb(III) complexes reacted with nitrosonium tetrafluoroborate in presence of air (O<sub>2</sub>) and generated *trans*-difluoro-corrolato Sb(V) species along with dinitration of corrole ring. These [*trans*-difluoro(3,17-dinitro–corrolato) antimony(V)] complexes were fully characterized via X-ray crystallography, UV-vis, FT-IR, and NMR spectroscopy. A [*trans*-dinitrosyl(corrolato)antimony(V)] compound has been proposed as a possible reaction intermediate. This intermediate was subsequently converted into an [*trans*-dinitro(corrolato)antimony(V)] species. The formation of these intermediate species has been established via in situ FT-IR spectra. This [*trans*-dinitro(corrolato)antimony(V)] species further transferred the nitro group in the  $\beta$ -positions (3 and 17) of corrole

periphery in antimony(V)corrole complexes *via* a radical pathway. Subsequently, the fluoride ion was inserted into the axial positions of antimony(V)corrole via nucleophilic attack of fluoride ion from  $\text{BF}_4^-$ . The *trans*-difluoro(3,17-dinitro–corrolato)antimony(V) showed oxygenation reaction under photo-redox conditions in presence of air and light at ambient temperature.



## References:

1. A. R. Battersby, C. Fookes, G. Matcham, E. McDonald, *Nature*. **1980**, 285, 17-21.
2. K. M. Kadish, Smith, K. M.; Guillard, R.; Editors, *The Porphyrin Handbook*; Volume 2, Heteroporphyrins, Expanded Porphyrins and Related Macrocycles. Academic Press: 2000.
3. Scott, A. I. *Accounts of Chemical Research* **1978**, 11, 1, 29-36.
4. Bonnett, R., *Chem. Rev.* **1963**, 63, 573-605.
5. Hodgkin, D. C.; Kamper, J.; Lindsey, J.; MacKay, M.; Pickworth, J.; Robertson, J.; Shoemaker, C. B.; White, J.; Prosen, R.; Trueblood, K., *Proc. R. Soc. Lond. A* **1957**, 242, 228-263.

6. Johnson, A.; Todd, A., *Vitam. Horm.* **1957**, 15, 1.
7. Johnson, A.; Price, R., *J. Chem. Soc.* **1960**, 1649-1653.
8. I. Aviv-Harel and Z. Gross, *Chem. Eur. J.*, **2009**, 15, 8382-8394.
9. Mondal, S.; Naik, P. K.; Adha, J. K.; Kar, S. *Coord. Chem. Rev.* **2019**, 400, 213043.
10. Patra, B.; Mondal, S.; Kar, S. Corroles, in: Scott, R. A.; Storr, T. (Eds.) *Encyclopedia of Inorganic and Bioinorganic Chemistry*, John Wiley & Sons, Ltd, Chichester, UK, **2020**, DOI: <https://doi.org/10.1002/9781119951438.eibc2729>.

## List of Tables

			Pages
1	<b>Table 2.1</b>	Scope of the synthesis of <i>meso</i> -substituted <i>trans</i> -A <sub>2</sub> B <sub>2</sub> -Porphyrins	48
2	<b>Table 2.2</b>	Composition of selected molecular orbitals of <b>7-Mn</b>	56
3	<b>Table 2.3</b>	Composition of selected molecular orbitals of 7-Mn	57
4	<b>Table 2.4</b>	TD-DFT transitions for <b>7-Mn</b>	57
5	<b>Table 2.5</b>	TD-DFT calculated IR frequencies for <b>7-M</b>	58
6	<b>Table 2.6</b>	UV–Vis. Data	77
7	<b>Table 3.1</b>	Crystallographic data of <b>1</b> for both the conformers	92
8	<b>Table 3.2</b>	UV-Vis data of <b>1</b> , <b>2</b> , <b>3</b> and <b>4</b>	99
9	<b>Table 4.1</b>	Optimization of reaction conditions for the conversion of tetrapyrane into porphyrin	121
10	<b>Table 4.2</b>	Optimization of reaction conditions for the conversion of tetrapyrane into porphyrin	122
11	<b>Table 4.3</b>	Optimization of reaction conditions for the conversion of tetrapyrane into porphyrin	123
12	<b>Table 4.4</b>	Scope of the synthesis of <i>meso</i> -substituted symmetric A <sub>4</sub> – porphyrins	124
13	<b>Table 4.5</b>	Scope of the synthesis of <i>meso</i> -substituted <i>trans</i> -A <sub>2</sub> B <sub>2</sub> -porphyrins	130
14	<b>Table 5.1</b>	Crystallographic data of <b>1</b> and <b>2</b>	193
15	<b>Table 5.2</b>	UV–Vis data for <b>1</b> and <b>2</b>	194
16	<b>Table 5.3</b>	Electrochemical data for <b>1</b> and <b>2</b>	197
17	<b>Table 5.4</b>	Catalytic oxidation reactions using [ <i>trans</i> -difluoro(3,17-dinitro– corrolato)antimony(V)] complexes	198

## List of Schemes

		Pages
1	<b>Scheme 1.1</b> An overview of heme activity	1
2	<b>Scheme 1.2</b> Synthesis of tetraphenylporphyrin using Rothmund protocol	10
3	<b>Scheme 1.3</b> Synthesis of tetraphenylporphyrin using Adler-Longo protocol	11
4	<b>Scheme 1.4</b> Synthesis of <i>meso</i> -substituted porphyrins using Lindsey methodology	12
5	<b>Scheme 1.5</b> Synthesis of the free-base corroles from cyclization of a,c-biladienes	19
6	<b>Scheme 1.6</b> Synthesis of free-base corroles from pyrrole and pentafluorobenzaldehyde	20
7	<b>Scheme 1.7</b> Synthesis of free-base corroles in acetic acid medium	21
8	<b>Scheme 1.8</b> Synthesis of free-base A <sub>3</sub> -corroles in water-MeOH/HCl medium	22
9	<b>Scheme 1.9</b> Synthesis of free-base trans-A <sub>2</sub> B-corrole in water-MeOH/HCl medium	22
10	<b>Scheme 2.1</b> Synthetic application of <i>meso</i> -substituted <i>trans</i> -A <sub>2</sub> B <sub>2</sub> -Porphyrins	47
11	<b>Scheme 2.2</b> Probable mechanism for the conversion of Mn(IV)-porphyrinogen derivatives to the porphyrin via hydrogen abstraction	61
12	<b>Scheme 3.1</b> Synthesis of <b>3</b> via oxidation of <b>1</b> by using iodosobenzene	88

13	<b>Scheme 3.2</b>	Structural parameters of <b>1</b> <sup>st</sup> and <b>2</b> <sup>nd</sup> conformers	90
14	<b>Scheme 4.1</b>	Synthetic application of <i>meso</i> -substituted symmetric A <sub>4</sub> -porphyrins and <i>trans</i> -A <sub>2</sub> B <sub>2</sub> -porphyrins	119
15	<b>Scheme 5.1</b>	Structures of the complexes: <b>1</b> and <b>2</b>	181
16	<b>Scheme 5.2</b>	Synthetic application of [ <i>trans</i> -difluoro(corrolato)antimony(V)] complexes: <b>1</b> and <b>2</b>	182
17	<b>Scheme 5.3</b>	Chemical reactivity of (corrolato)antimony(III) complex, <b>1A</b>	185
18	<b>Scheme 5.4</b>	Probable mechanism for the formation of <b>1</b> by the addition of NOBF <sub>4</sub> into the (corrolato)antimony(III) precursors in CH <sub>2</sub> Cl <sub>2</sub> -CH <sub>3</sub> CN mixture in the air (O <sub>2</sub> )	189



## List of Figures

			Pages
1	<b>Figure 1.1</b>	Structure of heme and its resemblance with porphyrin ring	2
2	<b>Figure 1.2</b>	Structure of chlorophyll a and its resemblance with chlorin ring	3
3	<b>Figure 1.3</b>	Structure of Vitamin B <sub>12</sub> and its resemblance with corrin ring	4
4	<b>Figure 1.4</b>	Structures of $\beta$ -modified and <i>meso</i> -substituted porphyrinoid macrocycles	5
5	<b>Figure 1.5</b>	Structure of core-modified porphyrinoid macrocycles	6
6	<b>Figure 1.6</b>	Structures of isomer-modified, expanded, and contracted porphyrinoid macrocycles	6
7	<b>Figure 1.7</b>	Structure of porphyrin macrocycle	8
8	<b>Figure 1.8</b>	Various structures of porphyrin dyes	13
9	<b>Figure 1.9</b>	Molecular structure of porphyrin wires	15
10	<b>Figure 1.10</b>	Molecular structure of some porphyrin-based inorganic nanoparticles (NPs)	16
11	<b>Figure 1.11</b>	Penta-coordinated mode of metallocorroles	24
12	<b>Figure 1.12</b>	Tetra-coordinated mode of metallocorroles	24
13	<b>Figure 1.13</b>	Hexa-coordinated mode of metallocorroles	25
14	<b>Figure 1.14</b>	Tri-coordinated mode of metallocorroles	25
15	<b>Figure 1.15</b>	Structures of representative metallocorroles which are used as catalysts	28

16	<b>Figure 1.16</b>	Structures of metallocorroles that are used for the decomposition of the peroxyxynitrite species	29
17	<b>Figure 1.17</b>	Structure of a representative cobalt(III) corrole which is used for CO sensing	30
18	<b>Figure 1.18</b>	Structures of metallocorroles that are used as sensitizers in dye-sensitized solar cells	30
19	<b>Figure 1.19</b>	Structure of the first reported water-soluble corrole which is applied in <i>in vivo</i> medical investigation	32
20	<b>Figure 2.1</b>	Proposed mechanism	51
21	<b>Figure 2.2</b>	Experimental X-band EPR spectrum (black) of <b>7-Mn</b> at 100 K in CH <sub>3</sub> OH-C <sub>2</sub> H <sub>5</sub> OH glass in a flat cell and the simulated spectrum (red)	52
22	<b>Figure 2.3</b>	Plot of the effective magnetic moment vs. temperature(from 2 to 300 K) for the complex <b>7-Mn</b>	52
23	<b>Figure 2.4</b>	Cyclic voltammogram (—) of <b>7-Mn</b> in CH <sub>3</sub> CN.	53
24	<b>Figure 2.5</b>	DFT optimized structure of <b>7-Mn</b>	54
25	<b>Figure 2.6</b>	UV-Vis spectra of <b>7-Mn</b> : Experimental UV-Vis absorption spectrum (—) and TDDFT (TD-B97D/6-31G*)-based absorption spectrum (—)	55
26	<b>Figure 2.7</b>	Chemical reduction of <b>7-Mn</b> via LiAlH <sub>4</sub> in DCM at RT. The black line indicates the absorption spectra before reduction, and the red line indicates the species obtained after reduction	56
27	<b>Figure 2.8</b>	IR spectrum of <b>7-Mn</b> : Experimentally recorded FT-IR spectrum (—) and IR spectrum (—) obtained from DFT (B97-D/6-31G*) computation	58

28	<b>Figure 2.9</b>	Calculated single occupied molecular orbitals (SOMO), lowest unoccupied molecular orbital (LUMO), and the corresponding orbital energies of <b>7-Mn</b>	59
29	<b>Figure 2.10</b>	Electronic absorption spectrum of a) <b>7-Mn</b> in CH <sub>2</sub> Cl <sub>2</sub> solution. After this, excess of PhIO was added to this solution; b) Recorded from the crude reaction mixture after 3 mins, c) after 6 mins, d) after 9 mins, e) after 12 mins, f) after 15 mins, g) 20 mins (passed through a silica gel filter to remove the residual Mn salt and excess PhIO, h) Pure <b>7</b> in CH <sub>2</sub> Cl <sub>2</sub> solution	60
30	<b>Figure 2.11</b>	<sup>1</sup> H NMR spectrum of <b>1</b> in CDCl <sub>3</sub>	68
31	<b>Figure 2.12</b>	<sup>1</sup> H NMR spectrum of <b>2</b> in CDCl <sub>3</sub>	69
32	<b>Figure 2.13</b>	<sup>1</sup> H NMR spectrum of <b>3</b> in CDCl <sub>3</sub>	70
33	<b>Figure 2.14</b>	<sup>1</sup> H NMR spectrum of <b>4</b> in CDCl <sub>3</sub>	71
34	<b>Figure 2.15</b>	<sup>1</sup> H NMR spectrum of <b>5</b> in CDCl <sub>3</sub>	72
35	<b>Figure 2.16</b>	<sup>1</sup> H NMR spectrum of <b>6</b> in CDCl <sub>3</sub>	73
36	<b>Figure 2.17</b>	<sup>1</sup> H NMR spectrum of <b>7</b> in CDCl <sub>3</sub>	74
37	<b>Figure 2.18</b>	<sup>1</sup> H NMR spectrum of <b>8</b> in CDCl <sub>3</sub>	75
38	<b>Figure 2.19</b>	<sup>1</sup> H NMR spectrum of <b>9</b> in CDCl <sub>3</sub>	76
39	<b>Figure 2.20</b>	ESI- MS spectrum in CH <sub>3</sub> CN shows the (a) measured spectrum, (b) isotopic distribution pattern (experimental), and (c) isotopic distribution pattern (simulated) of <b>7-Mn</b>	77
40	<b>Figure 2.21</b>	<sup>1</sup> H NMR spectrum of 5,15-bis(4-cyanophenyl)-10-(pentafluorophenyl)tetrapyranein CDCl <sub>3</sub>	78

41	<b>Figure 2.22</b>	ESI- MS spectrum in CH <sub>3</sub> CN shows the (a) measured spectrum, (b) isotopic distribution pattern of 5,15-bis(4-cyanophenyl)-10-pentafluorophenyl)tetrapyrane	79
42	<b>Figure 3.1</b>	Structures of <b>1</b> and <b>2</b>	87
43	<b>Figure 3.2</b>	Single-crystal X-ray structure of <b>1</b> . (a) 1 <sup>st</sup> conformer and (b) 2 <sup>nd</sup> conformer	90
44	<b>Figure 3.3</b>	Single-crystal X-ray analysis of <b>1</b> revealing the closest Sb–Sb distances (a) 1 <sup>st</sup> conformer and (b) 2 <sup>nd</sup> conformer	91
45	<b>Figure 3.4</b>	<sup>1</sup> H NMR spectrum of the complexes <b>3</b> and <b>1</b> in CDCl <sub>3</sub>	94
46	<b>Figure 3.5</b>	<sup>1</sup> H NMR spectra of <b>1</b> in CDCl <sub>3</sub> at variable temperatures	95
47	<b>Figure 3.6</b>	Electronic absorption spectra of complexes, <b>1</b> (black line) and <b>3</b> (red line) in CH <sub>2</sub> Cl <sub>2</sub> at room temperature	97
48	<b>Figure 3.7</b>	Electronic absorption spectra of complexes, <b>2</b> (black line) and <b>4</b> (red line) in CH <sub>2</sub> Cl <sub>2</sub> at room temperature	97
49	<b>Figure 3.8</b>	Normalized electronic emission spectra (excited at the Soret band) of the complexes, <b>1</b> (solid black line), <b>2</b> (dotted black line), <b>3</b> (solid red line), and <b>4</b> (dotted red line) in CH <sub>2</sub> Cl <sub>2</sub> at room temperature	98
50	<b>Figure 3.9</b>	Cyclic voltammograms of <b>1</b> in CH <sub>2</sub> Cl <sub>2</sub>	99
51	<b>Figure 3.10</b>	<sup>1</sup> H NMR spectrum of <b>1</b> in CDCl <sub>3</sub>	104
52	<b>Figure 3.11</b>	<sup>13</sup> C NMR spectrum of <b>1</b> in CDCl <sub>3</sub>	104
53	<b>Figure 3.12</b>	ESI- MS spectrum of <b>1</b> in CH <sub>3</sub> CN shows the measured spectrum with isotopic distribution pattern	105
54	<b>Figure 3.13</b>	<sup>1</sup> H NMR spectrum of <b>2</b> in CD <sub>2</sub> Cl <sub>2</sub>	106
55	<b>Figure 3.14</b>	<sup>13</sup> C NMR spectrum of <b>2</b> in CD <sub>2</sub> Cl <sub>2</sub>	107

56	<b>Figure 3.15</b>	ESI- MS spectrum of <b>2</b> in CH <sub>3</sub> CN shows the measured spectrum with isotopic distribution pattern	107
57	<b>Figure 3.16</b>	<sup>1</sup> H NMR spectrum of <b>3</b> in CDCl <sub>3</sub>	109
58	<b>Figure 3.17</b>	<sup>13</sup> C NMR spectrum of <b>3</b> in CDCl <sub>3</sub>	109
59	<b>Figure 3.18</b>	ESI- MS spectrum of <b>3</b> in CH <sub>3</sub> CN shows the measured spectrum with isotopic distribution pattern	110
60	<b>Figure 3.19</b>	<sup>1</sup> H NMR spectrum of <b>4</b> in CDCl <sub>3</sub>	111
61	<b>Figure 3.20</b>	<sup>13</sup> C NMR spectrum of <b>4</b> in CDCl <sub>3</sub>	112
62	<b>Figure 3.21</b>	ESI- MS spectrum of <b>4</b> in CH <sub>3</sub> CN shows the measured spectrum with isotopic distribution pattern	112
63	<b>Figure 4.1</b>	Proposed mechanism	133
64	<b>Figure 4.2</b>	<sup>1</sup> H NMR spectrum of <b>1</b> in CDCl <sub>3</sub>	136
65	<b>Figure 4.3</b>	<sup>1</sup> H NMR spectrum of <b>2</b> in CDCl <sub>3</sub>	138
66	<b>Figure 4.4</b>	<sup>1</sup> H NMR spectrum of <b>3</b> in CDCl <sub>3</sub>	139
67	<b>Figure 4.5</b>	ESI-MS spectrum of <b>3</b> in CH <sub>3</sub> CN shows the measured spectrum with isotopic distribution pattern	140
68	<b>Figure 4.6</b>	<sup>1</sup> H NMR spectrum of <b>4</b> in CDCl <sub>3</sub>	141
69	<b>Figure 4.7</b>	<sup>1</sup> H NMR spectrum of <b>5</b> in CDCl <sub>3</sub>	142
70	<b>Figure 4.8</b>	<sup>1</sup> H NMR spectrum of <b>6</b> in CDCl <sub>3</sub>	144
71	<b>Figure 4.9</b>	<sup>1</sup> H NMR spectrum of <b>7</b> in CDCl <sub>3</sub>	145
72	<b>Figure 4.10</b>	<sup>1</sup> H NMR spectrum of <b>8</b> in CDCl <sub>3</sub>	146
73	<b>Figure 4.11</b>	<sup>1</sup> H NMR spectrum of <b>9</b> in CDCl <sub>3</sub>	147
74	<b>Figure 4.12</b>	<sup>1</sup> H NMR spectrum of <b>10</b> in CDCl <sub>3</sub>	148
75	<b>Figure 4.13</b>	<sup>1</sup> H NMR spectrum of <b>11</b> in CDCl <sub>3</sub>	150
76	<b>Figure 4.14</b>	<sup>1</sup> H NMR spectrum of <b>12</b> in CDCl <sub>3</sub>	151

77	<b>Figure 4.15</b>	$^1\text{H}$ NMR spectrum of <b>13</b> in $\text{CDCl}_3$	152
78	<b>Figure 4.16</b>	$^1\text{H}$ NMR spectrum of <b>14</b> in $\text{CD}_2\text{Cl}_2$	154
79	<b>Figure 4.17</b>	$^1\text{H}$ NMR spectrum of <b>15</b> in $\text{CDCl}_3$	155
80	<b>Figure 4.18</b>	$^1\text{H}$ NMR spectrum of <b>16</b> in $\text{CDCl}_3$	156
81	<b>Figure 4.19</b>	$^{13}\text{C}\{^1\text{H}\}$ NMR (101 MHz) spectrum of <b>16</b> in $\text{CDCl}_3$	157
82	<b>Figure 4.20</b>	ESI-MS spectrum of <b>16</b> in $\text{CH}_3\text{CN}$ shows the measured spectrum with isotopic distribution pattern	158
83	<b>Figure 4.21</b>	$^1\text{H}$ NMR spectrum of <b>21</b> in $\text{CDCl}_3$	159
84	<b>Figure 4.22</b>	$^1\text{H}$ NMR spectrum of <b>22</b> in $\text{CDCl}_3$	160
85	<b>Figure 4.23</b>	$^1\text{H}$ NMR spectrum of <b>23</b> in $\text{CDCl}_3$	162
86	<b>Figure 4.24</b>	$^1\text{H}$ NMR spectrum of <b>24</b> in $\text{CDCl}_3$	163
87	<b>Figure 4.25</b>	$^{13}\text{C}\{^1\text{H}\}$ NMR (101 MHz) spectrum of <b>24</b> in $\text{CDCl}_3$	164
88	<b>Figure 4.26</b>	ESI-MS spectrum of <b>24</b> in $\text{CH}_3\text{CN}$ shows the measured spectrum with isotopic distribution pattern	165
89	<b>Figure 4.27</b>	$^1\text{H}$ NMR spectrum of <b>25</b> in $\text{CDCl}_3$	166
90	<b>Figure 4.28</b>	$^1\text{H}$ NMR spectrum of <b>26</b> in $\text{CDCl}_3$	167
91	<b>Figure 4.29</b>	$^1\text{H}$ NMR spectrum of <b>27</b> in $\text{CDCl}_3$	169
92	<b>Figure 4.30</b>	$^1\text{H}$ NMR spectrum of <b>28</b> in $\text{CDCl}_3$	170
93	<b>Figure 4.31</b>	$^1\text{H}$ NMR spectrum of <b>29</b> in $\text{CDCl}_3$	171
94	<b>Figure 4.32</b>	$^1\text{H}$ NMR spectrum of <b>30</b> in $\text{CDCl}_3$	173
95	<b>Figure 4.33</b>	$^1\text{H}$ NMR spectrum of <b>31</b> in $\text{CDCl}_3$	174
96	<b>Figure 4.34</b>	$^1\text{H}$ NMR spectrum of <b>32</b> in $\text{CDCl}_3$	175
97	<b>Figure 5.1</b>	$^1\text{H}$ NMR spectrum of <b>1</b> in $\text{CDCl}_3$	183
98	<b>Figure 5.2</b>	$^1\text{H}$ NMR spectrum of <b>2</b> in $\text{CDCl}_3$	184

99	<b>Figure 5.3</b>	Electronic absorption spectrum of (5,10,15-triphenylcorrolato)( <i>trans</i> -difluoro)antimony(V) in dichloromethane	186
100	<b>Figure 5.4</b>	ESI- MS spectrum of (5,10,15-triphenylcorrolato)( <i>trans</i> -difluoro) antimony(V) in CH <sub>3</sub> CN shows the measured spectrum with isotopic distribution pattern	186
101	<b>Figure 5.5</b>	Electronic absorption spectrum of (3,17-dinitro-5,10,15-triphenylcorrolato)(oxo)antimony(V) in CH <sub>2</sub> Cl <sub>2</sub> -CH <sub>3</sub> CN mixture	187
102	<b>Figure 5.6</b>	ESI- MS spectrum of (3,17-dinitro-5,10,15-triphenylcorrolato)(oxo)antimony(V) in CH <sub>3</sub> CN shows the measured spectrum with isotopic distribution pattern	188
103	<b>Figure 5.7</b>	Solution FT-IR spectra of (a) (5,10,15-triphenylcorrolato) antimony(III) in a CH <sub>2</sub> Cl <sub>2</sub> -CH <sub>3</sub> CN mixture (b) (5,10,15-triphenylcorrolato)antimony(III) complex was treated with excess NOBF <sub>4</sub> in a CH <sub>2</sub> Cl <sub>2</sub> -CH <sub>3</sub> CN mixture at 0°C after 3 minutes (c) after 15 minutes (d) after 25 minutes (e) after 35 minutes (f) after 60 minutes	190
104	<b>Figure 5.8</b>	Single-crystal X-ray structure of <b>2</b>	192
105	<b>Figure 5.9</b>	Single-crystal X-ray structure of <b>1</b>	192
106	<b>Figure 5.10</b>	Steady-state absorption (solid lines) and emission (dashed lines) spectra of <b>1</b> (black line) ( $\lambda_{\text{exc}}$ =424 nm) and <b>2</b> (red line) ( $\lambda_{\text{exc}}$ =430 nm) in aerated dichloromethane.	195
107	<b>Figure 5.11</b>	Cyclic voltammograms and differential pulse voltammogram of <b>1</b> in CH <sub>2</sub> Cl <sub>2</sub>	196

108	<b>Figure 5.12</b>	Cyclic voltammograms of <b>2</b> in CH <sub>2</sub> Cl <sub>2</sub>	197
109	<b>Figure 5.13</b>	<sup>1</sup> H (top) and <sup>13</sup> C (bottom) of compound <b>2a</b> in CDCl <sub>3</sub>	199
110	<b>Figure 5.14</b>	ESI-MS data of compound <b>2a</b> in CH <sub>3</sub> CN	200
111	<b>Figure 5.15</b>	<sup>1</sup> H (top) and <sup>13</sup> C (bottom) of compound <b>2b</b> in CDCl <sub>3</sub>	201
112	<b>Figure 5.16</b>	Mass spectrum (GC-EIMS) of compound <b>2b</b> detected by GC of the reaction mixture	202
113	<b>Figure 5.17</b>	Mass spectrum (GC-EIMS) of compound <b>2c</b> detected by GC of the reaction mixture	202
114	<b>Figure 5.18</b>	<sup>1</sup> H (top) and <sup>13</sup> C (bottom) of compound <b>2c</b> in CDCl <sub>3</sub>	203
115	<b>Figure 5.19</b>	HRMS data of compound <b>2c</b> in CH <sub>3</sub> CN	204
116	<b>Figure 5.20</b>	Electronic absorption spectrum of (a) pure <b>2</b> (—) in CH <sub>2</sub> Cl <sub>2</sub> at RT; (b) isolated compound (—) (in CH <sub>2</sub> Cl <sub>2</sub> at RT) obtained via the treatment of <b>2</b> (0.002 mmol) with PPh <sub>3</sub> (10 mmol) in CH <sub>2</sub> Cl <sub>2</sub> -CH <sub>3</sub> CN mixture at RT for 17h in air and light (20 W CFL bulb), followed by purification <i>via</i> column chromatography	206
117	<b>Figure 5.21</b>	<sup>1</sup> H NMR spectrum of (a) pure <b>2</b> (—) in CDCl <sub>3</sub> at RT; (b) crude reaction mixture (—) (in CDCl <sub>3</sub> at RT) obtained via the treatment of <b>2</b> (0.002 mmol) with PPh <sub>3</sub> (10 mmol) in CH <sub>2</sub> Cl <sub>2</sub> -CH <sub>3</sub> CN mixture at RT for 17h in air and light (20 W CFL bulb)	206
118	<b>Figure 5.22</b>	<sup>13</sup> C NMR spectrum of <b>1</b> in CDCl <sub>3</sub>	210
119	<b>Figure 5.23</b>	<sup>19</sup> F { <sup>1</sup> H} NMR (377 MHz) spectrum of <b>1</b> in CDCl <sub>3</sub>	211
120	<b>Figure 5.24</b>	ESI- MS spectrum of <b>1</b> in CH <sub>3</sub> CN shows the measured spectrum with isotopic distribution pattern	212
121	<b>Figure 5.25</b>	FT IR spectra of <b>1</b> as KBr Pellet	212



122	<b>Figure 5.26</b>	$^1\text{H}$ NMR spectrum of <b>2A</b> in $\text{CDCl}_3$	214
123	<b>Figure 5.27</b>	$^{13}\text{C}$ NMR spectrum of <b>2A</b> in $\text{CDCl}_3$	214
124	<b>Figure 5.28</b>	ESI- MS spectrum of <b>2A</b> in $\text{CH}_3\text{CN}$ shows the measured spectrum with isotopic distribution pattern	215
125	<b>Figure 5.29</b>	$^{13}\text{C}$ NMR spectrum of <b>2</b> in $\text{CDCl}_3$	216
126	<b>Figure 5.30</b>	$^{19}\text{F}\{^1\text{H}\}$ NMR (377 MHz) spectrum of <b>2</b> in $\text{CDCl}_3$	217
127	<b>Figure 5.31</b>	ESI- MS spectrum of <b>2</b> in $\text{CH}_3\text{CN}$ shows the measured spectrum with isotopic distribution pattern	218
128	<b>Figure 5.32</b>	FT IR spectra of <b>2</b> as KBr Pellet	218

## Glossary of Acronyms

$^1\text{H}$ NMR	Proton Nuclear Magnetic Resonance
DDQ	2,3-Dichloro-5,6-dicyano-1,4-benzoquinone
$\text{CH}_2\text{Cl}_2$	Dichloromethane
$\text{CHCl}_3$	Chloroform
$^{13}\text{C}$ NMR	Carbon-13 Nuclear Magnetic Resonance
$^{19}\text{F}$ NMR	Fluorine-19 Nuclear Magnetic Resonance
FTIR	Fourier Transform Infrared
EPR	Electron Paramagnetic Resonance
UV-Vis	Ultraviolet–Visible
NO	Nitric oxide
tpfc	5,10,15-tris(pentafluorophenyl)corrole
CO	Carbon monoxide
NIR	Near-Infrared
DFT	Density Functional Theory
cor	corrole
TD-DFT	Time-Dependent Density Functional Theory
HCl	Hydrogen chloride
TFA	Trifluoroacetic acid
$\text{NaNO}_2$	Sodium nitrite
KBr	Potassium bromide
$\text{CDCl}_3$	Deuterated chloroform
GOF	Goodness of Fit
CCDC	Cambridge Crystallographic Data Centre
TBAP	Tetrabutylammonium perchlorate
OTTLE	Optically Transparent Thin Layer

HOMO	Highest Occupied Molecular Orbital
SOMO	Singly Occupied Molecular Orbital
LUMO	Lowest Unoccupied Molecular Orbital
expt.	Experimental
Anal. Calcd	Analytically Calculated
CH <sub>3</sub> CN	Acetonitrile
SEM	Scanning Electron Microscopy
TEM	Transmission Electron Microscopy
EDX	Energy Dispersive X-Ray Spectroscopy
CAFM	Conductive Atomic Force Microscopy
FB	Free-Base
TLC	Thin Layer Chromatography
ESI	Electrospray Ionization
CH <sub>3</sub> OH	Methanol
KOH	Potassium hydroxide
CaH <sub>2</sub>	Calcium hydride
HPLC	High-Performance Liquid Chromatography
ILCT	Intra-Ligand Charge Transfer
MLCT	Metal to Ligand Charge Transfer
LMCT	Ligand to Metal Charge Transfer
Na <sub>2</sub> SO <sub>4</sub>	Sodium sulphate
CD <sub>2</sub> Cl <sub>2</sub>	Dideuteromethylenechloride
SbCl <sub>3</sub>	Antimony trichloride
NOBF <sub>4</sub>	Nitrosonium tetrafluoroborate
CD <sub>3</sub> CN	Trideuteroacetonitrile
PhIO	Iodosobenzene

# CHAPTER 1

---

## Evolution of Porphyrins and Corroles

---

### 1.1 Introduction

### 1.2 Nomenclature of porphyrins

### 1.3 Structural modifications of porphyrinoids

#### 1.3.1 Porphyrins

##### 1.3.1.1 Characteristic properties of porphyrins

##### 1.3.1.2 Synthesis of porphyrins

##### 1.3.1.3 Applications of porphyrins

###### 1.3.1.3.1 as organic solar cells

###### 1.3.1.3.2 as functional devices

###### 1.3.1.3.3 as porphyrin-based nanoparticles (NPs)

###### 1.3.1.3.4 as porphyrin-based polymers

#### 1.3.2 Corroles

##### 1.3.2.1 Characteristic properties of corroles

##### 1.3.2.2 Synthesis of corroles

##### 1.3.2.3 Metallocorrole complexes

##### 1.3.2.4 Coordination mode of corroles

##### 1.3.2.5 Applications of corroles

###### 1.3.2.5.1 as Catalysts

###### 1.3.2.5.2 as Sensors

###### 1.3.2.5.3 as Dye-Sensitized Solar Cells

###### 1.3.2.5.4 as Medicinal drugs

### 1.5 Scope and Objectives of the Present Thesis

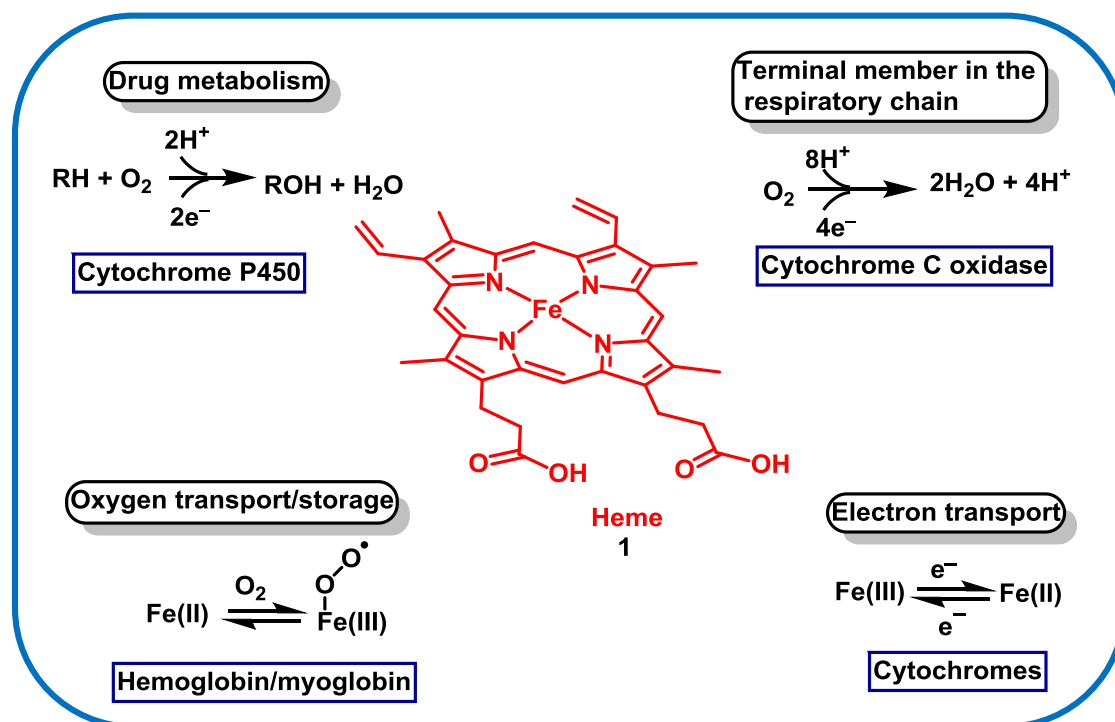
#### 1.5.1 Lacunae

#### 1.5.2 Objectives

## 1.1 Introduction

In nature, porphyrins are widely abundant, and it plays a pivotal role in various biological systems. Porphyrins are often referred to as the “Pigments of Life” due to their intense color, which arises from a highly conjugated  $\pi$  system.<sup>1</sup> Porphyrins<sup>2</sup>, and metallated porphyrins are present in various aromatic heterocyclic and different macrocyclic derivatives such as heme, **1** (iron porphyrin), (found in hemoglobins, myoglobins, catalases, cytochromes, and peroxidases, etc.), chlorophylls, bacteriochlorophylls, etc.

Porphyrins<sup>2</sup> have huge biological applications such as transportation of  $O_2$  in hemoglobin and storage of  $O_2$  in myoglobins, transportation and collection of light energy in antennae compounds, dioxygen reduction in oxidases, electron transfer in cytochromes, conversion of solar energy to chemical energy in photosynthetic reaction centers, and a large number of other enzymatic reactions (peroxidases, catalases, methylreductases, cytochrome P450, etc.) (Scheme 1.1).

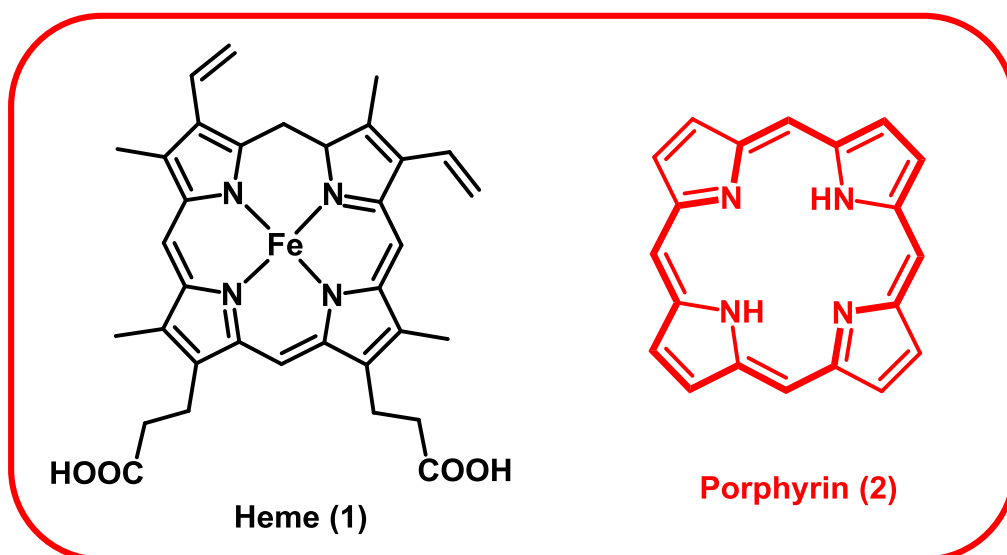


**Scheme 1.1** An overview of heme activity.<sup>2</sup>

---

Synthetic porphyrin derivatives and their metallated derivatives show unique chemical, physical and biological properties, which has attracted lots of interest in different interdisciplinary research fields such as supramolecular building blocks, molecular electronics, and photodynamic therapy.

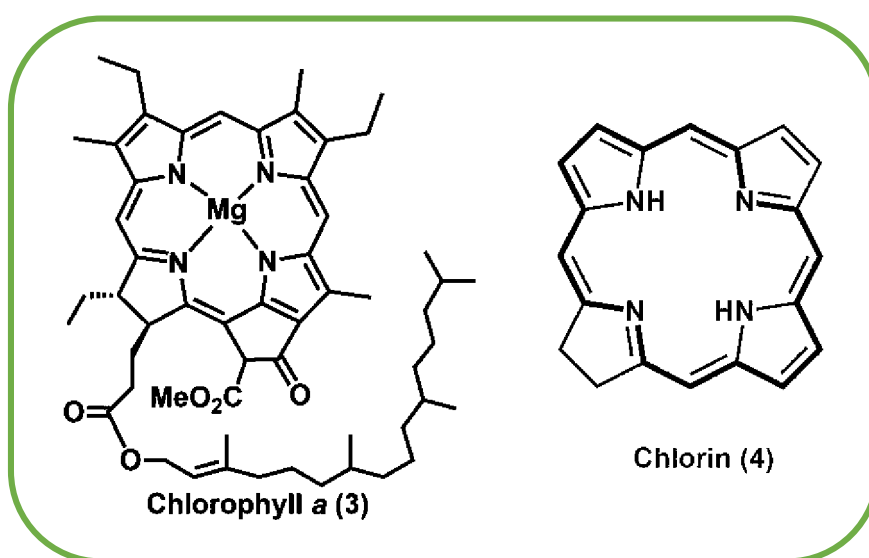
Hemoglobin (Heme + globin) is responsible for the transport of oxygen in the blood from the lungs to cells.<sup>3</sup> Porphyrin macrocycle, **2** containing iron metal atom in the center of the ring is often referred to as heme group, **1**. On the other hand, myoglobin is responsible for the transport of oxygen in muscle tissues. Both hemoglobin and myoglobin have the basic structure of the iron protoporphyrin XI unit, which is known as heme (Figure 1.1).



**Figure 1.1** Structure of heme and its resemblance with porphyrin ring.<sup>3</sup>

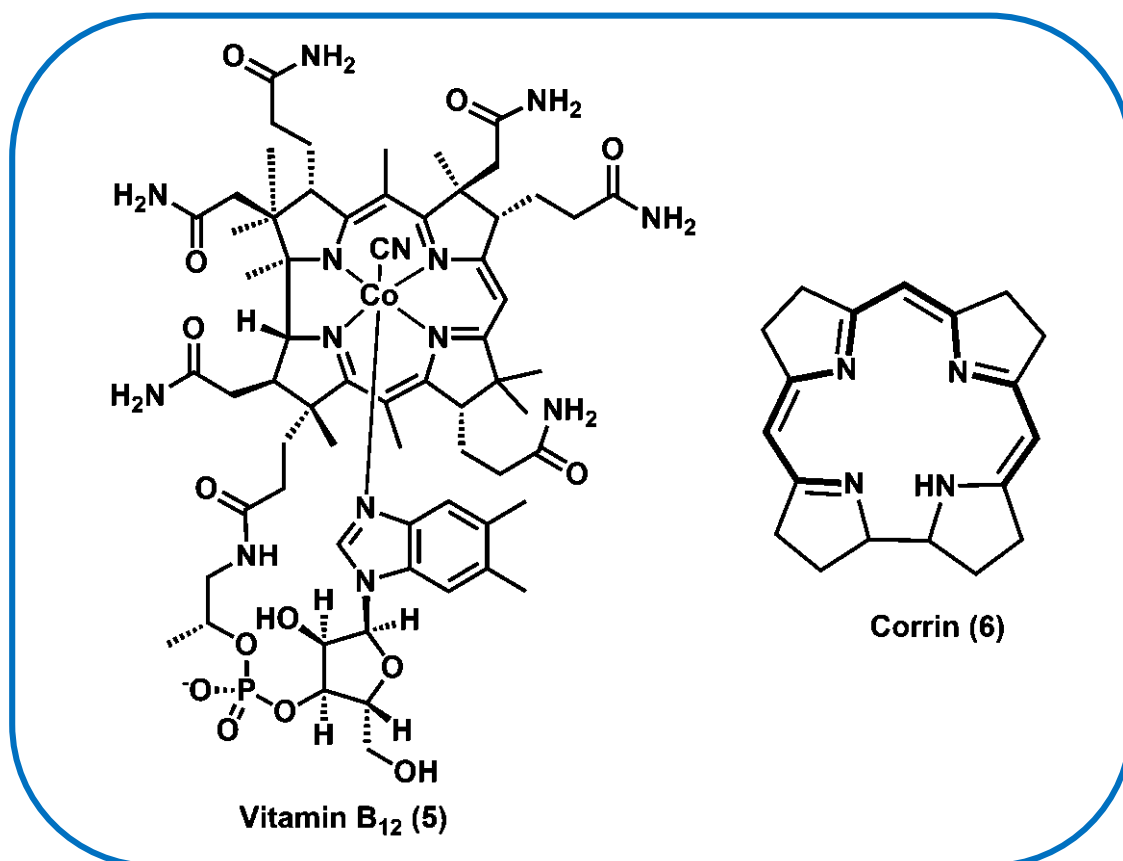
The existence of human life is dependent on one of the naturally occurring phenomena known as photosynthesis. In this process, plants and other living organisms capture light energy and convert it to chemical energy. This process begins with the absorbance of the light energy by proteins that contains chlorophyll, a green-colored chromophore. This chlorophyll molecule contains a porphyrin ring as the basic structure, and in this molecule, the inner core of the porphyrin ring is coordinated with a

magnesium metal atom. Chlorophyll *a*, **3** is a particular type of chlorophyll that is also involved in aerobic photosynthesis.<sup>4</sup> It absorbs light energy specifically in the range of blue and red region wavelength. Chlorophyll *a* has the basic structure constituted of a chlorin ring, **4**, and the inner core nitrogen atoms of the ring are coordinated with a magnesium metal atom with different side groups attached to it (Figure 1.2). The name chlorin is derived from the name chlorophyll.



**Figure 1.2** Structure of chlorophyll *a* and its resemblance with chlorin ring.<sup>4</sup>

Vitamin B<sub>12</sub>, <sup>5</sup> **5**, commonly known as cobalamin, plays a vital role in the metabolism process. The molecular structure of vitamin B<sub>12</sub> resembles the heterocyclic compound, corrin, **6** (Figure 1.3)<sup>6-8</sup>. The corrin ring acts as the parent molecule for the substituted derivative in vitamin B<sub>12</sub>. Again, this corrin moiety has an amazing resemblance with the porphyrin ring. But unlike porphyrin rings, corrin lacks one of the carbon atoms which is involved in the linkage of two subsequent pyrrole moieties. The conjugated  $\pi$  system in the corrin ring is less than that of the porphyrin ring, which makes the corrin ring more flexible and non-planar. On the other hand, the fully aromatic derivative of this corrin ring is known as corroles.



**Figure 1.3** Structure of Vitamin B<sub>12</sub> and its resemblance with corrin ring.<sup>5</sup>

### 1.2 Nomenclature of porphyrins:

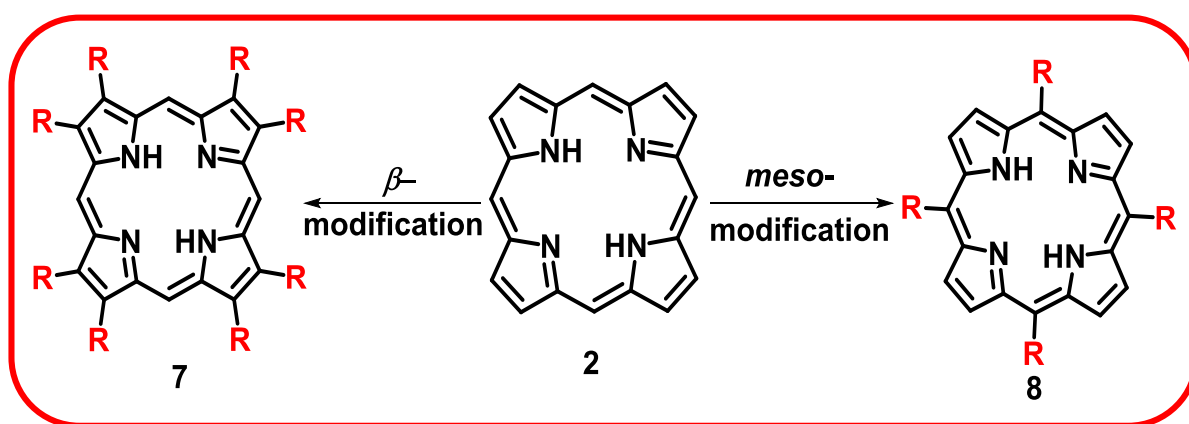
The porphyrins were given names depending on the nature of the color, size, and numbers of heterocyclic moiety with suffixes such as phyrin or rin.<sup>9</sup> Sapphyrin, pentapyrrolic porphyrinoid macrocycle is blue in color. Similarly, rubyrin is a red-colored porphyrinoid, whereas pentaphyrin is a porphyrinoid with five pyrrole units, and hexaphyrin is a porphyrinoid with six pyrrole units. This naming system of the porphyrinoid molecules was suggested by Frank and Nonn.<sup>10</sup> The name porphyrin emerged from the Greek word ‘porphura’, which means purple. Porphyrins with or without the presence of a metal center are also observed in different biological systems such as pheophytins, catabolites, and biosynthetic intermediates in metal-free porphyrin



and hemes containing iron, vitamin B<sub>12</sub> containing cobalt, chlorophylls containing magnesium, pigments containing copper, cofactor F<sub>430</sub> containing nickel, etc.

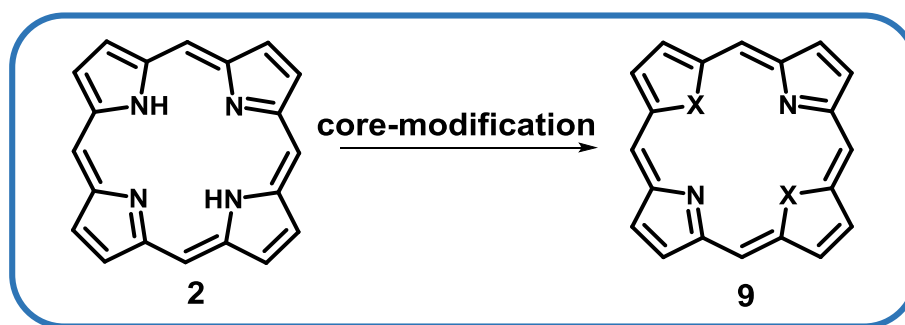
### 1.3 Structural modifications of porphyrinoids:

The attempt to synthesize artificial porphyrin derivatives has been made since the significance of the applications of these macrocycles came to light. While attempting to synthesize these macrocycles, different kinds of porphyrinoids have been synthesized with various modifications in various positions. This occurrence led to the structural modifications of porphyrinoids. These structurally modified porphyrinoid macrocycles have different structural and electronic properties when compared to the basic porphyrin framework. Structural modifications of porphyrin have been attained in various ways, out of which the two most popular strategies used are  $\beta$ -substitution and *meso*-substitution (Figure 1.4). Structurally modified porphyrins attained via  $\beta$ -substitution are octaalkyl porphyrins, **7**. Octaalkyl porphyrins can be both symmetric and asymmetric in structure. These octaalkyl porphyrins are quite similar to the protoporphyrin IX, which is found in nature. Structurally modified porphyrins attained via *meso*-substitution do not generally resemble the naturally occurring macrocycles, but these *meso*-substituted porphyrins, **8** are widely used in biological as well as materials chemistry.<sup>11-14</sup>



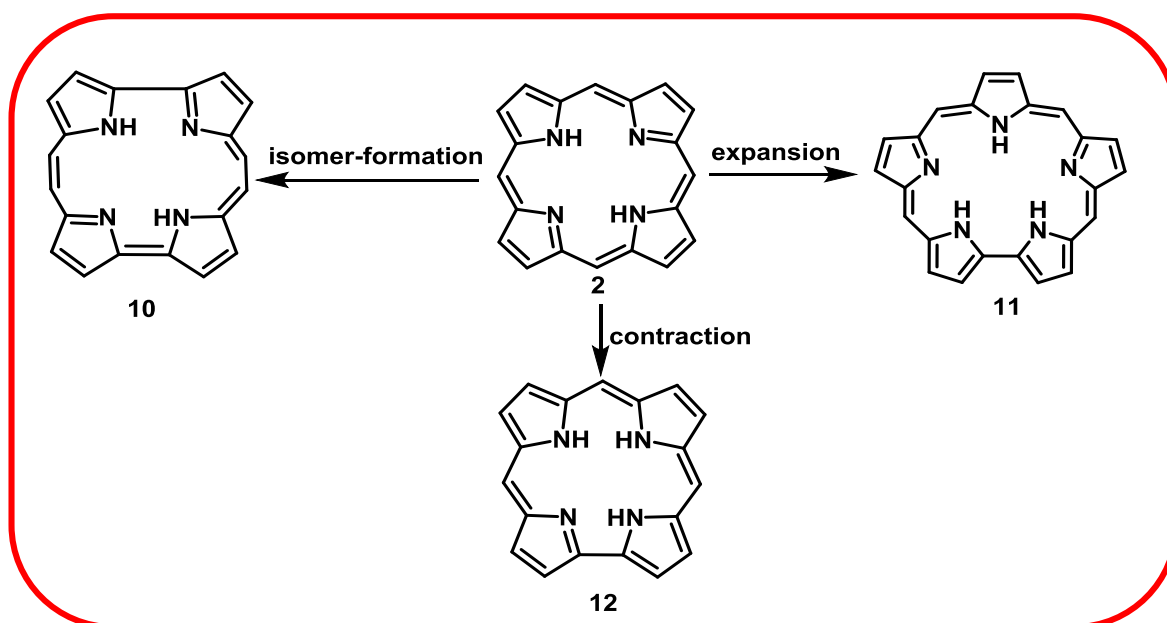
**Figure 1.4** Structures of  $\beta$ -modified and *meso*-substituted porphyrinoid macrocycles.

Another variety of structurally modified porphyrins is core-modified porphyrins, **9** (Figure 1.5).<sup>15-17</sup> In core-modified porphyrins, at least one or two  $\beta$ -pyrrolic nitrogen atoms of the porphyrin macrocycle are replaced by other donor heteroatoms such as O, S, Se, and Te.



**Figure 1.5** Structure of core-modified porphyrinoid macrocycles.

Other structurally modified porphyrins are isomeric porphyrins, **10** expanded porphyrins, **11**, and contracted porphyrins, **12** (Figure 1.6).<sup>18-20</sup>



**Figure 1.6** Structures of isomer-modified, expanded and contracted porphyrinoid macrocycles.

In isomeric porphyrins, **10**, the basic molecular formula ( $C_{20}H_{14}N_4$ ) of the porphyrin ring remains the same, but the position of the *meso* carbons and the pyrrole moiety gets alternated. In expanded porphyrins, **11**, the macrocycle contains more than

---

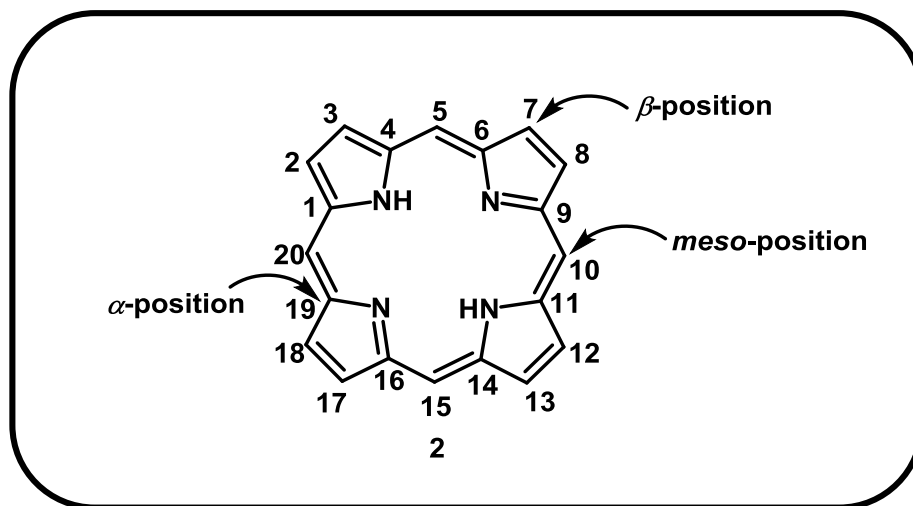
four pyrrolic rings which are bonded directly or indirectly (through spacer atom), and the framework contains a minimum of 17 conjugated atoms. In contracted porphyrins, **12**, the macrocycle contains one carbon atom short at *meso* position or one pyrrole moiety short of the parent porphyrin molecule, but it retains the aromaticity.

### 1.3.1 Porphyrins:

Porphyrin macrocycles are biologically important organic pigments which can be found in nature as well as can be artificially synthesized.<sup>21</sup> The chemistry of porphyrin macrocycles deals with different kinds of derivatives and analogs of porphyrin along with its metal complexes.<sup>22,23</sup> Porphyrin is an aromatic tetrapyrrolic ring system. The four pyrrole rings are connected by four  $sp^2$  hybridized *meso*-carbon atoms, which have been confirmed by various X-ray crystal structures. The very concept of the macrocyclic porphyrin structure was first suggested by Küster in 1912<sup>24</sup>, later which was confirmed by Fischer. The inner core of the porphyrin macrocycle is comprised of two amino nitrogen and two imino nitrogen. As porphyrin is a highly conjugated system, porphyrin derivatives are intense in color. The numbering of the porphyrin moiety occurs throughout the peripheral carbon atoms (Figure 1.7). The carbon atoms located in the 5,10,15- and 20 positions are often called *meso*-positions, whereas the carbon atoms located in the 2,3,7,8,12,13,17,18- are referred to as  $\beta$ -positions. The rest of the methine bridged carbons carbon atoms at 1,4,6,9,11,14,16,19- positions are known as the  $\alpha$ -carbons. These nomenclatures are done by following the convention of nomenclature used for the 5-membered heterocycles.

The most common synthetic substitution of porphyrin macrocycles occurs in the eight  $\beta$ -positions located on the pyrrole rings and on the four methine groups, which are represented as *meso*-positions. But in nature, the most common substitution of porphyrin

macrocycle is observed at  $\beta$ -positions in an unsymmetrical manner. The unsubstituted porphyrin macrocycle is called porphine.



**Figure 1.7** Structure of porphyrin macrocycle.

#### 1.3.1.1 Characteristic properties of porphyrins:

Porphyrin derivatives are intensely colored. In porphyrin derivatives, an intense absorption band is observed in the visible region. Porphyrin macrocycles usually display an intense absorption band named the Soret band between 350 and 450 nm with a high molar extinction coefficient ( $\epsilon > 100,000$ ). The Soret band is observed due to the highly conjugated  $\pi$  system. Besides the Soret band, a few other weaker characteristic absorption bands are also seen, called the Q-bands, in the range of 450-700 nm.<sup>25,26</sup>

Porphyrin macrocycles are aromatic in nature. It consists of 22  $\pi$ -electrons. Without any substitution in the  $\beta$ -pyrrole ring or *meso*-position in the parent porphyrin molecule is called porphine, whereas porphyrins are substituted porphines. The electron count is consistent with Hückel's  $[4n+2]$  rule for aromaticity, where  $n = 4$ . Porphyrin contains two inner-core NH groups and two pyrrolenine nitrogen atoms.

The aromaticity of the porphyrin compounds can be further manifested by the  $^1\text{H}$  NMR spectra. In the  $^1\text{H}$  NMR spectrum, the chemical shift of the different protons in the

---

porphyrin molecule differs widely due to the strong porphyrin ring current effect.<sup>27,28</sup> Downfield shifts are observed for the peripheral protons, whereas strong upfield shifts are observed for the inner core NH protons. In FB porphyrins, the chemical shift of the inner nitrogen protons is usually observed in the range of -4 and -2 ppm due to the shielding effect of the porphyrin ring current. The *meso*-protons of the porphyrin molecule usually resonate at ~ 10 ppm (low field region), so the *meso*-protons generally appear in the deshielded region. The protons at the  $\beta$ -pyrrolic position usually resonate in the range of ~8 to 9 ppm, so the  $\beta$ -pyrrolic protons are also deshielded, compared to that of pyrrole (~ 6 ppm). However, the formation of aggregates of these porphyrin macrocycles further complicates its NMR spectrum and is difficult to assign the peaks. This thesis contains the study of different synthetic methodologies for these porphyrin molecules.

Porphyrin macrocycles are weak bases. It can be easily protonated in the presence of bases to generate di-cations. In the free-base porphyrins, which are usually in the unprotonated form, the two NH protons in the inner core of the mean plane are labile.

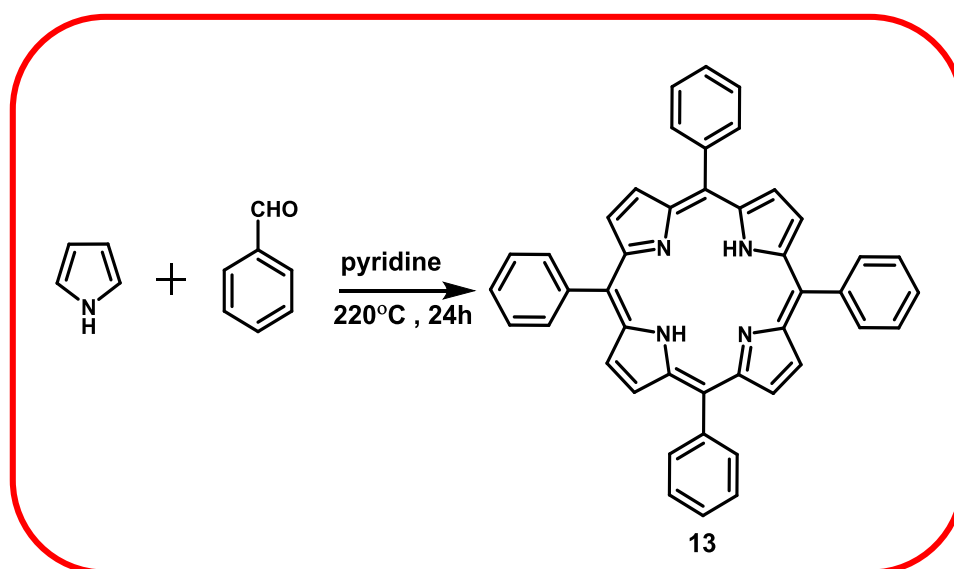
#### **1.3.1.2 Synthesis of porphyrins:**

The synthesis of porphyrin derivatives has gained attention since the first synthesis reported by Hans Fisher.<sup>29</sup> Since then, various attempts have been made to simplify the synthesis of porphyrin derivatives and modify their yield. The methodologies involved the synthesis of symmetric as well as asymmetric porphyrin derivatives.

---

### Using Rothemund synthetic protocol

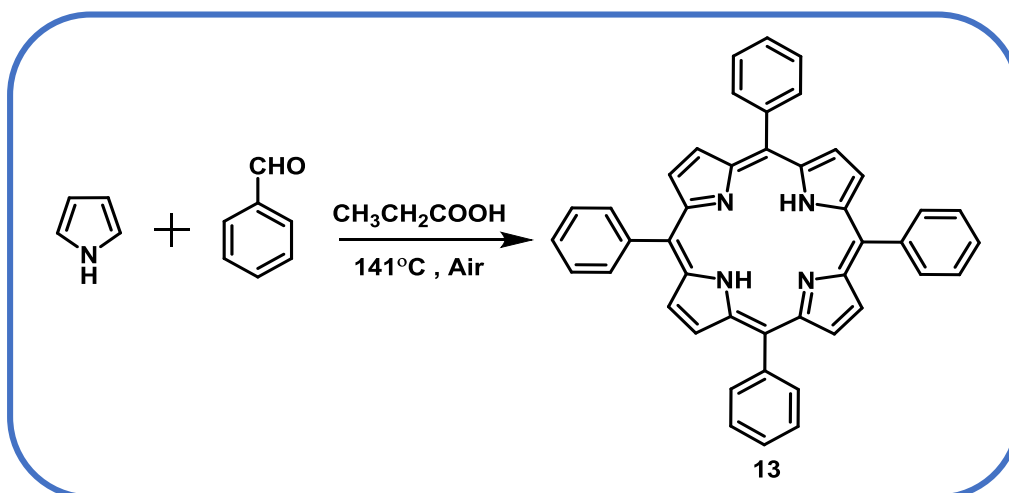
Rothemund *et al.* first reported the synthesis of *meso*-substituted porphyrins in 1935.<sup>30</sup> Tetraphenylporphyrin, **13** was synthesized by reacting aromatic aldehydes and pyrrole in a sealed tube using pyridine as solvent at a high temperature (Scheme 1.2). No oxidants were used in this reaction process. However, the yields of the porphyrins were considerably low as severe conditions were used during the reaction.



**Scheme 1.2** Synthesis of tetraphenylporphyrin using Rothemund protocol.<sup>30</sup>

### Using Adler-Longo synthetic protocol

Later in 1964, another synthetic methodology for porphyrins was developed by Adler-Longo (Scheme 1.3).<sup>31</sup> In this synthetic route, benzaldehyde and pyrrole were refluxed in propionic acid under aerial conditions at 141°C, which resulted in the formation of tetraphenylporphyrin, **13**.

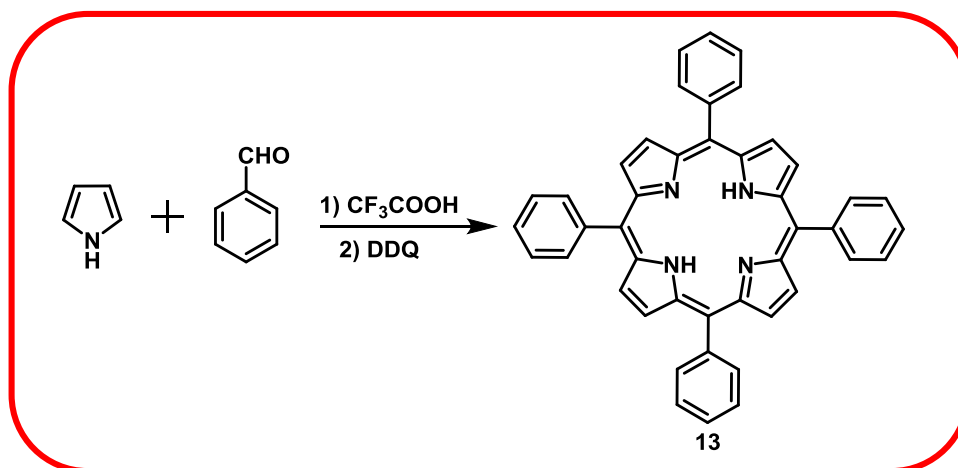


**Scheme 1.3** Synthesis of tetraphenylporphyrin using Adler-Longo protocol.<sup>31</sup>

This synthetic methodology is very useful for synthesizing porphyrin in a multigram amount. However, this synthetic route has a major limitation as aldehydes bearing acid-sensitive groups yields no porphyrin.

#### Using Lindsey's synthetic methodology

In 1986, Lindsey optimized the synthetic methodology for porphyrins and developed a two-step, one-pot methodology for the synthesis of *meso*-substituted porphyrins (Scheme 1.4).<sup>32,33</sup> In this synthetic route, the first step involves the acid-catalyzed condensation between pyrrole and aldehyde in an inert atmosphere which results in the formation of the porphyrinogen intermediate. And in the second step, the porphyrinogen intermediate was oxidized with quinone-based oxidants such as DDQ or *p*-chloranil, resulting in the formation of the desired porphyrin macrocycle, **13**. This methodology occurs in mild conditions, and the yields of the desired porphyrins are also reasonably satisfactory.



**Scheme 1.4** Synthesis of *meso*-substituted porphyrins using Lindsey methodology.<sup>32,33</sup>

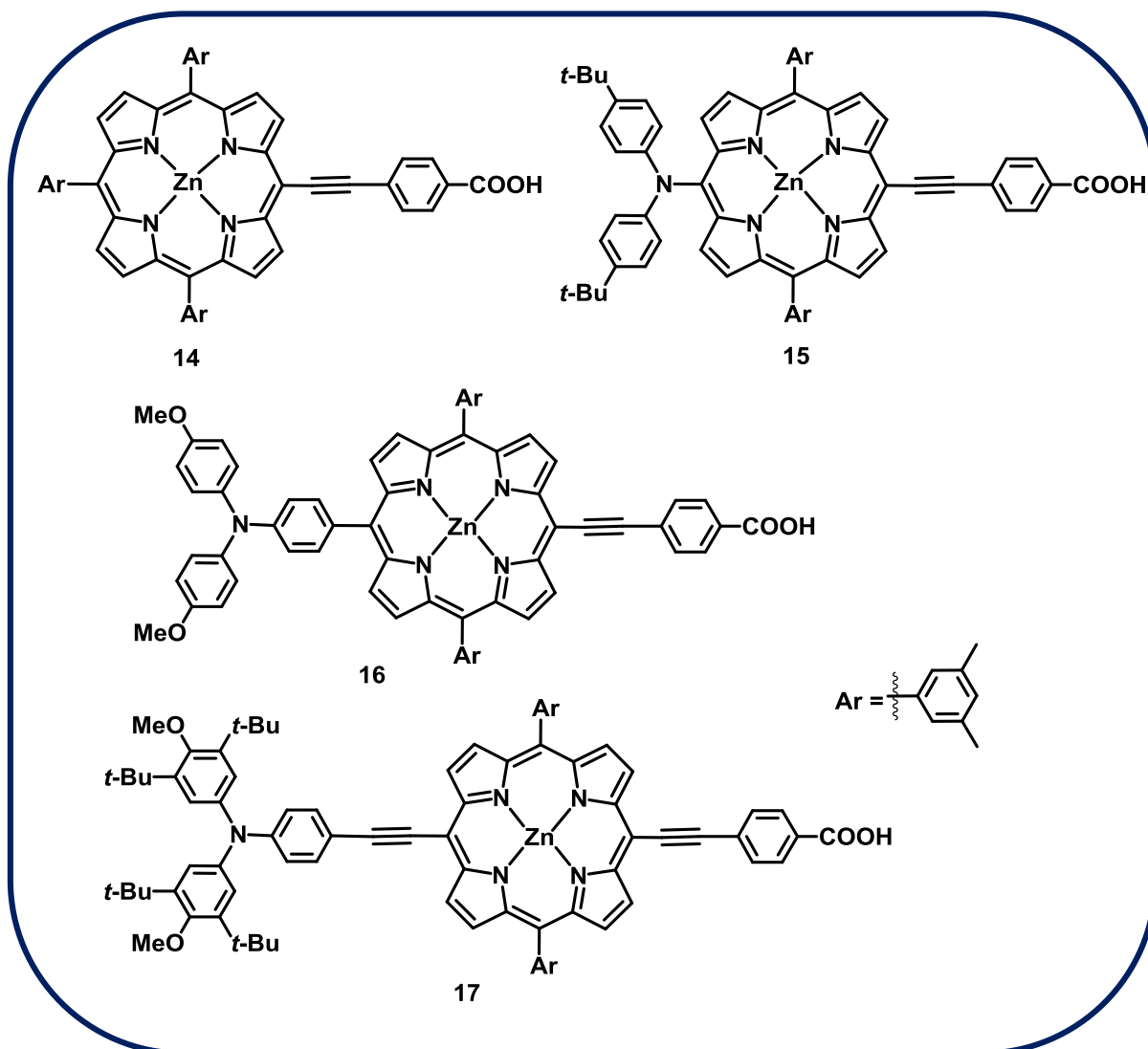
#### 1.3.1.3 Applications of porphyrins:

Porphyrin macrocycles absorb light in the visible region. Thus, porphyrins and metalloporphyrins both display unique photophysical, photoredox, and photochemical properties. Due to these properties, porphyrin and metalloporphyrin have been proven to be very useful in biological and medical applications. Porphyrins and substituted porphyrins have vast applications in different fields due to their unique and versatile properties. The various applications of porphyrins and metalloporphyrins are discussed below.

##### 1.3.1.3.1 as organic solar cells:

To harvest solar energy and to reduce the consumption of non-renewable energy, dye-sensitized solar cells (DSSC) are widely studied for the conversion of solar energy to chemical energy. Porphyrin complexes, **14-17**, are vastly used as sensitizers in dye-sensitized solar cells.<sup>34-36</sup>





**Figure 1.8** Various structures of porphyrin dyes.<sup>37</sup>

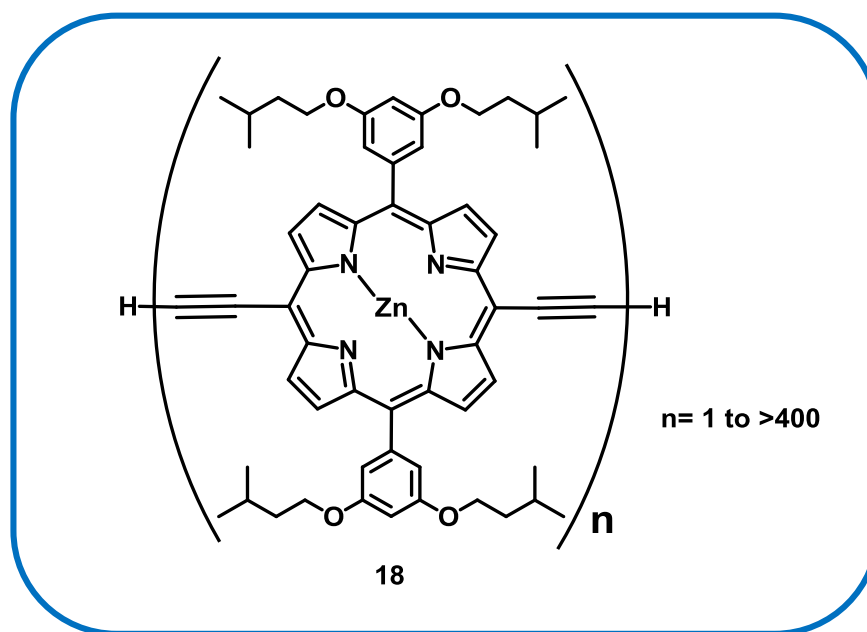
Dye-sensitized solar cells are usually made up of solar cells mimicking the photosynthesis process, which is, converting the solar energy to chemical energy. Porphyrins are significant macrocyclic ligands. In porphyrin derivatives, an intense absorption band is observed in the visible region, which is known as the Soret band, with a high molar extinction coefficient ( $\epsilon > 100,000$ ). Besides the Soret band, a few other weaker characteristic absorption bands are also observed, which are known as the Q-bands. Due to these features, porphyrins are thought to be ideal for dye-sensitized solar cells. Porphyrin derivatives containing different *meso*-, core-, and  $\beta$ -substituents, **14-17**

---

also play a major role in tuning the properties and functionalities as sensitizers in dye-sensitized solar cells (Figure 1.8).<sup>37</sup> In context to this, porphyrin derivatives containing conjugated polymers also show huge potential as optoelectronic devices in solar cells.

#### **1.3.1.3.2 as functional devices:**

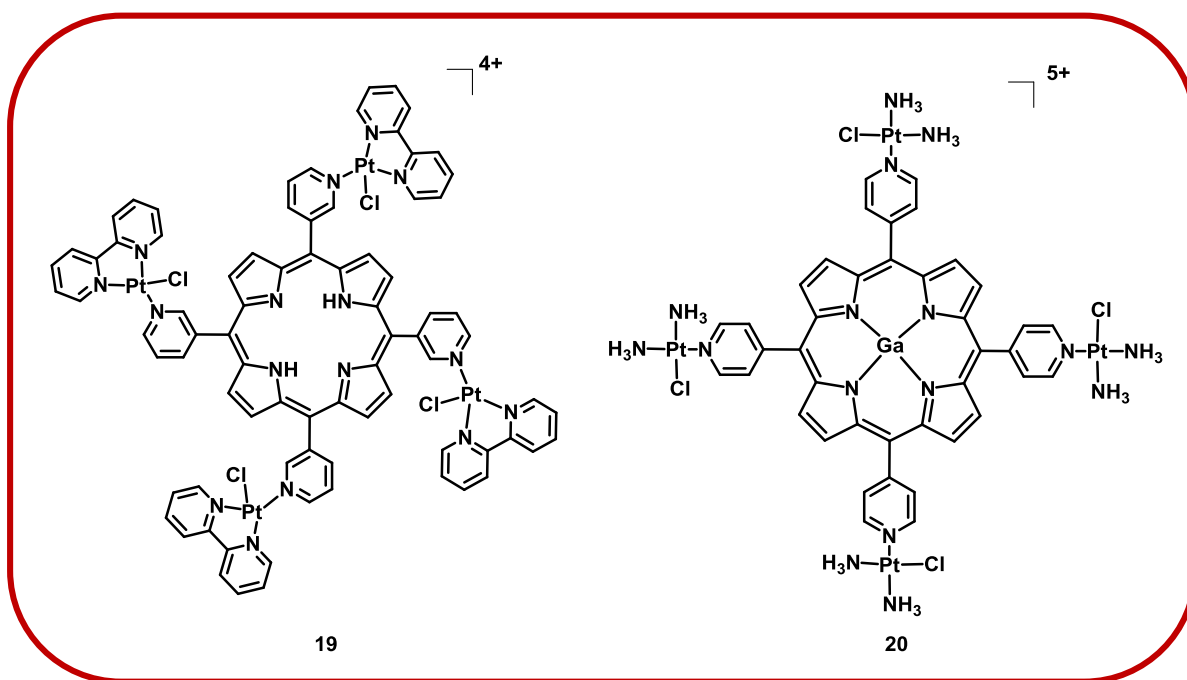
Recently, studies based on molecular functional devices have been a subject of great interest in molecular electronics.<sup>38,39</sup> The unique structures and properties of porphyrin derivatives promote the molecule to be studied as molecular devices. Porphyrin is an aromatic tetrapyrrolic ring system. The four pyrrole rings are connected by four  $sp^2$  hybridized *meso*-carbon atoms. It is a highly conjugated system. The energy gap between the HOMO and LUMO is less in porphyrin derivatives, which helps these types of molecules to perform enhanced electrical properties necessary for molecular wires. The properties of the porphyrin macrocycle can be varied by several means, such as metalation by different metal ions or modification of the substituents.<sup>40-42</sup> Usually, metalloporphyrins are formed by substituting the two protons located in the inner core of the macrocycle with the metal center. The photoelectric behavior can be changed by varying the substituents on *meso*-, core-, and  $\beta$ -positions, thus extending the ring size of the molecule. Thus, the porphyrin macrocycles **18** are the model complexes for the study of molecular devices (Figure 1.9).<sup>43</sup> Recent studies showed the formation and self-assembly of porphyrin molecular wires. A molecular wire is generally a connector that links between an electron donor and an electron acceptor.



**Figure 1.9** Molecular structure of porphyrin wires.<sup>43</sup>

#### 1.3.1.3.3 As porphyrin-based nanoparticles (NPs):

Nanoparticles have the ability to convey various theranostic agents due to their smaller size. Theranostic agents are those drugs that are used for both diagnostics and therapeutics purposes. These nanoparticles are also intensively studied in the field of photodynamic therapy (PDT). Porphyrins and metalloporphyrins have been taken into account as theranostic agents due to their unique size, shape, and properties.<sup>44</sup> Porphyrin, **19**<sup>45</sup> especially metal porphyrins, **20**<sup>46</sup> have shown selectivity towards tumor cell and anti-tumor activity (Figure 1.10). These porphyrin-based inorganic nanoparticles are also fabricated to show activity in the field of photodynamic therapy.



**Figure 1.10** Molecular structure of some porphyrin-based inorganic nanoparticles (NPs).<sup>45,46</sup>

#### 1.3.1.3.4 As porphyrin-based polymers:

Porphyrin-based polymers have huge applications in the field of catalysis, photovoltaic cells, biological and medicinal arena. Polymers that are naturally occurring and synthetically derived have wide applications in the field of photodynamic therapy. Porphyrin-based polymers are recently studied in the application as photosensitizers in the field of photodynamic therapy.<sup>47,48</sup> Metal-organic frameworks (MOFs) containing porphyrin macrocycle are prepared either by incorporating porphyrin derivatives inside the metal-organic frameworks or by utilizing porphyrin derivatives as linkers to generate MOFs. Various studies have been reported on porphyrin-based metal-organic frameworks as potential PDT agents for treating resistant cancers.<sup>47</sup>

#### 1.3.2 Corroles:

Researchers are relentlessly trying to synthesize various macrocyclic systems, which resemble the naturally occurring biologically important macrocycles. Corrole is a

---

tetrapyrrolic macrocyclic system that resembles the central corrin moiety of vitamin B<sub>12</sub>. This term ‘corrole’ was suggested by Johnson and Price because of its resemblance with the central corrin moiety of vitamin B<sub>12</sub>.<sup>49</sup> Corrole was first synthesized by Johnson and Kay in 1965. Corrole has an aromatic 18 $\pi$ -electron system that resembles porphyrin. Therefore, the corrole macrocycle is considered the intermediate between corrin and porphyrin macrocycle. Corroles behave as trianionic ligands, whereas porphyrins are dianionic, and corrin rings are monoanionic in nature. The inner core of the corrole macrocycle is comprised of three amino nitrogen and one imino nitrogen. The corrole macrocycle lacks a *meso*-carbon atom at the C-20 position compared to the porphyrin macrocycle. Due to the absence of the *meso*-carbon atom, corroles have a smaller cavity size than porphyrin, and the symmetry of the corrole macrocycle is also reduced from  $D_{4h}$  to  $C_{2v}$ .

### 1.3.2.1 Characteristic properties of corroles:

Corroles are stable tetrapyrrolic macrocyclic system, and it behaves as trianionic ligand. This property helps to stabilize metal atoms in higher oxidation states. Corrole macrocycle is intensely colored. Free-base corroles display a strong Soret band at ~400-420 nm and Q-bands at ~500-650 nm.<sup>50,51</sup> Corroles usually have a lower molar absorption coefficient than porphyrins, but the molar absorption coefficient of the Q bands is typically higher in corrole in comparison to porphyrins. Corroles are also fluorescent in nature, and it exhibits emission spectra at ~600-700 nm with a lifetime of few nanoseconds.

The <sup>1</sup>H NMR spectra of corroles show interesting features. The *meso*-protons of the corrole moiety generally appear in the deshielding zone. The chemical shift of the *meso*-protons of the corrole macrocycle is usually in the range of 8–9 ppm, and the  $\beta$ -

---

protons appear at ~10 ppm. The aromaticity of the corrole ring is also demonstrated by the diatropic ring current. The three protons located in the inner N4 core of the free-base corrole appear in the upfield region. These protons are shielded due to the ring current. The chemical shift of the imino protons is usually in the range of  $-2$  to  $-3$  ppm.<sup>52</sup> These imino protons generally show a broad singlet.

Corroles are acidic in nature. They are generally more acidic compared to the porphyrin macrocycles. Corroles can easily release the protons located in the inner N4 core of the free-base corrole in the presence of a base and form monoanionic species. And in the presence of an acid, it generates the monoprotonated species.<sup>53</sup> Both the species have been observed to retain their aromaticity.

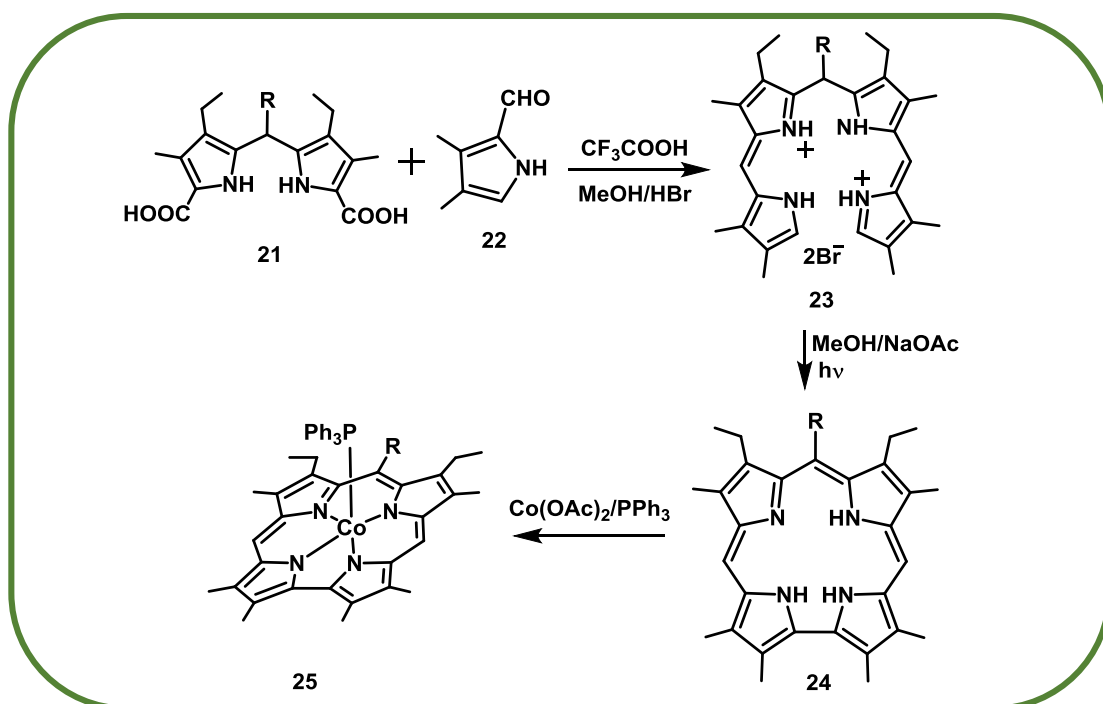
The free-base corrole displays two tautomers that are the same in energy, and both can exist in the same solution.<sup>54,55</sup> Both the tautomers are generally non-planar in geometry. The existence of both the tautomers has been proven by various spectroscopic techniques. 2D NMR spectroscopic experiment of H<sub>3</sub>[TPFPC] proved the presence of one of the tautomers at  $-70$  °C. Whereas the single-crystal X-ray structure of 2,3,7,8,12,13,17,18-octabromo-5,10,15-tris(pentafluorophenyl)-corrole proved the presence of the second tautomer. The first single-crystal X-ray structure of corrole was obtained by Crowfoot Hodgkin *et al.*<sup>56</sup> The single-crystal X-ray structure of 8,12-diethyl-2,3,7,13,17,18-hexamethyl corrole displayed a non-planar geometry. The deviation of this planarity is due to the direct linkage of the C1–C19 bond. While studying the single-crystal X-ray structure of A<sub>3</sub>–corrole, namely, 5,10,15-tris(pentafluorophenyl)corrole, it was observed that out of the three imino protons, only one proton of the inner core resides in the inner core plane, whereas the rest two imino protons reside above and below the inner core plane respectively.<sup>57</sup> This is because of the saddling of pyrrole moiety.

### 1.3.2.2 Synthesis of corroles:

The synthesis of corrole derivatives has gained attention since the first synthesis reported by Johnson and Kay.<sup>50</sup> Since then, various attempts have been made to simplify the synthesis of corrole derivatives and modify their yield. The methodologies involved the synthesis of symmetric as well as asymmetric corrole derivatives.

#### From cyclization of a,c-biladienes:

Johnson and Kay first reported the synthesis of corroles in 1965. The synthetic route is comprised of a photochemical cyclization between a,c-biladienes and sodium acetate or ammonium hydroxide in the presence of methanol.<sup>50</sup> Usually, a,c-biladienes are formed via a condensation reaction between dipyrromethanedicarboxylic acid (1 equivalent), **21** and 2-formylpyrrole (2 equivalents), **22** in the presence of methanol solvent and hydrobromic acid and are obtained as crystalline dihydrobromide salts, **23**. In the presence of cobalt acetate, the free-base corroles, **24**, yield their corresponding cobalt(III) corrole derivative, **25** (Scheme 1.5).

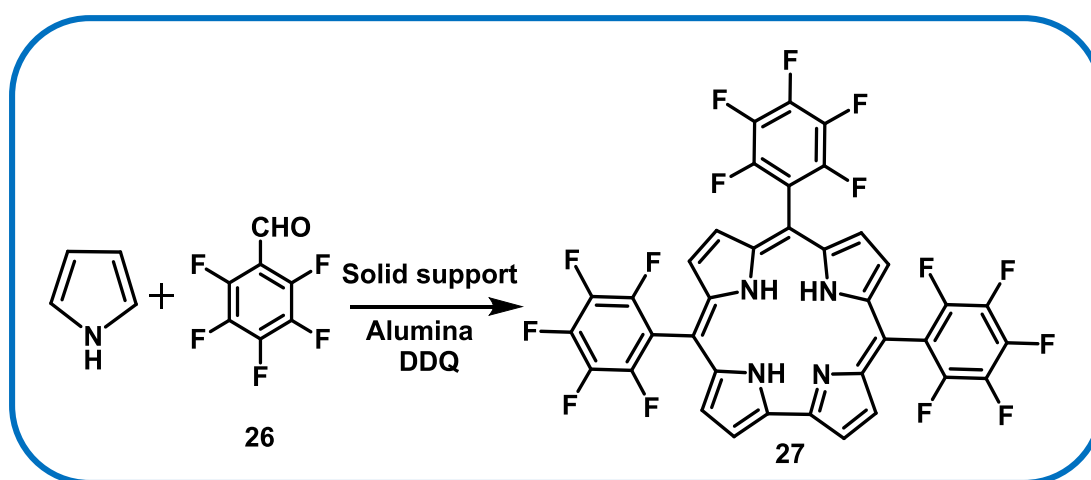


**Scheme 1.5** Synthesis of the free-base corroles from cyclization of a,c-biladienes.<sup>50</sup>

The cobalt(III) corrole derivative was synthesized to inspect the NMR broadening of the free-base corroles.<sup>58</sup> The yield obtained from this synthetic process varied from 20-60%, depending on the nature of the reactants.

#### From condensation of pyrrole and aldehyde without solvent:

Later in 1999, another synthetic methodology was developed by Gross *et al.*<sup>59</sup> They reported the direct synthetic route for 5,10,15-tri(2,3,4,5,6-pentafluorophenyl)corrole, **27**. In this synthetic route, an equimolar amount of 2,3,4,5,6-pentafluorobenzaldehyde, **26**, and pyrrole was taken in the reaction vessel, and the mixture was heated on a solid support at 100°C in aerial condition for 4 hours. Then, this reaction mixture was extracted, followed by the addition of an oxidant (DDQ). The corresponding free-base corrole, **27**, was obtained in 11% yield after separation through column chromatography (Scheme 1.6).



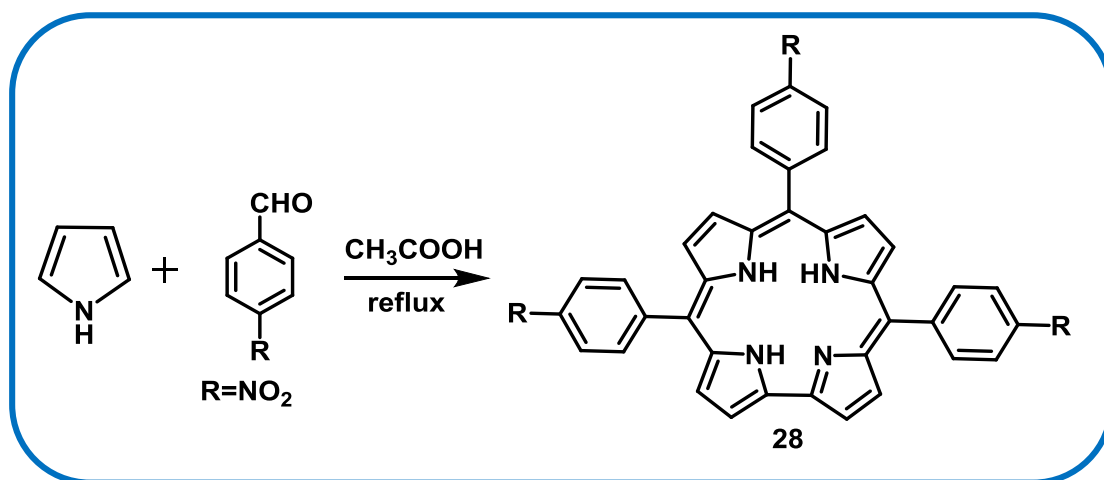
**Scheme 1.6** Synthesis of free-base corroles from pyrrole and pentafluorobenzaldehyde.<sup>59</sup>

#### From condensation of pyrrole and aldehyde in acetic acid:

Another synthetic methodology was developed by Paolesse *et al.*, modifying the Adler-Longo method.<sup>60</sup> In this synthetic route, three equivalents of pyrrole and one equivalent of aldehyde were refluxed in the presence of acetic acid. The corresponding free-base A<sub>3</sub>-corroles, **28**, were obtained in a 9% yield after chromatographic separation



(Scheme 1.7). A certain amount of A<sub>4</sub>-porphyrins was obtained as a side product which was difficult to separate from the desired product. The maximum yield obtained from this synthetic methodology was 22%, using 4-nitrobenzaldehyde as the starting material.<sup>61</sup>

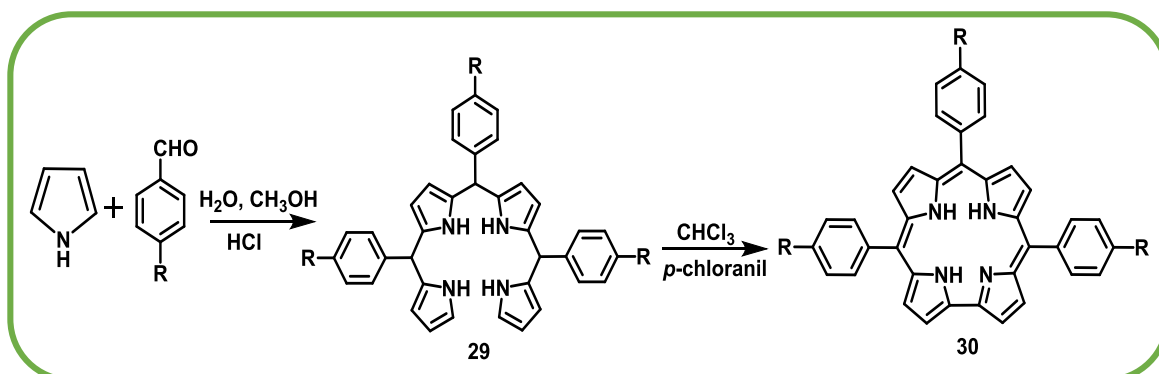


**Scheme 1.7** Synthesis of free-base corroles in acetic acid medium.<sup>60</sup>

#### **From condensation of pyrrole and aldehyde in water-MeOH/HCl medium:**

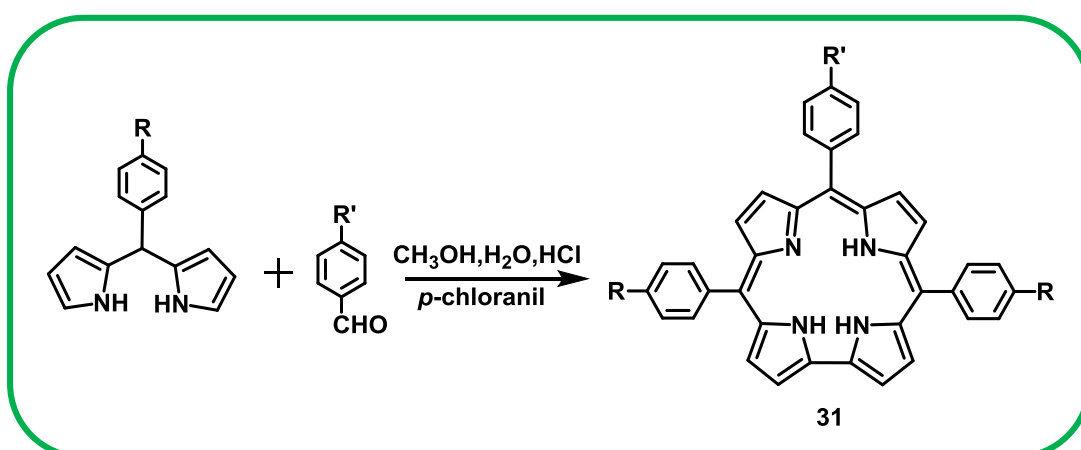
To avoid the definite formation of A<sub>4</sub>-porphyrins along with the desired free-base A<sub>3</sub>-corrole product, Gryko *et al.* developed a new synthetic methodology in 2006.<sup>61</sup> This synthetic methodology was inspired by the synthesis of dipyrromethane developed by Král *et al.*<sup>62</sup> This methodology involves the one-pot two-step synthesis of both *meso*-substituted A<sub>3</sub>-corroles and *trans*-A<sub>2</sub>B corroles with good yields. The major advantage of this synthetic route is a scrambling-free product, and this is one of the most efficient processes for the synthesis of free-base corroles. For the synthesis of A<sub>3</sub>-corroles, aldehyde and pyrrole were taken in a reaction vessel and were dissolved in a water-MeOH (1:1) solution, and subsequently, a concentrated HCl solution was added to this solution. The first step results in the formation of different kinds of oligocondensates such as tetrapyrane, **29**, dipyrromethane, etc. The second step involves the oxidation of

the resulted tetrapyrane with an oxidant (*p*-chloranil). The corresponding A<sub>3</sub>-corroles, **30**, were obtained with ~30% after chromatographic separation (Scheme 1.8).



**Scheme 1.8** Synthesis of free-base A<sub>3</sub>-corroles in water-MeOH/HCl medium.<sup>61</sup>

For the synthesis of A<sub>2</sub>B-corroles, dipyrromethane and aldehyde were taken in a reaction vessel and were dissolved in a water-MeOH (1:1) solution, and subsequently, concentrated HCl solution was added to this solution. After extraction, *p*-chloranil was added to the solution, and the corresponding *trans*-A<sub>2</sub>B corroles, **31**, were derived by performing column chromatography with good yields. The yield obtained for *trans*-A<sub>2</sub>B corrole using sterically unhindered dipyrromethane was ~56%, whereas for hindered dipyrromethane was about 27-31% (Scheme 1.9).<sup>61</sup>



**Scheme 1.9** Synthesis of free-base *trans*-A<sub>2</sub>B-corrole in water-MeOH/HCl medium.<sup>61</sup>

---

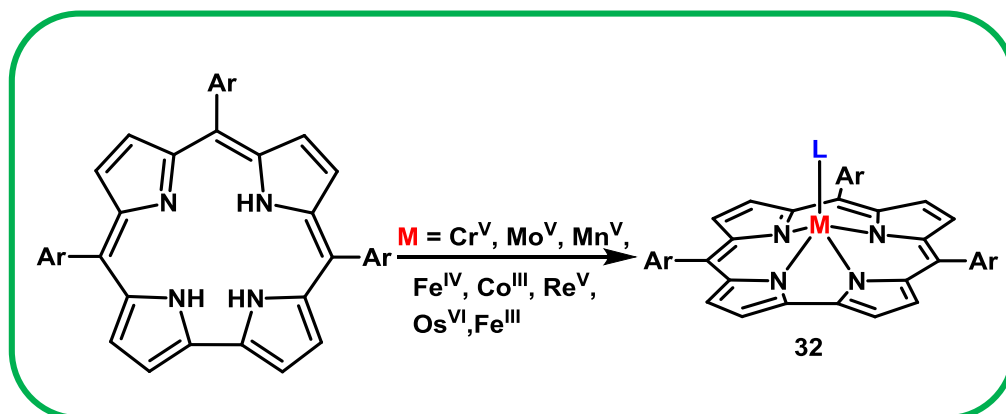
### 1.3.2.3 Metalloporphyrin complexes:

The inner core of the porphyrin macrocycle is comprised of three amino nitrogen and one imino nitrogen. The three NH protons of the inner-core porphyrin macrocycle are highly acidic in nature. These protons can be easily deprotonated, and thus the inner N atoms coordinate with the metal center. The porphyrin macrocycle stabilizes metals with a higher oxidation state. The porphyrin macrocycle is generally metallated by following two procedures, namely, cyclization of metallated tetrapyrrole (bilane) or by the insertion of the metal atom in the cavity.

Various types of metalloporphyrins have been explored throughout the years due to their different kinds of applications in several fields. Primarily, studies on metalloporphyrins were reported by only a few transition metal atoms. But in recent years, metalloporphyrins containing rare transition metals, main group metal atoms, lanthanides, and actinides are also reported. Metalloporphyrins containing the main group element display catalytic activity. They also show photocatalytic activity. This thesis contains the study of the synthesis, characterization, and catalytic activity of antimony porphyrins in various oxidation states.

### 1.3.2.4 Coordination mode of porphyrins:

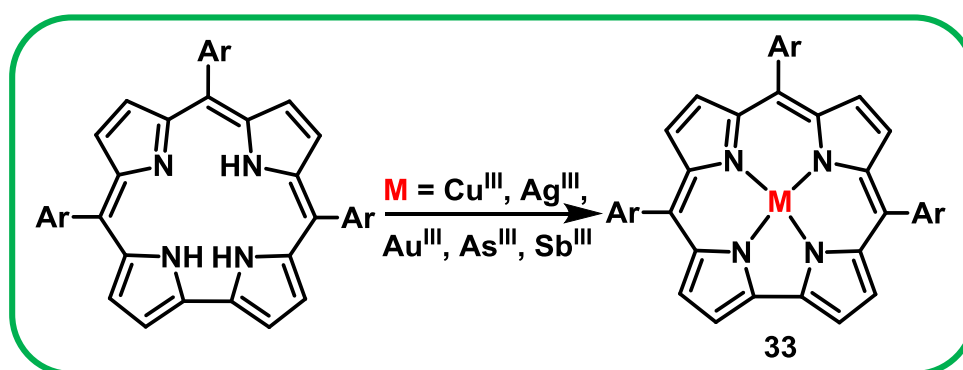
When the porphyrin macrocycle binds with the following transition metal and main group metal atoms, such as Cr(V), Mo(V), Mn(V), Fe, Co, Rh, Ge, Sn, or Pb, it displays square pyramidal geometry around the metal atom, **32** (Figure 1.11).<sup>63</sup> In this geometry, the coordination mode is penta-coordinated. Due to its penta-coordination mode, a domed shape configuration is observed where the metal atom is axially displaced from the plane of the inner core N4 atoms.



**Figure 1.11** Penta-coordinated mode of metallocorroles.<sup>63</sup>

The axial ligands ligated to the metal center in this penta-coordination mode are usually neutral or anionic in nature. The commonly used axial ligands are triphenylphosphine, pyridine or halides (fluoride, chloride, bromide, and iodide), phenyl, methyl, oxo, nitride, and nitrosyl moieties.<sup>64-66</sup>

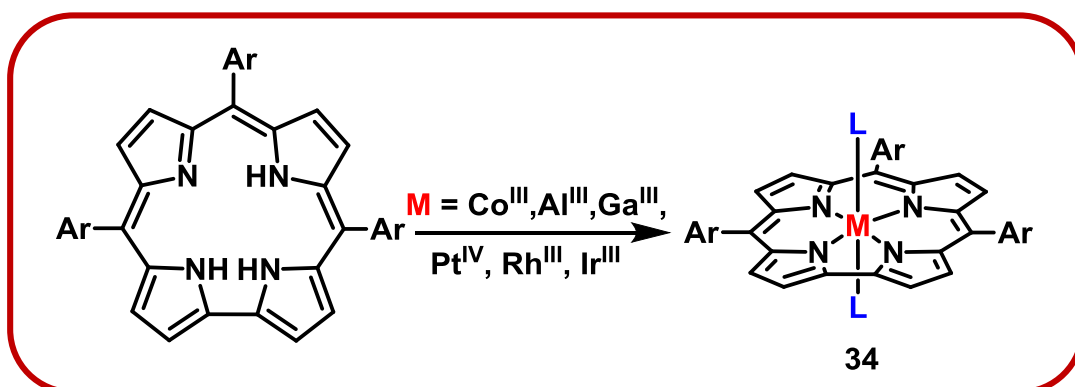
Corroles generally act as trianionic and tetradentate ligands. When the corrole macrocycle binds with the following transition metal and main group metal atoms, such as Cu(3+), Ag(3+), Au(3+), As(3+), Sb(3+), Bi(3+), it displays square planar geometry around the metal atom, **33** (Figure 1.12).<sup>67-70</sup>



**Figure 1.12** Tetra-coordinated mode of metallocorroles.<sup>67-70</sup>

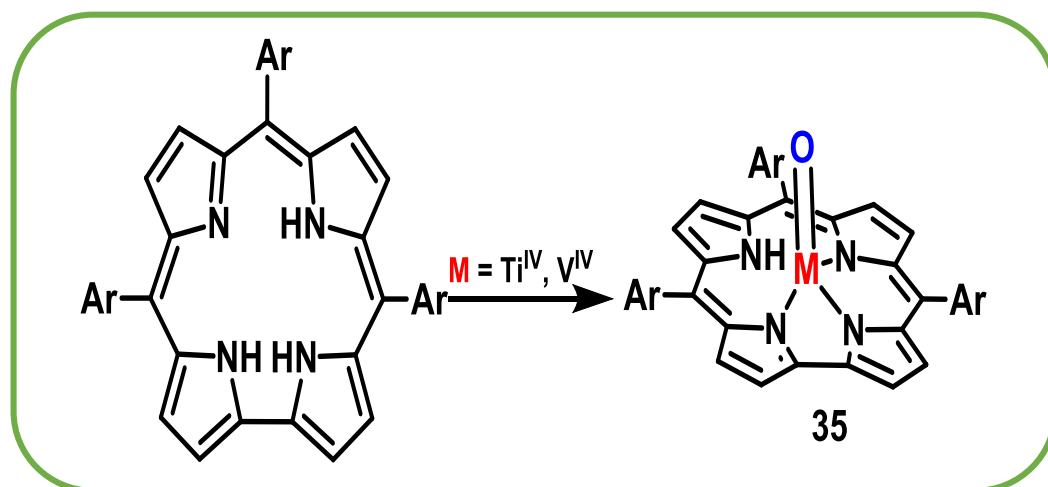
Corroles also display hexa-coordinated complexes, **34** with metal centers such as Al(III), Co(III), Ga(III), and Ir(III) (Figure 1.13).<sup>71-74</sup> In this hexa-coordinated mode, the

geometry around the metal center is octahedral. The commonly ligated axial ligands in these complexes are pyridine or triethylamine.



**Figure 1.13** Hexa-coordinated mode of metallocorroles.<sup>71-74</sup>

Corrole macrocycle also displays di-coordinated complexes and tri-coordinated complexes, **35** with metal atoms such as  $\text{Ti}(4+)$  and  $\text{V}(4+)$  (Figure 1.14).<sup>75</sup> The axially ligated ligand in these complexes is oxide.



**Figure 1.14** Tri-coordinated mode of metallocorroles.<sup>75</sup>

The metallocorrole chemistry is not as vast as the chemistry of metalloporphyrins. Yet certain developments have occurred in recent years.<sup>76</sup> The immense applications of metallocorroles in various fields have encouraged researchers to explore metallocorroles which are air-sensitive and hard to synthesize. No studies on metallocorroles were reported with metals like alkali metals, early transition metals, lanthanides, and actinide

---

elements until 2012, and the studies on metallocorroles with metals like third-row transition metals and heavier metals of the main group elements are hardly reported.<sup>77</sup> Recent studies showed metallocorroles bearing alkali metal (Li),<sup>78</sup> early main group elements, lanthanides (La, Gd, and Tb)<sup>79</sup>, and actinides (Th and U).<sup>79</sup> The metallocorroles have been thoroughly investigated through absorption and emission spectroscopy, mass spectrometer, <sup>1</sup>H NMR spectra, and <sup>13</sup>C NMR spectra, cyclic voltammetry and differential pulse voltammetry, single-crystal X-ray crystallography, etc. Some of the metallocorroles have also been explored via thin-layer spectroelectrochemical analysis. This measurement includes UV-Vis, FT-IR, and EPR spectroscopy. The electro-reduced and electro-oxidized species generated by this spectroelectrochemical equipment *in situ* are helpful in predicting the spectral change of the species upon reduction and oxidation, the position where the electron transfer process occurs, and the reversibility nature of the species.

### 1.3.2.5 Applications of corroles:

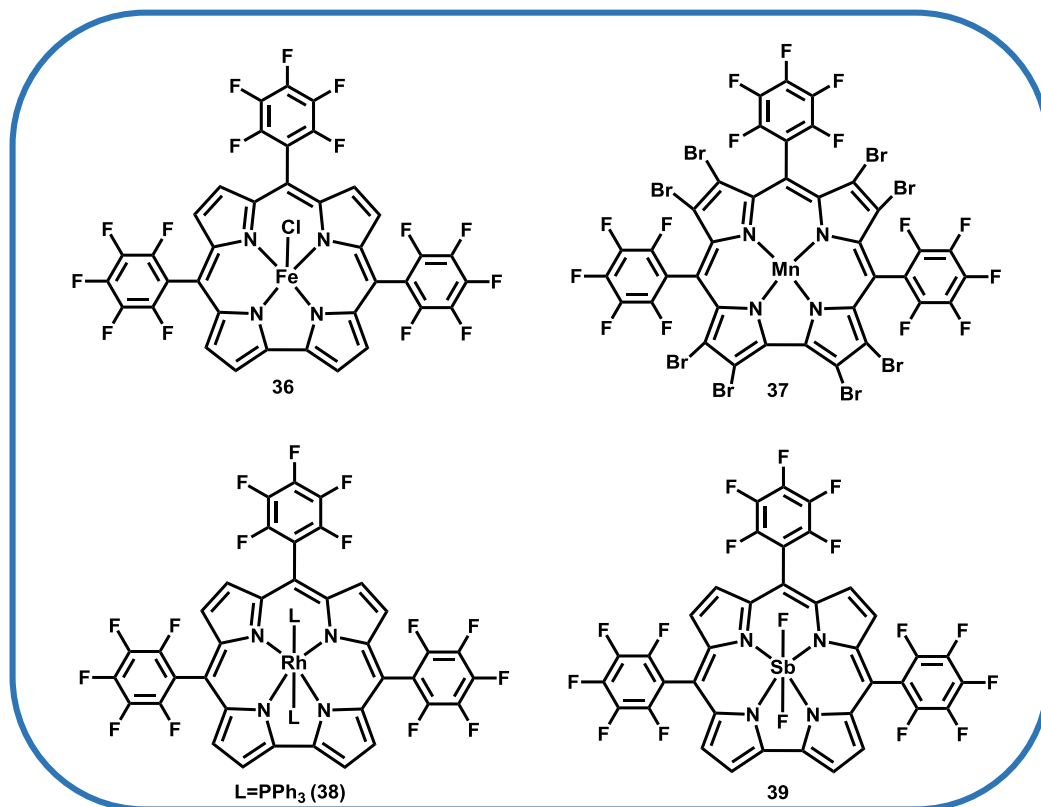
Metallocorroles have broad applications in various fields such as photodynamic therapy, dye-sensitized solar cells, bioimaging, catalysis, etc.<sup>63,80-100</sup> Corroles, bearing similar skeleton structures with the naturally occurring heme-containing enzymes, like Cytochrome P450, can be used as oxidation catalysts. Metallocorroles and other related macrocyclic ligands can also be used for this purpose. The various applications of corroles and metallocorroles are discussed below.

#### 1.3.2.5.1 As Catalysts

Metallocorroles bearing different metal centers show efficient catalytic activities in various reaction conditions (Figure 1.15). Gross *et al.* first reported the usage of iron corroles, Fe(tpfc)Cl, **36** as oxidation catalysts for hydroxylation of alkane compounds

---

and epoxidation of alkenes to their corresponding alcohols, ketones, and epoxides in the presence of iodosobenzene in 1999.<sup>101</sup> When the same catalytic reactions were studied using analogous porphyrin derivatives, it was observed that the porphyrin derivatives obtained better yields for the oxidized products for both the reactions. Manganese(III) corrole, **37** were also used to study the catalytic activity for the oxidation of cyclohexene in the presence of iodosobenzene. In this case, it was observed that the manganese(III) corrole derivatives yielded better results in comparison to their analogous porphyrin derivatives in every aspect, such as reaction time, yield, stability, and turnover frequency.<sup>102,103</sup> Iron corroles and rhodium corrole complexes, **38** are efficient catalysts for cyclopropanation of alkenes in the presence of ethyl diazoacetate.<sup>65,104,105</sup> In 2006, antimony corroles also showed high selectivity and activity as a photocatalytic agent. *Trans*-difluoroantimony(V)corroles, **39** oxidized hydrocarbons to their respective hydroperoxides in the presence of molecular O<sub>2</sub>.<sup>106</sup> Cr(V)-oxo corroles also display efficient catalytic activity.<sup>107</sup> It can easily oxidize small organic molecules such as triphenylphosphine to triphenylphosphine oxide.<sup>108</sup> The Cr<sup>V</sup>oxo/Cr<sup>III</sup> couple is involved in this catalytic process. Metallocorroles show better catalytic activity in the cyclopropanation reaction of olefins in comparison to their analogous metalloporphyrin derivatives.



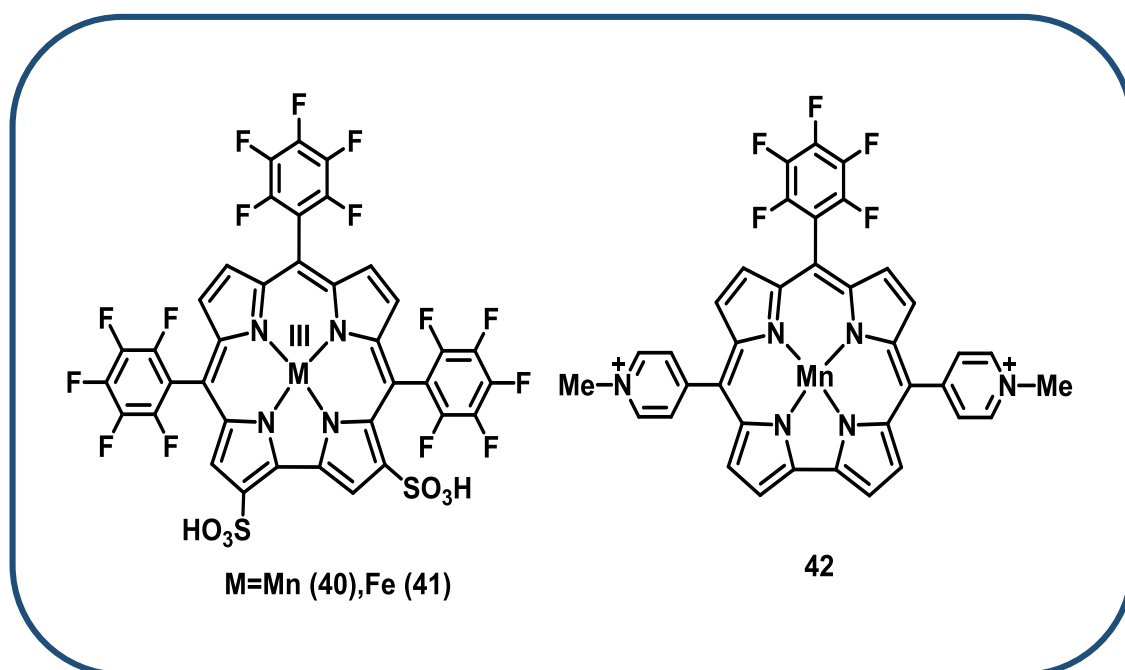
**Figure 1.15** Structures of representative metallocorroles which are used as catalysts.<sup>101-</sup>

106

Metallocorroles work as an efficient catalyst for the decomposition of the reactive oxygen species.<sup>109,110</sup> Hydrogen peroxide and peroxynitrite are among some of the reactive oxygen species. The reactive oxygen species, along with the reactive nitrogen species, give rise to the nitration of biologically important molecules. This phenomenon is also called nitrooxidative stress. Due to this stress, different types of neurodegenerative disorder occurs. In this process, peroxynitrite is formed *in vivo*. The protonated species of the peroxynitrite can easily decompose to harmful radicals. As there is no enzyme to stop this reaction, peroxynitrite specifically is dangerous for biological systems. In this context, it has been found that the Mn(III) corrole complexes, **40** and Fe(III)corrole complexes, **41** have huge applications for this purpose.<sup>110</sup> It was also found that the water-soluble Mn(III) corrole derivatives with *p*-pyridinium substitution, **42**, act as an



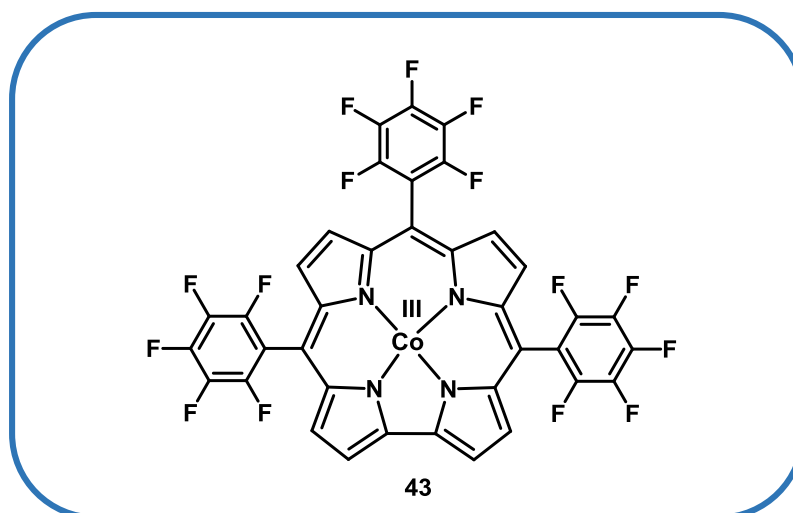
even better catalyst than negatively charged Mn(III) corrole complex in the decomposition of the peroxynitrite species (Figure 1.16).<sup>111</sup>



**Figure 1.16** Structures of metallocorroles that are used for the decomposition of the peroxynitrite species.<sup>110,111</sup>

#### 1.3.2.5.2 As Sensors

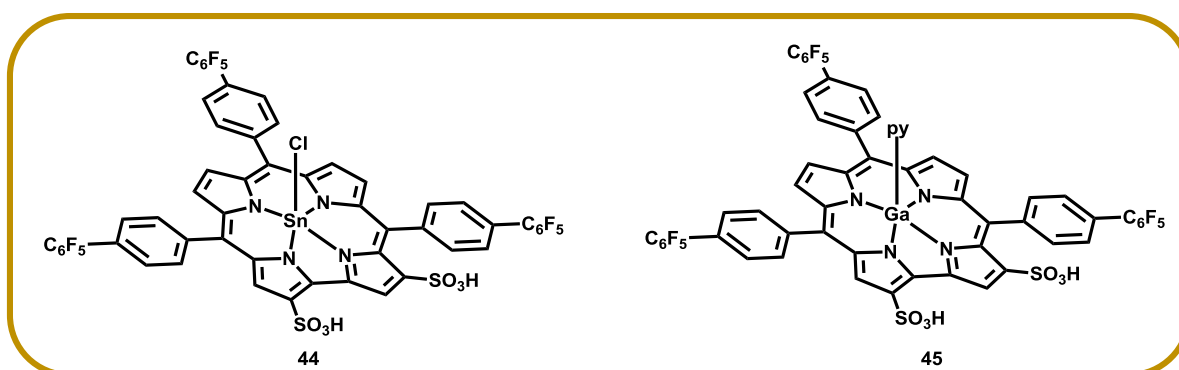
Metallocorroles act as sensors of carbon monoxide gas. It was observed that the cobalt(III) corroles could bind very efficiently and selectively with carbon monoxide vs. oxygen molecule and nitrogen gas (Figure 1.17).<sup>112,113</sup> The study of adsorption properties of CO gas on cobalt(III) corroles, **43** was performed on various cobalt(III) corrole complexes varying the substituents on the *meso*-positions.<sup>114</sup> From this study, it was observed that when the electron density on the central metal atom increases, the affinity towards CO binding decreases.



**Figure 1.17** Structure of a representative cobalt(III) corrole, which is used for CO sensing.<sup>114</sup>

#### 1.3.2.5.3 As Dye Sensitized Solar Cells

To harvest solar energy and to reduce the consumption of non-renewable energy, dye-sensitized solar cells are widely studied for the conversion of solar energy to chemical energy. Ruthenium bipyridine derivatives and different porphyrinoids are widely studied for dye-sensitized solar cells.<sup>115-117</sup> However, ruthenium complexes being expensive, alternative compounds are explored for this purpose. Various porphyrinoid and metalloporphyrinoid complexes also have been studied due to their unique photophysical properties for this purpose.



**Figure 1.18** Structures of metallocorroles that are used as sensitizers in dye-sensitized solar cells.<sup>118</sup>

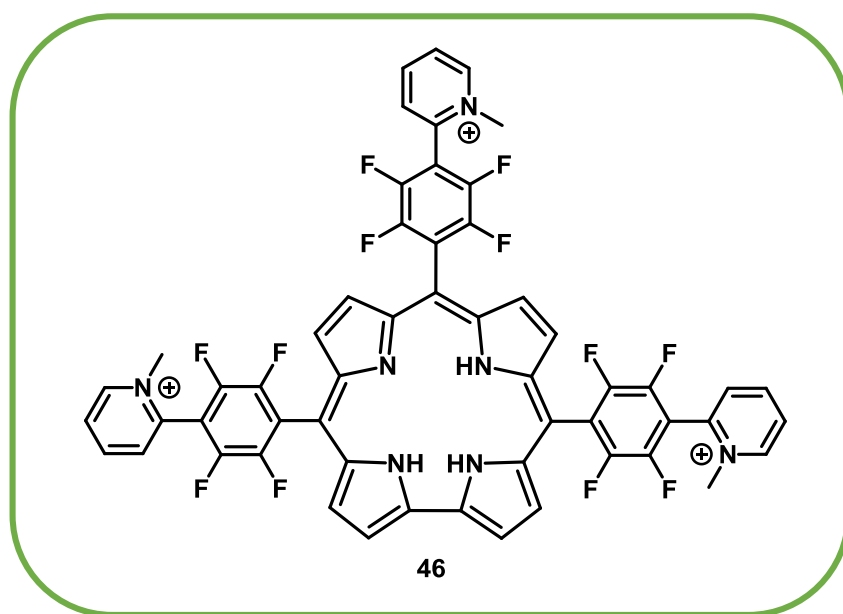
---

To explore the activity of the corrole macrocycles as dye-sensitized solar cells, bisulfonated tris(pentafluorophenyl)corrole and its tin corrole complexes, **44** and gallium corrole complexes, **45** have also been studied (Figure 1.18).<sup>118</sup> The study shows that these complexes bind with the mesoporous material TiO<sub>2</sub> with varying efficiencies.

#### 1.3.2.5.4 As Medicinal drugs:

Water-soluble corroles can be a potent candidate for medicinal drugs. The first water-soluble corrole, **46**, was synthesized by changing the *para*-F atoms of (H<sub>3</sub>)tpfc complex by C-alkylation by pyridine and further N-alkylation (Figure 1.19).<sup>119</sup> The study for the medicinal applications of this water-soluble corrole was performed, and it was observed that this corrole macrocycle showed better results than the porphyrin complexes. The water-soluble corrole showed efficiency in inhibiting endothelial cell proliferation, tumor progression, and metastasis. Iron (III) corroles and manganese (III) corroles have the ability to decompose peroxynitrite, which results in the prevention of harming the low-density lipoproteins and high-density lipoproteins.<sup>120</sup>

Another medicinal application of corrole macrocycles was observed by gallium(III) corrole complexes.<sup>121</sup> Gallium(III) corrole complexes exhibited intense fluorescence, which helped in imaging purposes. Gallium(III) corrole complexes were tested on mice containing human breast cancer tumors.<sup>122</sup> When the Ga-corrole complexes along with the carrier proteins were injected into those mice, the detection of those tumors was done by *in vivo* fluorescence-based imaging. It was also observed that the Ga-corrole complexes were able to suppress the tumor growth without showing side effects. The amount required for the treatment for the suppression of the tumor growth was minimal with respect to doxorubicin (anti-cancer drug). It was also observed that the sulfonated corrole derivatives showed cytotoxicity towards ErbB2-positive breast cancer cells when the compound was delivered via a cell-penetrating protein molecule.<sup>122,</sup>



**Figure 1.19** Structure of the first reported water-soluble corrole, which is applied in *in vivo* medical investigation.<sup>119</sup>

### 1.5 Scope and Objectives of the Present Thesis

In this thesis, several efforts have been made to explore the easiest and cheapest method to synthesize symmetric A<sub>4</sub>-porphyrins from aromatic aldehydes and *trans*-A<sub>2</sub>B<sub>2</sub>-porphyrins from dipyrromethanes using [2+2] synthesis in good yields. Attempts have also been made to synthesize various antimony corrole derivatives having different substituents. And also to characterize the antimony corrole derivatives thoroughly by using various spectroscopic techniques. The catalytic activity of the antimony corroles has also been explored.

#### 1.5.1 Lacunae

1. Metalloporphyrins are a very important class of molecules having a key role in various biological relevant processes. A few of the important biological processes where the metalloporphyrins are relevant include photosynthesis, transport and

---

storage of dioxygen, and various other electron transfer reactions. Thus there is a constant strive to synthesize newer varieties of porphyrin scaffolds in order to mimic the naturally occurring metalloporphyrins. The synthetic approach for the production of artificial porphyrin derivatives has been a major field of attraction since the 1930s. Several synthetic methodologies were reported by various pioneer researchers. But all the methodologies either have harsh reaction conditions, which leads to by-products that are hard to separate, show scrambling, or have narrow substrate scope and occur in a very low concentration (~10 mM) which hinders its industrial-scale applications.

2. Several attempts have been made to study photocatalytic substrate oxidation at room temperature, and it is often observed that the best possible choice is a metal complex bearing a tetrapyrrolic macrocycle as a ligand and a redox-active group 14 or 15 element. A metal-centered (MC) triplet state is responsible for the photocatalytic activity of these low valent groups 14 and 15 (main group) metal complexes. Being a group 15 redox-active element, the most commonly found oxidation states of antimony are +III and +V. High-valent antimony(V)-porphyrin complexes are extensively studied for various applications due to their propensity to attach to a wide variety of axial ligands (*e.g.*, O-, N-, and S-donor ligands). Very limited studies have been carried out on antimony corrole complexes as photocatalysts using a visible light source for organic transformations.
3. Porphyrin, a natural pigment, is present in a large number of metalloenzymes, like, heme, chlorophyll, bacteriochlorophyll, siroheme, heme d<sub>1</sub>, and factor F<sub>430</sub>. Synthetic porphyrinoids and their metallated versions have diverse applications in various areas like oxidation of organic molecules (as catalysts), water splitting reactions (as catalysts), as possible components in molecular electronics, as the dye

---

in dye-sensitized solar cells, in supramolecular chemistry, and also in photodynamic therapy (PDT). Thus, a great deal of research interest is involved in the synthesis of artificial porphyrin. Although numerous synthetic procedures are developed, a careful observation tells us that the choice of reagents and reaction solvents is somewhat limited. The major obstacle involved in the traditional synthetic pathways is that they are most successful in the small (milligram) scale synthesis of porphyrin.

4. Metallo-porphyrinoids constitute the most important class of naturally occurring and also artificially obtained photosensitizers. Metallo-porphyrinoids can also participate in multiple electron transfer reactions due to the involvement of judiciously chosen central metal ions and the equatorially bound porphyrinoid ligands. High valent metalloporphyrinoid complexes bearing  $\text{Sn}^{\text{IV}}$ ,  $\text{Sb}^{\text{V}}$ ,  $\text{As}^{\text{V}}$ , and  $\text{P}^{\text{V}}$  centers have the propensity to bind axial ligands covalently, and they differ largely from their transition metalloporphyrinoid counterparts. The axial ligands can bind and activate a series of substrates. Antimony porphyrinoid complexes are the ideal choice for photocatalytic multiple electron transfer reactions due to their excellent photostability, which arises due to the highly reversible shuttling of  $s^2$ (low valent) to  $s^0$ (high valent) electronic configuration. Although antimony is the main group element, still, Sb-porphyrin complexes can efficiently replace various transition metal complexes in catalytic oxidation reactions and have the propensity to fulfill as a spectroscopic and functional model of the cytochrome P450 family of metalloenzymes. Antimony is an ideal choice for two-electron transfer reactions due to the availability of thermodynamically stable Sb(III) and Sb(V) oxidation states. Although sparsely reported, but still various researchers have discovered intriguing properties of different antimony corrole complexes.

---

### 1.5.2 Objectives

1. To develop an efficient, milder (occurs at RT), cheap (while using aerial oxygen), and environmentally benign synthetic methodology for the facile synthesis of porphyrin (symmetric A<sub>4</sub>–porphyrins and *trans*-A<sub>2</sub>B<sub>2</sub>-Porphyrin) derivatives using manganese templated ring formation reaction as intermediate and which can also be easily scaled up for the gram-scale synthesis without scrambling; and to explore the putative reactive intermediate (Mn–porphyrinogen complex) using a combined analytical, electrochemical, spectroscopic techniques, and DFT studies.
2. To synthesize antimony-corrole complexes, including two corrolato-antimony(III) complexes and two (corrolato)(oxo)antimony(V) complexes, and to characterize all the antimony-corrole complexes using analytical, electrochemical, spectroscopic techniques, and crystallographic studies and to investigate its catalytic activity.
3. To develop the easiest and cheapest method to synthesize symmetric A<sub>4</sub>-porphyrins from aromatic aldehydes and *trans*-A<sub>2</sub>B<sub>2</sub>-porphyrins from dipyrromethanes using [2+2] synthesis in good yields without using any expensive traditional oxidizers like DDQ, chloranil, *etc.*, a large volume of dry chlorinated solvents, and metal salts.
4. To synthesize metallocorrole complexes, which contain *trans*-difluoro-corrolato Sb(V) species along with dinitration of corrole ring, and to fully characterize them via X-ray crystallography, UV-vis, FT-IR, and NMR spectroscopy and to explore the intermediate species, [*trans*-dinitrosyl (corrolato)antimony(V)] compound generated from this synthesis via IR and NMR spectroscopy. And also to investigate the catalytic activity of these [*trans*-difluoro(3,17-dinitro–corrolato)antimony(V)] complexes.

---

## References

1. Battersby, A. R.; Fookes, C.; Matcham, G.; McDonald, E., *Nature*. **1980**, 285, 17-21.
2. Kadish, K. M.; Smith, K. M.; Guillard, R.; Editors, *The Porphyrin Handbook; Volume 2, Heteroporphyrins, Expanded Porphyrins and Related Macrocycles*. Academic Press: **2000**.
3. Berg, J. M.; Lippard, S., *Principles of bioinorganic chemistry*. Mill Valley, 411s.ed. ; University Science Books: **1994**.
4. Borbas, K. E., in *Handbook of Porphyrin Science: With Applications to Chemistry, Physics, Materials Science, Engineering, Biology and Medicine—Volume 36: BODIPYs and Chlorins: Powerful Related Porphyrin Fluorophores*, World Scientific, **2016**, 1-149.
5. Scott, A. I. *Accounts of Chemical Research* **1978**, 11, 1, 29-36.
6. Bonnett, R., *Chem. Rev.* **1963**, 63, 573-605.
7. Hodgkin, D. C.; Kamper, J.; Lindsey, J.; MacKay, M.; Pickworth, J.; Robertson, J.; Shoemaker, C. B.; White, J.; Prosen, R.; Trueblood, K., *Proc. R. Soc. Lond. A* **1957**, 242, 228-263.
8. Johnson, A.; Todd, A., *Vitam. Horm.* **1957**, 15, 1.
9. Sessler, J. L.; Weghorn, S. J., *Expanded, contracted & isomeric porphyrins*. Elsevier: **1997**, 15.
10. Franck, B.; Nonn, A., *Angew. Chem. Int. Ed.* **1995**, 34, 1795-1811.



- 
11. Kadish, K. M.; Smith, K. M.; Guillard, R.; Editors, *The Porphyrin Handbook; Volume 1, Synthesis and Organic Chemistry*. Academic Press: **2000**.
  12. Lai, D.; Khan, F. S. T.; Rath, S. P., *Dalton Trans.* **2018**, 47, 14388-14401.
  13. Mondal, P.; Rath, S. P., *Coord. Chem. Rev.* **2020**, 405, 213117.
  14. Guchhait, T.; Sarkar, S.; Pandit, Y. A.; Rath, S. P., *Chem. Eur. J.* **2017**, 23, 10270-10275.
  15. Yedukondalu, M.; Ravikanth, M., *Coord. Chem. Rev.* **2011**, 255, 547-573.
  16. Gupta, I.; Hung, C. H.; Ravikanth, M., *European Journal of Organic Chemistry*, **2003**, 2003, 4392-4400.
  17. Alka, A.; Shetti, V. S.; Ravikanth, M., *Dalton Trans.* **2019**, 48, 4444-4459.
  18. Misra, R.; Chandrashekar, T. K., *Acc. Chem. Res.* **2008**, 41, 265-279.
  19. Rath, H.; Sankar, J.; PrabhuRaja, V.; Chandrashekar, T. K.; Nag, A.; Goswami, D., *J. Am. Chem. Soc.* **2005**, 127, 11608-11609.
  20. Chandrashekar, T.; Prabhuraja, V.; Gokulnath, S.; Sabarinathan R.; Srinivasan, A.; *Chem. Commun.* **2010**, 46, 5915-5917.
  21. Groves, J. T., *J. Inorg. Biochem.* **2006**, 100, 434-447.
  22. Meunier, B., *Chem. Rev.* **1992**, 92, 1411-1456.
  23. Sessler, J. L.; Burrell, A. K., in *Macrocycles*, Springer, **1992**, 177-273
  24. Küster, W.; Hoppe-Seyler's *Z. Physiol. Chem.* **1912**, 82, 463.
  25. Weiss, C., *J. Mol. Spectrosc.* **1972**, 44, 37-80.
  26. Soret, J.-L., *Compt. Rend.* **1883**, 97, 1269-1273.
  27. Senge, M. O.; Smith, K. M., *Photochem. Photobiol.* **1991**, 54, 841-846.
-

- 
28. Smith, K. M.; Goff, D. A.; Abraham, R. J., *Org. Magn. Resonance* **1984**, 22, 779-783.
29. Fischer H.; Gleim W., *Justus Liebigs Ann. Chem.* **1936**, 521, 157-160.
30. Rothmund, P., *J. Am. Chem. Soc.* **1936**, 58, 625-627.
31. Adler, A. D.; Longo, F. R.; Finarelli, J. D.; Goldmacher, J.; Assour, J.; Korsakoff, L., *J. Org. Chem.* **1967**, 32, 476-476.
32. Geier III, G. R.; Lindsey, J. S., *J. Chem. Soc., Perkin Trans 2* **2001**, 677-686.
33. Littler, B. J.; Ciringh, Y.; Lindsey, J. S., *J. Org. Chem.* **1999**, 64, 2864-2872.
34. Cárdenas-Jirón, G.; Borges-Martínez, M.; Mera-Adasme, R.; Pino-Rios, R. *Int. J. Quantum Chem.* **2019**, 119, 25821.
35. Lu, Y.; Liu, Q.; Luo, J.; Wang, B.; Feng, T.; Zhou, X.; Liu, X.; Xie, Y. *ChemSusChem* **2019**, 12, 2802-2809.
36. Zeng, K.; Chen, Y.; Zhu, W.-H.; Tian, H.; Xie, Y. *J. Am. Chem. Soc.* **2020**, 142, 5154-5161.
37. Hsieh, C.-P.; Lu, H.-P.; Chiu, C.-L.; Lee, C.-W.; Chuang, S.-H.; Mai, C.-L.; Yen, W.-N.; Hsu, S.-J.; Diao, E. W.-G.; Yeh, C.-Y. *J. Mater. Chem.* **2010**, 20, 1127-1134.
38. Barigelletti, F.; Flamigni, L. *Chem. Soc. Rev.* **2000**, 29, 1-12.
39. Robertson, N.; McGowan, C. A. *Chem. Soc. Rev.* **2003**, 32, 96-103.
40. Collman, J. P.; McDevitt, J. T.; Yee, G. T.; Zisk, M. B.; Torrance, J. B.; Little, W. *A. Synthetic metals* **1986**, 15, 129-140.
-

- 
41. Sandanayaka, A. S.; Araki, Y.; Wada, T.; Hasobe, T. *J. Phys. Chem. C* **2008**, *112*, 19209-19216.
  42. Danger, B. R.; Bedient, K.; Maiti, M.; Burgess, I. J.; Steer, R. P. *J. Phys. Chem. A* **2010**, *114*, 10960-10968.
  43. Kawao, M.; Ozawa, H.; Tanaka, H.; Ogawa, T. *Thin Solid Films* **2006**, *499*, (1-2), 23-28.
  44. Lovejoy, K. S.; Lippard, S. J. *Dalton Trans.* **2009**, (48), 10651-10659.
  45. Shi, Y.; Zhang, F.; Linhardt, R. J. *Dyes and Pigments* **2021**, 109136.
  46. Hu, X.; Ogawa, K.; Kiwada, T.; Odani, A. *J. Inorg. Biochem.* **2017**, *170*, 1-7.
  47. K. Lu, C. He and W. Lin, *J. Am. Chem. Soc.* **2014**, *136*, 16712-16715.
  48. Chen, Y. Zhu and S. Kaskel, *Angew. Chem. Int. Ed.* **2021**, *60*, 5010-5035.
  49. Johnson, A.; Price, R., *J. Chem. Soc.* **1960**, 1649-1653.
  50. Johnson, A.; Kay, I., *J. Chem. Soc.* **1965**, 1620-1629.
  51. Paolesse, R.; Sagone, F.; Macagnano, A.; Boschi, T.; Prodi, L.; Montalti, M.; Zaccheroni, N.; Bolletta, F.; Smith, K. M., *J. Porphyr. Phthalocyanines* **1999**, *3*, 364-370.
  52. Balazs, Y. S.; Saltsman, I.; Mahammed, A.; Tkachenko, E.; Golubkov, G.; Levine, J.; Gross, Z., *Magn. Reson. Chem.* **2004**, *42*, 624-635.
  53. Broadhurst, M. J.; Grigg, R.; Shelton, G.; Johnson, A. W., *J. Chem. Soc., Perkin Trans. I* **1972**, 143-151.
  54. Dyke, J.; Hush, N.; Williams, M.; Woolsey, I., *Mol. Phys.* **1971**, *20*, 1149-1152.
  55. Ghosh, A.; Jynge, K., *Chem. Eur. J.* **1997**, *3*, 823-833.
-

- 
56. Harrison, H. R.; Hodder, O. J. R.; Hodgkin, D. C., *J. Chem. Soc. B* **1971**, 640.
57. Gross, Z.; Galili, N.; Simkhovich, L.; Saltsman, I.; Botoshansky, M.; Blaeser, D.; Boese, R.; Goldberg, I., *Org. Lett.* **1999**, *1*, 599-602.
58. Paolesse, R.; Pandey, R. K.; Forsyth, T. P.; Jaquinod, L.; Gerzevske, K. R.; Nurco, D. J.; Senge, M. O.; Licoccia, S.; Boschi, T.; Smith, K. M., *J. Am. Chem. Soc.* **1996**, *118*, 3869-3882.
59. Z. Gross, N. Galili, L. Simkhovich, I. Saltsman, M. Botoshnsky, D. Blaser, R. Boese and I. Goldberg, *Org. Lett.*, **1999**, *1*, 599.
60. R. Paolesse, L. Jaquinod, D. J. Nurco, S. Mini, F. Sagone, T. Boschi and K. M. Smith, *Chem. Commun.* **1999**, 1307–1308.
61. R. Orłowski, D. Gryko and D. T. Gryko, *Chem. Rev.*, **2017**, *117*, 3102–3137.
62. V. Král, P. Vašek and B. Dolensky, *Collect. Czech. Chem. Commun.*, **2004**, *69*, 1126-1136.
63. Aviv-Harel, I.; Gross, Z., *Chem. Eur. J.* **2009**, *15*, 8382-94.
64. Gross, Z., *J. Biol. Inorg. Chem.* **2001**, *6*, 733-738.
65. Simkhovich, L.; Mahammed, A.; Goldberg, I.; Gross, Z., *Chem. Eur. J.* **2001**, *7*, 1041-55.
66. Sinha, W.; Deibel, N.; Agarwala, H.; Garai, A.; Schweinfurth, D.; Purohit, C.S.; Lahiri, G. K.; Sarkar, B.; Kar, S., *Inorg. Chem.* **2014**, *53*, 1417-1429.
67. Will, S.; Lex, J.; Vogel, E.; Schmickler, H.; Gisselbrecht, J.-P.; Haubtmann, C.; Bernard, M.; Gorss, M., *Angew. Chem. Int. Ed. Engl.* **1997**, *36*, 357-361.
68. Kadish, K. M.; Erben, C.; Ou, Z.; Adamian, V. A.; Will, S.; Vogel, E., *Inorg. Chem.* **2000**, *39*, 3312-3319.
-

- 
69. Thomas, K. E.; Alemayehu, A. B.; Conradie, J.; Beavers, C.; Ghosh, A., *Inorg. Chem.* **2011**, *50*, 12844-12851.
70. Brückner, C.; Barta, C. A.; Brinas, R. P.; Krause Bauer, J. A., *Inorg. Chem.* **2003**, *42*, 1673-1680.
71. Palmer, J. H.; Day, M. W.; Wilson, A. D.; Henling, L. M.; Gross, Z.; Gray, H. B., *J. Am. Chem. Soc.* **2008**, *130*, 7786-7787.
72. Mahammed, A.; Giladi, I.; Goldberg, I.; Gross, Z., *Chem. Eur. J.* **2001**, *7*, 4259-65.
73. Bendix, J.; Dmochowski, I. J.; Gray, H. B.; Mahammed, A.; Simkhovich, L.; Gross, Z., *Angew. Chem. Int. Ed.* **2000**, *39*, 4048-4051.
74. Mahammed, A.; Gross, Z., *J. Inorg. Biochem.* **2002**, *88*, 305-309.
75. Licoccia, S.; Paolesse, R.; Tassoni, E.; Polizio, F.; Boschi, T., *J. Chem. Soc., Dalton Trans.* **1995**, 3617-21.
76. Buckley, H. L.; Arnold, J., *Dalton Trans.* **2015**, *44*, 30-6.
77. Aviv-Harel, I.; Gross, Z., *Coord. Chem. Rev.* **2011**, *255*, 717-736.
78. Buckley, H. L.; Chomitz, W. A.; Koszarna, B.; Tasior, M.; Gryko, D. T.; Brothers, P. J.; Arnold, J., *Chem. Commun.* **2012**, *48*, 10766-10768.
79. Ward, A. L.; Buckley, H. L.; Lukens, W. W.; Arnold, J., *J. Am. Chem. Soc.* **2013**, *135*, 13965-13971.
80. Aviv, I.; Gross, Z., *Chem. Commun.* **2007**, 1987.
81. Sujesh, S.; Basumatary, B.; Kumar, A.; Sankar, J., *Eur. J. Inorg. Chem.* **2021**, *2021*, 540-547.
-

- 
82. Basumatary, B.; Rai, J.; Reddy, R. R.; Sankar, J., *Chem. Eur. J.* **2017**, *23*, 17458-17462.
83. Mondal, B.; Chattopadhyay, S.; Dey, S.; Mahammed, A.; Mittra, K.; Rana, A.; Gross, Z.; Dey, A., *J. Am. Chem. Soc.* **2020**, *142*, 21040-21049.
84. Srikanth, M.; Sastry, G. N.; Soujanya, Y., *Int. J. Quantum Chem.* **2015**, *115*, 745-752.
85. De, R.; Gonglach, S.; Paul, S.; Haas, M.; Sreejith, S.; Gerschel, P.; Apfel, U. P.; Vuong, T. H.; Rabeah, J.; Roy, S., *Angew. Chem.* **2020**, *132*, 10614-10621.
86. Sudhakar, K.; Giribabu, L.; Salvatori, P.; Angelis, F. D., *physica status solidi (a)*, **2015**, *212*, 194-202.
87. Gonglach, S.; Paul, S.; Haas, M.; Pillwein, F.; Sreejith, S. S.; Barman, S.; De, R.; Müllegger, S.; Gerschel, P.; Apfel, U.-P., *Nat. Commun.* **2019**, *10*, 1-10.
88. Sudhakar, K.; Gokulnath, S.; Giribabu, L.; Lim, G. N.; Trâm, T.; D'Souza, F., *Chem. Asian J.* **2015**, *10*, 2708-2719.
89. Mahammed, A.; Mondal, B.; Rana, A.; Dey, A.; Gross, Z., *Chem. Commun.* **2014**, *50*, 2725-2727.
90. Mondal, S.; Naik, P. K.; Adha, J. K.; Kar, S. *Coord. Chem. Rev.* **2019**, *400*, 213043.
91. Balsukuri, N.; Das, S.; Gupta, I., *New J. Chem.* **2015**, *39*, 482-491.
92. Bose, S.; Pariyar, A.; Biswas, A. N.; Das, P.; Bandyopadhyay, P., *Catal. Commun.* **2011**, *12*, 1193-1197.
93. Giribabu, L.; Kandhadi, J.; Kanaparthi, R. K., *J. Fluoresc.* **2014**, *24*, 569-577.
-

- 
94. Sankar, J.; Rath, H.; Prabhuraja, V.; Gokulnath, S.; Chandrashekar, T. K.; Purohit, C. S.; Verma, S., *Chem. Eur. J.* **2007**, *13*, 105-114.
95. Adinarayana, B.; Thomas, A. P.; Yadav, P.; Kumar, A.; Srinivasan, A., *Angew. Chem.* **2016**, *128*, 981-985.
96. Mondal, B.; Sengupta, K.; Rana, A.; Mahammed, A.; Botoshansky, M.; Dey, S. G.; Gross, Z.; Dey, A., *Inorg. Chem.* **2013**, *52*, 3381-3387.
97. Mishra, R.; Basumatary, B.; Singhal, R.; Sharma, G. D.; Sankar, J., *ACS Appl. Mater. Interfaces* **2018**, *10*, 31462-31471.
98. Ghosh, A., *Chem. Rev.* **2017**, *117*, 3798-3881.
99. Anusha, P.; Swain, D.; Hamad, S.; Giribabu, L.; Prashant, T. S.; Tewari, S. P.; Rao, S. V., *J. Phys. Chem. C*, **2012**, *116*, 17828-17837.
100. Yadav, I.; Dhiman, D.; Sankar, M., *J. Porphyr. Phthalocyanines* **2021**, *25*, 547-554.
101. Gross, Z.; Simkhovich, L.; Galili, N., *Chem. Commun.* **1999**, 599-600.
102. Golubkov, G.; Bendix, J.; Gray, H. B.; Mahammed, A.; Goldberg, I.; DiBilio, A. J.; Gross, Z., *Angew. Chem. Int. Ed. Engl.* **2001**, *40*, 2132-2134.
103. Liu, H. Y.; Lai, T. S.; Yeung, L. L.; Chang, C. K., *Org. Lett.* **2003**, *5*, 617-20.
104. L. Simkhovich, I. Goldberg and Z. Gross, *J. Porphyrins Phthalocyanines*, **2002**, *6*, 439-444.
105. I. Aviv and Z. Gross, *Synlett*, 2006, **2006**, 951-953.
106. Luobeznova, I.; Raizman, M.; Goldberg, I.; Gross, Z., *Inorg. Chem.* **2006**, *45*, 386-94.
-

- 
107. Meier-Callahan, A. E.; Di Bilio, A. J.; Simkhovich, L.; Mahammed, A.; Goldberg, I.; Gray, H. B.; Gross, Z., *Inorg. Chem.* **2001**, *40*, 6788-93.
108. A. Mahammed, H. B. Gray, A. E. Meier-Callahan and Z. Gross, *J. Am. Chem. Soc.*, **2003**, *125*, 1162-1163.
109. Mahammed, A.; Gross, Z., *J. Am. Chem. Soc.* **2005**, *127*, 2883-7.
110. Mahammed, A.; Gross, Z., *Angew. Chem. Int. Ed. Engl.* **2006**, *45*, 6544-7.
111. Gershman, Z.; Goldberg, I.; Gross, Z., *Angew. Chem. Int. Ed. Engl.* **2007**, *46*, 4320-4.
112. Guillard, R.; Gros, C. P.; Bolze, F.; Jerome, F.; Ou, Z.; Shao, J.; Fischer, J.; Weiss, R.; Kadish, K. M., *Inorg. Chem.* **2001**, *40*, 4845-55.
113. Kadish, K. M.; Ou, Z.; Shao, J.; Gros, C. P.; Barbe, J. M.; Jerome, F.; Bolze, F.; Burdet, F.; Guillard, R., *Inorg. Chem.* **2002**, *41*, 3990-4005.
114. Barbe, J. M.; Canard, G.; Brandes, S.; Jerome, F.; Dubois, G.; Guillard, R., *Dalton Trans.* **2004**, 1208-14.
115. Campbell, W. M.; Burrell, A. K.; Officer, D. L.; Jolley, K. W., *Coord. Chem. Rev.* **2004**, *248*, 1363-1379.
116. Wang, Q.; Campbell, W. M.; Bonfantani, E. E.; Jolley, K. W.; Officer, D. L.; Walsh, P. J.; Gordon, K.; Humphry-Baker, R.; Nazeeruddin, M. K.; Gratzel, M., *J. Phys. Chem. B* **2005**, *109*, 15397-409.
117. Urbani, M.; Gratzel, M.; Nazeeruddin, M. K.; Torres, T., *Chem. Rev.* **2014**, *114*, 12330-96.
118. Walker, D.; Chappel, S.; Mahammed, A.; Brunschwig, B. S.; Winkler, J. R.; Gray, H. B.; Zaban, A.; Gross, Z., *J. Porphyr. Phthalocyanines* **2006**, *10*, 1259-1262.
-



- 
119. Gershman Z. I. Goldberg, Z. Gross., *Angew. Chem.* **2007**, *119*, 4398.
120. Haber, A.; Mahammed, A.; Fuhrman, B.; Volkova, N.; Coleman, R.; Hayek, T.; Aviram, M.; Gross, Z., *Angew. Chem. Int. Ed. Engl.* **2008**, *47*, 7896-900.
121. Agadjanian, H.; Ma, J.; Rentsendorj, A.; Valluripalli, V.; Hwang, J. Y.; Mahammed, A.; Farkas, D. L.; Gray, H. B.; Gross, Z.; Medina-Kauwe, L. K., *Proc. Natl. Acad. Sci. U. S. A.* **2009**, *106*, 6105-10.
122. Agadjanian, H.; Weaver, J. J.; Mahammed, A.; Rentsendorj, A.; Bass, S.; Kim, J.; Dmochowski, I. J.; Margalit, R.; Gray, H. B.; Gross, Z.; Medina-Kauwe, L. K., *Pharm. Res.* **2006**, *23*, 367-77.

# CHAPTER 2

---

## A new synthesis of porphyrin via a putative *trans*-manganese(IV)-dihydroxide intermediate

---

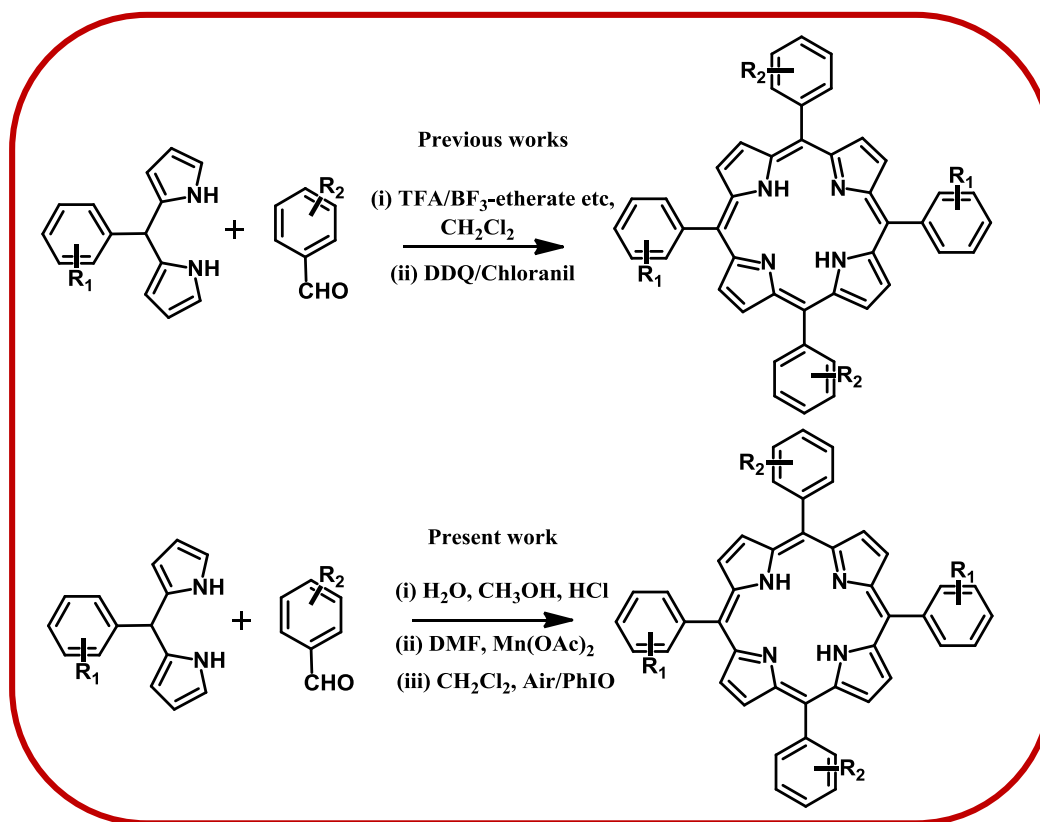
- 2.1 Introduction
- 2.2 Results and discussion
  - 2.2.1 Synthesis and Characterization
  - 2.2.2 TD-DFT Calculations
- 2.3 Conclusions
- 2.4 Experimental section
  - 2.4.1 Materials
  - 2.4.2 Characterization
  - 2.4.3 Computational Method
  - 2.4.4 Syntheses
    - 2.4.4.1 Synthesis of *trans*-A<sub>2</sub>B<sub>2</sub>-porphyrins, **1-7**
    - 2.4.4.2 Synthesis of 5,15-Bis(4-cyanophenyl)-10,20-diphenylporphyrin, **5**
    - 2.4.4.3 Synthesis of 5,10,15,20-Tetraphenylporphyrin, **8**
    - 2.4.4.4 Synthesis of 5,10,15,20-Tetrakis(4-methoxyphenyl)porphyrin, **9**
    - 2.4.4.5 Synthesis of Mn(IV)- porphyrinogen derivative, **7-Mn**
    - 2.4.4.6 Synthesis of 5,15-bis(4-cyanophenyl)-10-(pentafluorophenyl)tetrapyrane

---

## 2.1 Introduction

Metalloporphyrins are a very important class of molecules having a key role in various biological relevant processes.<sup>1</sup> Few of the important biological processes where the metalloporphyrins are relevant include photosynthesis, transport and storage of dioxygen, and various other electron transfer reactions.<sup>2</sup> Thus, there is a constant strive to synthesize newer varieties of porphyrin scaffolds in order to mimic the naturally occurring metalloporphyrins.<sup>3</sup> The synthetic approach to synthesizing artificial porphyrin derivatives has been a major field of attraction since the 1930s. Hans Fisher is the pioneer in the synthesis of porphyrin derivatives.<sup>4</sup> Rothmund *et al.* synthesized the tetraphenyl porphyrin via a direct condensation reaction of pyrrole and aldehyde in the presence of pyridine in a sealed tube at around 220°C.<sup>5</sup> A milder version has been reported by Adler *et al.* Aldehydes and pyrroles condense in the presence of propionic acid at 141°C in the presence of air.<sup>6</sup> Lindsey developed the two-step one flask methodology in mild conditions and with satisfactory yields.<sup>7</sup> First step is an acid-catalyzed condensation reaction and formation of porphyrinogen, and the second step involves the oxidation of porphyrinogen to porphyrin by using a quinone-based oxidant (Scheme 2.1). One of the important porphyrin-based analogs is the *trans*-A<sub>2</sub>B<sub>2</sub>-porphyrins, which have versatile applications in many areas.<sup>8</sup> It is clearly observed from the above discussions that the choice of reagents in porphyrin synthesis owing to mild conditions with wide substrate scope is still rather small in number. Herein, an attempt has been made to decipher a new synthetic strategy for the facile synthesis of a series of *meso*-substituted porphyrins in mild conditions. The first step of the synthesis involves the condensation of aldehyde and pyrrole/dipyrromethane in acidic conditions (Scheme 2.1). The second step involves the manganese templated ring formation reaction. Finally on oxidation via PhIO/air resulted the formation of *meso*-substituted porphyrins in good/moderate yields. This strategy has

been extended for the synthesis of *meso*-substituted *trans*-A<sub>2</sub>B<sub>2</sub>-porphyrins and symmetric A<sub>4</sub>-porphyrins.



**Scheme 2.1** Synthetic application of *meso*-substituted *trans*-A<sub>2</sub>B<sub>2</sub>-Porphyrins.

In order to understand the role of manganese in the ring formation reaction, we have isolated and characterized a representative Mn-porphyrinogen complex as a putative reaction intermediate. A combined analytical, electrochemical, spectroscopic techniques and DFT studies are presented to confirm the structure of this putative reactive intermediate (Mn-porphyrinogen complex) and to unravel the role of this reaction intermediate in porphyrin synthesis.

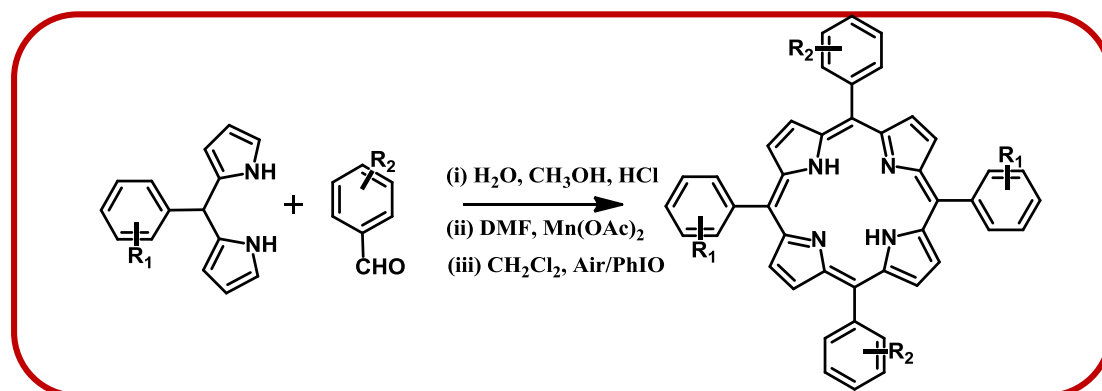
## 2.2 Results and discussion

### 2.2.1 Synthesis and Characterization

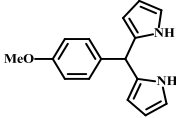
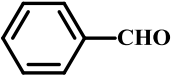
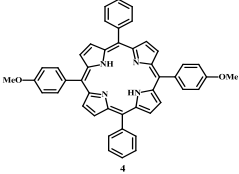
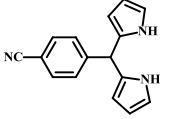
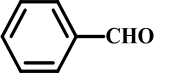
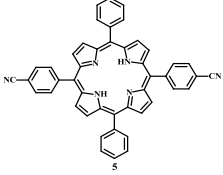
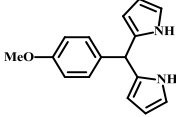
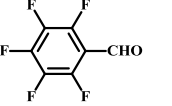
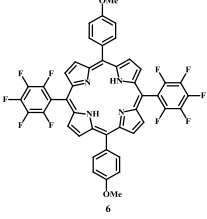
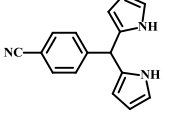
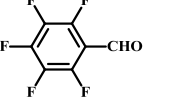
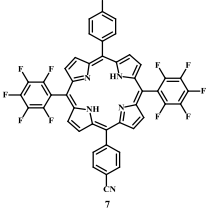
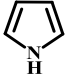
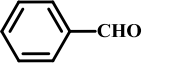
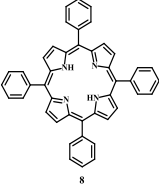
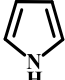
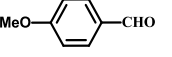
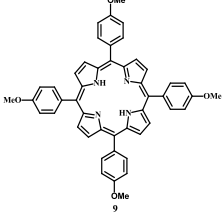
In order to establish the general nature of the synthetic strategy (Table 2.1), we have explored the scope of this newly designed porphyrin synthesis by synthesizing a

series of porphyrin derivatives bearing both electron donating as well as electron-withdrawing functional groups at the porphyrin periphery.

**Table 2.1** Scope of the synthesis of *meso*-substituted *trans*-A<sub>2</sub>B<sub>2</sub>-Porphyrins.



DPM/ Pyrrole	Aldehyde	Porphyrin	Yield (%)
			28
			25
			20

DPM/ Pyrrole	Aldehyde	Porphyrin	Yield (%)
			19
			18
			15
			15
			13
			10

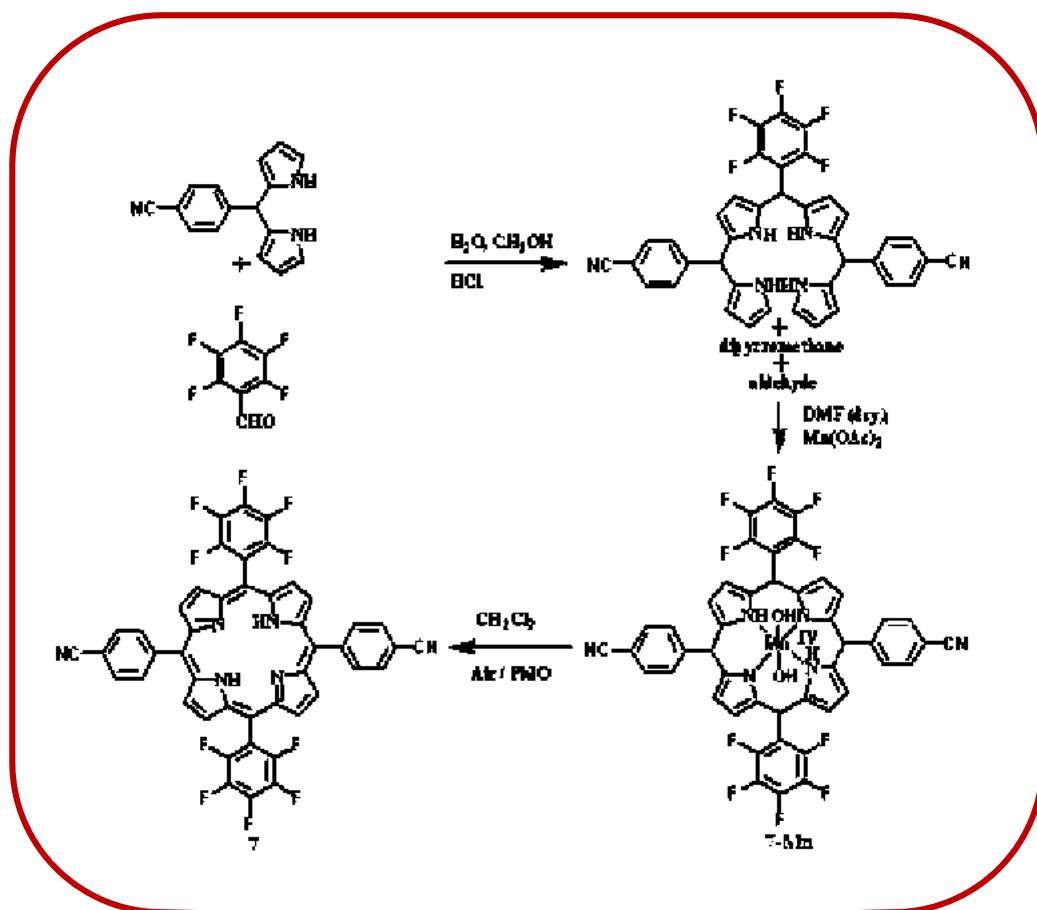
---

Under the optimized reaction conditions, the respective aldehyde and the corresponding dipyrromethane were dissolved in a (2:1) CH<sub>3</sub>OH and water mixture. After treatment with aqueous HCl, the reaction mixture was kept on stirring for approx. 2 hours at room temperature. The extracted product was dissolved in dry DMF, and anhydrous Mn(OAc)<sub>2</sub> was added to it and was stirred for another one hour. It is worthwhile to mention here that while using the Mn(OAc)<sub>2</sub>-tetrahydrate as a metal source, tetrapyrromethanes as the precursor ligand and followed by workup mostly in the non-chlorinated solvents, Kumar *et al.* have obtained the Mn(III) corroles.<sup>9</sup> The compound obtained on drying was dissolved in CH<sub>2</sub>Cl<sub>2</sub> and was kept for stirring overnight with silica gel. The crude product was purified over silica gel chromatography and resulted in the formation of pure *trans*-A<sub>2</sub>B<sub>2</sub>-Porphyrins in good yields (Figs S3-S11, and Table 2.1). Iodosyl benzene is the effective oxidizing agent for this transformation. However, in half of these cases, aerial oxidation is sufficient enough to lead the desired conversion to occur. The same reaction was successful across a broad range of dry solvents like dichloromethane, methanol, acetonitrile, toluene, and THF. However, we have observed that DMF is the most suitable solvent for this purpose.

In order to understand the reaction mechanism better, we have isolated a green color reaction intermediate by using column chromatography. We assume that these compounds may be the true intermediates as they deliver the porphyrin derivatives upon oxidation (Figure 2.1).

Unfortunately, these intermediate compounds are not sufficiently stable, and thus, we were unable to get single crystals of these species. However, we have characterized a representative derivative (**7-Mn**) thoroughly by using various techniques like CHN analysis, ESI-MS analysis, conductivity measurements, UV-Vis, FT-IR, ESR, and magnetic susceptibility measurements. The composition of this compound (**7-Mn**) was

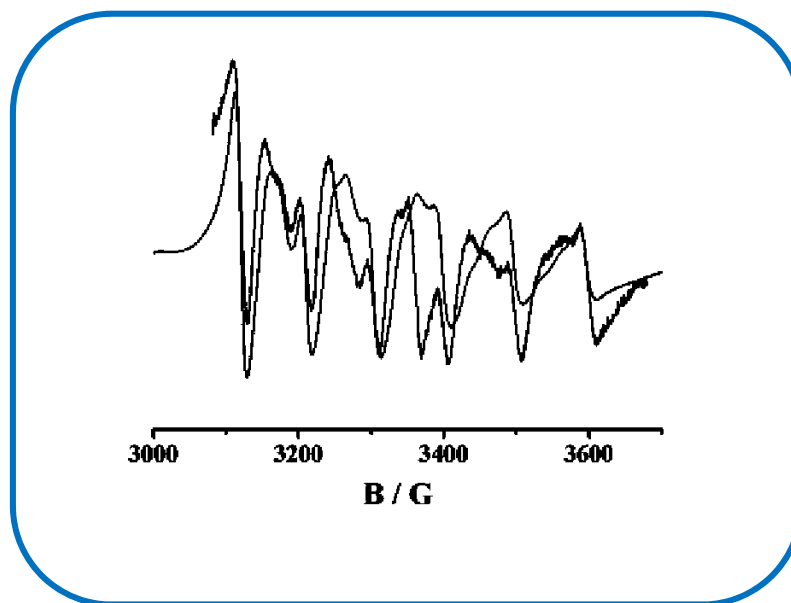
confirmed by using CHN analysis and also by ESI-MS analysis. From the conductivity measurements, the compound, **7-Mn**, shows no conductivity in acetonitrile solution. This clearly indicates that there are no dissociable counter ions in the compound (**7-Mn**).



**Figure 2.1** Proposed mechanism.

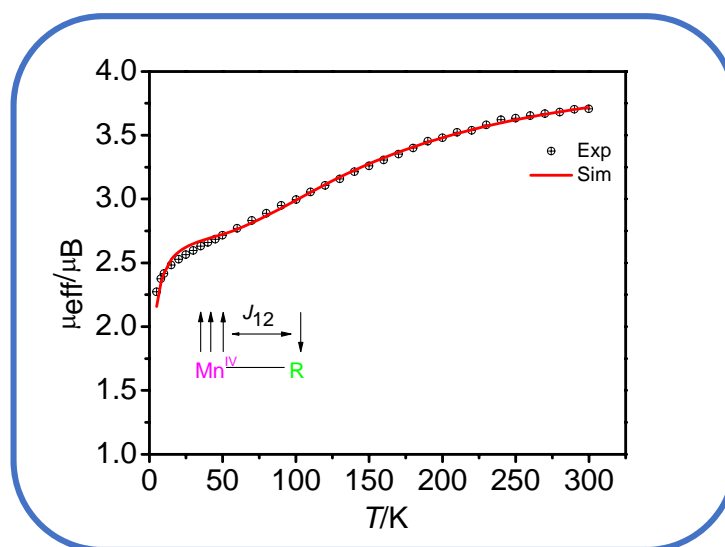
The EPR spectrum (Figure 2.2), which is observed in  $\text{CH}_3\text{OH-C}_2\text{H}_5\text{OH}$  glass at 100 K, displays a sextet ( $g \sim 2.003$ ) originating from the hyperfine coupling of the unpaired electron with  $^{55}\text{Mn}$  nucleus ( $^{55}\text{Mn}$ , 100%,  $I = 5/2$ ). An approximate  $A$ -value of 95 G,  $D$ -value of 180 G, and  $E$ -value of 20 G were determined from simulations of the experimental data, and these values are within the ranges of the reported values of other Mn-complexes.<sup>10</sup> This conforms to the paramagnetic nature of the Mn-complex, **7-Mn**.





**Figure 2.2** Experimental X-band EPR spectrum (black) of **7-Mn** at 100 K in CH<sub>3</sub>OH-C<sub>2</sub>H<sub>5</sub>OH glass in a flat cell and the simulated spectrum (red).

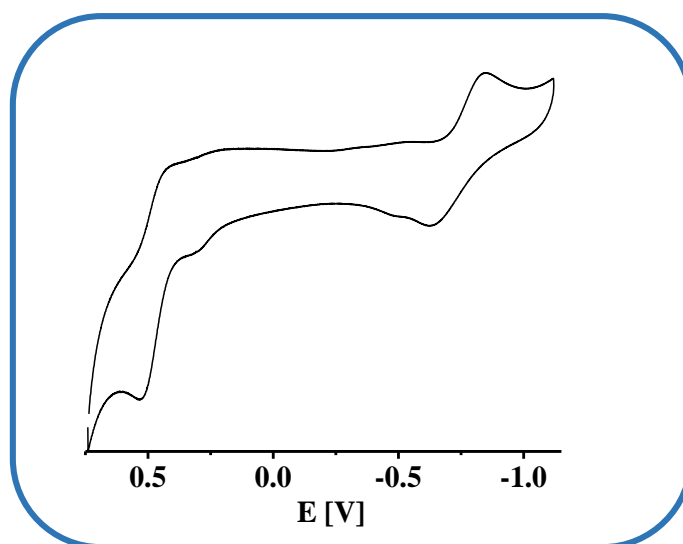
From the variable temperature magnetic susceptibility measurements (300K to 2K) (Figure 2.3), we have observed that the room temperature magnetic moment is  $3.71\mu_B$  at 300K.<sup>11</sup>



**Figure 2.3** Plot of the effective magnetic moment vs. temperature (from 2 to 300 K) for the complex **7-Mn**.

Figure 2.3 shows a plot of the  $\mu_{\text{eff}}$  versus temperature ( $T$ ) for a polycrystalline sample of **7-Mn**. A satisfactory fit, displayed in Figure 2.3, was obtained with  $J_{12} = -51 \text{ cm}^{-1}$ ,  $g_1 = 1.980$ ,  $g_2 = 2.000$ , and  $\theta = -3.36 \text{ K}$ . Fitting of the magnetic data indicates the presence of both Mn(IV) and porphyrinogen radical. An antiferromagnetic interaction exists between the Mn(IV) ion ( $S_{\text{Mn}}=3/2$ ) and the porphyrinogen radical ( $S_{\text{rad}} = 1/2$ ).

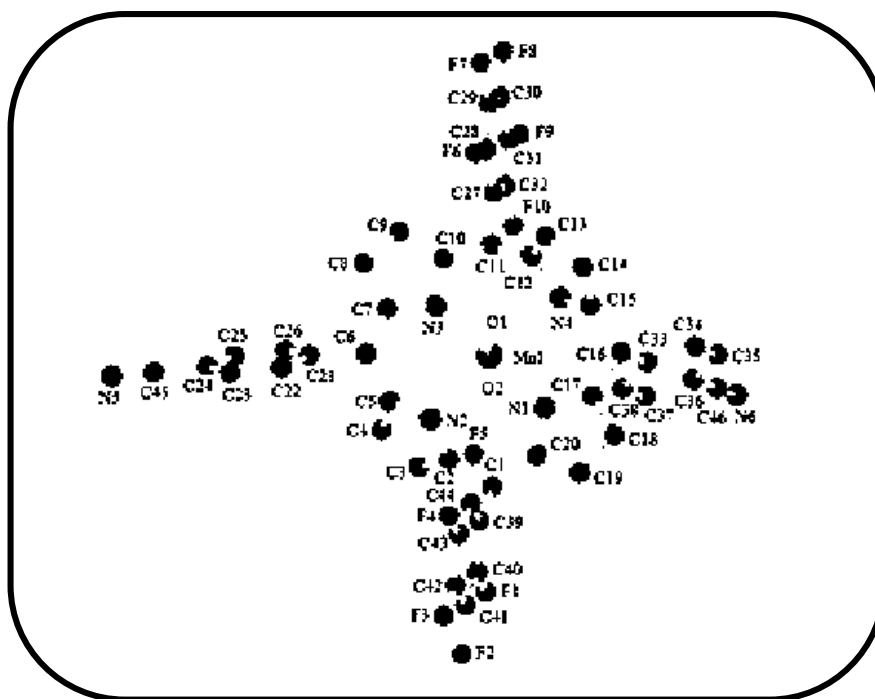
The cyclic voltammogram (Figure 2.4) of **7-Mn** in  $\text{CH}_3\text{CN}$  reveals a reversible couple at 0.48 V and a quasi-reversible couple at -0.73 V vs.  $\text{Fc}/\text{Fc}^+$ . While comparing with analogous Mn(IV) complexes, we have assigned the couple at 0.48 V as Mn(IV)/Mn(III) couple and at -0.73 V as Mn(III)/Mn(II) couple.<sup>12</sup>



**Figure 2.4** Cyclic voltammogram (—) of **7-Mn** in  $\text{CH}_3\text{CN}$ . The potentials are vs. ferrocene/ferricinium.

To support the experimental observation and to get better insight into the structural parameters, DFT calculations were carried out on **7-Mn** as a representative example (Figure 2.5 and Table 2.2-2.5). The bond lengths and angles of DFT optimized structures match reasonably well with the previously reported other Mn(IV) hydroxide complexes. In the optimized structure (Figure 2.5), the two Mn–OH bond distances are

1.86 and 1.87 Å, respectively. These distances fall in the ranges of previously reported and well-characterized L Mn<sup>IV</sup>(OH) complexes.<sup>13a</sup>



**Figure 2.5** DFT optimized structure of **7-Mn**

For these complexes, the Mn–OH bond distances are in the range of 1.79–1.88 Å. These values are significantly longer than related Mn<sup>IV</sup>=O complexes,<sup>13</sup> which are reported to be in the range of 1.57–1.72 Å. The Mn···N(pyrrolic NH) (Mn···N2 and Mn···N4) bond distances in **7-Mn** are 2.50 and 2.60 Å, respectively. These values are outside the typical range of Mn–N bond distances. However, the Mn···N(pyridine) bond distances in an Mn(III)–peroxo intermediate has been reported to be as high as 2.49 Å.<sup>13d</sup> However, the Mn···N(pyrrolic N) (Mn···N1 and Mn···N3) bond distances are usual and matches nicely with the earlier reports of similar bond distances.<sup>13</sup>

### 2.2.2 TD-DFT Calculations

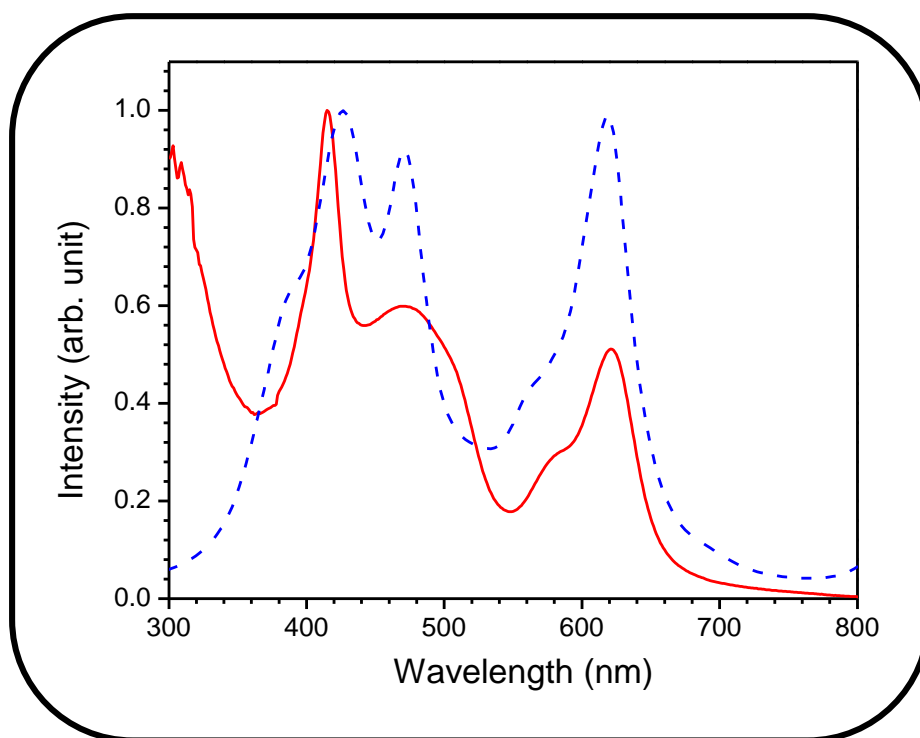
The DFT calculated UV-Vis and FT-IR spectra corroborate well with the experimentally obtained spectra (Figure 2.6, Figure 2.8, and Table 2.2-2.5). The

---

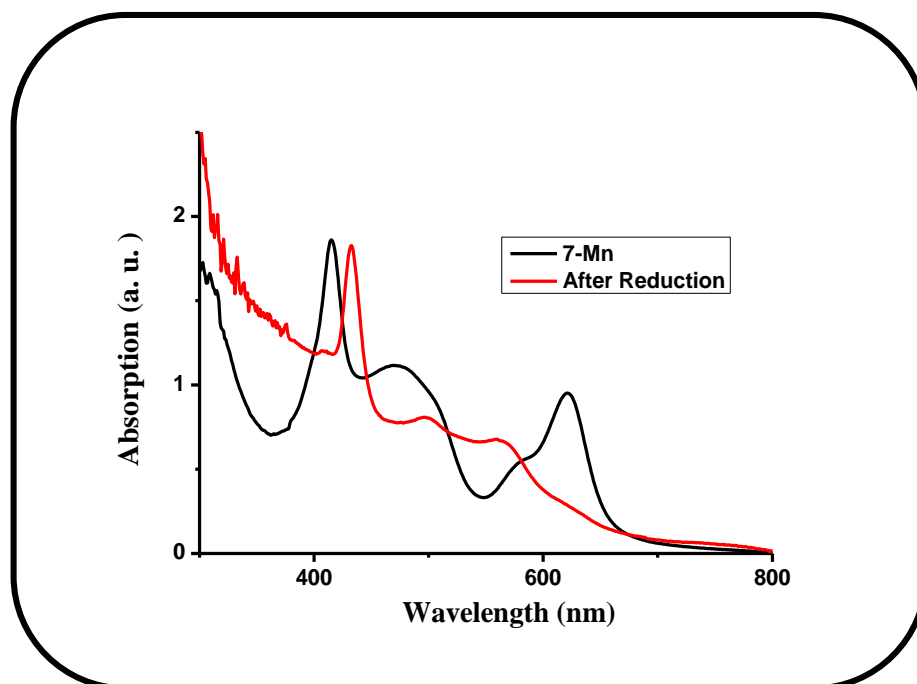
experimentally obtained UV–Vis spectrum of the **7-Mn** in its native state is fully consistent with the calculated values (Table 2.4).

For example, **7-Mn** displays an intense band in the visible spectrum at 416, 470, and 621 nm (Table S1), the TD-DFT computed values for these transitions are at 432 nm (SOMO-3 to LUMO), 472nm (SOMO-2 to LUMO), and 620 nm (SOMO-11 to LUMO).

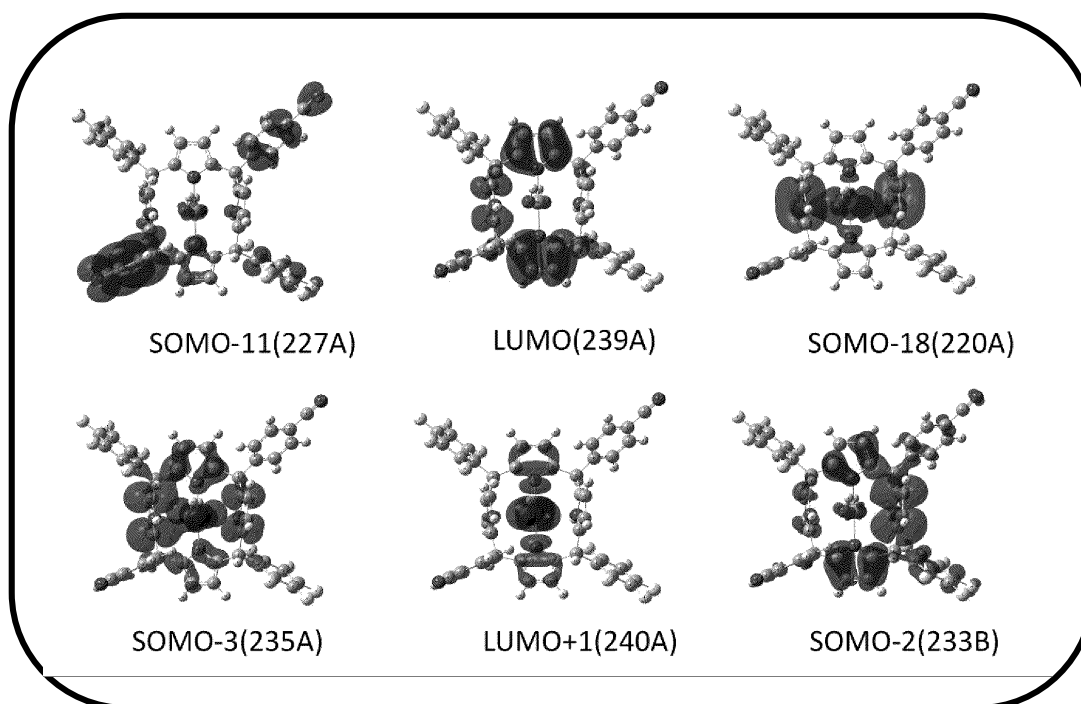
The origin of the bands at 416, 470, and 621 nm is attributed to the LMCT, LMCT, and ILCT transitions, respectively (Figure 2.9). While reducing the compound by using LiAlH<sub>4</sub> in DCM solution, the band at 416 nm is red shifted to 432 nm, and other bands in the visible region lose their intensity significantly (Figure 2.7).



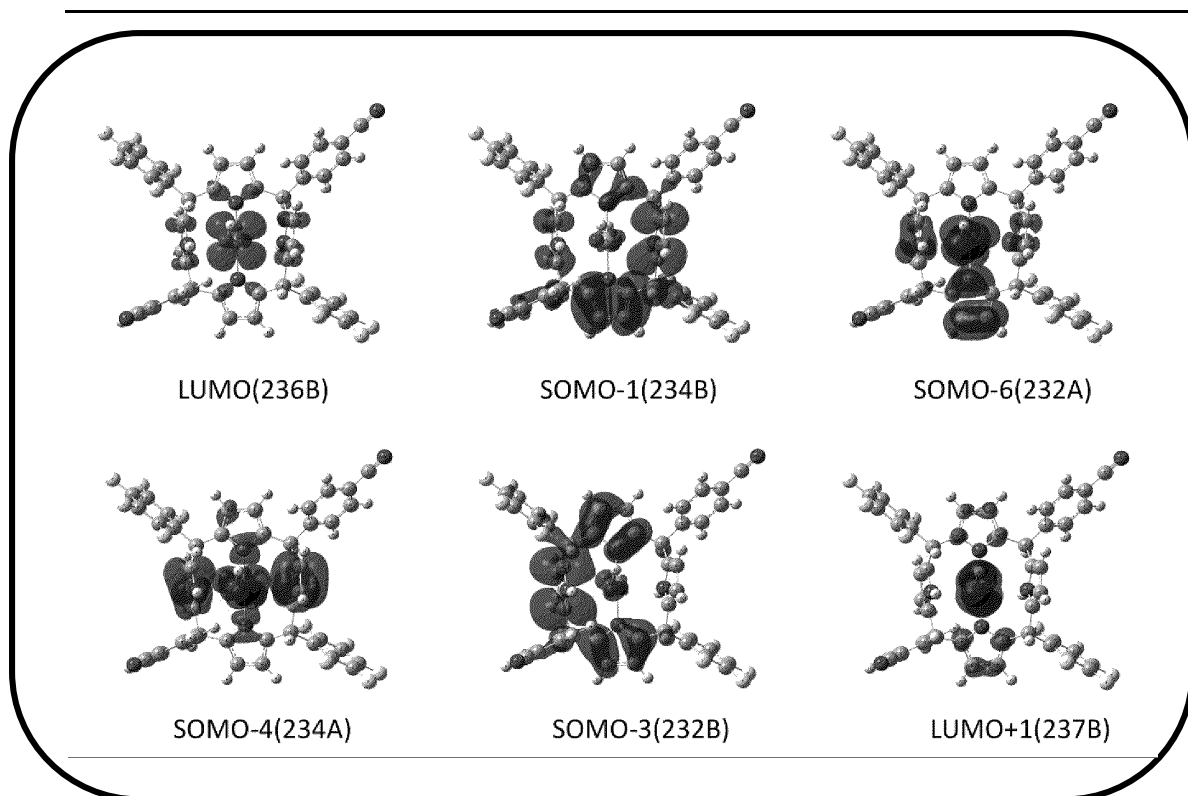
**Figure 2.6** UV-Vis spectra of **7-Mn**: Experimental UV-Vis absorption spectrum (—) and TDDFT (TD-B97D/6-31G\*)-based absorption spectrum (---) (Lorentzian broadening with FWHM ~ 25 nm).



**Figure 2.7** Chemical reduction of **7-Mn** via  $\text{LiAlH}_4$  in DCM solution at RT. The black line indicates the absorption spectra before reduction, and the red line indicates the species obtained after reduction.



**Table 2.2** Composition of selected molecular orbitals of **7-Mn**.

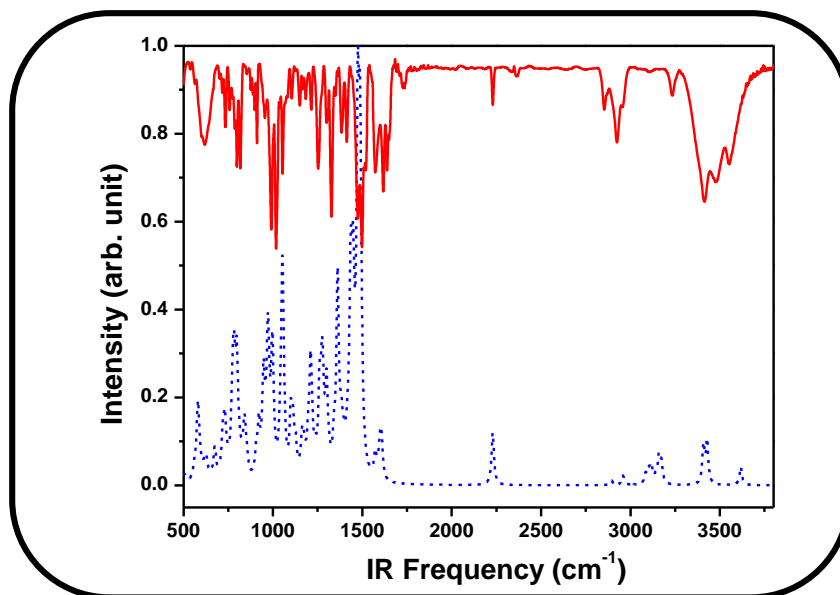


**Table 2.3**      Composition of selected molecular orbitals of **7-Mn**

State	E(eV)	Transition Orbitals	Contribution	Character
<b>S<sub>13</sub></b>	1.76	SOMO-11(227A) to LUMO(239A)	0.99(100%)	ILCT
<b>S<sub>26</sub></b>	2.31	SOMO-18(220A) to LUMO239A)	0.11(1.19%)	LMCT
		SOMO-3(235A) to LUMO+1(240A)	0.11(1.30%)	LMCT
		SOMO-2(233B) to LUMO(236B)	0.98(96.30%)	LMCT
		SOMO-1(234B) to LUMO(236B)	0.11(1.20%)	LMCT
<b>S<sub>29</sub></b>	2.52	SOMO-6(232A) to LUMO+1(240A)	0.22(4.87%)	LMCT
		SOMO-4(234A) to LUMO+1(240A)	0.66(44.37%)	LMCT
		SOMO-3(232B) to LUMO(236B)	0.69(48.37%)	LMCT
		SOMO-1(234B) to LUMO+1(237B)	0.14(1.92%)	LMCT

**Table 2.4**    TD-DFT transitions for **7-Mn**.

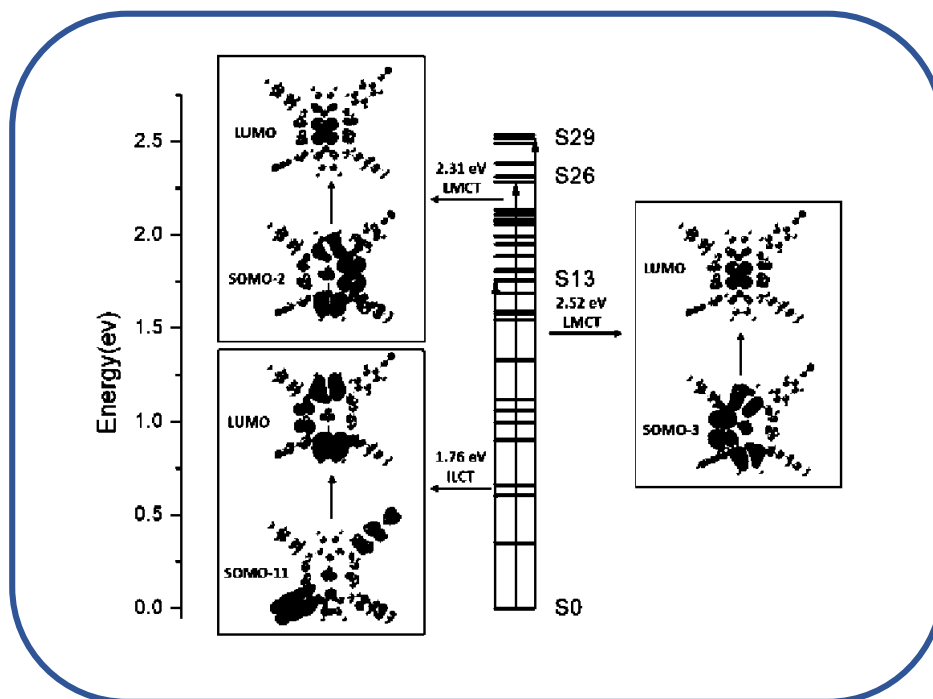
As shown in Figure 2.8, not only UV-Vis spectra but also the experimental IR spectra of **7-Mn** can be reproduced with reasonable accuracy by DFT calculation. Some of the significant and distinguishable IR stretching and bending frequencies of **7-Mn** are listed in Table 2.5.



**Figure 2.8** IR spectrum of **7-Mn**: Experimentally recorded FT-IR spectrum (—) and IR spectrum (—) obtained from DFT (B97-D/6-31G\*) computation (scaling factor; 0.90, Lorentzian broadening with FWHM ~ 25 cm<sup>-1</sup>).

**Table 2.5** TD-DFT calculated IR frequencies for **7-Mn**.

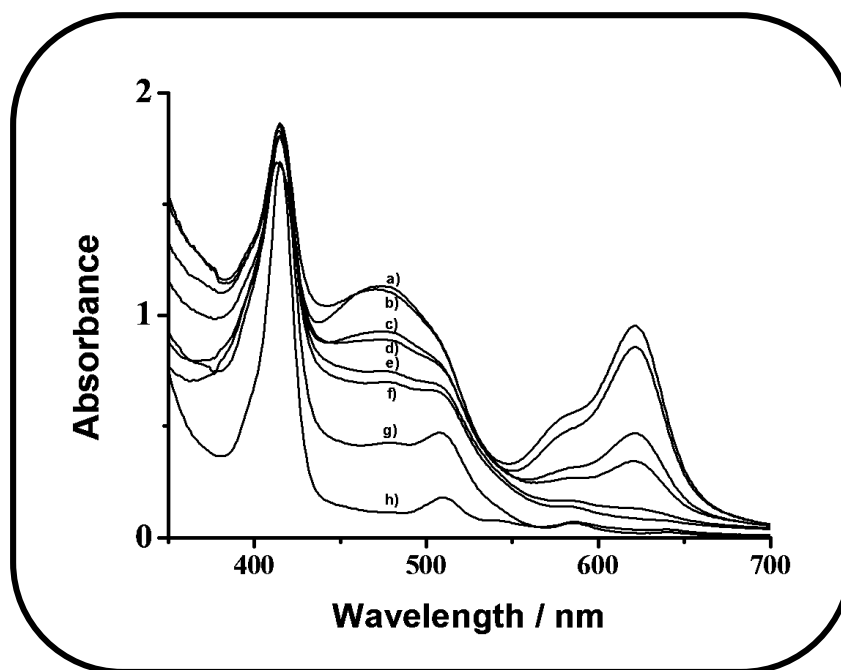
Functional Group	IR frequency (cm <sup>-1</sup> )
Water stretch	3667.10
	3664.82
Pyrrole NH	3466.32
	3437.08
Pyrrole CH	3235.57-3176.80
Benzonitrile CH	3153.95-3119.51
PFB	2993-2924
CN stretch	2257.96
	2257.83
Aromatic C=C bending	1627.74-900
OH bending	700-900



**Figure 2.9** Calculated single occupied molecular orbitals (SOMO), lowest unoccupied molecular orbital (LUMO), and the corresponding orbital energies of **7-Mn**.

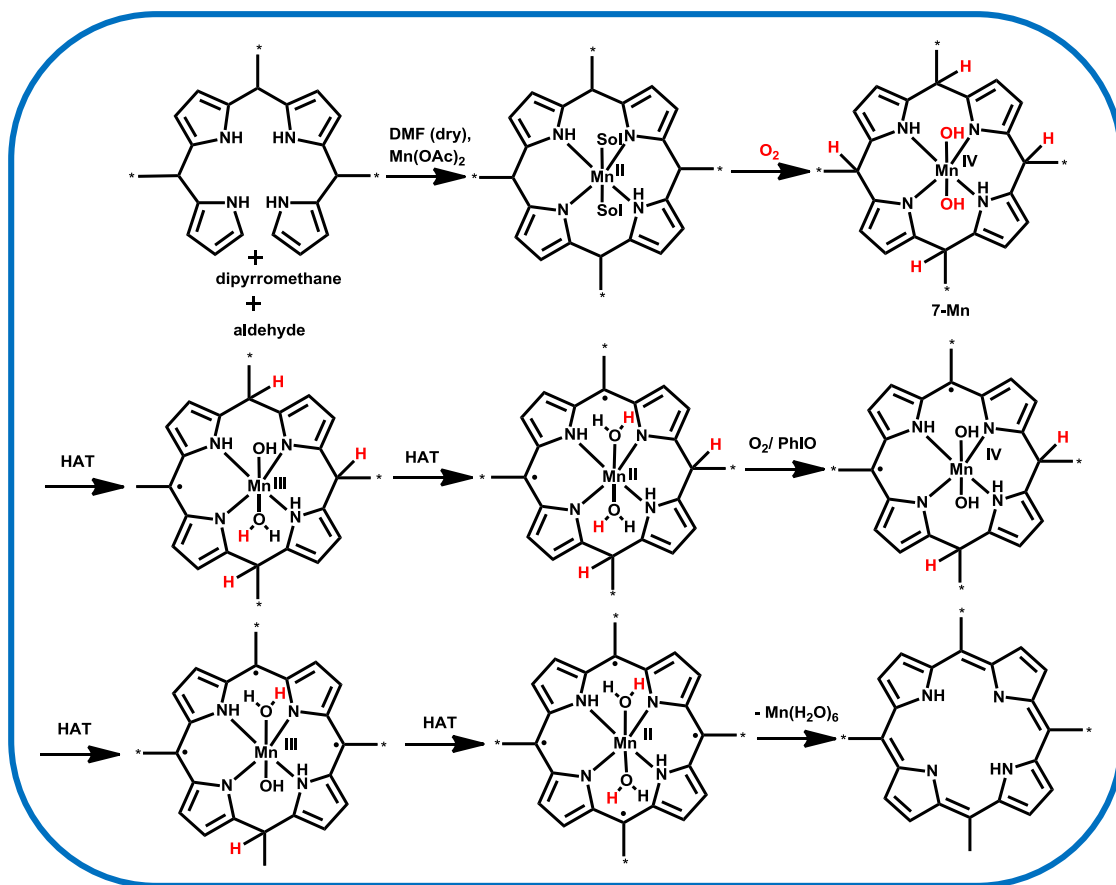
*In-situ* UV-Vis experiments (Figure 2.10) support that the Mn-complex, **7-Mn** is the intermediate for the desired transformation to occur. For this purpose, the isolated Mn-complex, **7-Mn**, is treated with excess iodosyl benzene, and it yields the *trans*-A<sub>2</sub>B<sub>2</sub>-Porphyrins instantly. Iodosyl benzene is the effective oxidizing agent which can convert the Mn(IV)- porphyrinogen derivatives to the corresponding *trans*-A<sub>2</sub>B<sub>2</sub>-porphyrins. However, in half of these cases, aerial oxidation is sufficient enough to lead the desired conversion to occur. Conversion of Mn(IV)- porphyrinogen derivatives to the *trans*-A<sub>2</sub>B<sub>2</sub>-porphyrins occurs very fast in the time scale. Literature reports suggest that the Mn(IV)-OH intermediate<sup>14</sup> (**7-Mn**) is a potent H-atom abstractor and has the ability to carry out the H-atom abstraction reaction efficiently (Scheme 2.2); it is even more potent than its analogous Mn=O species.<sup>14</sup> The resultant Mn(II) porphyrin (Scheme 2.2) is unstable at the experimental condition and thus demetalates easily.<sup>2c</sup>





**Figure 2.10** Electronic absorption spectrum of a) **7-Mn** in  $\text{CH}_2\text{Cl}_2$  solution. After this, excess PhIO was added to this solution; b) Recorded from the crude reaction mixture after 3 mins, c) crude reaction mixture after 6 mins, d) crude reaction mixture after 9 mins, e) crude reaction mixture after 12 mins, f) crude reaction mixture after 15 mins, g) reaction mixture after 20 mins (passed through a silica gel filter to remove the residual Mn salt and excess PhIO, and h) Pure **7** in  $\text{CH}_2\text{Cl}_2$  solution.

Based on these observations, we can conclude that the metal has performed a dual role in the present case. Firstly, it acts as a chelating agent and brings the aldehyde and the corresponding tetrapyrromethanes into a planar conformation and leads to the macrocycle formation; secondly, it provides the redox equivalents for the reaction. Oxidative macro-cyclization mediated by metal salts has been reported extensively in the literature.<sup>15</sup> However, it was limited mostly to the cyclization of a,c-biladienes.<sup>16</sup> One major drawback is that one needs to demetallate the porphyrin derivatives, and also, the substrate scope is very narrow.<sup>17</sup>



**Scheme 2.2** Probable mechanism for the conversion of Mn(IV)- porphyrinogen derivatives to the porphyrins via hydrogen abstraction (HAT=hydrogen abstraction).

### 2.3 Conclusions

In summary, we have developed an efficient, milder (occurs at RT), cheap (while using aerial oxygen), and environment benign methodology for the facile synthesis of porphyrin (including *trans*-A<sub>2</sub>B<sub>2</sub>-Porphyrin) derivatives. Most interestingly, these reactions can be easily scaled up and can be useful for the gram-scale synthesis of porphyrins. Negligible to no scrambling (for *trans*-A<sub>2</sub>B<sub>2</sub>-Porphyrin) is observed in almost all of these cases. In half of these representative syntheses, excess iodosylbenzene is used as an oxidizing agent, and in the rest examples, the air is used as an oxidizing agent. Excess iodosylbenzene is obviously more expensive than the traditionally used

---

oxidizing agent like DDQ. However, in the traditional synthetic routes, using DDQ as an oxidizing agent, a large excess of chlorinated solvents was used as a reaction medium. In the present cases, we can limit the use of chlorinated solvents in the reaction medium. Thus the commercial feasibility of this new method may arise while performing these reactions on a large scale and using air as an oxidizing agent. *In-situ* UV-vis experiments support that the *trans*-Mn(IV)-dihydroxide is the putative intermediate for the desired transformation to occur. To support the experimental observation and to get better insight into the structural parameters, DFT calculations were carried out on **7-Mn** as a representative example. The DFT calculated UV-Vis, and FT-IR spectra corroborate well with the experimentally obtained spectra. The role of the *trans*-Mn(IV)-dihydroxide putative intermediate has been appreciated as a potent H-atom abstractor, which ultimately leads to the generation of free-base porphyrins.

## **2.4 Experimental section**

### **2.4.1 Materials**

The precursor's pyrrole, manganese(II) acetate (98%), and aldehydes were purchased from Aldrich, USA. Other chemicals were of reagent grade. Hexane and CH<sub>2</sub>Cl<sub>2</sub> were distilled from KOH and CaH<sub>2</sub>, respectively. For spectroscopy studies, HPLC-grade solvents were used. 5-phenyldipyrromethane, 5-(4-methoxyphenyl)dipyrromethane, and 5-(4-cyanophenyl)dipyrromethane were prepared by following an earlier literature report.<sup>18</sup>

### **2.4.2 Characterization**

UV-Vis spectral studies were performed on a Perkin-Elmer LAMBDA-750 spectrophotometer. The elemental analyses were carried out with a Perkin-Elmer 240C elemental analyzer. FT-IR spectra were recorded on a Perkin-Elmer spectrophotometer

---

with samples prepared as KBr pellets. The NMR measurements were carried out using a Bruker 400 and 700 MHz NMR spectrometer. Chemical shifts are expressed in parts per million (ppm) relative to residual chloroform. Electrospray mass spectra were recorded on a Bruker Micro TOF—QII mass spectrometer. The magnetic susceptibility of the samples was measured by using a superconducting quantum interference device (SQUID) manufactured by Quantum Design, USA. Simulations of the experimentally obtained magnetic measurements were performed using julX programme developed by Dr. E. Bill, Max-Planck Institute, Muelheim an der Ruhr, Germany. Cyclic voltammetry measurements were carried out using a CH Instruments model *CHI1120A* electrochemistry system. A glassy-carbon working electrode, a platinum wire as an auxiliary electrode, and a saturated calomel reference electrode (SCE) were used in a three-electrode configuration. Tetrabutyl ammonium perchlorate (TBAP) was the supporting electrolyte (0.1M), and the concentration of the solution was  $10^{-3}$ M with respect to the complex. The half-wave potential  $E_{298}^0$  was set equal to  $0.5(E_{pa} + E_{pc})$ , where  $E_{pa}$  and  $E_{pc}$  are anodic and cathodic cyclic voltammetric peak potentials, respectively. The scan rate used was  $100 \text{ mV s}^{-1}$ . The solution electrical conductivity was checked using a CON 700 Conductivity/°C/°F Bench Meter. EPR spectra at X-band frequency (ca. 9.5 GHz) were obtained with a Bruker EMX (ER 073) System. The EPR spectra were simulated on a home-written program using C language and used a third-order perturbation treatment.

### **2.4.3 Computational Method**

The geometry optimization was carried out at the density-functional theory (DFT) level using the B97 functional with dispersion correction as implemented in the Turbomole program.<sup>19-22</sup> The resolution of the identity (RI) approximation, as well as the multipole-accelerated RI (MARIJ) approximation<sup>23</sup>, were employed to speed up the

---

calculation. The 6-31G(d) basis set was used for hydrogen, carbon, nitrogen, oxygen, and fluorine, and def-TZVP basis set was used for manganese. The harmonic vibrational frequencies of **7-Mn** were calculated numerically at the same level of theory. The time-dependent DFT calculations were also performed at the same level of theory and basis sets with Gaussian-09 software.<sup>24</sup>

#### 2.4.4 Syntheses

##### 2.4.4.1 Synthesis of *trans*-A<sub>2</sub>B<sub>2</sub>-porphyrins, **1-7**

The *trans*-A<sub>2</sub>B<sub>2</sub>-porphyrins (**1-7**) were prepared by following a general procedure. Hence, only one representative case is discussed below. 0.100 g (0.4 mmol) of 5-(4-cyanophenyl)dipyrromethane and 49.3  $\mu$ L (0.4 mmol) of 2,3,4,5,6-pentafluorobenzaldehyde were dissolved in 50 mL MeOH and 25 mL water (2:1) mixture. Subsequently, 5 mL of aqueous HCl (36%) was added to it. The reaction mixture was kept on stirring for 2 hours at room temperature. The crude product was washed and extracted several times with chloroform and water and dried over anhydrous Na<sub>2</sub>SO<sub>4</sub>. The solvent was evaporated to dryness. The extracted product was dissolved in dry DMF, and 0.173 g (1 mmol) of manganese(II) acetate was added to it. The mixture was stirred for another one hour at RT. The dark-colored product was evaporated to dryness. The crude product was dissolved in minimum dichloromethane and excess PhIO was added to it, and it was stirred at room temperature in the presence of air, and the rate of the reaction was monitored through thin layer chromatography (**1**, **2**, **6**, and **7**). The reaction generally yields the desired product in 10-15 minutes. The reaction mixture was immediately purged through a previously packed silica gel (100-200 mesh) column. The final product was eluted using pure DCM as eluent. In half of these cases, the desired product is formed without the addition of any external oxidant, like PhIO, and the aerial oxygen is sufficient enough to perform the reaction (**3**, **4**, and **5**).

---

#### **2.4.4.2 Synthesis of 5,15-Bis(4-cyanophenyl)-10,20-diphenylporphyrin, 5**

4.2 g (17 mmol) of 5-(4-cyanophenyl)dipyrromethane and 1.8 mL (17 mmol) of benzaldehyde were dissolved in 1L MeOH and 500 mL water (2:1) mixture with the subsequent addition of 50 mL of aqueous HCl. The reaction mixture was kept on stirring for 2 hours at room temperature. The crude product was washed and extracted several times with chloroform and water and dried over anhydrous Na<sub>2</sub>SO<sub>4</sub>. The solvent was evaporated to dryness. The extracted product was dissolved in 100ml dry DMF, and 7.3 g (42.5 mmol) of manganese(II) acetate was added to it. The mixture was stirred for another one hour at RT. The dark-colored product was evaporated to dryness. The crude product was dissolved in minimum dichloromethane and was stirred overnight at room temperature in the presence of air. The reaction mixture was purged through a silica gel (100-200 mesh) column.

#### **2.4.4.3 Synthesis of 5,10,15,20-Tetraphenylporphyrin, 8**

6.8 mL (0.098 mol) of pyrrole and 10 mL (0.098 mol) of benzaldehyde were dissolved in a 2 L MeOH and 1 L water (2:1) mixture. Subsequently, 100 mL of aqueous HCl (36%) was added to it. The reaction mixture was kept on stirring for 2 hours at room temperature. The crude product was washed and extracted several times with chloroform and water and dried over anhydrous Na<sub>2</sub>SO<sub>4</sub>. The solvent was evaporated to dryness. The extracted product was dissolved in 200ml dry DMF, and 30 g (0.173 mol) of manganese(II) acetate was added to it. The mixture was stirred for another one hour at RT. The dark-colored product was evaporated to dryness. The crude product was dissolved in minimum dichloromethane, excess PhIO was added to it, and it was stirred at room temperature in the presence of air, and the rate of the reaction was monitored through thin layer chromatography. The reaction generally yields the desired product in 30 minutes. The reaction mixture was immediately purged through a previously packed

---

silica gel (100-200 mesh) column. The final product was eluted using DCM-hexane (1:1) mixture as an eluent.

#### **2.4.4.4 Synthesis of 5,10,15,20-Tetrakis(4-methoxyphenyl)porphyrin, 9**

0.5 mL (7.34 mmol) of pyrrole and 1.0 gm (7.34 mmol) of 4-methoxybenzaldehyde were dissolved in 300 mL MeOH and 150 mL water (2:1) mixture. Subsequently, 30 mL of aqueous HCl (36%) was added to it. The reaction mixture was kept on stirring for 2 hours at room temperature. The crude product was washed and extracted several times with chloroform and water and dried over anhydrous Na<sub>2</sub>SO<sub>4</sub>. The solvent was evaporated to dryness. The extracted product was dissolved in dry DMF, and 3.175 g (18.35 mmol) of manganese(II) acetate was added to it. The mixture was stirred for another one hour at RT. The dark-colored product was evaporated to dryness. The crude product was dissolved in minimum dichloromethane, excess PhIO was added to it, and it was stirred at room temperature in the presence of air, and the rate of the reaction was monitored through thin layer chromatography. The reaction generally yields the desired product in 10-15 minutes. The reaction mixture was immediately purged through a previously packed silica gel (100-200 mesh) column. The final product was eluted using DCM-hexane (1:1) mixture as an eluent.

#### **2.4.4.5 Synthesis of Mn(IV)- porphyrinogen derivative, 7-Mn**

0.100 g (0.4 mmol) of 5-(4-cyanophenyl)dipyrromethane and 49.3  $\mu$ L (0.4 mmol) of 2,3,4,5,6-pentafluorobenzaldehyde was dissolved in 50mL MeOH and 25 mL water (2:1) mixture. Subsequently, 5 mL of aqueous HCl (36%) was added to it. The reaction mixture was kept on stirring for 2 hours at room temperature. The crude product was washed and extracted several times with chloroform and water and dried over anhydrous Na<sub>2</sub>SO<sub>4</sub>. The solvent was evaporated to dryness. The extracted product was dissolved in

---

dry DMF, and 0.173 g (1 mmol) of manganese(II) acetate was added to it. The mixture was stirred for another one hour at RT. The dark-colored product was evaporated to dryness. The reaction mixture was purged through a silica gel (100-200 mesh) column. The final green color product was eluted using DCM-hexane (2:3) mixture as an eluent.

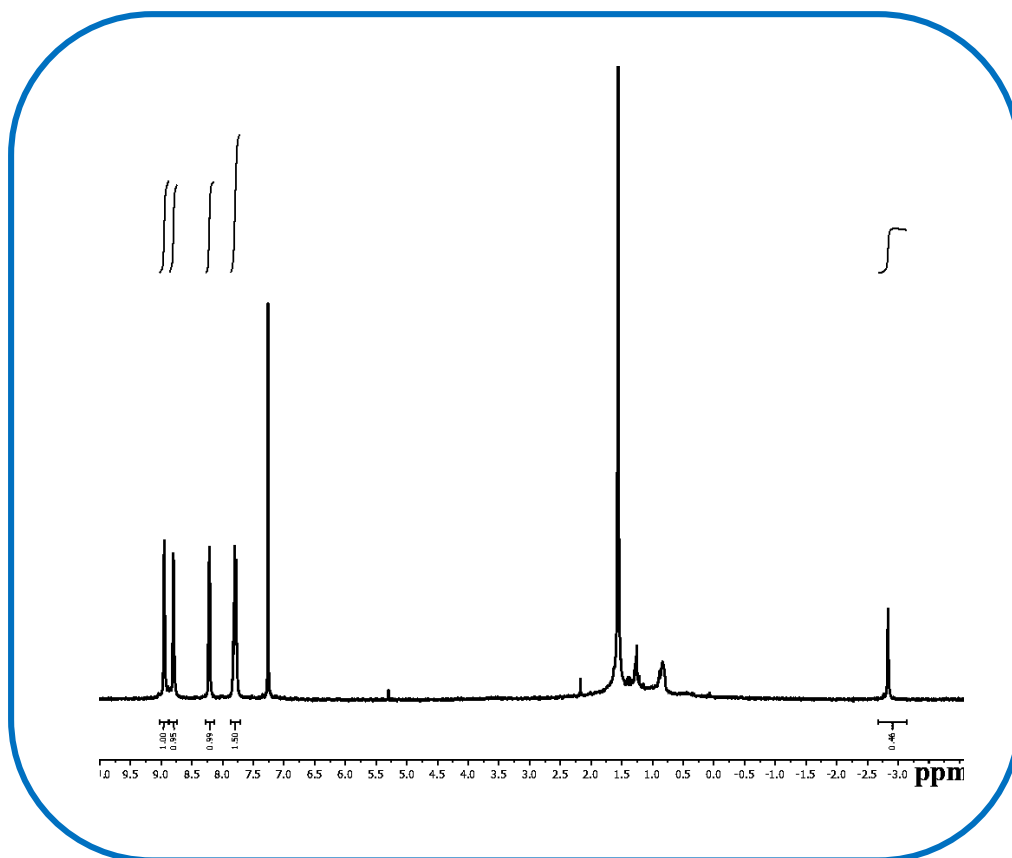
#### **2.4.4.6 Synthesis of 5,15-bis(4-cyanophenyl)-10-(pentafluorophenyl)tetrapyrane**

The following synthesis was performed by following a protocol reported earlier.<sup>1</sup> 0.100 g (0.4 mmol) of 5-(4-cyanophenyl)dipyrromethane and 49.3  $\mu$ L (0.4 mmol) of 2,3,4,5,6-pentafluorobenzaldehyde were dissolved in 50 mL MeOH and 25 mL water (2:1) mixture. Subsequently, 5 mL of aqueous HCl (36%) was added to it. The reaction mixture was kept on stirring for 2 hours at room temperature. The crude product was washed and extracted several times with chloroform and water and dried over anhydrous Na<sub>2</sub>SO<sub>4</sub>. The solvent was evaporated to dryness. The reaction mixture was purged through a silica gel (100-200 mesh) column. The final product was eluted using EtOAc/hexane mixture as an eluent.

#### **For 5,15-Bis(pentafluorophenyl)-10,20-diphenylporphyrin, 1**

Yield: 28% (49 mg). Anal. Calcd (found) for C<sub>44</sub>H<sub>20</sub>F<sub>10</sub>N<sub>4</sub> (**1**): C, 66.50 (66.67); H, 2.54 (2.32); N, 7.05 (7.16). <sup>1</sup>H NMR (400 MHz, Chloroform-*d*)  $\delta$  8.95 (d, *J* = 4.9 Hz, 4H), 8.80 (d, *J* = 4.9 Hz, 4H), 8.22 (d, *J* = 6.9 Hz, 4H), 7.79 (q, *J* = 7.9, 7.1 Hz, 6H), -2.84 (br s, 2 H) (Figure 2.11). Other analytical data are consistent with the previously reported authentic compounds.<sup>25</sup>



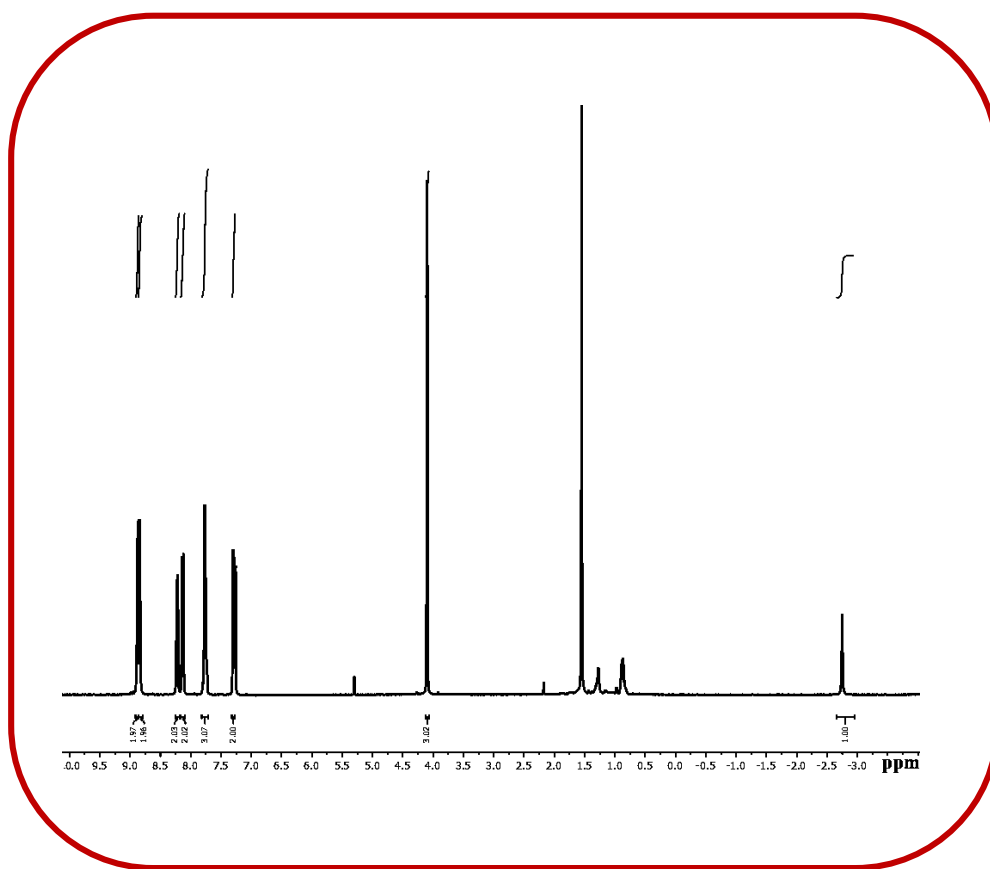


**Figure 2.11**  $^1\text{H}$  NMR spectrum of 5,15-Bis(pentafluorophenyl)-10,20-diphenylporphyrin, **1** in  $\text{CDCl}_3$ .

**For 5,15-Bis(4-cyanophenyl)-10,20-bis(4-methoxyphenyl)porphyrin, 2**

Yield: 25% (35 mg). Anal. Calcd (found) for  $\text{C}_{48}\text{H}_{32}\text{N}_6\text{O}_2$  (**2**): C, 79.54 (79.66); H, 4.45 (4.36); N, 11.59 (11.64).  $^1\text{H}$  NMR (400 MHz, Chloroform-*d*)  $\delta$  8.92 (m, 4H), 8.74 (m, 4H), 8.35 (m, 4H), 8.12 (m, 4H), 8.08 (m, 4H), 7.32 (m, 4H), 4.11 (s, 6H), -2.80 (br s, 2H) (Figure 2.12). Other analytical data are consistent with the previously reported authentic compounds.<sup>26</sup>

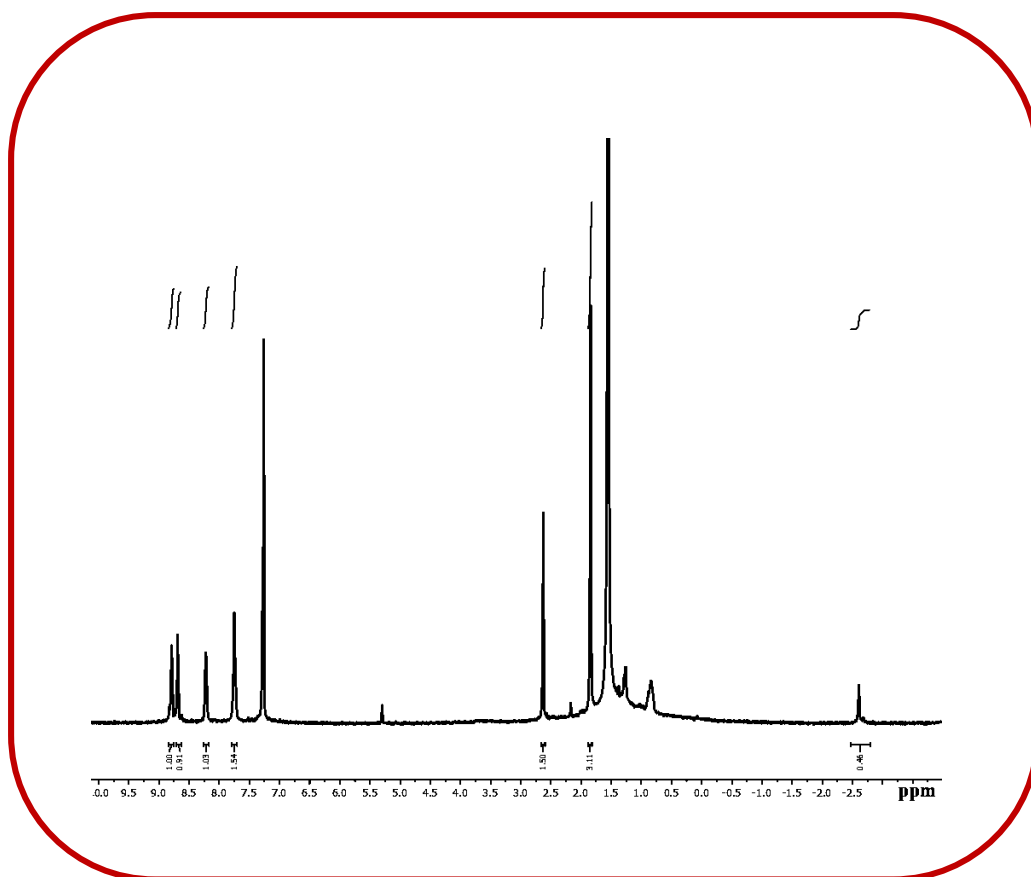




**Figure 2.13**  $^1\text{H}$  NMR spectrum of 5,15-Dimesityl-10,20-diphenylporphyrin, **3** in  $\text{CDCl}_3$ .

**For 5,15-Bis(4-methoxyphenyl)-10,20-diphenylporphyrin, 4**

Yield: 19% (24 mg). Anal. Calcd (found) for  $\text{C}_{46}\text{H}_{34}\text{N}_4\text{O}_2$  (**4**): C, 81.88 (81.78); H, 5.08 (5.17); N, 8.30 (8.39).  $^1\text{H}$  NMR (400 MHz, Chloroform-*d*)  $\delta$  8.91 – 8.81 (m, 8H), 8.23 – 8.21 (m, 4H), 8.13 (d,  $J = 8.2$  Hz, 4H), 7.76 (td,  $J = 8.2, 7.5, 5.3$  Hz, 6H), 7.29 (d,  $J = 8.3$  Hz, 4H), 4.10 (s, 6H), -2.76 (s, 2H) (Figure 2.14). Other analytical data are consistent with the previously reported authentic compounds.<sup>28</sup>

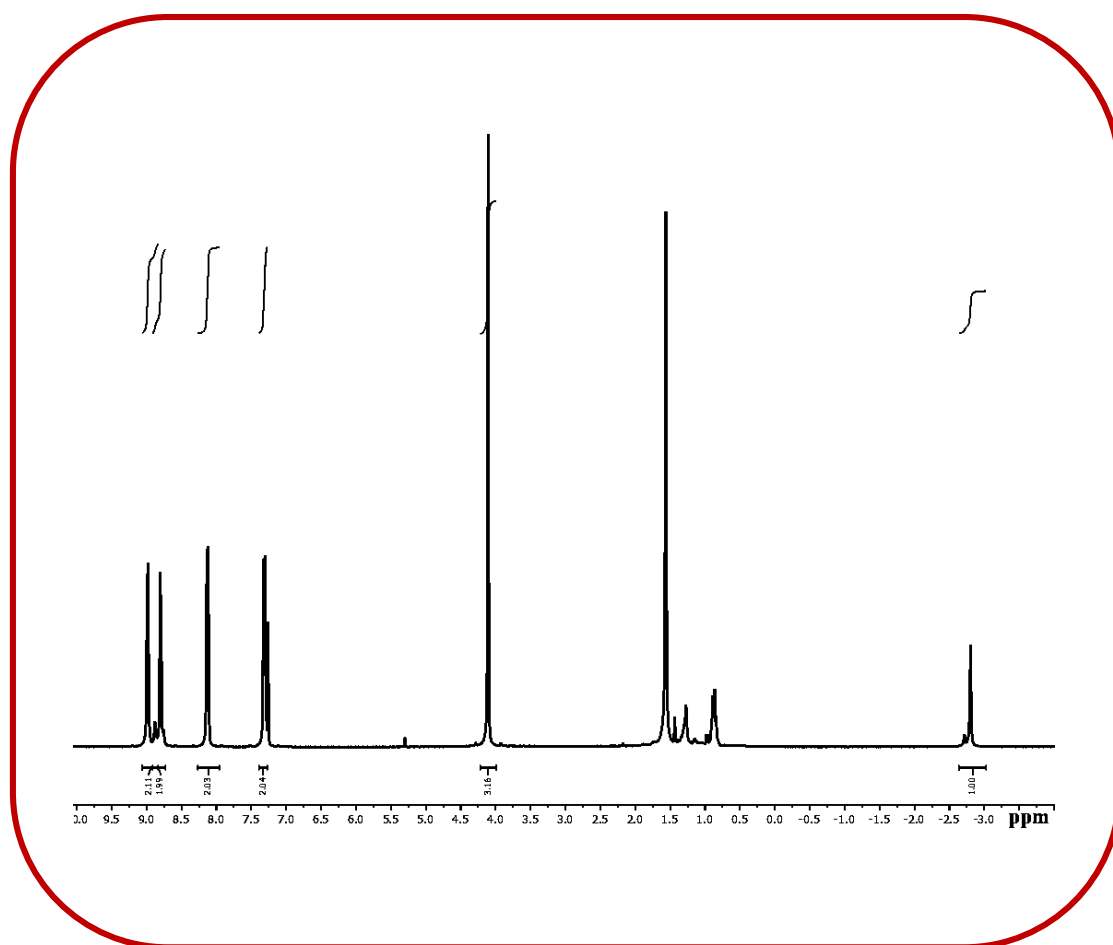


**Figure 2.14**  $^1\text{H}$  NMR spectrum of 5,15-Bis(4-methoxyphenyl)-10,20-diphenylporphyrin, **4** in  $\text{CDCl}_3$ .

**For 5,15-Bis(4-cyanophenyl)-10,20-diphenylporphyrin, **5****

Yield: 18% (1g). Anal. Calcd (found) for  $\text{C}_{46}\text{H}_{28}\text{N}_6$  (**5**): C, 83.11 (83.10); H, 4.25 (4.33); N, 12.64 (12.77).  $^1\text{H}$  NMR (400 MHz, Chloroform-*d*)  $\delta$  8.90 (d,  $J = 4.8$  Hz, 4H), 8.74 (d,  $J = 4.9$  Hz, 4H), 8.34 (d,  $J = 7.8$  Hz, 4H), 8.25 – 8.17 (m, 4H), 8.08 (d,  $J = 7.8$  Hz, 4H), 7.85 – 7.73 (m, 6H), -2.82 (s, 2H) (Figure 2.15). Other analytical data are consistent with the previously reported authentic compounds. <sup>29</sup>

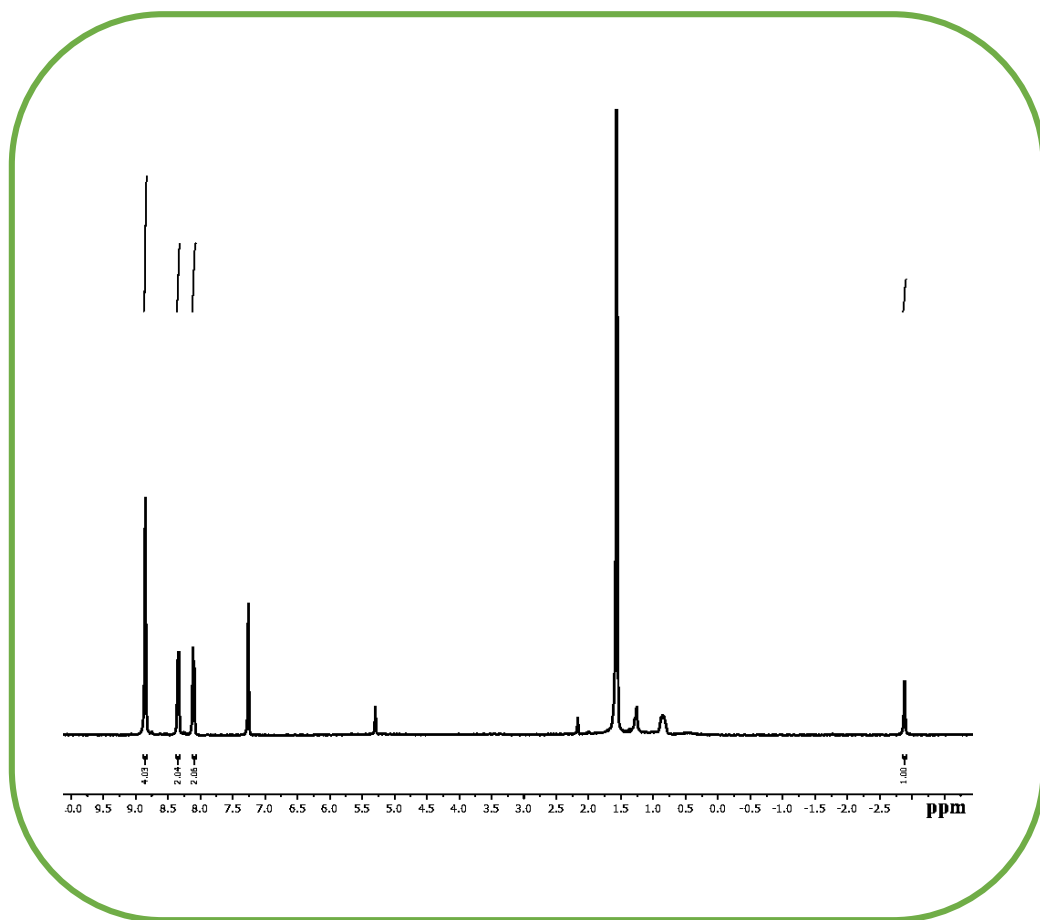




**Figure 2.16**  $^1\text{H}$  NMR spectrum of 5,15-Bis(4-methoxyphenyl)-10,20-bis(pentafluorophenyl)porphyrin, **6** in  $\text{CDCl}_3$ .

**For 5,15-bis(4-cyanophenyl)-10,20-bis(pentafluorophenyl)porphyrin, **7****

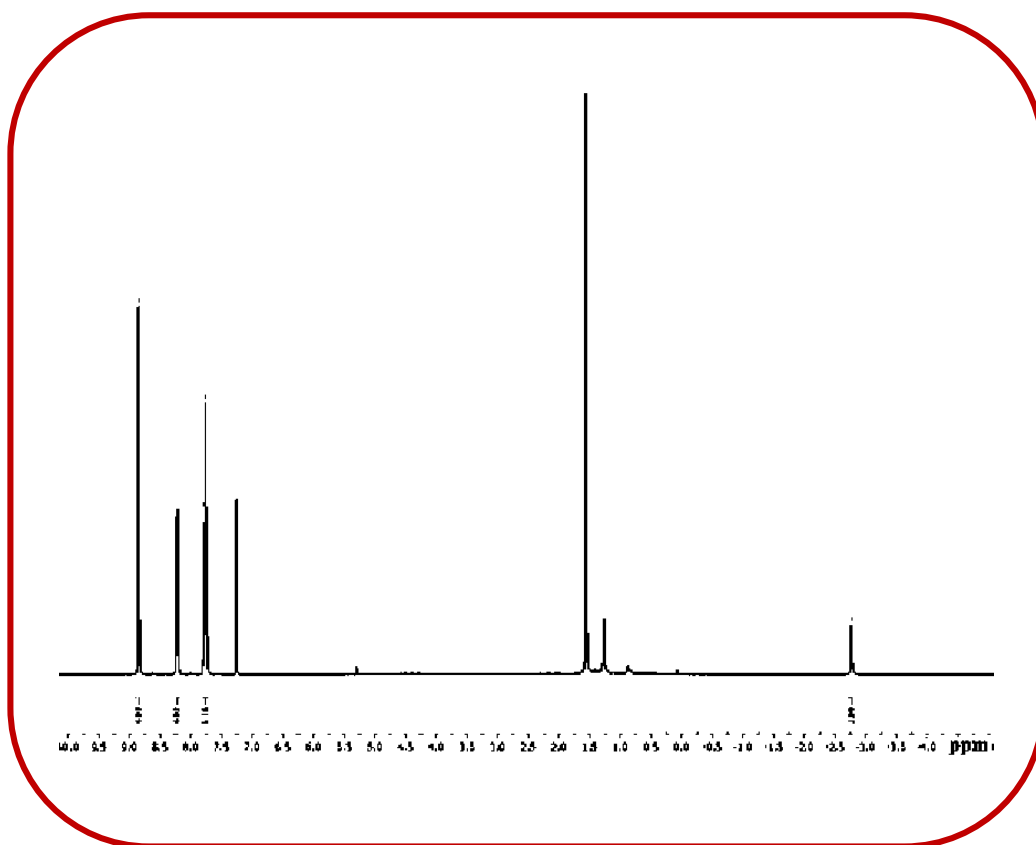
Yield: 15% (25 mg). Anal. Calcd (found) for  $\text{C}_{46}\text{H}_{18}\text{F}_{10}\text{N}_6$  (**7**): C, 65.41 (65.54); H, 2.15 (2.32); N, 9.95 (9.86).  $^1\text{H}$  NMR (400 MHz, Chloroform-*d*)  $\delta$  8.86 (s, 8H), 8.35 (d,  $J = 7.7$  Hz, 4H), 8.11 (d,  $J = 7.7$  Hz, 4H), -2.89 (s, 2H) (Figure 2.17). Other analytical data are consistent with the previously reported authentic compounds.<sup>30</sup>



**Figure 2.17**  $^1\text{H}$  NMR spectrum of 5,15-bis(4-cyanophenyl)-10,20-bis(pentafluorophenyl)porphyrin, **7** in  $\text{CDCl}_3$ .

#### For 5,10,15,20-Tetraphenylporphyrin, **8**

Yield: 13% (1.9 g). Anal. Calcd (found) for  $\text{C}_{44}\text{H}_{30}\text{N}_4$  (**8**): C, 85.97 (85.83); H, 4.92 (5.01); N, 9.11 (9.16).  $^1\text{H}$  NMR (400 MHz, Chloroform-*d*)  $\delta$  8.85 (s, 8H), 8.23 (m, 8H), 7.77 (m, 12H), -2.77 (s, 2H) (Figure 2.18). Other analytical data are consistent with the previously reported authentic compounds.<sup>31</sup>

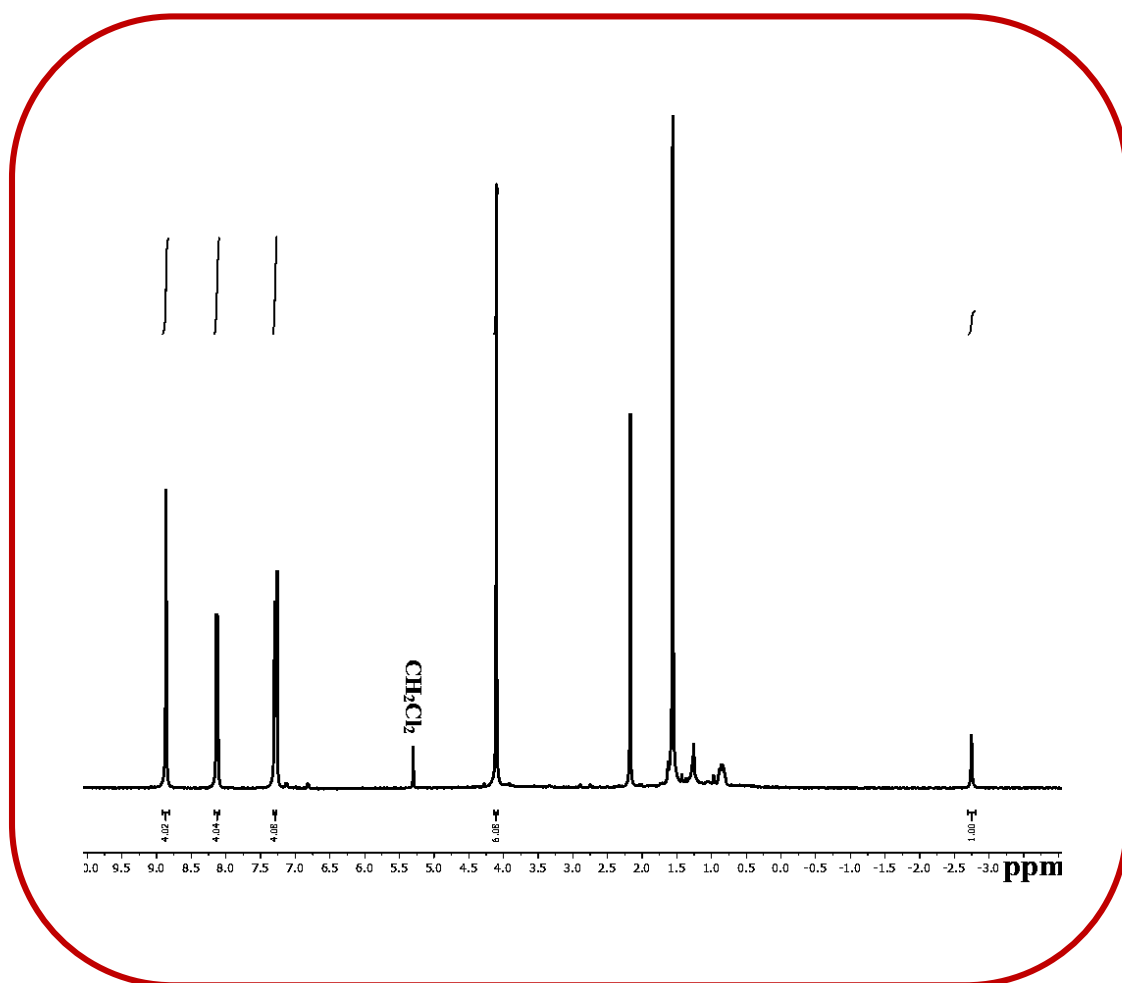


**Figure 2.18**  $^1\text{H}$  NMR spectrum of 5,10,15,20-tetraphenylporphyrin, **8** in  $\text{CDCl}_3$ .

**For 5,10,15,20-Tetrakis(4-methoxyphenyl)porphyrin, **9****

Yield: 10% (140 mg). Anal. Calcd (found) for  $\text{C}_{48}\text{H}_{38}\text{N}_4\text{O}_4$  (**9**): C, 78.45 (78.51); H, 5.21 (5.32); N, 7.62 (7.77).  $^1\text{H}$  NMR (400 MHz, Chloroform- $d$ )  $\delta$  8.86 (s, 8H), 8.14 (m, 8H), 7.30 (m, 8H), 4.10 (s, 12H), -2.75 (s, 2H) (Figure 2.19). Other analytical data are consistent with the previously reported authentic compounds.<sup>32</sup>





**Figure 2.19**  $^1\text{H}$  NMR spectrum of 5,10,15,20-tetrakis(4-methoxyphenyl)porphyrin, **9** in  $\text{CDCl}_3$ .

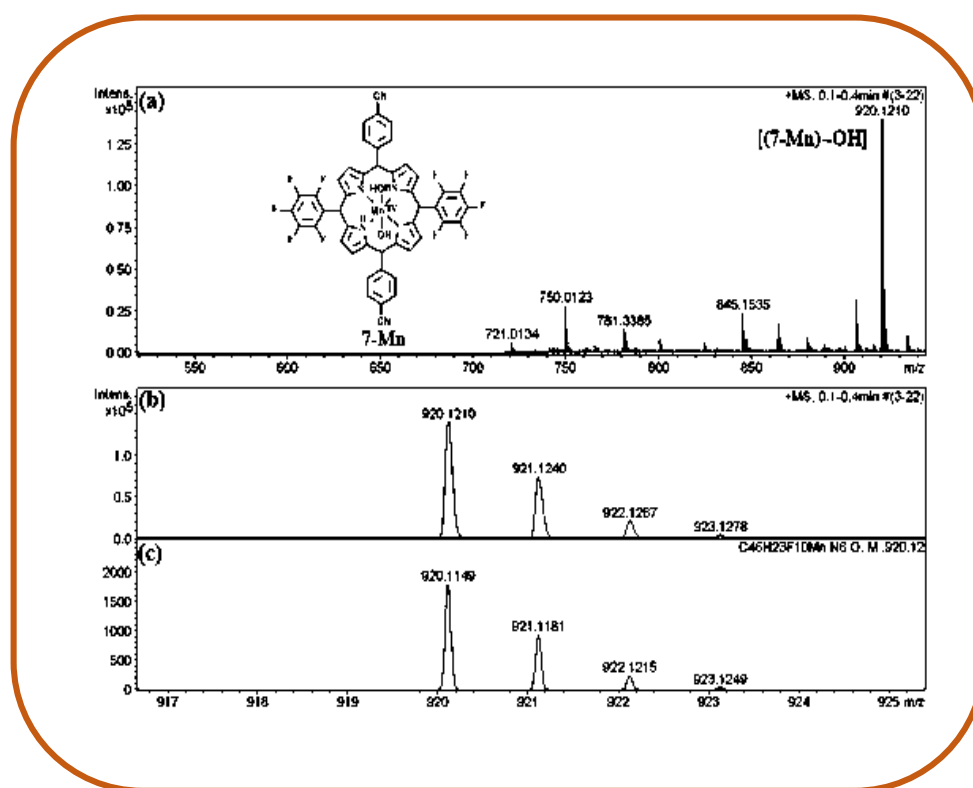
#### For Mn(IV)- porphyrinogen derivative, **7-Mn**

Anal. Calcd (found) for  $\text{C}_{46}\text{H}_{24}\text{F}_{10}\text{MnN}_6\text{O}_2$  (**7-Mn**): C, 58.92 (58.81); H, 2.58 (2.67); N, 8.96 (8.85).  $\lambda_{\text{max}}/\text{nm}$  ( $\epsilon/\text{M}^{-1}\text{cm}^{-1}$ ) in dichloromethane: 416 (10860), 470 (7970), 576 (4020), 621 (7140) (Table 2.6). The electrospray mass spectrum in acetonitrile showed peaks centred at  $m/z = 920.1210$  correspond to  $[\mathbf{7-Mn-OH}]^+$  (920.1149 calcd for  $\text{C}_{46}\text{H}_{23}\text{F}_{10}\text{MnN}_6\text{O}$ ) (Figure 2.20).

**Table 2.6** UV–Vis. Data <sup>a</sup>

Compound	UV–vis. Data <sup>a</sup>
	$\lambda_{\text{max}}$ / nm ( $\epsilon$ / M <sup>-1</sup> cm <sup>-1</sup> )
<b>7-Mn</b> <sup>a</sup>	416 (10,860), 470 (7970), 576 (4020), 621 (7140)

<sup>a</sup> In dichloromethane.

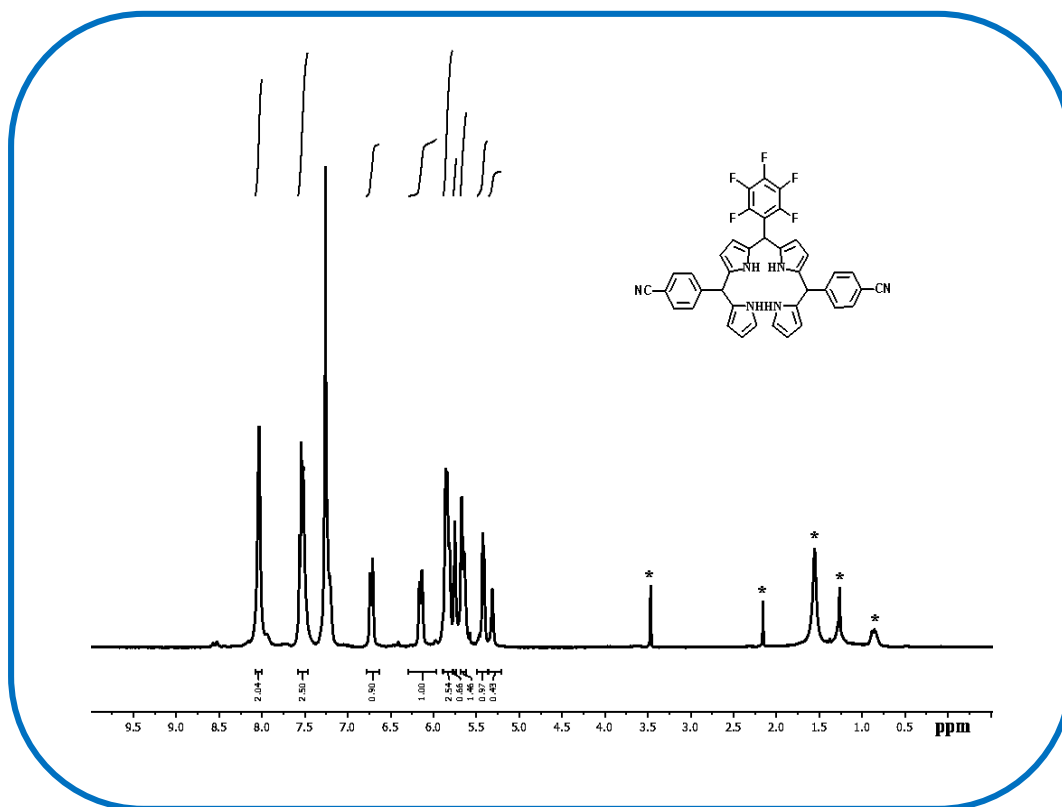


**Figure 2.20** ESI- MS spectrum in CH<sub>3</sub>CN shows the (a) measured spectrum, (b) isotopic distribution pattern (experimental), and (c) isotopic distribution pattern (simulated) of **7-Mn**.

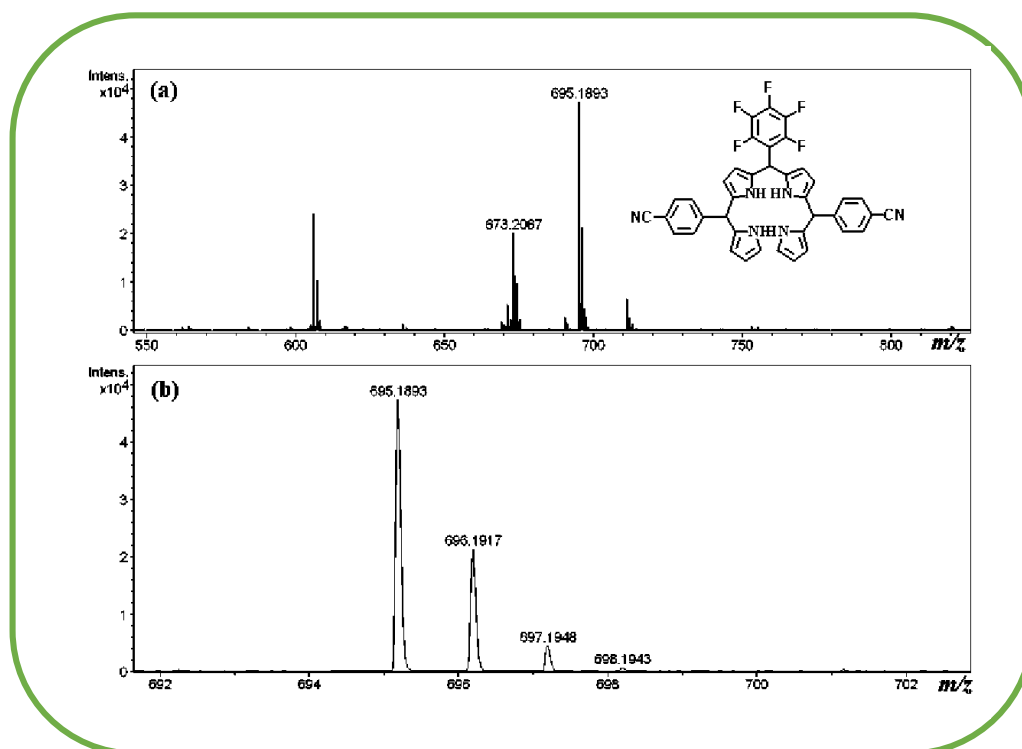
---

**For 5,15-bis(4-cyanophenyl)-10-(pentafluorophenyl) tetrapyrane**

Yield: 30% (41 mg). Anal. Calcd (found) for  $C_{39}H_{25}F_5N_6$ : C, 69.64 (69.77); H, 3.75 (3.84); N, 12.49 (12.37).  $^1H$  NMR (400 MHz, Chloroform-*d*)  $\delta$  8.14 – 7.86 (br s, 4H), 7.53 (m, 5H), 6.79 – 6.60 (m, 2H), 6.15 (dt,  $J = 11.2, 3.0$  Hz, 2H), 5.97 – 5.53 (m, 9H), 5.42 (d,  $J = 6.3$  Hz, 2H), 5.31 (s, 1H) (Figure 2.21). The electrospray mass spectrum in acetonitrile showed peaks centred at  $m/z = 695.1893$  correspond to  $[M+Na^+]$  (695.196 calcd for  $C_{39}H_{25}F_5N_6Na$ ) (Figure 2.22).



**Figure 2.21**  $^1H$  NMR spectrum of 5,15-bis(4-cyanophenyl)-10-(pentafluorophenyl) tetrapyrane in  $CDCl_3$ .



**Figure 2.22** ESI- MS spectrum in CH<sub>3</sub>CN shows the (a) measured spectrum, (b) isotopic distribution pattern of 5,15-bis(4-cyanophenyl)-10-(pentafluorophenyl)tetrapyrane.

---

## References

- (1) (a) Groves, J. T., *J. Inorg. Biochem.* **2006**, *100*, 434-447; (b) Que Jr, L.; Tolman, W. B., *Nature* **2008**, *455*, 333; (c) Collman, J. P.; Brauman, J. I.; Halbert, T. R.; Suslick, K. S., *Proc. Natl. Acad. Sci. U.S.A.* **1976**, *73*, 3333-3337; (d) Dolphin, D., *The Porphyrins V7: Biochemistry*, Elsevier, **2012**.
- (2) (a) Fukuzumi, S.; Imahori, H., *Electron Transfer in Chemistry* **2001**, 927-975; (b) Seely, G., *Photochem. Photobiol.* **1978**, *27*, 639-654; (c) Kadish, K. M.; Smith, K. M.; Guillard, R., *The Porphyrin Handbook: Inorganic, organometallic and coordination chemistry, Vol. 1-20*, Elsevier, **2000**; (d) Kadish, K. M., *Porphyrin Science: With Applications to Chemistry, Physics, Materials Science, Engineering, Biology and Medicine, Vol. 1*, World Scientific, 2010.
- (3) (a) Meunier, B., *Chem. Rev.* **1992**, *92*, 1411-1456; (b) Smith, K. M., *Porphyrins and metalloporphyrins, Vol. 9*, Elsevier Amsterdam, **1975**; (c) Fleischer, E. B., *Acc. Chem. Res.* **1970**, *3*, 105-112; (d) Nakano, A.; Osuka, A.; Yamazaki, I.; Yamazaki, T.; Nishimura, Y., *Angew. Chem. Int. Ed.* **1998**, *37*, 3023-3027; (e) Osuka, A.; Mataga, N.; Okada, T., *Pure Appl. Chem.* **1997**, *69*, 797-802; (f) Furuta, H.; Asano, T.; Ogawa, T., *J. Am. Chem. Soc.* **1994**, *116*, 767-768; (g) Sessler, J. L.; Burrell, A. K., *Macrocycles* **1992**, 177-273; (h) Lemon, C. M.; Brothers, P. J.; Boitrel, B., *Dalton Trans.* **2011**, *40*, 6591-6609; (i) Sinha, W.; Sommer, M. G.; Deibel, N.; Ehret, F.; Sarkar, B.; Kar, S., *Chem. Eur. J.* **2014**, *20*, 15920-15932; (j) Sinha, W.; Sommer, M. G.; Deibel, N.; Ehret, F.; Bauer, M.; Sarkar, B.; Kar, S., *Angew. Chem. Int. Ed.* **2015**, *54*, 13769-13774; (k) Sinha, W.; Sommer, M. G.; Hettmanczyk, L.; Patra, B.; Filippou, V.; Sarkar, B.; Kar, S., *Chem. Eur. J.* **2017**, *23*, 2396-2404; (l) Patra, B.; Sobottka, S.; Sinha, W.; Sarkar, B.; Kar, S., *Chem. Eur. J.* **2017**, *23*, 13858-13863; (m) Garai, A.;
-

- 
- Sobottka, S.; Schepper, R.; Sinha, W.; Bauer, M.; Sarkar, B.; Kar, S., *Chem. - Eur. J.* **2018**, *24*, 12613-12622; (n) Patra, B.; Sobottka, S.; Mondal, S.; Sarkar, B.; Kar, S., *Chem. Commun.* **2018**, *54*, 9945-9948; (o) Padilla, R.; Buckley, H. L.; Ward, A. L.; Arnold, J., *Chem. Commun.* **2014**, *50*, 2922-2924; (p) Gros, C. P.; Brisach, F.; Meristoudi, A.; Espinosa, E.; Guillard, R.; Harvey, P. D., *Inorg. Chem.* **2007**, *46*, 125– 135; (q) Ward, A. L.; Buckley, H. L.; Lukens, W. W.; Arnold, J., *J. Am. Chem. Soc.* **2013**, *135*, 13965-13971.
- (4) (a) Fischer H.; Gleim W., *Justus Liebigs Ann. Chem.* **1936**, *521*, 157-160; (b) Vicente, M. G. H.; Smith, K. M., *Curr. Org. Chem.* **2000**, *4*, 139-174.
- (5) Rothmund, P., *J. Am. Chem. Soc.* **1936**, *58*, 625-627.
- (6) Adler, A. D.; Longo, F. R.; Finarelli, J. D.; Goldmacher, J.; Assour, J.; Korsakoff, L., *J. Org. Chem.* **1967**, *32*, 476-476.
- (7) (a) Geier III, G. R.; Lindsey, J. S., *J. Chem. Soc., Perkin Trans 2* **2001**, 677-686; (b) Littler, B. J.; Ciringh, Y.; Lindsey, J. S., *J. Org. Chem.* **1999**, *64*, 2864-2872.
- (8) (a) Salamończyk, M.; Pocięcha, D.; Nowak-Król, A.; Koszelewski, D.; Gryko, D. T.; Górecka, E., *Chem. Eur. J.* **2015**, *21*, 7384-7388; (b) Beyzavi, M. H.; Nietzold, C.; Reissig, H. U.; Wiehe, A., *Adv. Synth. Catal.* **2013**, *355*, 1409-1422; (c) Youngblood, W. J., *J. Org. Chem.* **2006**, *71*, 3345-3356.
- (9) Yadav, O.; Varshney, A.; Kumar, A., *Inorg. Chem. Commun.* **2017**, *86*, 168-171.
- (10) (a) Richens, D. T.; Sawyer, D. T., *J. Am. Chem. Soc.* **1979**, *101*, 3681-3683; (b) Romain, S.; Baffert, C.; Duboc, C.; Leprêtre, J.-C.; Deronzier, A.; Collomb, M.-N. I., *Inorg. Chem.* **2009**, *48*, 3125-3131; (c) Gupta, R.; Taguchi, T.; Borovik, A.; Hendrich, M. P., *Inorg. Chem.* **2013**, *52*, 12568-12575; (d) Chun, H.; Chaudhuri, P.; Weyhermüller, T.; Wieghardt, K., *Inorg. chem.* **2002**, *41*, 790-795; (e) Bougher, C. J.; Liu, S.; Hicks, S. D.; Abu-Omar, M. M., *J. Am. Chem. Soc.* **2015**,
-

- 
- 137, 14481-14487; (f) Ding, M.; Cutsail III, G.; Aravena, D.; Amoza, M.; Rouzières, M.; Dechambenoit, P.; Losovyj, Y.; Pink, M.; Ruiz, E.; Clérac, R., *Chem. Sci.* **2016**, 7, 6132-6140; (g) Halbach, R. L.; Gygi, D.; Bloch, E. D.; Anderson, B. L.; Nocera, D. G., *Chem. Sci.* **2018**, 9, 4524-4528.
- (11) (a) Wieghardt, K.; Bossek, U.; Nuber, B.; Weiss, J.; Bonvoisin, J.; Corbella, M.; Vitols, S.; Girerd, J., *J. Am. Chem. Soc.* **1988**, 110, 7398-7411; (b) Mukherjee, S.; Weyhermüller, T.; Bothe, E.; Wieghardt, K.; Chaudhuri, P., *Dalton Trans.* **2004**, 3842-3853.
- (12) (a) Passard, G.; Dogutan, D. K.; Qiu, M.; Costentin, C.; Nocera, D. G., *ACS Catalysis* **2018**, 8, 8671-8679; (b) Chan, M. K.; Armstrong, W. H., *Inorg. Chem.* **1989**, 28, 3777-3779.
- (13) (a) Zaragoza, J. P. T.; Siegler, M. A.; Goldberg, D. P., *J. Am. Chem. Soc.* **2018**, 140, 4380-4390; (b) Kurahashi, T.; Kikuchi, A.; Tosha, T.; Shiro, Y.; Kitagawa, T.; Fujii, H., *Inorg. Chem.* **2008**, 47, 1674-1686; (c) Charnock, J. M.; Garner, C. D.; Trautwein, A. X.; Bill, E.; Winkler, H.; Ayougou, K.; Mandon, D.; Weiss, R., *Angew. Chem., Int. Ed.* **1995**, 34, 343-346; (d) Kovacs, J. A., *Acc. Chem. Res.* **2015**, 48, 2744-2753.
- (14) (a) Kim, S. H.; Park, H.; Seo, M. S.; Kubo, M.; Ogura, T.; Klajn, J.; Gryko, D. T.; Valentine, J. S.; Nam, W., *J. Am. Chem. Soc.* **2010**, 132, 14030-14032; (b) Sawant, S. C.; Wu, X.; Cho, J.; Cho, K. B.; Kim, S. H.; Seo, M. S.; Lee, Y. M.; Kubo, M.; Ogura, T.; Shaik, S., *Angew. Chem., Int. Ed.* **2010**, 122, 8366-8370; (c) Fukuzumi, S.; Fujioka, N.; Kotani, H.; Ohkubo, K.; Lee, Y.-M.; Nam, W., *J. Am. Chem. Soc.* **2009**, 131, 17127-17134; (d) Naruta, Y.; Maruyama, K., *J. Am. Chem. Soc.* **1991**, 113, 3595-3596; (e) Shimazaki, Y.; Nagano, T.; Takesue, H.; Ye, B. H.; Tani, F.; Naruta, Y., *Angew. Chem.* **2004**, 43, 98-100; (f) Guo, M.;
-

- 
- Corona, T.; Ray, K.; Nam, W., *ACS Central Science* **2018**, *5*, 13-28; (g) Brazzolotto, D.; Cantú Reinhard, F. G.; Smith-Jones, J.; Retegan, M.; Amidani, L.; Faponle, A. S.; Ray, K.; Philouze, C.; de Visser, S. P.; Gennari, M., *Angew. Chem.* **2017**, *129*, 8323-8327; (h) Leto, D. F.; Jackson, T. A., *Inorg. Chem.* **2014**, *53*, 6179-6194; (i) Shi, S.; Wang, Y.; Xu, A.; Wang, H.; Zhu, D.; Roy, S. B.; Jackson, T. A.; Busch, D. H.; Yin, G., *Angew. Chem. Int. Ed.* **2011**, *123*, 7459-7462; (j) Leto, D. F.; Ingram, R.; Day, V. W.; Jackson, T. A., *Chem. Commun.* **2013**, *49*, 5378-5380; (k) Chattopadhyay, S.; Geiger, R. A.; Yin, G.; Busch, D. H.; Jackson, T. A., *Inorg. Chem.* **2010**, *49*, 7530-7535; (l) Yin, G.; Danby, A. M.; Kitko, D.; Carter, J. D.; Scheper, W. M.; Busch, D. H., *J. Am. Chem. Soc.* **2008**, *130*, 16245-16253; (m) Rice, D. B.; Massie, A. A.; Jackson, T. A., *Acc. Chem. Res.* **2017**, *50*, 2706-2717.
- (15) (a) da GH Vicente, M.; M Smith, K., *Curr. Org. Synth.* **2014**, *11*, 3-28; (b) Gradillas, A.; del Campo, C.; Sinisterra, J. V.; Llama, E. F., *J. Chem. Soc. Perkin Trans. I* **1995**, 2611-2613.
- (16) (a) Liddell, P. A.; Olmstead, M. M.; Smith, K. M., *J. Am. Chem. Soc.* **1990**, *112*, 2038-2040; (b) Licoccia, S.; Di Vona, M. L.; Paolesse, R., *J. Org. Chem.* **1998**, *63*, 3190-3195; (c) Bröring, M.; Hell, C., *Chem. Commun.* **2001**, 2336-2337.
- (17) Lin, J. J.; Gerzevske, K. R.; Liddell, P. A.; Senge, M. O.; Olmstead, M. M.; Khoury, R. G.; Weeth, B. E.; Tsao, S. A.; Smith, K. M., *J. Org. Chem.* **1997**, *62*, 4266-4276.
- (18) Koszarna, B.; Gryko, D. T., *J. Org. Chem.* **2006**, *71*, 3707-3717.
- (19) Ahlrichs, R.; Bär, M.; Häser, M.; Horn, H.; Kölmel, C., *Chem. Phys. Lett.* **1989**, *162*, 165-169.
- (20) Treutler, O.; Ahlrichs, R., *J. Chem. Phys.* **1995**, *102*, 346-354.
-



- 
- (21) Eichkorn, K.; Treutler, O.; Oehm, H.; Häser, M.; Ahlrichs, R., *Chem. Phys.* **1995**, *242*, 652-660.
- (22) Eichkorn, K.; Weigend, F.; Treutler, O.; Ahlrichs, R., *Theor. Chem. Acc.* **1997**, *97*, 119-124.
- (23) Sierka, M.; Hogekamp, A.; Ahlrichs, R., *J. Chem. Phys.* **2003**, *118*, 9136-9148.
- (24) Frisch, M. J. ; Trucks, G. W.; Schlegel, H. B.; Scuseria, G. E.; Robb, M. A.; Cheeseman, J. R.; Scalmani, G.; Barone, V.; Mennucci, B., *Gaussian 09, Revision C.01*; Gaussian, Inc.: Wallingford, CT, **2011**.
- (25) Rao, P. D.; Littler, B. J.; Geier, G. R.; Lindsey, J. S., *J. Org. Chem.* **2000**, *65*, 1084-1092.
- (26) Lang, T.; Guenet, A.; Graf, E.; Kyritsakas, N.; Hosseini, M. W., *Chem. Commun.* **2010**, *46*, 3508-3510.
- (27) Littler, B. J.; Ciringh, Y.; Lindsey, J. S., *J. Org. Chem.* **1999**, *64*, 2864-2872.
- (28) Goldberg, P. K.; Pundsack, T. J.; Splan, K. E., *J. Phys. Chem. A* **2011**, *115*, 10452-10460.
- (29) Krebs, F. C.; Hagemann, O.; Spanggaard, H., *J. Org. Chem.* **2003**, *68*, 2463-2466.
- (30) Kooriyaden, F. R.; Sujatha, S.; Varghese, B.; Arunkumar, C., *J. Fluorine Chem.* **2015**, *170*, 10-16.
- (31) Saucedo, L.; Mink, L. M., *J. Chem. Educ.* **2005**, *82*, 790.
- (32) Milanesio, M.; Alvarez, M.; Yslas, E.; Borsarelli, C.; Silber, J.; Rivarola, V.; Durantini, E., *Photochem. Photobiol.* **2001**, *74*, 14-21.

# CHAPTER 3

## Synthesis and characterization of Antimony(V)–oxo corrole complexes

- 3.1 Introduction
- 3.2 Results and discussion
  - 3.2.1 Synthesis and characterization
  - 3.2.2 Crystal structure
  - 3.2.3 NMR spectra
  - 3.2.4 UV-Vis and emission spectroscopy
  - 3.2.5 Redox properties
- 3.3 Conclusions
- 3.4 Experimental section
  - 3.4.1 Materials
  - 3.4.2 Physical Measurements
  - 3.4.3 Crystal Structure Determination
  - 3.4.4 Synthesis
    - 3.4.4.1 Synthesis of 5,10,15-Triphenylcorrolato-antimony(III), **1**
    - 3.4.4.2 Synthesis of 5,10,15-Tris[3,4-(1,4-dioxan)phenyl]corrolato-antimony(III), **2**
    - 3.4.4.3 Synthesis of (5,10,15-Triphenylcorrolato)(oxo)antimony(V), **3**
    - 3.4.4.4 Synthesis of (5,10,15-Tris[3,4-(1,4-dioxan)phenyl]corrolato)(oxo) antimony(V), **4**

---

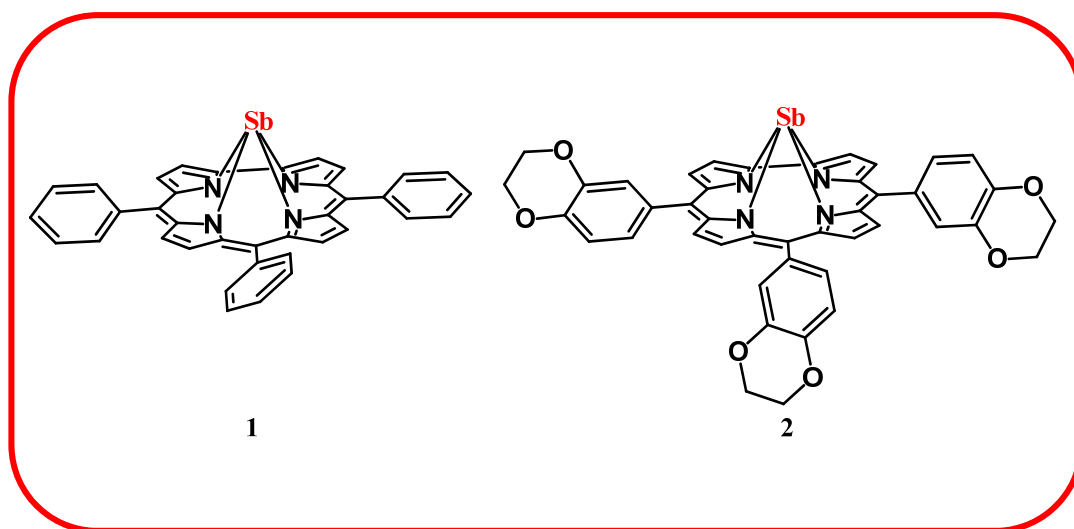
### 3.1 Introduction

For the photocatalytic substrate oxidation at room temperature, it is often invoked that the best possible choice is a metal complex bearing a tetrapyrrolic macrocycle as a ligand and a redox-active group 14 or 15 element<sup>1</sup>. A metal-centered (MC) triplet state is responsible for the photocatalytic activity of these low valent groups 14 and 15 (main group) metal complexes<sup>2-5</sup>. Being a group 15 redox-active element, the most commonly found oxidation states of antimony are +III and +V<sup>6</sup>. High-valent antimony(V)–porphyrin complexes are extensively studied for various applications due to their propensity to attach to a wide variety of axial ligands (*e.g.*, O<sup>−</sup>, N<sup>−</sup>, and S–donor ligands)<sup>7-13</sup>. A series of electron-rich molecules like phosphine, alkene, etc., can be conveniently oxidized by antimony-porphyrin cation radicals owing to the high redox potential of antimony-porphyrin complexes<sup>14-21</sup>. Antimony porphyrin complexes are extensively used as photocatalysts using a visible light source for various organic transformations<sup>14-21</sup>. Although there are few reports on the antimony-porphyrin complexes as a potent photocatalyst for various organic reactions<sup>14-21</sup>. However, such reports on corrole, a contracted version of porphyrin are very limited<sup>22-27</sup>. Among the tetrapyrrolic macrocycle, the corrole chemistry is recently gaining a lot of interest<sup>28-48</sup>. In this context, it is important that contrary to porphyrin, corrole is trianionic in nature and thus stabilizes metals in higher oxidation states. The fascinating chemistry of antimony corroles is rarely reported in the literature<sup>22-27</sup>. In this context, Kadish *et al.* have synthesized and characterized the antimony complex of octaethylcorroles in three (+III, +IV, +V) different oxidation states<sup>22</sup>. Gross *et al.* have successfully synthesized and characterized antimony corroles and used them in aerobic oxygenation reactions<sup>23</sup>. Nocera *et al.* have synthesized and characterized Sb(III) and Sb(V) corrole complexes bearing chloride and bromide as axial ligands. They have further demonstrated that the

---

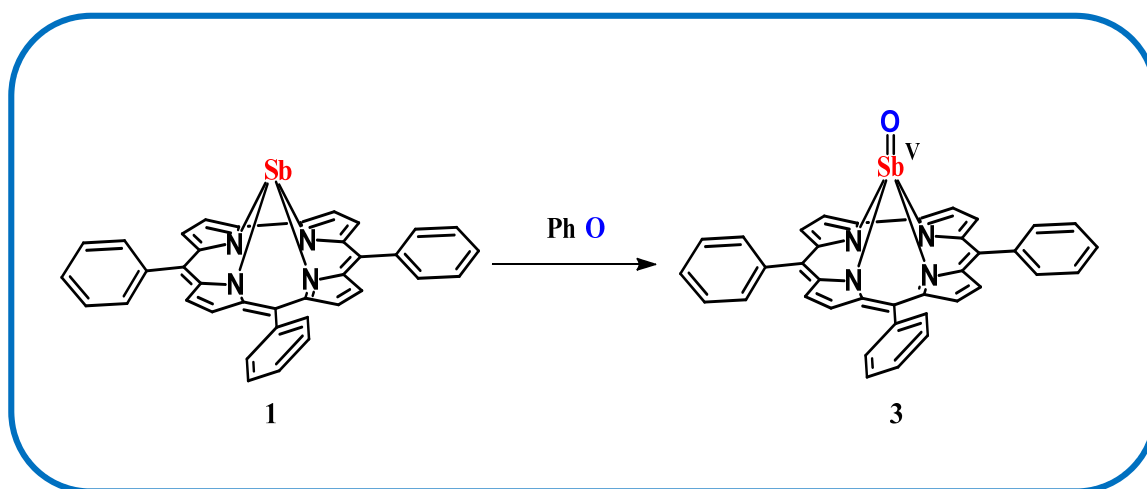
interconversion from Sb(V) to Sb(III) corroles can occur via photo-elimination of axial halide ligands<sup>24</sup>. Gross *et al.* have reported that difluoroantimony(V) corrole complex can act as a potent photocatalyst and perform the bromide to bromine conversion while using visible light<sup>25</sup>.

The present report describes the synthesis and characterization of two novel corrolato-Sb<sup>III</sup> complexes namely, 5,10,15-Triphenylcorrolato-antimony(III), **1**; 5,10,15-Tris[3,4-(1,4-dioxan)phenyl]corrolato-antimony(III), **2** (Figure 3.1). The generated corrolato-antimony(III) complexes were characterized by various spectroscopic techniques, including single-crystal X-ray structure of a representative complex 5,10,15-Triphenylcorrolato-antimony(III), **1**. The choice of the ligand framework is obvious here, as 5,10,15,20-tetraphenylporphyrinato is the most common framework in porphyrin research; thus, in analogy with that, we have chosen here 5,10,15-triphenylcorrolato. In addition to that, another ligand framework that bears electron-donating substituents, *i.e.*, 1,4-dioxan moiety at its periphery, is also chosen. Benzodioxan has been chosen here in the periphery of the corrole ligand as it contains the basic oxygen atoms and which are available for coordination with the central metal ion. Literature report suggests that the high-valent antimony (V) –porphyrin complexes have the propensity to attach to a wide variety of axial ligands like O–donor ligands<sup>7-13</sup>. Thus it is obvious that the oxygenated functional groups like benzodioxan in the periphery of the corrole ligand will dictate the self-assembly formation. These self-assembled systems, in turn, can tune the stability of the generated antimony (V)–oxo complexes.



**Figure 3.1** Structures of the 5,10,15-Triphenylcorrolato-antimony(III), **1**; 5,10,15-Tris[3,4-(1,4-dioxan)phenyl]corrolato-antimony(III), **2**.

While using the representative corrolato-antimony (III) complexes as the precursor complex and upon treatment with iodosobenzene as oxidant, the corresponding high-valent (corrolato)(oxo)antimony(V) complexes (Scheme 3.1) have been successfully synthesized. The respective (corrolato)(oxo) antimony(V) complexes (5,10,15-Triphenylcorrolato)(oxo)antimony(V), **3** and (5,10,15-Tris[3,4-(1,4-dioxan)phenyl] corrolato)(oxo)antimony(V), **4** were obtained in good yields. The generated high-valent antimony(V)–oxo corroles were characterized by various spectroscopic techniques. The photophysical aspects of all the four antimony–corroles have also been investigated here.



**Scheme 3.1** Synthesis of (5,10,15-Triphenylcorrolato)(oxo)antimony(V), **3** via oxidation of 5,10,15-Triphenylcorrolato-antimony(III), **1** by using iodosobenzene (PhIO).

## 3.2 Results and discussion

### 3.2.1 Synthesis and characterization

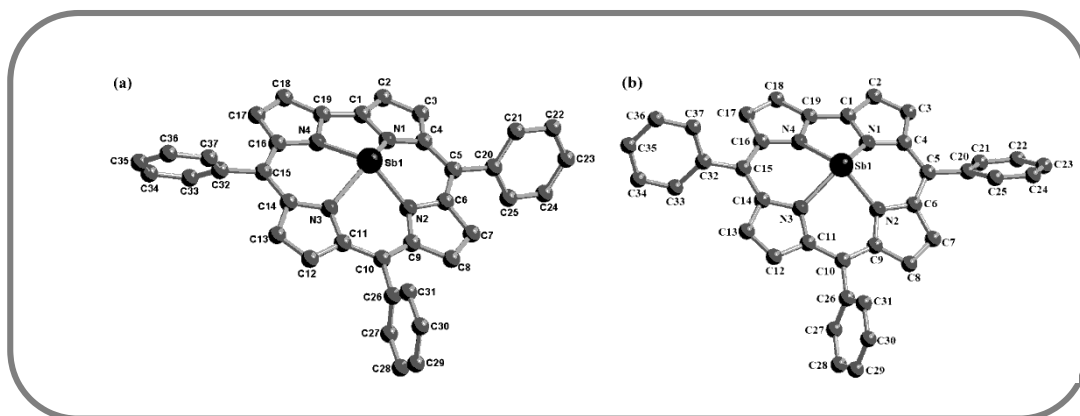
The Sb<sup>III</sup> corrole derivatives were synthesized by following an earlier literature report <sup>22</sup>. A mixture of the respective FB corroles and SbCl<sub>3</sub> was refluxed in a solution of pyridine till the fluorescence of starting FB corrole completely disappeared. Upon chromatographic separation, the corresponding Sb<sup>III</sup> corrole derivatives **1** and **2** were formed in good yields. The purity and identity of the Sb<sup>III</sup> corrole derivatives (**1** and **2**) have been demonstrated by their satisfactory CHN analyses and also by the *ESI*-MS data. The electrospray mass spectrum of **1** in acetonitrile (Figure 3.12) shows peaks centered at  $m/z = 644.068$ , corresponding to [M<sup>+</sup>] (calculated molecular mass: 644.096). The corrolato-oxo-antimony(V) derivatives were prepared by following an earlier literature report <sup>23</sup>. A mixture of the respective Sb<sup>III</sup> corrole and PhIO was stirred in a solution of

---

CH<sub>2</sub>Cl<sub>2</sub> till the starting corrolato-antimony(III) completely disappeared. Upon chromatographic separation, the corresponding corrolato-oxo-antimony(V) derivatives **3** and **4** were formed in good yields. The purity and identity of the corrolato-oxo-antimony(V) derivatives have been demonstrated by their satisfactory CHN analyses and also by the *ESI*-MS data.

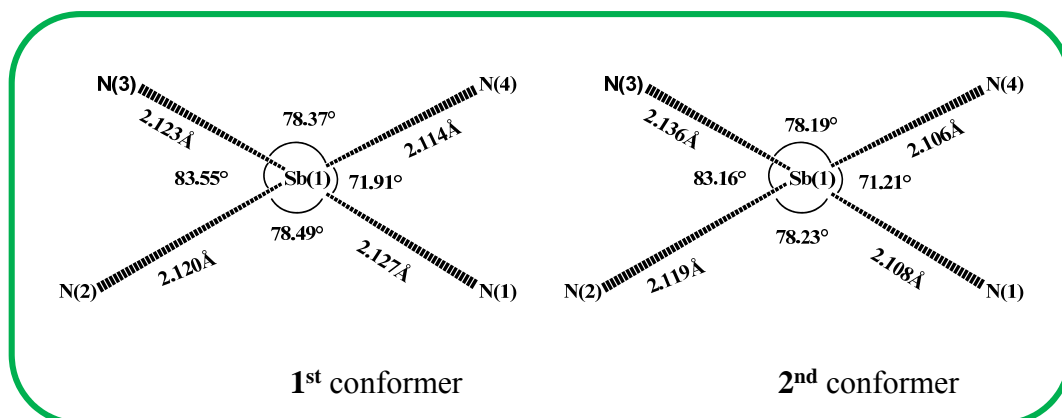
### 3.2.2 Crystal structure

The compound (5,10,15-Trisphenylcorrolato)antimony(III), **1**, crystallizes in two different conformations with slightly different bond lengths and angles in two different solvents. The crystal structures of both the conformers of **1** are shown in Figure 3.2. The compound crystallized in the triclinic space group as the 1<sup>st</sup> conformation with two molecules of **1** in each unit cell (Table 3.1). The 2<sup>nd</sup> conformation crystallized in the [monoclinic](#) space group with four molecules of **1** in each unit cell (Table 3.1). Selected crystallographic parameters of both the conformations have been reported in Table 3.1. The Sb<sup>III</sup> corrole is dome-shaped, and the deviation of the Sb<sup>III</sup> ion with respect to a plane consisting of four pyrrolic nitrogen atoms is ~0.963 Å ( 1<sup>st</sup> conformer) and ~0.966 Å ( 2<sup>nd</sup> conformer), respectively. This kind of dome-shaped geometry is frequently observed when a large central metal ion like Sb(III) is chelated with porphyrin/corrole cores. If the metal-nitrogen bond distances are significantly larger than one-half of the length of the diagonal N-N distances in the porphyrin/corrole core, a dome-shaped structure prevails. This is indeed the case here.



**Figure 3.2** Single-crystal X-ray structure of **1** (both the conformers are shown). (a) 1<sup>st</sup> conformer and (b) 2<sup>nd</sup> conformer.

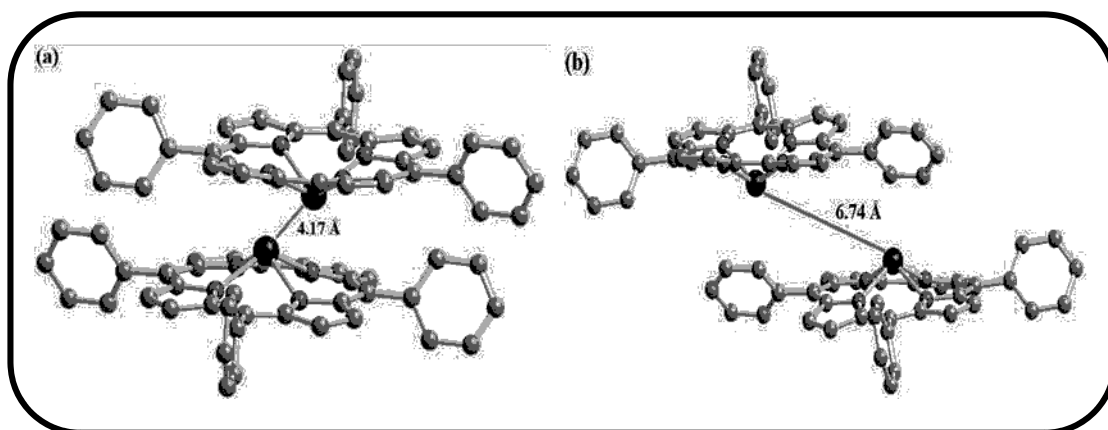
Herein, the Sb–N bond distances ( $\sim 2.12$  Å) are appreciably larger than the one-half of the diagonal N–N distances ( $\sim 1.90$  Å). Thus Sb(III) ion cannot fit into the corrole cavity and resides above the N<sub>4</sub> corrole core. The Sb–N bond distances are 2.127 Å (for Sb1–N1), 2.120 Å (for Sb1–N2), 2.123 Å (for Sb1–N3), and 2.114 Å (for Sb1–N4) in the 1<sup>st</sup> conformer. The Sb–N bond distances are 2.108 Å (for Sb1–N1), 2.119 Å (for Sb1–N2), 2.136 Å (for Sb1–N3), and 2.106 Å (for Sb1–N4) in the 2<sup>nd</sup> conformer. The N–Sb–N bond angles are 78.49°, 83.55°, 78.37°, and 71.91° in the 1<sup>st</sup> conformer. The N–Sb–N bond angles are 78.23°, 83.16°, 78.19°, and 71.21° in the 2<sup>nd</sup> conformer (Scheme 3.2).



**Scheme 3.2** Structural parameters of **1**<sup>st</sup> and **2**<sup>nd</sup> conformers



The dihedral angles between the *meso*-substituents at 5-, 10-, and 15- positions and the plane consisting of four pyrrolic nitrogen atoms are 57.67°, 88.62° and 71.69°, respectively, in the 1<sup>st</sup> conformer. The dihedral angles between the *meso*-substituents at 5-, 10-, and 15- positions and the plane consisting of four pyrrolic nitrogen atoms are 49.46°, 74.97°, and 48.66°, respectively, in the 2<sup>nd</sup> conformer. The closest Sb-Sb distance between a pair of **1** molecule is 4.17 Å in the 1<sup>st</sup> conformer (Figure 3.3). The closest Sb-Sb distance between a pair of **1** molecule is 6.74 Å in the 2<sup>nd</sup> conformer. Sb<sup>III</sup>-N bond lengths and N-Sb-N angles corroborated well with the previously reported Sb<sup>III</sup>-N bond lengths and N-Sb-N angles in relation to the Sb<sup>III</sup> corrole derivatives <sup>24</sup>.



**Figure 3.3** Single-crystal X-ray analysis of **1** revealing the closest Sb-Sb distances

(a) 1<sup>st</sup> conformer and (b) 2<sup>nd</sup> conformer.

**Table 3.1** Crystallographic data of **1** for both the conformers.

compound code	<b>1</b> (1 <sup>st</sup> conformer)	<b>1</b> (2 <sup>nd</sup> conformer)
molecular formula	<u>C<sub>37</sub>H<sub>23</sub>N<sub>4</sub>Sb</u>	<u>C<sub>37</sub>H<sub>23</sub>N<sub>4</sub>Sb</u>
Fw	645.35	645.35
Radiation	<u>Mo K<math>\alpha</math></u>	<u>Mo K<math>\alpha</math></u>
crystal symmetry	<u>Triclinic</u>	<u>Monoclinic</u>
space group	P-1	<u>P2<sub>1</sub>/c</u>
<i>a</i> (Å)	<u>10.8994 (4)</u> ,	<u>12.4741 (8)</u>
<i>b</i> (Å)	<u>11.3461 (5)</u> ,	<u>21.8912 (10)</u>
<i>c</i> (Å)	<u>12.0068 (5)</u>	<u>10.7274 (6)</u>
<i>a</i> (deg)	<u>76.495 (3)</u> ,	90
$\beta$ (deg)	<u>79.268 (3)</u> ,	<u>99.256 (5)</u>
<i>g</i> (deg)	<u>84.733 (3)</u>	90
<i>V</i> (Å <sup>3</sup> )	<u>1416.71 (10)</u>	<u>2891.2 (3)</u>
<i>Z</i>	<u>2</u>	<u>4</u>
$\mu$ (mm <sup>-1</sup> )	<u>1.01</u>	<u>0.99</u>
<i>T</i> (K)	<u>293</u>	298
<i>D</i> <sub>calcd</sub> (g cm <sup>-3</sup> )	1.513	1.483
2 $\theta$ range (deg)	4.52 to 60.48	6.612 to 53.464
<i>e</i> data ( <i>R</i> <sub>int</sub> )	<u>8247 (0.059)</u>	<u>6112 (0.073)</u>
<i>R</i> 1 ( <i>I</i> > 2 $\sigma$ ( <i>I</i> ))	0.0515	<u>0.037</u>
WR2 (all data)	0.1425	<u>0.081</u>
GOF	0.894	<u>1.02</u>
$\Delta\rho_{\text{max}}, \Delta\rho_{\text{min}}$ (e Å <sup>-3</sup> )	<u>1.47, -0.62</u>	<u>0.64, -0.36</u>

---

### 3.2.3 NMR spectra

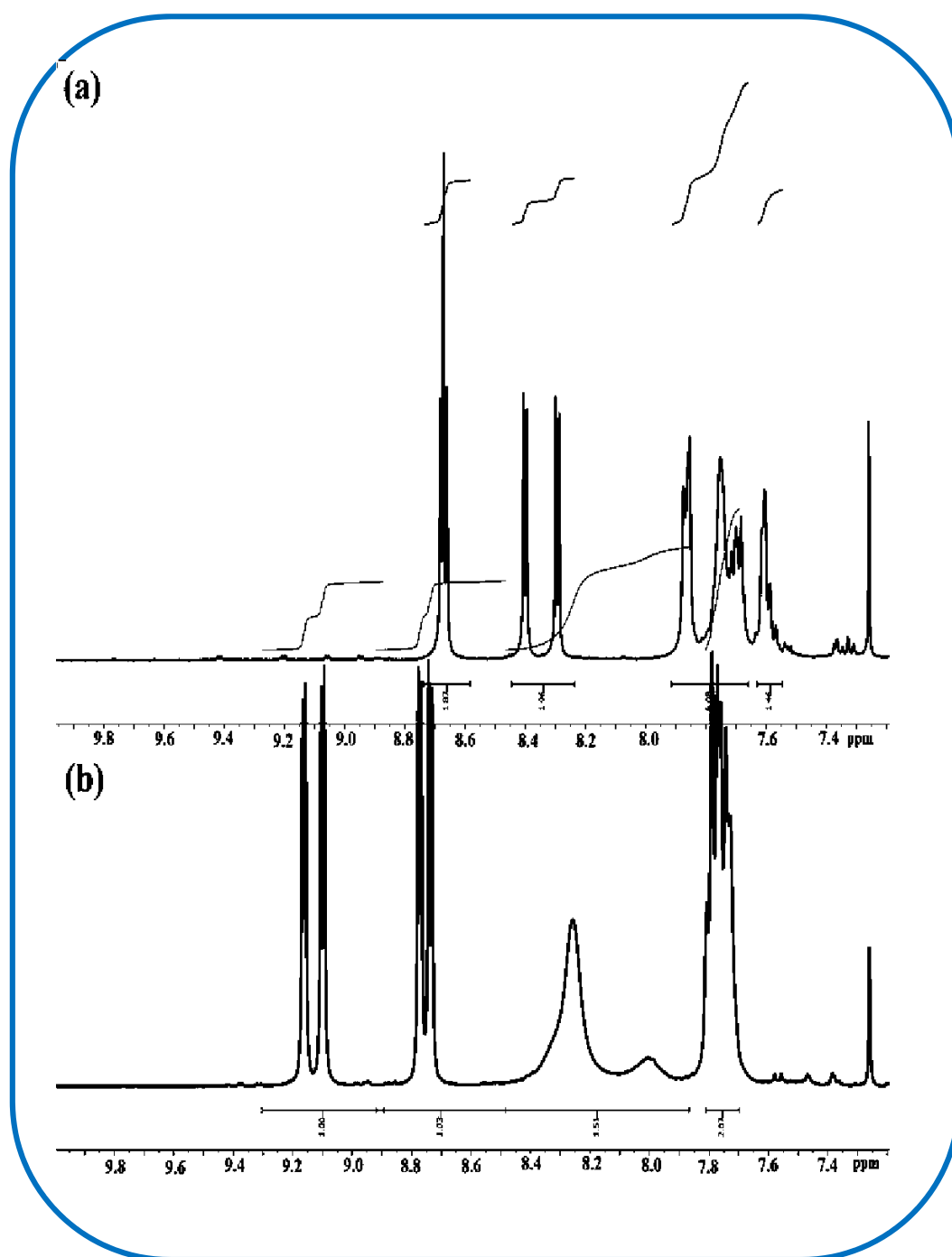
In the native states, all these antimony corroles are diamagnetic in nature (Figs. S5-S12) and are evident from the appearance of sharp peaks with normal chemical shifts in the  $^1\text{H}$  NMR spectrum of these complexes. **1** exhibit twenty-three partially overlapping aromatic protons in the region  $\delta$ , 9.2–7.7 ppm (Figure 3.4, Figure 3.5, and Figure 3.10). Out of these signals, four doublets ( $\delta$ =9.19, 9.13, 8.80, 8.76) are easily identifiable, with expected coupling constants of  $\sim 5.0$  Hz. One can safely assign these doublets as originating from  $\beta$ -pyrrolic hydrogen atoms based on the coupling constant values. The *meso*-aryl protons are observed at 8.42 – 7.70 ppm region. The signals of the *meso*-aryl protons are broadened at room temperature.

The  $^1\text{H}$  NMR spectrum of **2** exhibits the expected number of seventeen partially overlapping aromatic protons in the region  $\delta$ = 9.22–7.06 ppm (Figure 3.13). Twelve ethylene protons of the 1, 4-dioxan moiety appear in the region of 4.61 – 4.35 ppm as a broad singlet. All the signals in the Sb-corrole derivatives show a downfield shift compared to the FB corroles.

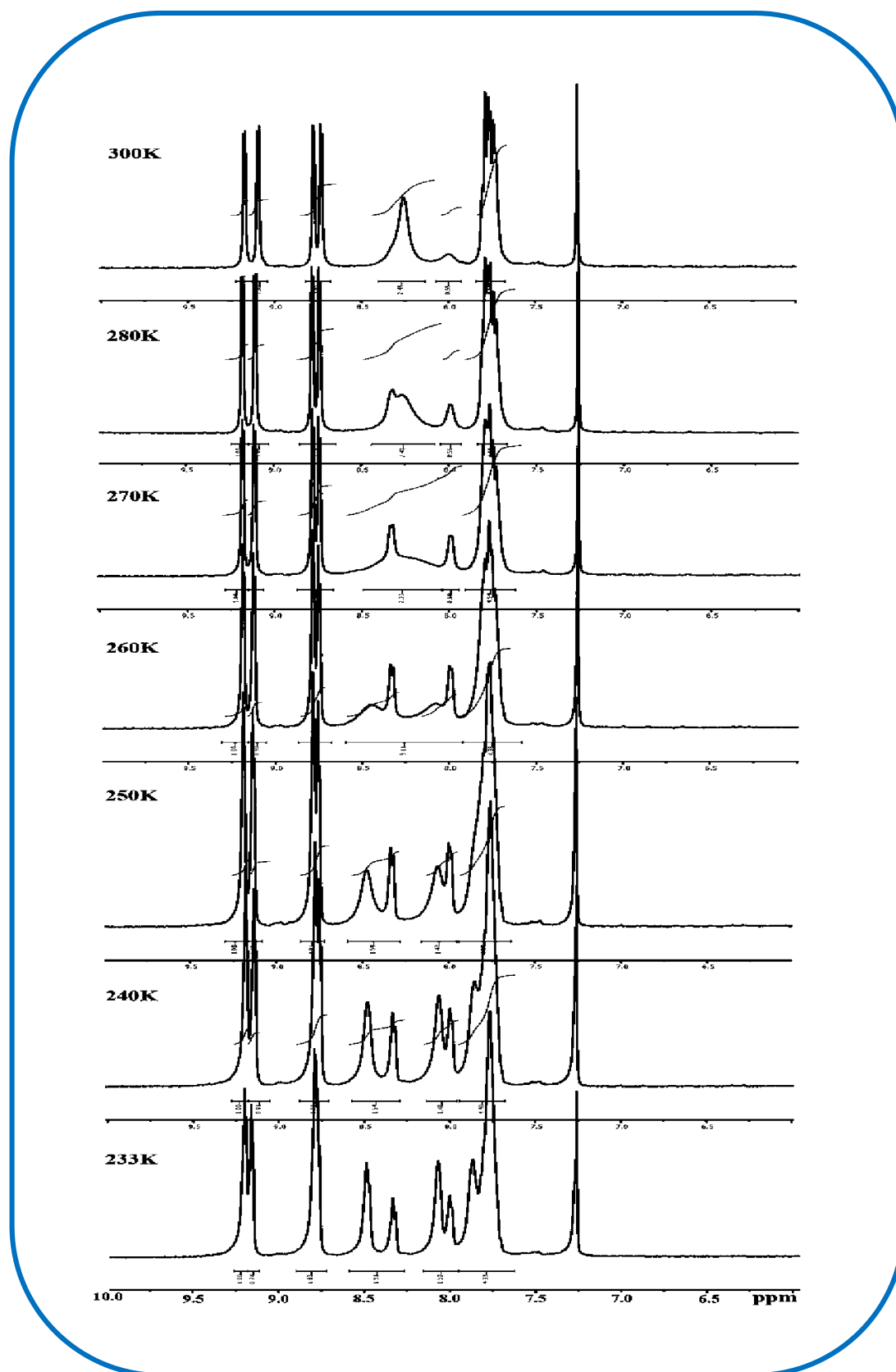
Complex **3** exhibits twenty-three partially overlapping aromatic protons in the region  $\delta$ , 8.67–7.56 ppm (Figure 3.16). Out of these signals, four doublets ( $\delta$ =8.67, 8.40, 8.29) are easily identifiable, with expected coupling constants of  $\sim 5.0$  Hz.

One can safely assign these doublets as originating from  $\beta$ -pyrrolic hydrogen atoms based on the coupling constant values. The *meso*-aryl protons are observed in 7.86 – 7.56 ppm region. All the signals in the corrolato-oxo-antimony(V) complexes show increased shielding compared to the corrolato-antimony(III). Variable temperature NMR spectra

suggest the pyrrolic protons and the *meso*-phenyl ring protons behave differently with temperature variations (Figure 3.5).



**Figure 3.4**  $^1\text{H}$  NMR spectrum of the complexes (a) (5,10,15-Triphenylcorrolato)(oxo)antimony(V), 3 and (b) 5,10,15-Triphenylcorrolato-antimony(III), 1 in  $\text{CDCl}_3$ .



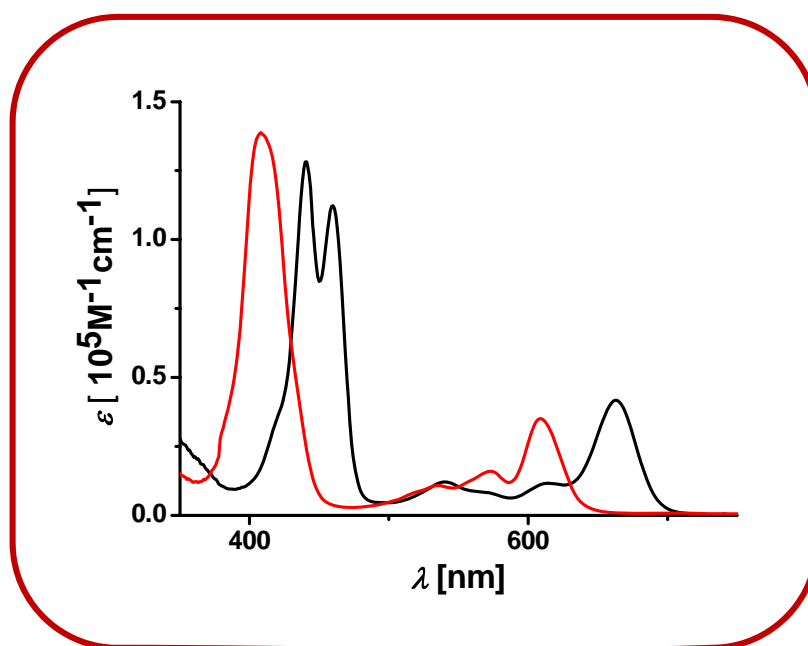
**Figure 3.5**  $^1\text{H}$  NMR spectra of **1** in  $\text{CDCl}_3$  at variable temperatures.

---

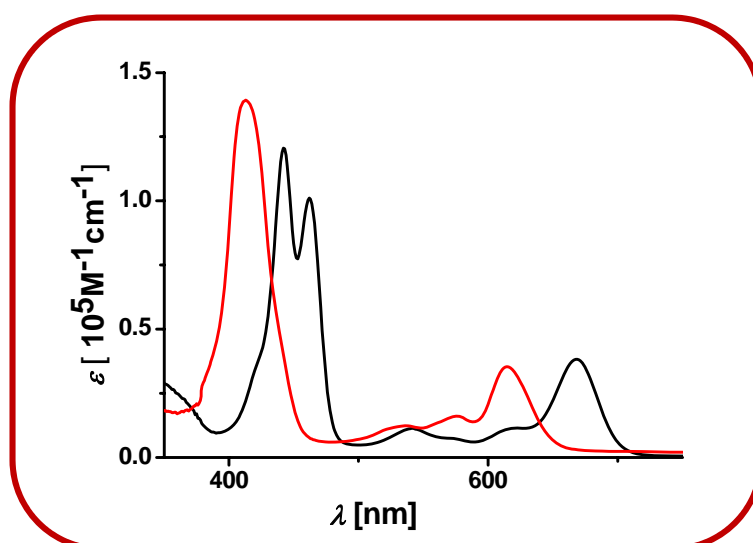
While lowering the temperature, the signals due to the pyrrolic protons *collapses* from well-defined doublets to a near singlet peak. On the other hand, the broad signals of *meso*-phenyl ring protons are converted into well-resolved signals at 233 K. This indicates different aggregation behavior ( $\pi$ - $\pi$  stacking driven intermolecular self-assembly formation<sup>53</sup>) of the corrolato-antimony(III) complex, **1** at different temperatures. This observation supports the formation of different conformers of **1** during crystallization with different solvents.

### 3.2.4 UV-Vis and emission spectroscopy

Electronic spectral data of the compounds (**1–4**) in CH<sub>2</sub>Cl<sub>2</sub> (Figure 3.6 and Figure 3.7) are shown in Table 3.2. All the two corrolato-antimony(III) complexes **1** and **2** exhibit Soret bands in the range of 440-462 nm. Interestingly, these typical split Soret bands reflect the low symmetric nature of these molecules<sup>24</sup>. This kind of splitting of the Soret bands arises due to the removal of polarization degeneracy (x and y) <sup>24</sup>. Another four weak bands arise in the visible region in the range of 539-668 nm. The molar absorption coefficient of the Soret bands in **1** and **2** are in the range of  $1-1.3 \times 10^5$  M<sup>-1</sup>cm<sup>-1</sup>, and the molar absorption coefficient of the Q-type bands in **1** and **2** are in the range of  $7-42 \times 10^3$  M<sup>-1</sup>cm<sup>-1</sup>. All the two (corrolato)(oxo)antimony(V) complexes **3** and **4** exhibit Soret bands in the range of 408-413 nm. Unlike **1** and **2**, there is no splitting in the Soret bands of compounds **3** and **4**. The presence of a single Soret band in **3** and **4** indicates their gain in symmetry in comparison with **1** and **2**. The molar absorption coefficient of the Soret bands in **3** and **4** are in the range of  $1.4 \times 10^5$  M<sup>-1</sup>cm<sup>-1</sup>, and the molar absorption coefficient of the Q-type bands in **3** and **4** are in the range of  $16-36 \times 10^3$  M<sup>-1</sup>cm<sup>-1</sup>.

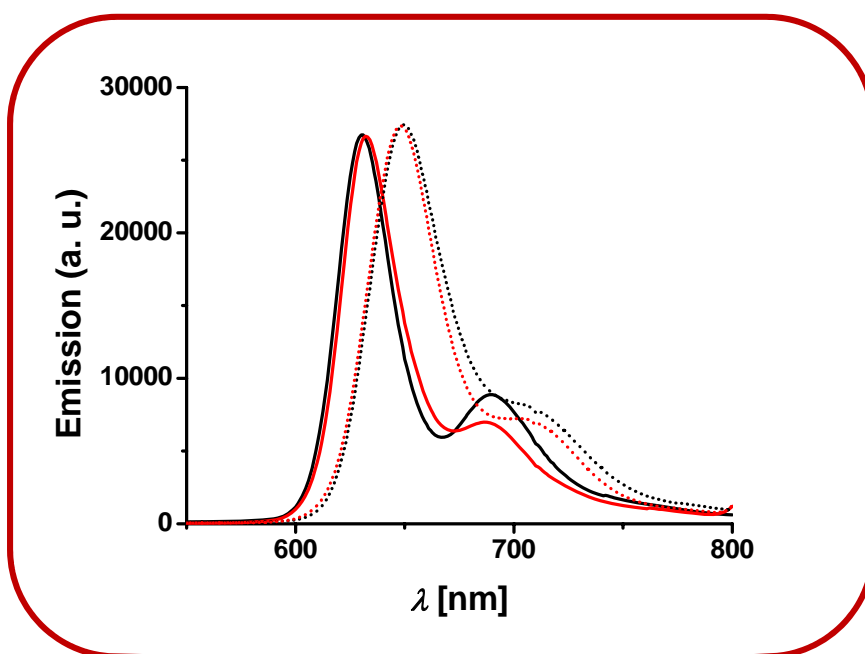


**Figure 3.6** Electronic absorption spectra of complexes, **1** (black line) and **3** (red line) in  $\text{CH}_2\text{Cl}_2$  at room temperature.



**Figure 3.7** Electronic absorption spectra of complexes 5,10,15-Tris[3,4-(1,4-dioxan)phenyl]corrolato-antimony(III), **2** (black line) and (5,10,15-Tris[3,4-(1,4-dioxan)phenyl]corrolato)(oxo)antimony(V), **4** (red line) in  $\text{CH}_2\text{Cl}_2$  at room temperature.

Compound **1** displayed weak emission at 630 nm and a shoulder at 690 nm in CH<sub>2</sub>Cl<sub>2</sub> (Figure 3.8). **2** displayed weak emission at 649 nm and a shoulder at 710 nm in CH<sub>2</sub>Cl<sub>2</sub>. **3** displayed weak emission at 632 nm and a shoulder at 688 nm in CH<sub>2</sub>Cl<sub>2</sub>. **4** displayed weak emission at 647 nm and a shoulder at 711 nm in CH<sub>2</sub>Cl<sub>2</sub>. These emission bands are assigned as fluorescence bands due to the observation of smaller Stokes shifts in reference to the lowest energy Q-type bands <sup>26</sup>.



**Figure 3.8** Normalized electronic emission spectra (excited at the Soret band) of the complexes 5,10,15-Triphenylcorrolato-antimony(III), **1** (solid black line), 5,10,15-Tris[3,4-(1,4-dioxan)phenyl] corrolato-antimony(III), **2** (dotted black line), (5,10,15-Triphenylcorrolato) (oxo) antimony(V), **3** (solid red line), and (5,10,15-Tris[3,4-(1,4-dioxan)phenyl] corrolato) (oxo) antimony(V), **4** (dotted red line) in CH<sub>2</sub>Cl<sub>2</sub> at room temperature.



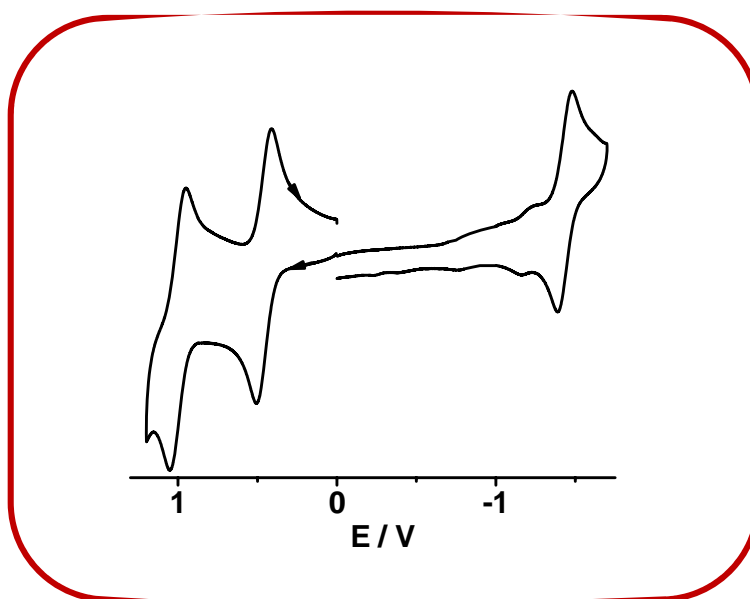
**Table 3.2** UV-Vis data of **1**, **2**, **3** and **4**.<sup>a</sup>

complex	$\lambda_{\text{max}}$ [nm] ( $\varepsilon$ [ $\text{M}^{-1}\text{cm}^{-1}$ ])
<b>1</b>	440(128000), 459(112000), 539(12800), 570(9000), 613(12000), 663(42400).
<b>2</b>	442(121000), 462(101000), 540(12300), 574(7400), 618(11400), 668(38300).
<b>3</b>	408(140000), 534(11100), 573(16700), 608(35900).
<b>4</b>	413(140000), 534(12700), 576(16900), 615(36100).

<sup>a</sup> Measurements in  $\text{CH}_2\text{Cl}_2$ .

### 3.2.5 Redox properties

The redox properties of **1** was investigated in  $\text{CH}_2\text{Cl}_2/0.1 \text{ M TBAP}$  by using cyclic voltammetric techniques (Figure 3.9). Antimony corrole complex **1** exhibited two successive one electron reversible oxidative couple and one reversible reductive couple *versus* Ag-AgCl reference electrode.



**Figure 3.9** Cyclic voltammograms of **1** in  $\text{CH}_2\text{Cl}_2$ . The potentials are vs. Ag/AgCl.

---

The first oxidation was observed at  $E_{298}^0$ , V ( $\Delta E_p$ , mV): 0.45(80), and the second oxidation process was observed at  $E_{298}^0$ , V ( $\Delta E_p$ , mV): 0.99(90) for **1**. They also showed one reversible reductive couple  $E_{298}^0$ , V ( $\Delta E_p$ , mV): -1.45(90) (**1**) *versus* Ag-AgCl. These values are in line with the previously reported other antimony corroles<sup>22</sup>.

### 3.3 Conclusions

We have presented here the synthesis of four new antimony-corrole complexes, including two corrolato-antimony(III) complexes and two (corrolato)(oxo)antimony(V) complexes. The purity and identity of these new antimony(III) and antimony(V)-oxo complexes have been demonstrated by their satisfactory elemental analysis and also by various other spectroscopic techniques. The <sup>1</sup>H NMR spectra of this new antimony (III) and antimony(V)-oxo complexes demonstrate sharp resonances with normal ‘chemical shifts’ and thus indicate their diamagnetic nature in the native states. As both Sb (III) {4d<sup>10</sup>5s<sup>2</sup>} and Sb (V) {4d<sup>10</sup>5s<sup>0</sup>} has closed-shell electronic configuration thus antimony-corroles are expected to be diamagnetic in nature. One of the representative corrolato-antimony(III) complexes has been characterized by X-ray diffraction. While using two different solvents for crystallization, we have obtained two different conformers for the corrolato-antimony(III) complex, **1**. There is a slight change in bond lengths and angles in these two conformations. In both the conformers, Sb<sup>III</sup> corrole is dome-shaped, and the deviation of Sb<sup>III</sup> ion with respect to the mean corrole plane (consists of four pyrrolic nitrogen atoms) is ~0.963-0.966 Å. This clearly indicates that the metal ion is significantly displaced from the mean corrole plane. Till date, the crystal structure of related Sb<sup>III</sup> corroles is rarely reported in the literature. The luminescent properties of Sb<sup>III</sup> corroles and Sb<sup>V</sup>=O corroles are also reported herein, and this paves the way for the future utilization of these classes of molecules in various photocatalytic oxygen atom

---

transfer reactions. Future work from our laboratories will be focused on the photocatalytic applications of these classes of molecules.

### **3.4 Experimental section**

#### **3.4.1 Materials**

The precursors pyrrole, *p*-chloranil, benzaldehyde, and 1,4-benzodioxan-6-carboxaldehyde were purchased from Aldrich, USA. SbCl<sub>3</sub> and pyridine were purchased from Merck, India. Other chemicals were of reagent grade. Hexane and CH<sub>2</sub>Cl<sub>2</sub> were distilled from KOH and CaH<sub>2</sub>, respectively. For spectroscopic and electrochemical studies, HPLC grade solvents were used. The free base corroles; 5,10,15-Triphenylcorrole and 5,10,15-Tris[3,4-(1,4-dioxan)phenyl]corrole were prepared according to the published procedures<sup>49-50</sup>.

#### **3.4.2 Physical Measurements**

UV–Vis spectral studies were performed on a Perkin–Elmer LAMBDA-750 spectrophotometer. Emission spectral studies were performed on a Perkin Elmer, LS 55 spectrophotometer using an optical cell of 1 cm path length. The elemental analyses were carried out with a Perkin–Elmer 240C elemental analyzer. FT–IR spectra were recorded on a Perkin–Elmer spectrophotometer with samples prepared as KBr pellets. The NMR measurements were carried out using a Bruker AVANCE 400 NMR spectrometer. Tetramethylsilane (TMS) was the internal standard. Electrospray mass spectra were recorded on a Bruker Micro TOF–QII mass spectrometer. Cyclic voltammetry measurements were carried out using a CH Instruments model *CHI1120A* electrochemistry system. A glassy carbon working electrode, a platinum wire as an auxiliary electrode and an Ag–AgCl reference electrode were used in a three–electrode configuration. Tetrabutyl ammonium perchlorate (TBAP) was the supporting electrolyte

---

(0.1M) and the concentration of the solution was  $10^{-3}\text{M}$  with respect to the complex. The half-wave potential  $E_{298}^0$  was set equal to  $0.5(E_{\text{pa}} + E_{\text{pc}})$ , where  $E_{\text{pa}}$  and  $E_{\text{pc}}$  are anodic and cathodic cyclic voltammetric peak potentials, respectively. The scan rate used was  $100\text{ mV s}^{-1}$ .

### 3.4.3 Crystal Structure Determination

Single crystals of 5,10,15-Triphenylcorrolato-antimony(III), **1** were grown by slow diffusion of solution of **1** in dichloromethane into hexane, followed by slow evaporation under atmospheric conditions. This resulted in the formation of the 1<sup>st</sup> conformer of **1**. On the other hand, slow evaporation from the dichloromethane-ethanol mixture resulted in the formation of the 2<sup>nd</sup> conformer. The crystal data of **1** (1<sup>st</sup> conformer) was collected on a Bruker Kappa APEX II CCD diffractometer at 293 K. The crystal data of **1** (2<sup>nd</sup> conformer) were collected on a Rigaku Oxford diffractometer at 293 K. Selected data collection parameters and other crystallographic results are summarized in Table 3.1. All data were corrected for Lorentz polarization and absorption effects. The program package SHELXTL<sup>51</sup> was used for structure solution and full-matrix least-squares refinement on  $F^2$ . Hydrogen atoms were included in the refinement using the riding model. Contributions of H atoms for the water molecules were included but were not fixed. Disordered solvent molecules were taken out using SQUEEZE command in PLATON<sup>52</sup>. CCDC 1943791 contains the supplementary crystallographic data for **1** (1<sup>st</sup> conformer). CCDC 1943792 contains the supplementary crystallographic data for **1** (2<sup>nd</sup> conformer). These data can be obtained free of charge via [www.ccdc.cam.ac.uk/data\\_request/cif](http://www.ccdc.cam.ac.uk/data_request/cif).

---

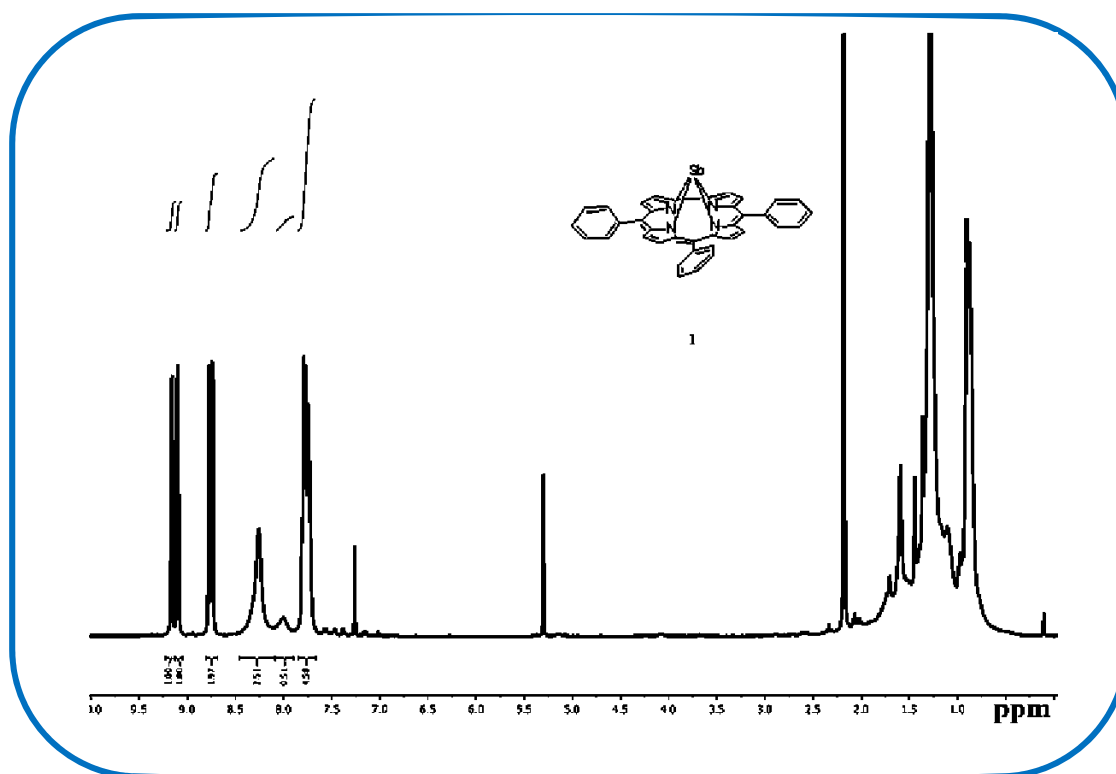
### 3.4.4 Synthesis

#### 3.4.4.1 Synthesis of 5,10,15-Triphenylcorrolato-antimony(III), **1**:

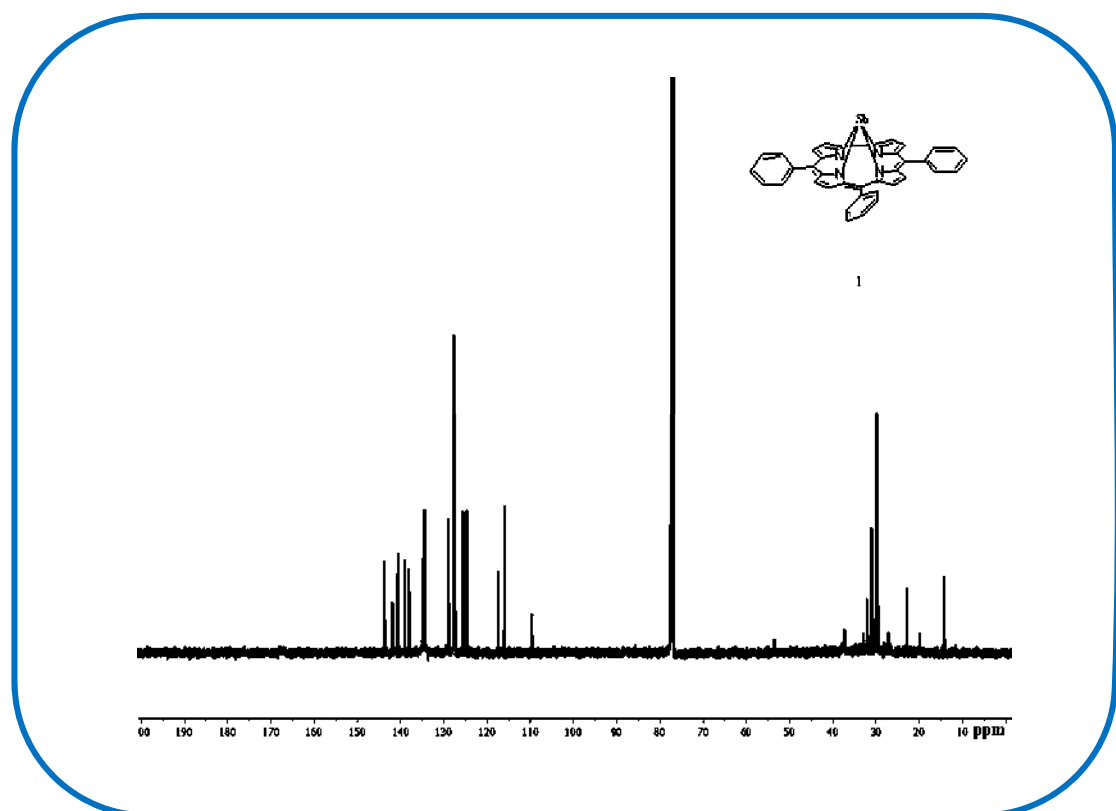
**1** was prepared by a slight modification of a general procedure for the synthesis of Sb–corrole developed by Kadish *et al.* [22]. 100 mg (0.19 mmol) of 5,10,15-Triphenylcorrole, and 300 mg (0.76 mmol) of SbCl<sub>3</sub> were added to a 20 mL of pyridine solution. The solution was then heated to reflux at 100°C till the fluorescence of starting FB corrole completely disappeared. The solution was then dried in a vacuum. The residue was then purified by chromatography on a silica gel column using CH<sub>2</sub>Cl<sub>2</sub>–hexane mixture (6:4) as eluent. The green fraction containing antimony corrole was further purified by recrystallization from dichloromethane/hexane mixture to give 105 mg of pure **1**. Average R<sub>f</sub> values (1:1 CH<sub>2</sub>Cl<sub>2</sub>: hexane mixture / silica gel plates): 0.75.

#### For (5,10,15-Trisphenylcorrolato)antimony(III), **1**:

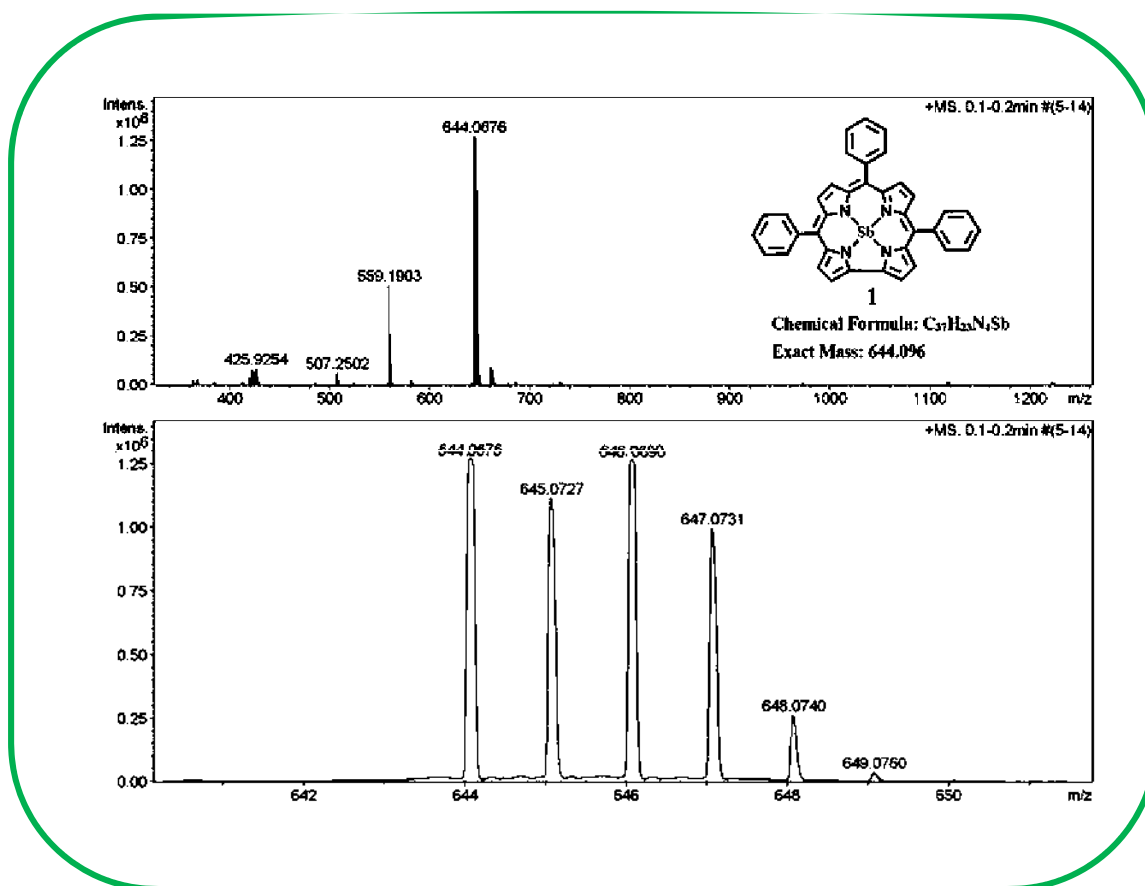
Yield 105 mg, (85%). Anal. Calcd (found) for C<sub>37</sub>H<sub>23</sub>N<sub>4</sub>Sb (**1**): C, 68.86 (68.71); H, 3.59 (3.70); N, 8.68 (8.81). UV-Vis (dichloromethane)  $\lambda_{\text{max}}$ /nm ( $\epsilon$ /M<sup>-1</sup>cm<sup>-1</sup>): 440(128000), 459(112000), 539(12800), 570(9000), 613(12000), 663(42400). <sup>1</sup>H NMR (400 MHz, Chloroform-*d*)  $\delta$  9.19 (d, *J* = 4.1 Hz, 2H,  $\beta$ -pyrrolic), 9.13 (d, *J* = 4.7 Hz, 2H,  $\beta$ -pyrrolic), 8.80 (d, *J* = 4.2 Hz, 2H,  $\beta$ -pyrrolic), 8.76 (d, *J* = 4.8 Hz, 2H,  $\beta$ -pyrrolic), 8.42-7.94 (m, 6H, *meso*-aryl), 7.89-7.70 (m, 9H, *meso*-aryl) (Figure 3.10). <sup>13</sup>C NMR (101 MHz, CDCl<sub>3</sub>)  $\delta$  143.76, 141.86, 140.63, 139.00, 138.07, 134.91, 134.51, 128.94, 127.73, 127.67, 127.45, 125.62, 124.72, 117.43, 115.97, 109.63 (Figure 3.11). The electrospray mass spectrum in acetonitrile showed peaks centered at *m/z* = 644.0676 correspond to [**1**]<sup>+</sup> (644.096 calcd for C<sub>37</sub>H<sub>23</sub>N<sub>4</sub>Sb) (Figure 3.12). **1** displayed weak emission at 630 nm and a shoulder at 690 nm in CH<sub>2</sub>Cl<sub>2</sub> (Excited at the Soret band).



**Figure 3.10**  $^1\text{H}$  NMR spectrum of **1** in  $\text{CDCl}_3$ .



**Figure 3.11**  $^{13}\text{C}$  NMR spectrum of **1** in  $\text{CDCl}_3$ .



**Figure 3.12** ESI- MS spectrum of **1** in CH<sub>3</sub>CN shows the measured spectrum with isotopic distribution pattern.

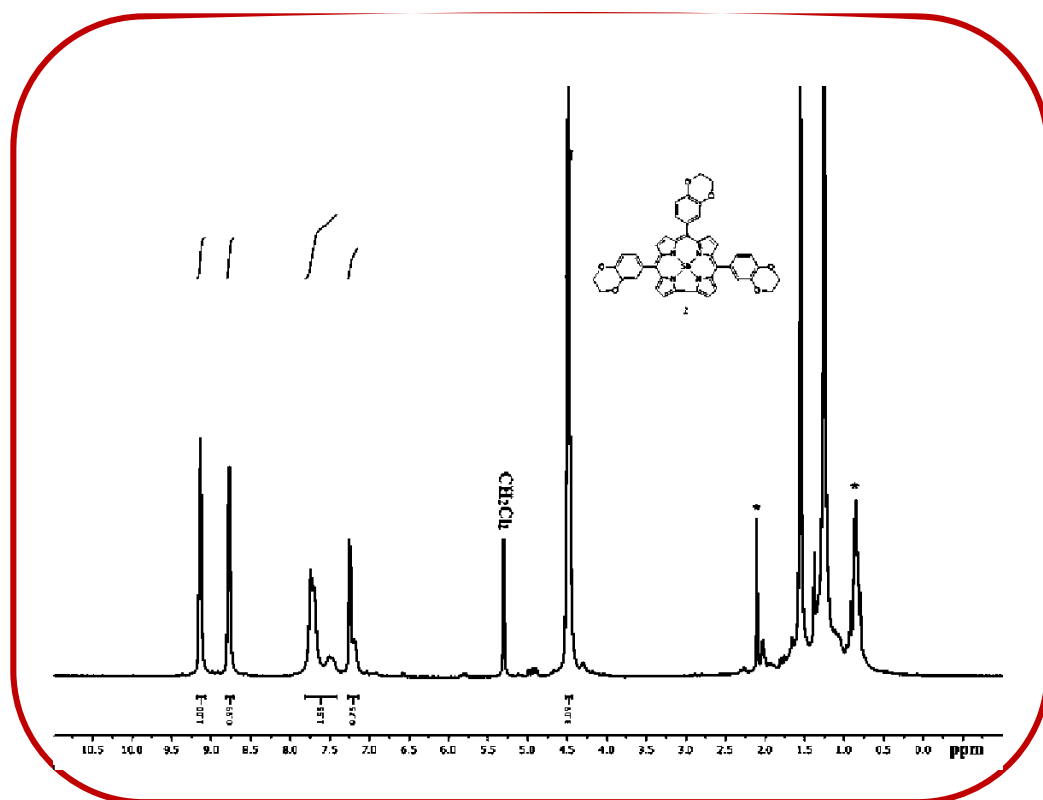
#### 3.4.4.2 Synthesis of 5,10,15-Tris[3,4-(1,4-dioxan)phenyl]corrolato-antimony(III), **2**:

100 mg (0.14 mmol) of 5,10,15-Tris[3,4-(1,4-dioxan)phenyl]corrole, and 300 mg (0.76 mmol) of SbCl<sub>3</sub> were added to a 20 mL of pyridine solution. The solution was then heated to reflux at 100°C till the fluorescence of starting FB corrole completely disappeared. The solution was then dried in a vacuum. The residue was then purified by chromatography on silica using pure CH<sub>2</sub>Cl<sub>2</sub> as eluent. The green fraction containing antimony corrole was further purified by recrystallization from dichloromethane/hexane mixture to give 100 mg of pure **2**. Average R<sub>f</sub> values (1:1 CH<sub>2</sub>Cl<sub>2</sub>: hexane mixture / silica gel plates): 0.11.

---

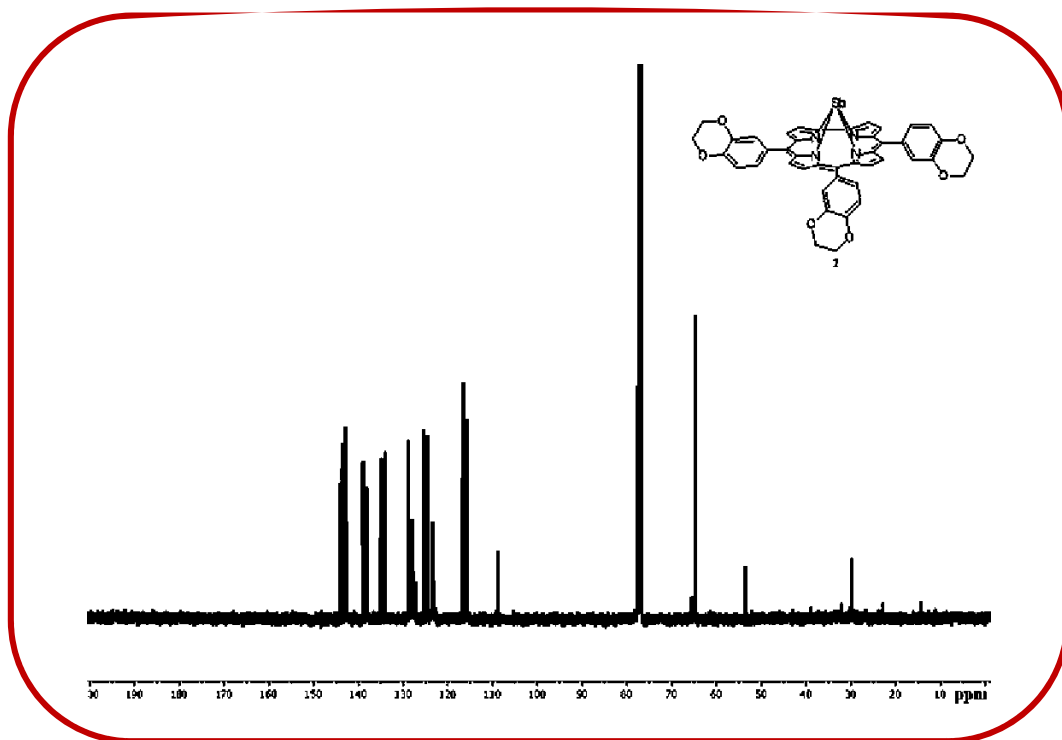
**For 5,10,15-Tris[3,4-(1,4-dioxan)phenyl]corrolato-antimony(III), **2**:**

Yield 100mg (86%). Anal. Calcd (found) for  $C_{43}H_{29}N_4O_6Sb$  (**2**): C, 63.02 (63.18); H, 3.57 (3.72); N, 6.84 (6.74). UV-Vis (dichloromethane):  $\lambda_{max}/nm$  ( $\epsilon/M^{-1}cm^{-1}$ ): 442(121000), 462(101000), 540(12300), 574(7400), 618(11400), 668(38300).  $^1H$  NMR (400 MHz, Methylene Chloride- $d_2$ )  $\delta$  9.22 – 9.05 (m, 4H), 8.77 (dd,  $J = 7.6, 4.4$  Hz, 4H), 7.82 – 7.34 (m, 6H), 7.34 – 7.06 (m, 3H), 4.61 – 4.35 (m, 12H) (Figure 3.13).  $^{13}C$  NMR (101 MHz,  $CDCl_3$ )  $\delta$  143.94, 143.64, 143.34, 142.97, 142.60, 139.00, 138.12, 135.17, 134.79, 133.98, 128.91, 128.67, 127.89, 125.51, 124.63, 123.33, 116.79, 116.50, 116.09, 115.72, 108.80, 64.82, 64.79, 64.74, 53.56 (Figure 3.14). The electrospray mass spectrum of **2** in acetonitrile showed peaks centered at  $m/z = 818.147$  correspond to  $[2]^+$  (818.113 calcd for  $C_{43}H_{29}N_4O_6Sb$ ) (Figure 3.15). **2** displayed weak emission at 649 nm and a shoulder at 710 nm in  $CH_2Cl_2$  (Excited at the Soret band).

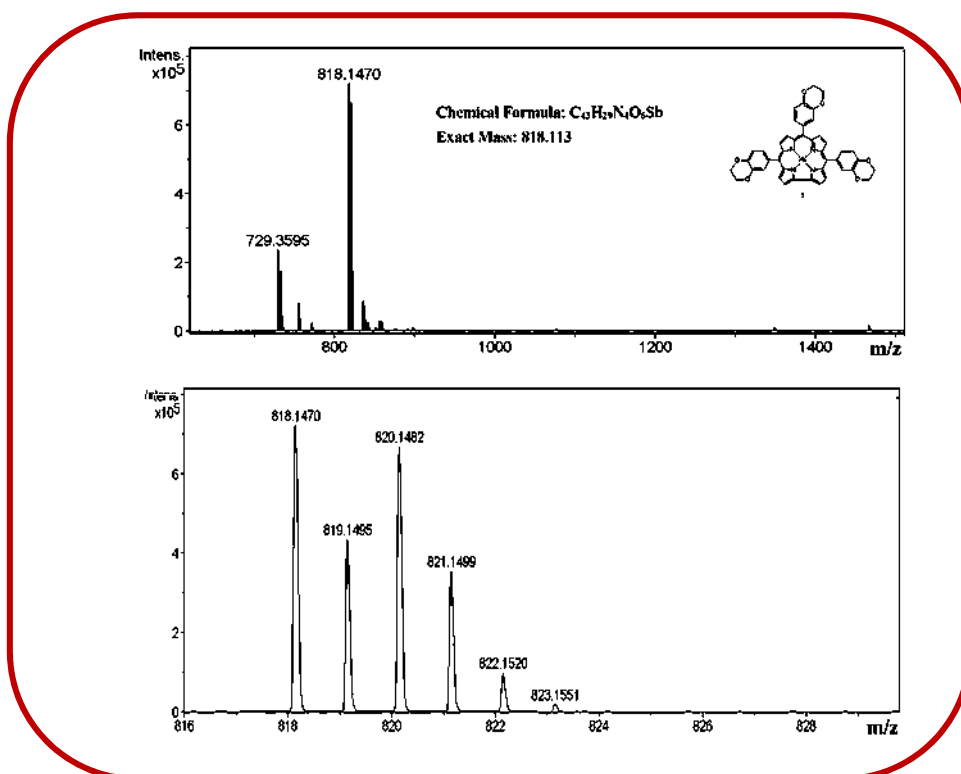


**Figure 3.13**  $^1H$  NMR spectrum of **2** in  $CD_2Cl_2$ .





**Figure 3.14**  $^{13}\text{C}$  NMR spectrum of **2** in  $\text{CD}_2\text{Cl}_2$ .



**Figure 3.15** ESI- MS spectrum of **2** in  $\text{CH}_3\text{CN}$  shows the measured spectrum with isotopic distribution pattern.

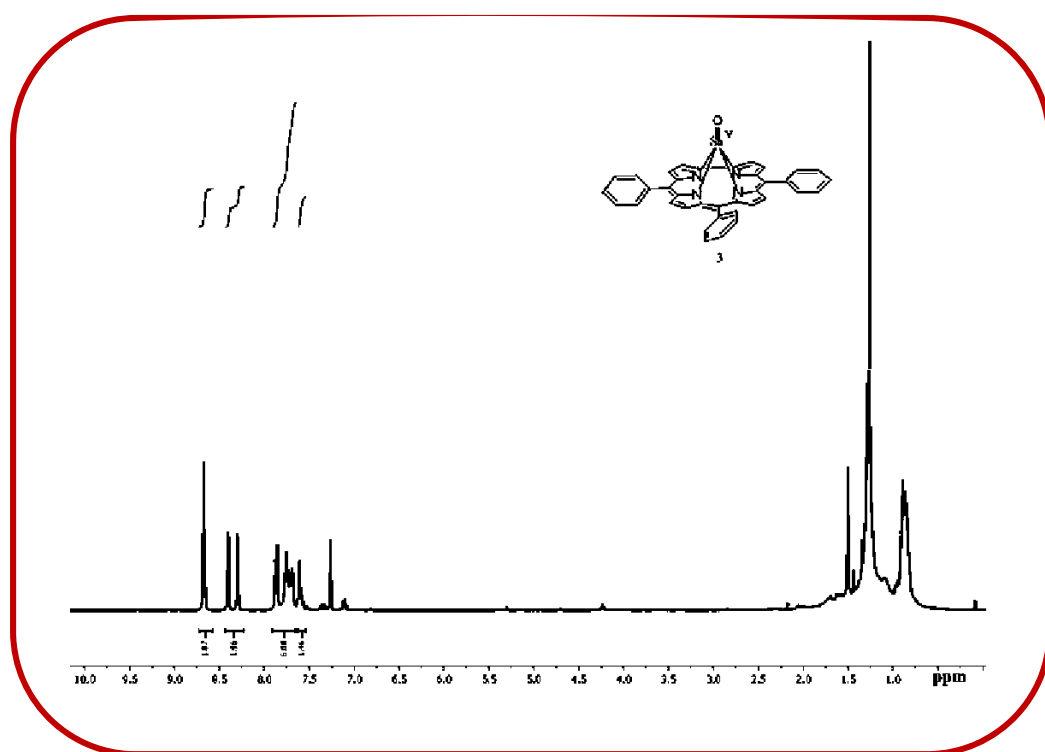
---

#### 3.4.4.3 Synthesis of (5,10,15-Triphenylcorrolato)(oxo)antimony(V), **3**:

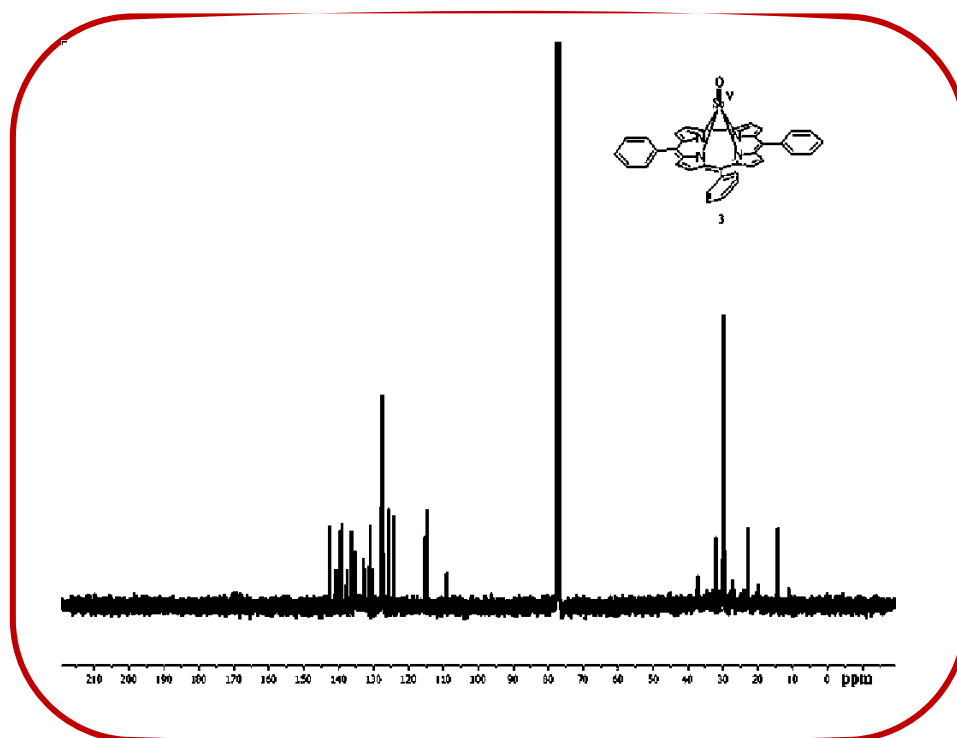
**3** was prepared by a slight modification of a general procedure for the synthesis of (corrolato)(oxo)antimony(V) developed by Gross *et al*<sup>23</sup>. 10 mg (0.016 mmol) of 5,10,15-Triphenylcorrolato-antimony(III), **1**, and 10 mg (0.048 mmol) of PhIO were added to a 10 mL of CH<sub>2</sub>Cl<sub>2</sub> solution. The solution was then stirred well at RT till the starting corrolato-antimony(III) completely disappeared. The solution was then purified by chromatography on neutral alumina using pure CH<sub>2</sub>Cl<sub>2</sub> as an eluent. The blueish-green fraction containing (corrolato)(oxo)antimony(V) was further purified by recrystallization from dichloromethane/hexane mixture to give 7 mg of pure **3**. Average R<sub>f</sub> values (1:1 CH<sub>2</sub>Cl<sub>2</sub>: hexane mixture / *neutral aluminium oxide* plates): 0.89.

#### For (5,10,15-Triphenylcorrolato)(oxo)antimony(V), **3**:

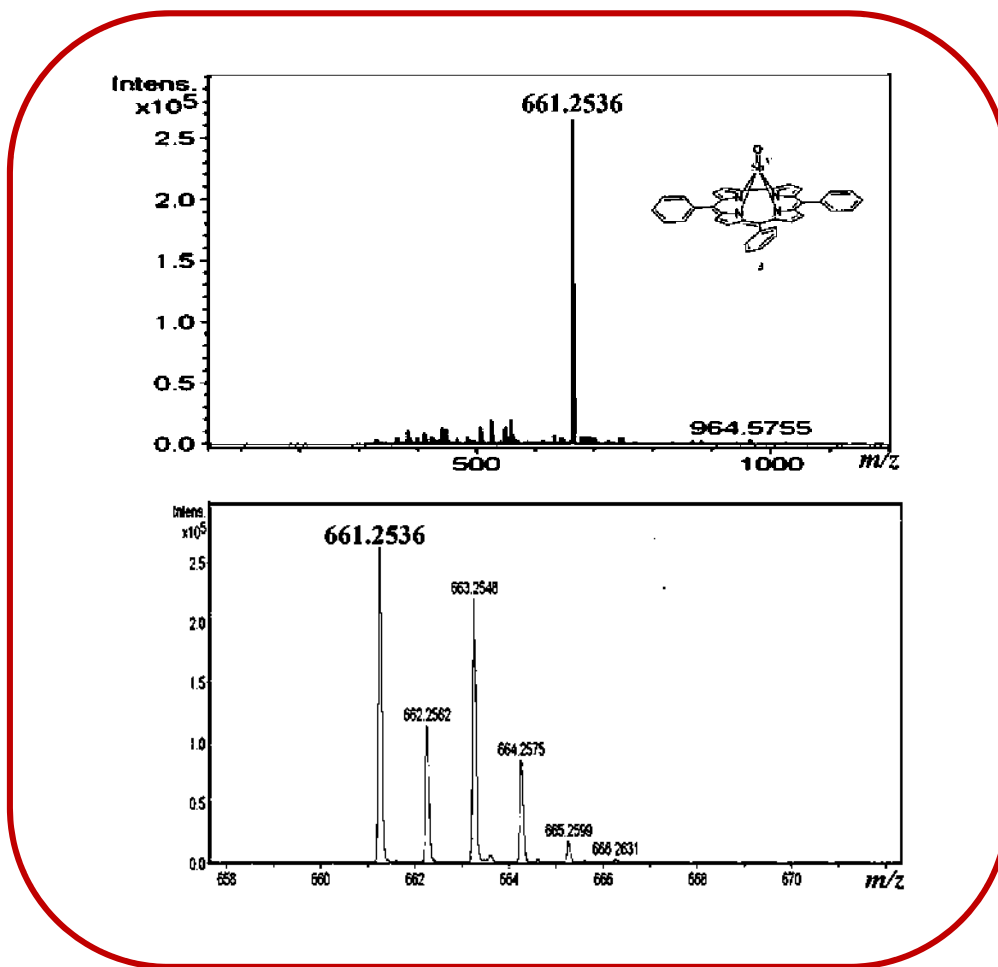
Yield 7 mg, (68%). Anal. Calcd (found) for C<sub>37</sub>H<sub>23</sub>N<sub>4</sub>OSb (**3**): C, 67.19 (67.35); H, 3.51 (3.64); N, 8.47 (8.32). UV-Vis (dichloromethane)  $\lambda_{\text{max}}$ /nm ( $\epsilon$  /M<sup>-1</sup>cm<sup>-1</sup>): 408(140000), 534(11100), 573(16700), 608(35900). <sup>1</sup>H NMR (400 MHz, Chloroform-*d*)  $\delta$  8.67 (dd, *J* = 11.0, 4.5 Hz, 4H), 8.40 (d, *J* = 4.2 Hz, 2H), 8.29 (d, *J* = 4.7 Hz, 2H), 7.86 (m, *J* = 6.8 Hz, 4H), 7.80 – 7.56 (m, 11H) (Figure 3.16). <sup>13</sup>C NMR (101 MHz, CDCl<sub>3</sub>)  $\delta$  142.71, 140.81, 139.76, 139.14, 137.64, 136.33, 135.17, 132.86, 131.07, 130.38, 127.93, 127.60, 127.56, 127.39, 127.21, 127.12, 125.70, 124.24, 115.38, 114.80, 109.09 (Figure 3.17). The electrospray mass spectrum of **3** in acetonitrile (Fig. S3) showed peaks centered at *m/z* = 661.2356 correspond to [**3**+H]<sup>+</sup> (661.091 calcd for C<sub>37</sub>H<sub>24</sub>N<sub>4</sub>OSb) (Figure 3.18). **3** displayed weak emission at 632 nm and a shoulder at 688 nm in CH<sub>2</sub>Cl<sub>2</sub> (Excited at the Soret band).



**Figure 3.16**  $^1\text{H}$  NMR spectrum of **3** in  $\text{CDCl}_3$ .



**Figure 3.17**  $^{13}\text{C}$  NMR spectrum of **3** in  $\text{CDCl}_3$ .

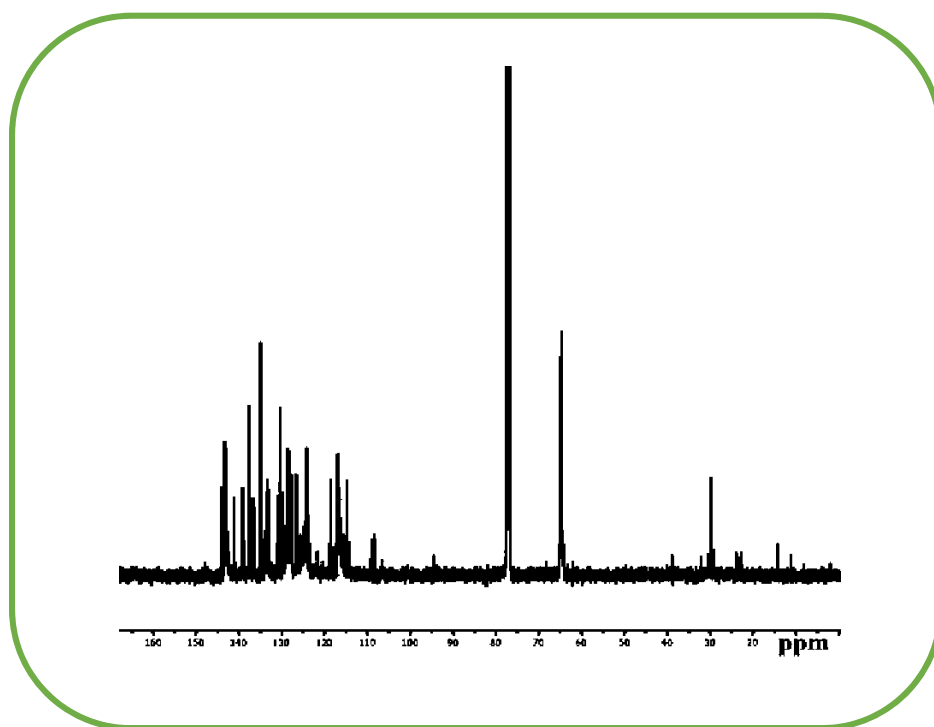


**Figure 3.18** ESI- MS spectrum of **3** in CH<sub>3</sub>CN shows the measured spectrum with isotopic distribution pattern.

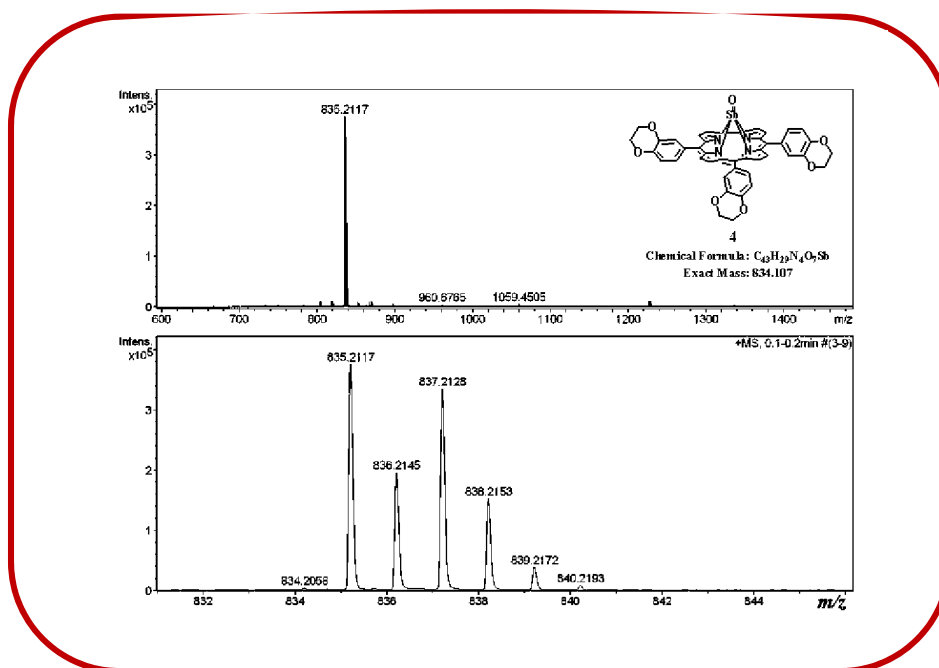
#### 3.4.4.4 Synthesis of (5,10,15-Tris[3,4-(1,4-dioxan)phenyl]corrolato)(oxo)antimony (V), **4**:

**4** was prepared by a slight modification of a general procedure for the synthesis of (corrolato)(oxo)antimony(V) developed by Gross *et al.*<sup>23</sup>. 10 mg (0.012 mmol) of 5,10,15-Tris[3,4-(1,4-dioxan)phenyl]corrolato-antimony(III), **2**, and 10 mg (0.048 mmol) of PhIO were added to a 10 mL of CH<sub>2</sub>Cl<sub>2</sub> solution. The solution was then stirred well at RT till the starting corrolato-antimony(III) completely disappeared. The residue was then purified by chromatography on neutral alumina using CH<sub>3</sub>CN–CH<sub>2</sub>Cl<sub>2</sub> mixture (1:20) as eluent. The blueish-green fraction containing (corrolato)(oxo)antimony(V) was





**Figure 3.20**  $^{13}\text{C}$  NMR spectrum of **4** in  $\text{CDCl}_3$ .



**Figure 3.21** ESI- MS spectrum of **4** in  $\text{CH}_3\text{CN}$  shows the measured spectrum with isotopic distribution pattern.

---

## References

1. *Inorganic Photochemistry* Edited by Rudi van Eldik, Grażyna Stochel, **2011**, 63, 2-448.
2. Shiragami, T.; Matsumoto, J.; Inoue, H.; Yasuda, M., *Journal of Photochemistry and Photobiology C: Photochemistry Reviews* **2005**, 6, 227-248.
3. DeAngelis, A. D.; Kemp, K. C.; Gaillard, N.; Kim, K. S., *ACS Appl. Mater. Interfaces* **2016**, 8, 8445-8451.
4. Niishiro, R.; Konta, R.; Kato, H.; Chun, W.-J.; Asakura, K.; Kudo, A., *J. Phys. Chem. C*, **2007**, 111, 17420-17426.
5. Knoer, G.; Vogler, A., *Inorg. Chem.* **1994**, 33, 314-318.
6. McAuliffe, C.A., *Transition Metal Complexes of Phosphorus, Arsenic & Antimony Ligands*, Macmillan International Higher Education, **2015**.
7. Lucia, L. A.; Yui, T.; Sasai, R.; Takagi, S.; Takagi, K.; Yoshida, H.; Whitten, D. G.; Inoue, H., *J. Phys. Chem. B* **2003**, 107, 3789-3797.
8. Kadish, K. M.; Autret, M.; Ou, Z.; Akiba, K.-y.; Masumoto, S.; Wada, R.; Yamamoto, Y., *Inorg. Chem.* **1996**, 35, 5564-5569.
9. Kalyanasundaram, K.; Shelnutt, J. A.; Graetzel, M., *Inorg. chem.* **1988**, 27, 2820-2825.
10. Akiba, K.-y.; Onzuka, Y.; Itagaki, M.; Hirota, H.; Yamamoto, Y., *Organometallics* **1994**, 13, 2800-2803.
11. Tsukamoto, T.; Shimada, T.; Takagi, S., *J. Phys. Chem. A* **2013**, 117, 7823-7832.
12. Knör, G.; Vogler, A.; Roffia, S.; Paolucci, F.; Balzani, V., *Chem. Commun.* **1996**, 1643-1644.
13. Tsukamoto, T.; Shimada, T.; Takagi, S., *RSC Adv.* **2015**, 5, 8479-8485.

- 
14. Knör, G., *Coord. Chem. Rev.* **1998**, *171*, 61-70.
  15. Takagi, S.; Suzuki, M.; Shiragami, T.; Inoue, H., *J. Am. Chem. Soc.* **1997**, *119*, 8712-8713.
  16. Jiang, J.; Materna, K. L.; Hedström, S.; Yang, K. R.; Crabtree, R. H.; Batista, V. S.; Brudvig, G. W., *Angew. Chem. Int. Ed.* **2017**, *56*, 9111-9115.
  17. Knör, G.; Vogler, A.; Roffia, S.; Paolucci, F.; Balzani, V., *Chem. Commun.* **1996**, 1643-1644.
  18. Ertl, M.; Wöb, E.; Knör, G., *Photochem. Photobiol. Sci.* **2015**, *14*, 1826-1830.
  19. Harvey, J. D.; Ziegler, C. J., *Coord. Chem. Rev.* **2003**, *247*, 1-19.
  20. Knör, G., *Inorg. Chem. Commun.* **2000**, *3*, 505-507.
  21. Liu, J.-C.; Ishizuka, T.; Osuka, A.; Furuta, H., *Chem. Commun.* **2003**, 1908-1909.
  22. Kadish, K. M.; Erben, C.; Ou, Z.; Adamian, V. A.; Will, S.; Vogel, E., *Inorg. Chem.* **2000**, *39*, 3312-3319.
  23. Luobeznova, I.; Raizman, M.; Goldberg, I.; Gross, Z., *Inorg. Chem.* **2006**, *45*, 386-94.
  24. Lemon, C. M.; Hwang, S. J.; Maher, A. G.; Powers, D. C.; Nocera, D. G., *Inorg. Chem.* **2018**, *57*, 5333-5342.
  25. Mahammed, A.; Gross, Z., *Angew. Chem. Int. Ed.* **2015**, *127*, 12547-12550.
  26. Wagnert, L.; Berg, A.; Stavitski, E.; Luobeznova, I.; Gross, Z.; Levanon, H., *J. Porphyr. Phthalocyanines* **2007**, *11*, 645-651.
  27. Preuß, A.; Saltsman, I.; Mahammed, A.; Pfitzner, M.; Goldberg, I.; Gross, Z.; Röder, B., *J. Photochem. Photobiol. B: Biology* **2014**, *133*, 39-46.
  28. Roznyatovskiy, V. V.; Lee, C.-H.; Sessler, J. L., *Chem. Soc. Rev.* **2013**, *42*, 1921-1933.
-



- 
29. Gross, Z., *J. Biol. Inorg. Chem.* **2001**, *6*, 733-738.
30. Paolesse, R., Nardis, S., Stefanelli, M., Fronczek, F. R. and Vicente, M. G. H., *Angew. Chem. Int. Ed.* **2005**, *44*, 3047-3050.
31. Czernuszewicz, R. S.; Mody, V.; Czader, A.; Gałęzowski, M.; Gryko, D. T., *J. Am. Chem. Soc.* **2009**, *131*, 14214-14215.
32. Brothers, P. J., *Chem. Commun.* **2008**, 2090-2102.
33. Palmer, J. H.; Durrell, A. C.; Gross, Z.; Winkler, J. R.; Gray, H. B., *J. Am. Chem. Soc.* **2010**, *132*, 9230-9231.
34. Liu, H.-Y., Yam, F., Xie, Y.-T., Li, X.-Y. and Chang, C. K., *J. Am. Chem. Soc.* **2009**, *131*, 12890-12891.
35. Brizet, B., Desbois, N., Bonnot, A., Langlois, A., Dubois, A., Barbe, J.-M., Gros, C. P., Goze, C., Denat, F. and Harvey, P. D., *Inorg. Chem.* **2014**, *53*, 3392-3403.
36. Kuck, S.; Hoffmann, G.; Bröring, M.; Fechtel, M.; Funk, M.; Wiesendanger, R., *J. Am. Chem. Soc.* **2008**, *130*, 14072-14073.
37. Thomas, K. E., Vazquez-Lima, H., Fang, Y., Song, Y., Gagnon, K. J., Beavers, C. M., Kadish, K. M. and Ghosh, A., *Chem. Eur. J.* **2015**, *21*, 16839-16847.
38. Bröring, M.; Brégier, F.; Cónsul Tejero, E.; Hell, C.; Holthausen, M. C *Angew. Chem. Int. Ed.* **2007**, *46*, 445-448.
39. Ghosh, A., *Chem. Rev.* **2017**, *117*, 3798-3881.
40. Orłowski, R., Gryko, D. and Gryko, D. T., *Chem. Rev.* **2017**, *117*, 3102-3137.
41. Fang, Y., Ou, Z. and Kadish, K. M., *Chem. Rev.* **2017**, *117*, 3377-3419.
42. Fujino, K., Hirata, Y., Kawabe, Y., Morimoto, T., Srinivasan, A., Toganoh, M., Miseki, Y., Kudo, A. and Furuta, H., *Angew. Chem. Int. Ed.* **2011**, *50*, 6855-6859.
-

- 
43. Sinha, W.; Sommer, M. G.; Deibel, N.; Ehret, F.; Sarkar, B.; Kar, S., *Chem. Eur. J.* **2014**, *20*, 15920-15932.
44. Sinha, W.; Sommer, M. G.; Deibel, N.; Ehret, F.; Bauer, M.; Sarkar, B.; Kar, S., *Angew.Chem. Int. Ed.* **2015**, *54*, 13769-13774.
45. Sinha, W.; Sommer, M. G.; Hettmanczyk, L.; Patra, B.; Filippou, V.; Sarkar, B.; Kar, S., *Chem. Eur. J.* **2017**, *23*, 2396-2404.
46. Patra, B.; Sobottka, S.; Sinha, W.; Sarkar, B.; Kar, S., *Chem. Eur. J.* **2017**, *23*, 13858-13863.
47. Garai, A.; Sobottka, S.; Schepper, R.; Sinha, W.; Bauer, M.; Sarkar, B.; Kar, S., *Chem. Eur. J.* **2018**, *24*, 12613-12622.
48. Patra, B.; Sobottka, S.; Mondal, S.; Sarkar, B.; Kar, S., *Chem. Commun.* **2018**, *54*, 9945-9948.
49. Koszarna, B.; Gryko, D. T., *J. Org. Chem.* **2006**, *71*, 3707-3717.
50. Garai, A.; Kumar, S.; Sinha, W.; Purohit, C. S.; Das, R.; Kar, S., *RSC Adv.* **2015**, *5*, 28643-28651.
51. Sheldrick, G. M., *Acta Crystallogr., Sect. A: Found. Crystallogr.* **2008**, *64*, 112-122.
52. Van der Sluis, P. V.; Spek, A. L., *Acta Crystallogr., Sect. A: Found. Crystallogr.* **1990**, *46*, 194-201.
53. Leung, S. Y.-L.; Wong, K. M.-C.; Yam, V. W.-W., *Proc Natl Acad Sci U S A* **2016**, *113*, 2845-2850.
-

# CHAPTER 4

---

## Large Scale Green Synthesis of Porphyrins

---

### 4.1 Introduction

### 4.2 Results and Discussions

#### 4.2.1 A<sub>4</sub>-porphyrins. Optimization Study

#### 4.2.2 *Trans*-A<sub>2</sub>B<sub>2</sub>-porphyrins. Optimization Study

### 4.3 Analysis of the reaction mechanism

### 4.4 Conclusions

### 4.5 Experimental Section

#### 4.5.1 Materials

#### 4.5.2 Physical Measurements

#### 4.5.3 Syntheses

---

## 4.1 Introduction

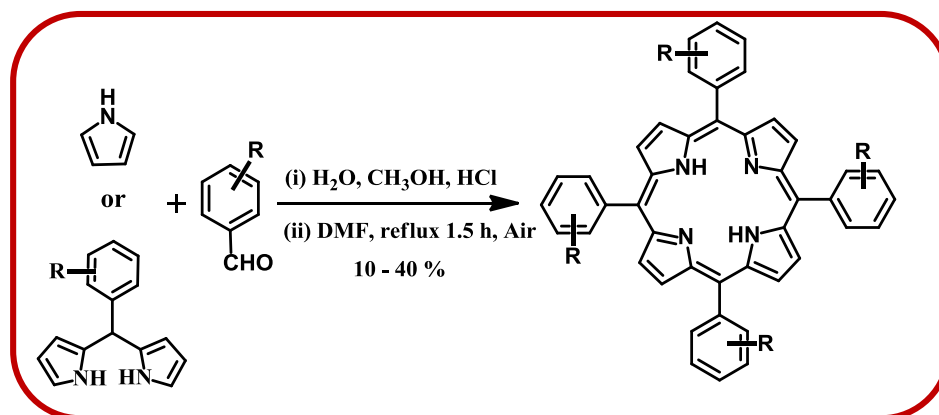
Porphyrin, a natural pigment, is present in a large number of metalloenzymes, like, heme,<sup>1</sup> chlorophyll,<sup>2</sup> bacteriochlorophyll,<sup>3</sup> siroheme,<sup>4</sup> heme d<sub>1</sub>,<sup>5</sup> and factor F<sub>430</sub>.<sup>6</sup> Synthetic porphyrinoids and their metallated versions have diverse applications in various areas like oxidation of organic molecules (as catalysts),<sup>7, 8</sup> water splitting reactions (as catalysts),<sup>9,10</sup> as possible components in molecular electronics,<sup>11</sup> as the dye in dye-sensitized solar cells,<sup>12</sup> in supramolecular chemistry,<sup>13,14</sup> and also in photodynamic therapy (PDT).<sup>15,16</sup> Thus, a great deal of research interest is involved in the synthesis of artificial porphyrin.<sup>17-28</sup> Although numerous synthetic procedures are developed, a careful observation tells us that the choice of reagents and reaction solvents is somewhat limited.<sup>29-34</sup> The major obstacle involved in the traditional synthetic pathways is that they are most successful in the small (milligram) scale synthesis of porphyrin.<sup>33-34</sup> An earlier version of porphyrin synthesis by Rothemund *et al.* describes the synthesis of porphyrin via the reaction of pyrrole and aldehyde in pyridine in a sealed tube at 220°C.<sup>31</sup> However, the reaction yield was as low as 5% in the case of *meso*-tetraphenylporphyrin.<sup>31</sup> Two synthetic methods are nowadays commonly used in porphyrin synthesis.<sup>32-34</sup> The Adler-Longo process is a one-step methodology using acetic or propionic acid as a solvent in aerobic conditions at around 141°C, which results in the formation of the desired porphyrin in 10-30% yield.<sup>32</sup> The formation of the tar-like product makes the purification process difficult in many cases. Lindsey's one flask two-step methodology was very successful in the synthesis of a large number of porphyrin derivatives (10-60% yield).<sup>33-34</sup> One of the major drawbacks of this synthesis is that it normally requires a large amount of chlorinated organic solvents, as pyrrole and aldehyde need to be maintained in very low concentration (~10 mM) and thus essentially hinders its industrial-scale applications.<sup>33-34</sup> In addition to that, in the second step, an expensive

---

oxidizer such as DDQ { DDQ=2,3-dichloro-5,6-dicyanobenzoquinone } was necessary. That eventually makes this synthetic methodology more costly. From the above discussion, it is clear that an industrial-scale cheap synthesis of porphyrin will have tremendous potential and will eventually make these molecules more relevant for various commercial applications. In Adler- Longo methodology, pyrrole and benzaldehyde were refluxed in propionic acid and resulted in the formation of tetraphenylporphyrin.<sup>32</sup> Thus, a direct condensation of pyrrole and benzaldehyde occurs; however, a problem is associated with the generation of different undesired aldehyde-pyrrole oligocondensates. Thus, it lowers the reaction yield and makes the purification of porphyrin quite difficult. Gryko *et al.* have described the synthesis of tetrapyrane in high yield in an H<sub>2</sub>O-CH<sub>3</sub>OH mixture catalyzed by HCl.<sup>35</sup> They have further used this tetrapyrane as a direct precursor of corrole synthesis. Herein, we have observed that this tetrapyrane can be an important intermediate for porphyrin synthesis and will eventually cut down the possibility of the formation of different undesired aldehyde-pyrrole oligocondensates. Thus it will be easier to get the desired porphyrin in high yield without any difficulty in the purification step.

Herein, we have demonstrated a new synthetic protocol for the simplified synthesis of a series of *meso*-substituted symmetric A<sub>4</sub>-porphyrins and *trans*-A<sub>2</sub>B<sub>2</sub>-porphyrins in mild conditions (Scheme 4.1). The first step is the facile condensation of pyrrole and aldehyde in a water-methanol solvent mixture using HCl as the catalyst at RT {RT= room temperature}. After this reaction, the precipitate was filtered out and was dissolved in reagent grade or ACS grade DMF {DMF= Dimethylformamide}, and refluxed in the air for 1-2 hours. After cooling, it was stirred overnight in the air at RT, dried in a vacuum, and purified using column chromatography. The yield of the obtained porphyrins is mostly satisfactory (10-40 %). In a few cases, it is possible to get pure

porphyrin via a simple crystallization technique, and thus one can also get rid of column chromatography.



**Scheme 4.1** Synthetic application of *meso*-substituted symmetric A<sub>4</sub>-porphyrins and *trans*-A<sub>2</sub>B<sub>2</sub>-porphyrins.

## 4.2 Results and Discussion

### 4.2.1 A<sub>4</sub>-porphyrins. Optimization Study

The acid-catalyzed condensation reaction of pyrrole and aldehyde in the HCl/H<sub>2</sub>O/MeOH system and the formation of different oligocondensates are already reported in the literature.<sup>35</sup> A slight modification of the earlier optimized protocol was used here. *Following the previous synthetic approach*, we have performed the synthesis of tetrapyrane. For a representative example, 2.0 mmol of aldehyde and 2.0 mmol of pyrrole were added to a 100 ml MeOH and 50 ml water mixture, followed by 10 ml of HCl. The reaction mixture was stirred at RT for 2 hours. The resulting mixture was filtered, and the precipitate was collected for the succeeding reaction. It is worthwhile to mention here that the resulting pink color oligocondensates contain a mixture of tetrapyrane, unreacted aldehyde, and some residual HCl. Gryko *et al.* have extracted this mixture in CHCl<sub>3</sub>, washed it several times with water, and dried it over Na<sub>2</sub>SO<sub>4</sub>. After further dilution in CHCl<sub>3</sub>, it was oxidized with *p*-chloranil. This process is now

---

considered the best protocol for the synthesis of corrole macrocycle.<sup>35</sup> While synthesizing A<sub>3</sub>-corroles, Gryko *et al.* have always observed A<sub>4</sub>-porphyrins as a side product with an average yield of 1-3%. It was suggested that the bilane (tetrapyrane) scrambling is responsible for this side reaction. This observation indeed promoted us to investigate further the reactivities of tetrapyrane. Hypothetically, tetrapyrane can be converted into a porphyrinogen derivative via simple condensation with one aldehyde moiety. A porphyrinogen derivative is considered a direct precursor for porphyrin synthesis. Keeping all these things in mind, we have tried to apply the Adler- Longo methodology here. Thus, we took the crude product directly obtained from HCl/H<sub>2</sub>O/MeOH system, the pink color oligocondensates (tetrapyrane), and refluxed it with propionic acid. However, this reaction is unsuccessful due to the poor solubility of tetrapyrane in propionic acid. The resulting mixture is very difficult to purify via column chromatography. We have recrystallized it a couple of times but were unable to get any convincing result to proceed further. Our main aim was to replicate the Adler-Longo methodology. Thus we were looking for an oxidation protocol devoid of quinone type oxidants like DDQ or *p*-chloranil. Thus we have tried a series of other solvents, specifically alcohols, like CH<sub>3</sub>OH, 1-butanol, etc. (Table 4.1). To our utter surprise, we have observed a definitive formation of porphyrin via TLC {TLC = thin layer chromatography}. It is indeed possible to separate the generated porphyrin via column chromatography without much difficulty. However, the obtained yield was not satisfactory. While using *p*-anisaldehyde as aldehyde, the obtained yield of 5,10,15,20-tetrakis(4-methoxyphenyl)porphyrin was 4% in CH<sub>3</sub>OH and 7% in 1-butanol.

The change of reflux time has not any significant effect on the yield of the porphyrin. Prolonged reflux eventually decreases the reaction yield further. Using basic solvents like Et<sub>3</sub>N also does not improve the situation further.

**Table 4.1** Optimization of reaction conditions for the conversion of tetrapyrane into porphyrin <sup>a</sup>.

Entry	Solvent	The yield of Porphyrin <sup>a</sup> (%)
1	DMF	29
2	CH <sub>3</sub> CN	5
3	CH <sub>3</sub> OH	4
4	Et <sub>3</sub> N	1-2
5	C <sub>5</sub> H <sub>9</sub> NO	14
6	1-Butanol	7
7	DCM	10
8	Toluene	13
9	Propionic acid	0 <sup>b</sup>

<sup>a</sup>5,10,15,20-Tetrakis(4-methoxyphenyl)porphyrin, **2**. <sup>b</sup>tetrapyrane is mostly insoluble in propionic acid.

Although, porphyrin was formed, however, the isolated yield was as low as 1-2%. While using other solvents like dichloromethane, acetonitrile, and toluene, the yield of the porphyrin was also not satisfactory. The obtained yield for the aforementioned solvents were 10%, 5%, and 13%, respectively. But when DMF was used as a solvent under the same reaction condition, our preliminary observation is that the porphyrin was formed at a reasonable yield. In this context, we have tried to change the solvent from propionic acid to DMF in the Adler-Longo methodology; however, the reaction remains unsuccessful. The reaction condition in DMF was further optimized by varying the reaction time (Table 4.2). The initial progress of the reaction was monitored by TLC.



The following experiment was carried out by using 5,10,15,20-tetraphenylporphyrin synthesis as a representative example. When the tetrapyrane was refluxed in DMF for 0.5 hr, the desired product was formed in moderate yield. When the reaction was further continued for 0.5 hr, there was a slight increase in the yield of the desired porphyrin. The yield of the porphyrin further slightly increased by continuing the reaction for another 0.5 hr. When the reaction was further continued for 0.5 hr, the yield of the desired porphyrin gradually decreases. But in a similar condition, when the reaction was stirred at room temperature for 1.5 hours in DMF solvent, the desired porphyrin was formed in much lesser quantities. Thus it was observed from the model studies, using 5,10,15,20-tetraphenylporphyrin as a representative example, when the tetrapyrane was refluxed in DMF for 1.5 hrs, the desired porphyrin was formed in satisfactory yield.

**Table 4.2** Optimization of reaction conditions for the conversion of tetrapyrane into porphyrin <sup>a</sup>.

Entry	Temperature	Time (h)	The yield of Porphyrin <sup>a</sup> (%)
1	RT	1.5	7
2	Reflux	0.5	11
3	Reflux	1	16
<b>4</b>	<b>Reflux</b>	<b>1.5</b>	<b>21</b>
5	Reflux	2	17

<sup>a</sup> 5,10,15,20-tetraphenylporphyrin, **1**.

However, it was further observed that the reaction yield is significantly increased by stirring the same reaction mixture overnight at room temperature. Thus, we can conclude that the optimum yield can be obtained by refluxing the reaction mixture in

DMF for 1.5 hours, followed by stirring the mixture overnight at RT in air. Overall, we have observed that the reaction yield for 5,10,15,20-tetraphenylporphyrin synthesis is 21%. As NMP {NMP=N-methyl-2-pyrrolidone} has similar properties to DMF, thus the reaction was also performed in NMP as the reaction solvent. In the case of NMP solvent, in similar reaction conditions, the obtained yield for the desired product was 14%. The optimization study was further carried out by varying the solvent from pure DMF to a DMF-water mixed solvent system (Table 4.3).

**Table 4.3** Optimization of reaction conditions for the conversion of tetrapyrane into porphyrin <sup>a</sup>.

Entry	Solvent	Yield of Porphyrin <sup>a</sup> (%)
1	DMF (dry)	21
2	DMF (HPLC)	21
3	DMF (reagent grade)	21
4	DMF: H <sub>2</sub> O (4:1)	15
5	DMF: H <sub>2</sub> O (1:1)	10
6	DMF: H <sub>2</sub> O (1:4)	6

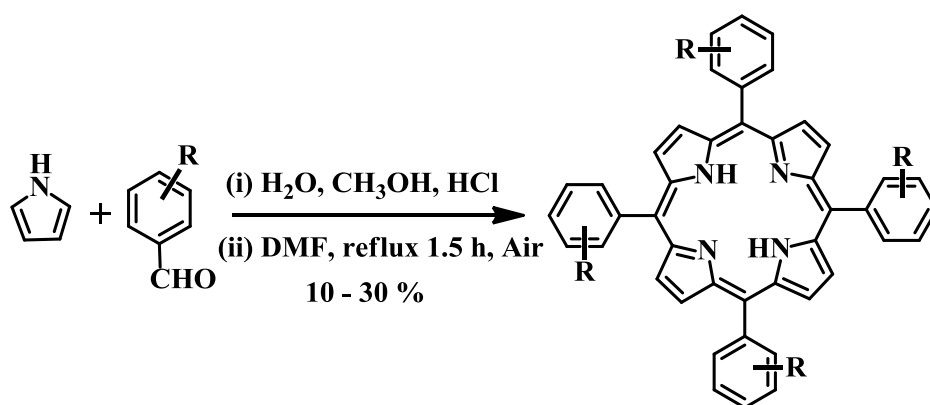
<sup>a</sup> 5,10,15,20-tetraphenylporphyrin, **1**.

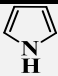
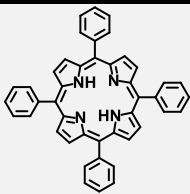
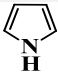
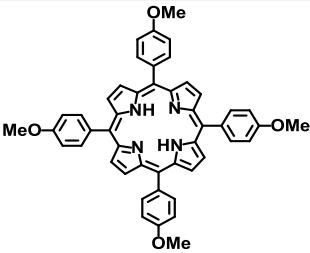
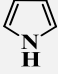
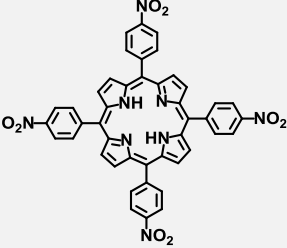
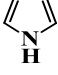
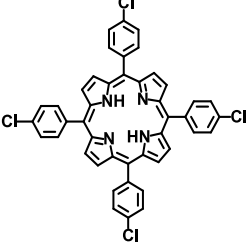
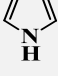
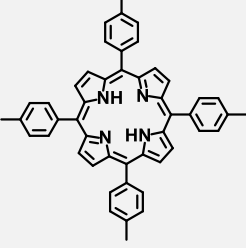
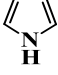
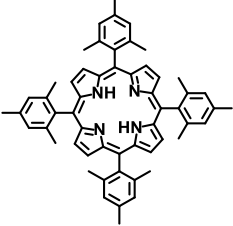
There was no significant change in the yield of the desired porphyrin by varying the quality of the solvent. By changing the solvent from dry DMF to HPLC grade DMF to reagent grade DMF, the same reaction was performed by following the similar optimized reaction condition, and it was observed that the yield of the porphyrin remained unchanged. Thus, it can be concluded that the yield of the porphyrin is not dependent on the purity of the DMF solvent. So the reaction can be easily carried out in

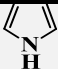
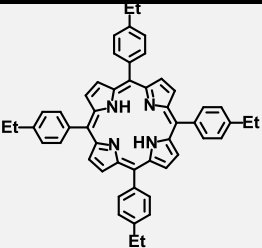
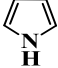
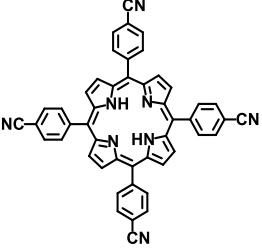
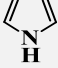
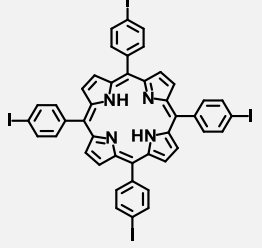
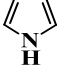
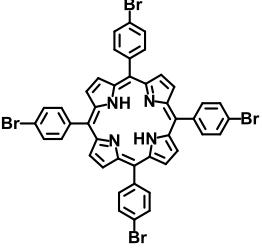
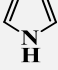
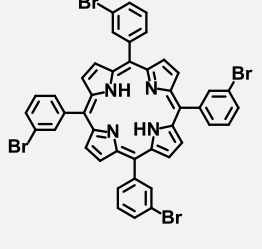

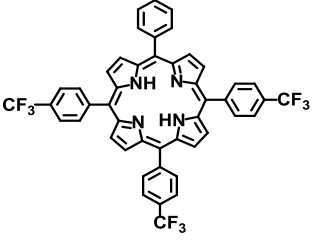
DMF-water mixed solvent system also. The reaction was performed in varying concentrations of reagent grade DMF with distilled water to further optimize the reaction conditions. For a representative example, 5,10,15,20-tetraphenylporphyrin, when 20% distilled water was added to 80% reagent grade DMF, the desired porphyrin was formed in a moderate yield. Further diluting the reagent grade DMF with distilled water (1:1), the desired porphyrin was formed but not in satisfactory yield. When reagent grade DMF was further diluted with distilled water (1:4), the yield of the desired porphyrin further decreased.

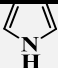
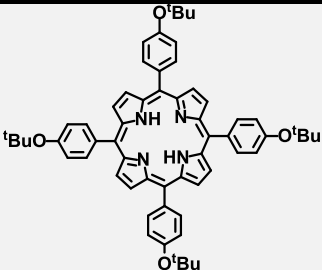

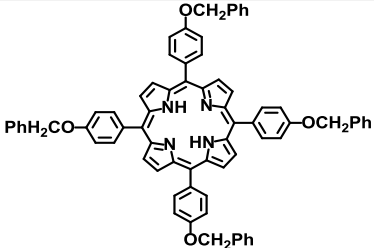
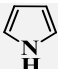
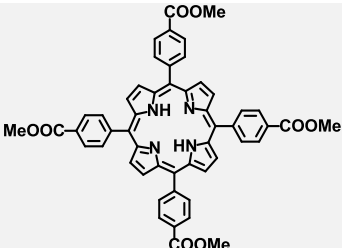
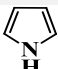
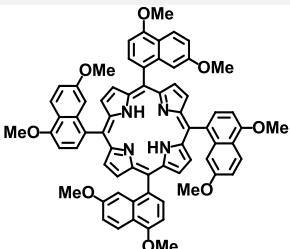
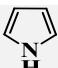
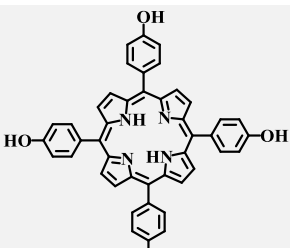
Aldehydes with varying electronic nature have been tested to synthesize a series of A<sub>4</sub>-porphyrins; however, it does not change much to the reaction yields. Moderate to good yields of A<sub>4</sub>-porphyrins are obtained regardless of the electronic nature of the aldehydes (Table 4.4).

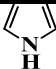
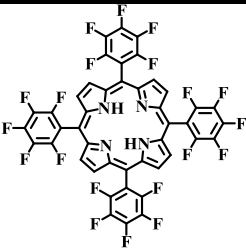
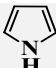
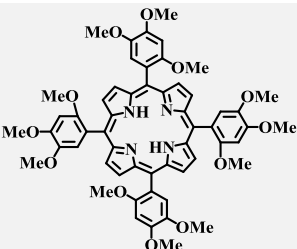
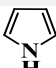
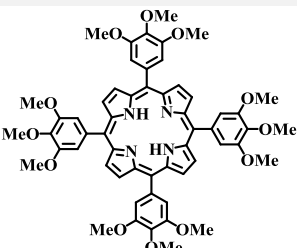
**Table 4.4** Scope of the synthesis of *meso*-substituted symmetric A<sub>4</sub>-porphyrins



Entry	Pyrrole	Porphyrin	Code	Yield (%)
1			1	21
2			2	29
3			3	28
4			4	20
5			5	20
			6	20

Entry	Pyrrole	Porphyrin	Code	Yield (%)
7			7	17
8			8	12
9			9	12
10			10	9
11			11	7
12			12	4

Entry	Pyrrole	Porphyrin	Code	Yield (%)
13			13	12
14			14	16
15			15	10
16			16	17
17			17	0

Entry	Pyrrole	Porphyrin	Code	Yield (%)
18			18	0
19			19	0
20			20	0

To prove the scalability of the process, a large-scale synthesis of A<sub>4</sub>-porphyrins was attempted. For a representative example, 10.0 mmol of aldehyde and 10.0 mmol of pyrrole were added to a 500 ml MeOH and 250 ml water mixture, followed by 20 ml of HCl. The reaction mixture was stirred at RT for 2 hours. The resulting mixture was filtered, and the precipitate was collected. The precipitate was further dissolved in 100 mL of reagent grade DMF and was refluxed for 1.5 hours. After cooling, the reaction mixture was transferred to the beaker and stirred overnight in the air. Finally, the crude product was purified by column chromatography through silica gel. These scale-up processes furnish similar yields to the small-scale synthesis.

For example, in the case of 5,10,15,20-tetraphenylporphyrin, we have obtained 261 mg (17%) of pure porphyrin, and for 5,10,15,20-tetrakis(4-methoxyphenyl)

---

porphyrin, we have obtained 441 mg (24 %) of pure porphyrin in gram-scale synthesis. No scrambling was detected via TLC and ESI-MS spectra of the crude reaction mixture. Although tetrapyrane is a direct precursor for corrole synthesis, we have not obtained any A<sub>3</sub>-corroles in the reaction mixture in the present case.

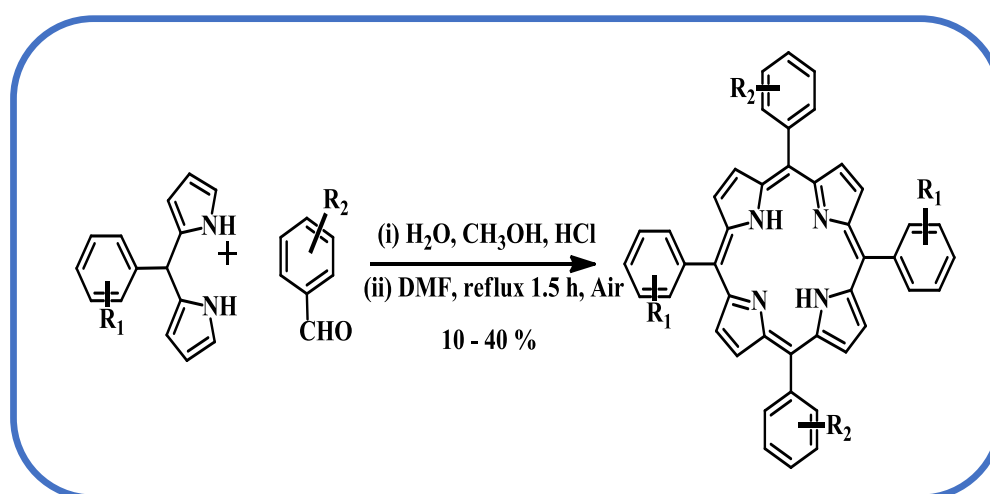
#### 4.2.2 *Trans*-A<sub>2</sub>B<sub>2</sub>-porphyrins. Optimization Study

*Trans*-A<sub>2</sub>B<sub>2</sub>-porphyrins are generally synthesized by following the MacDonald-Type [2+2] condensation reaction.<sup>36</sup> The limitation of this methodology is the formation of a mixture of different porphyrins often rather than the desired porphyrin, which makes the purification process more difficult. *Trans*-A<sub>2</sub>B<sub>2</sub>-porphyrins were synthesized by following the present optimized synthetic methodology. In this present methodology, the purification of the desired porphyrin is rather convenient. For the synthesis of various *trans*-A<sub>2</sub>B<sub>2</sub>-porphyrins, dipyrromethanes were used instead of pyrrole (Table 4.5). Dipyrromethanes are usually synthesized by reacting an aldehyde with pyrrole in the presence of trifluoroacetic acid. In a typical procedure, 1.0 mmol of aldehyde and 1.0 mmol of dipyrromethane were added to a 100 ml MeOH and 50 ml water mixture, followed by 10 ml of HCl. The reaction mixture was stirred at RT for 2 hours. The resulting mixture was filtered, and the precipitate was collected for the succeeding reaction. The precipitate was further dissolved in a minimum quantity of reagent grade DMF and was refluxed for 1.5 hours. After cooling, the reaction mixture was transferred to the beaker and stirred overnight in the air. Finally, the crude product was purified by column chromatography through silica gel in some cases. And for the rest of the cases, the desired porphyrin precipitated out from the solution. The crystals of the desired porphyrin can be easily collected by filtration and purified by washing the precipitate with MeOH. Dipyrromethanes with varying electron-withdrawing and electron releasing groups were tested for the synthesis of a series of *trans*-A<sub>2</sub>B<sub>2</sub>-porphyrins; however, no

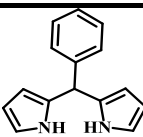
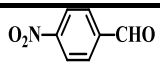
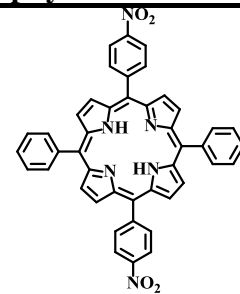
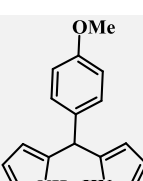
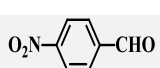
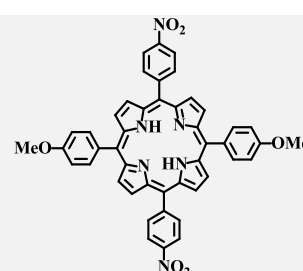
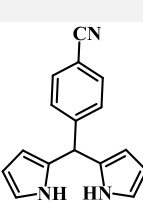
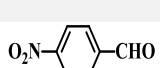
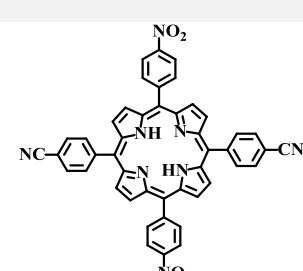
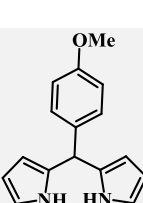
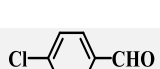
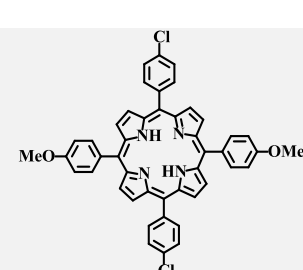
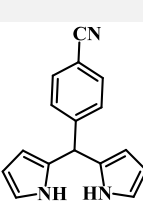
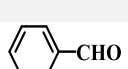
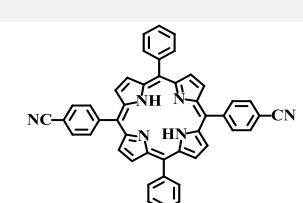
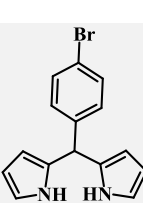
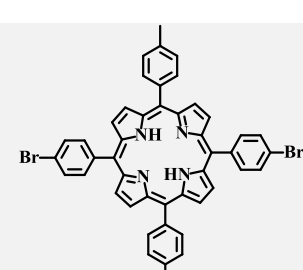


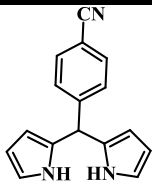
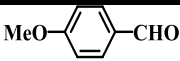
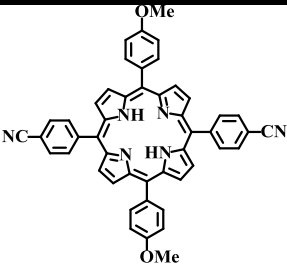
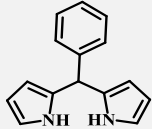
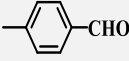
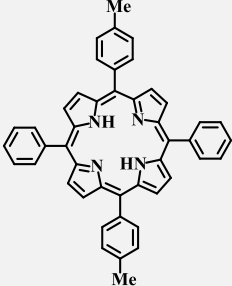
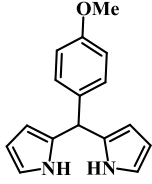
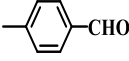
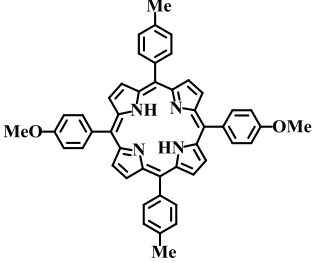
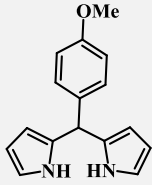
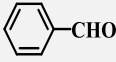
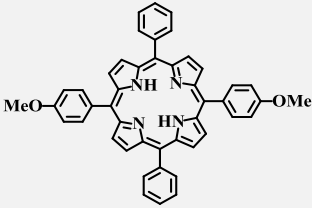
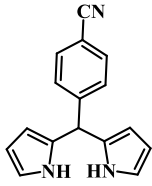
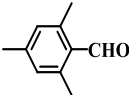
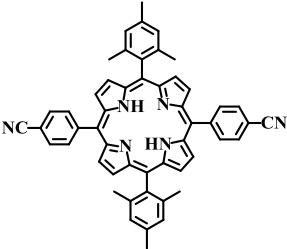
clear-cut electronic effect was observed. Moderate to good yields of *trans*-A<sub>2</sub>B<sub>2</sub>-porphyrins are obtained regardless of the electronic structure of the dipyrromethanes. No scrambling was detected via TLC and ESI-MS spectra of the crude reaction mixture. The mechanism of the reaction can be assigned based on the Adler-Longo methodology of porphyrin synthesis. The tetrapyrane derivative and the unreacted aldehyde, and some residual HCl obtained from the first step is possibly converted into a porphyrinogen derivative in DMF solvent and is further oxidized by aerial O<sub>2</sub> and generate the desired porphyrin.

**Table 4.5** Scope of the synthesis of *meso*-substituted *trans*-A<sub>2</sub>B<sub>2</sub>-porphyrins



Entry	DPM	Aldehyde	<i>trans</i> -A <sub>2</sub> B <sub>2</sub> -porphyrins	Code	Yield(%)
1				21	40

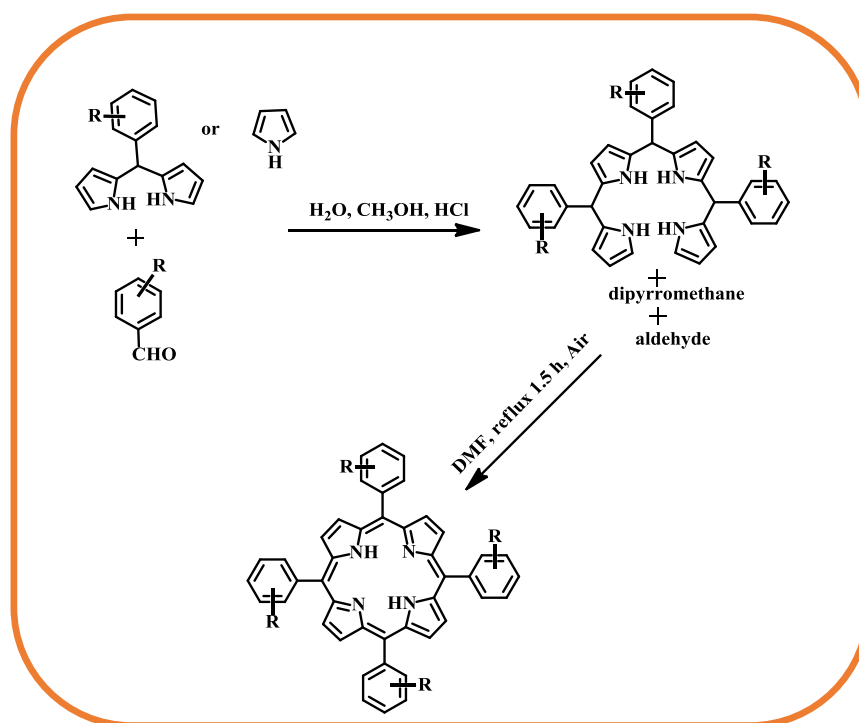
Entry	DPM	Aldehyde	<i>trans</i> -A <sub>2</sub> B <sub>2</sub> - porphyrins	Code	Yield(%)
2				22	31
3				23	30
4				24	23
5				25	19
6				26	17
7				27	13

Entry	DPM	Aldehyde	<i>trans</i> -A <sub>2</sub> B <sub>2</sub> - porphyrins	Code	Yield(%)
8				28	13
9				29	11
10				30	9
11				31	9
12				32	5

### 4.3 Analysis of the reaction mechanism

Based on these observations, we can postulate the probable mechanism for the porphyrin synthesis (Figure 4.1). The first step involves a simple condensation reaction

between pyrrole/ dipyrromethane with a suitable aldehyde in a water-methanol mixture via HCl catalysis and the generation of the corresponding tetrapyranes. The earlier researchers have well documented this step.<sup>35</sup> In the subsequent step, a coupling of tetrapyranes with the suitable aldehyde is imminent and aerobic oxidation is responsible for the generation of corresponding porphyrin derivatives.<sup>32</sup>



**Figure 4.1** Proposed mechanism.

#### 4.4 Conclusions

Synthesis of symmetric A<sub>4</sub>-porphyrins from aromatic aldehydes possessing a variety of substituents having the highest yield of 29%, and the [2+2] synthesis of *trans*-A<sub>2</sub>B<sub>2</sub>-porphyrins from dipyrromethanes bearing different substituents having the highest yield of 40% were reported herein. The first step involves the HCl catalyzed condensation reaction of pyrrole and aldehyde in an H<sub>2</sub>O-MeOH mixture. In the subsequent step, the obtained precipitate was dissolved in reagent grade DMF, refluxed (1-2 h), stirred overnight in the air at RT, and followed by purification via column

---

chromatography/crystallization, which resulted in the formation of pure porphyrins. The conditions described in this paper provide the easiest and cheapest synthesis of porphyrin on a large scale for getting a reproducible yield of 10-40% having high purity. The synthesis of *trans*-A<sub>2</sub>B<sub>2</sub>-porphyrins from dipyrromethanes is also scrambling free. Advantageously, this methodology does not need any expensive traditional oxidizers like DDQ, chloranil, *etc.* This reaction also does not need a large volume of dry chlorinated solvents. The present synthetic approach thus can open up an avenue for the synthesis of a wide range of symmetric-A<sub>4</sub> and *trans*-A<sub>2</sub>B<sub>2</sub> –porphyrins on a large scale, which will further widen the practical applications of these important classes of molecules. In essence, the present methodology does not represent the synthesis having the highest yield in the literature; however, it does represent the easiest and cheapest synthesis of porphyrin on a large scale for getting a reproducible yield of 10-40% having high purity.

## **4.5 Experimental Section**

### **4.5.1 Materials**

The precursor's pyrrole and aldehydes were purchased from Aldrich, USA. DMF was purchased from Merck Pvt. Ltd chemicals. Other chemicals were of reagent grade. Hexane, CH<sub>2</sub>Cl<sub>2</sub>, CH<sub>3</sub>CN were distilled from KOH and CaH<sub>2</sub>, respectively. For spectroscopy studies, HPLC-grade solvents were used. 5-phenyldipyrromethane, 5-(4-methoxyphenyl)dipyrromethane, 5-(4-bromophenyl) dipyrromethane, and 5-(4-cyanophenyl)dipyrromethane were prepared by following an earlier literature report.<sup>35</sup>

### **4.5.2 Physical Measurements**

The elemental analyses were carried out with a Euro EA elemental analyzer. UV–Vis spectral studies were performed on a Perkin–Elmer LAMBDA-750 spectrophotometer. Emission spectral studies were performed on a Perkin Elmer, LS 55

---

spectrophotometer using an optical cell of 1 cm path length. The NMR measurements were carried out using a Bruker 400 MHz NMR spectrometer. Chemical shifts are expressed in parts per million (ppm) relative to residual solvents. Electrospray mass spectra were recorded on a Bruker Micro TOF—QII mass spectrometer.

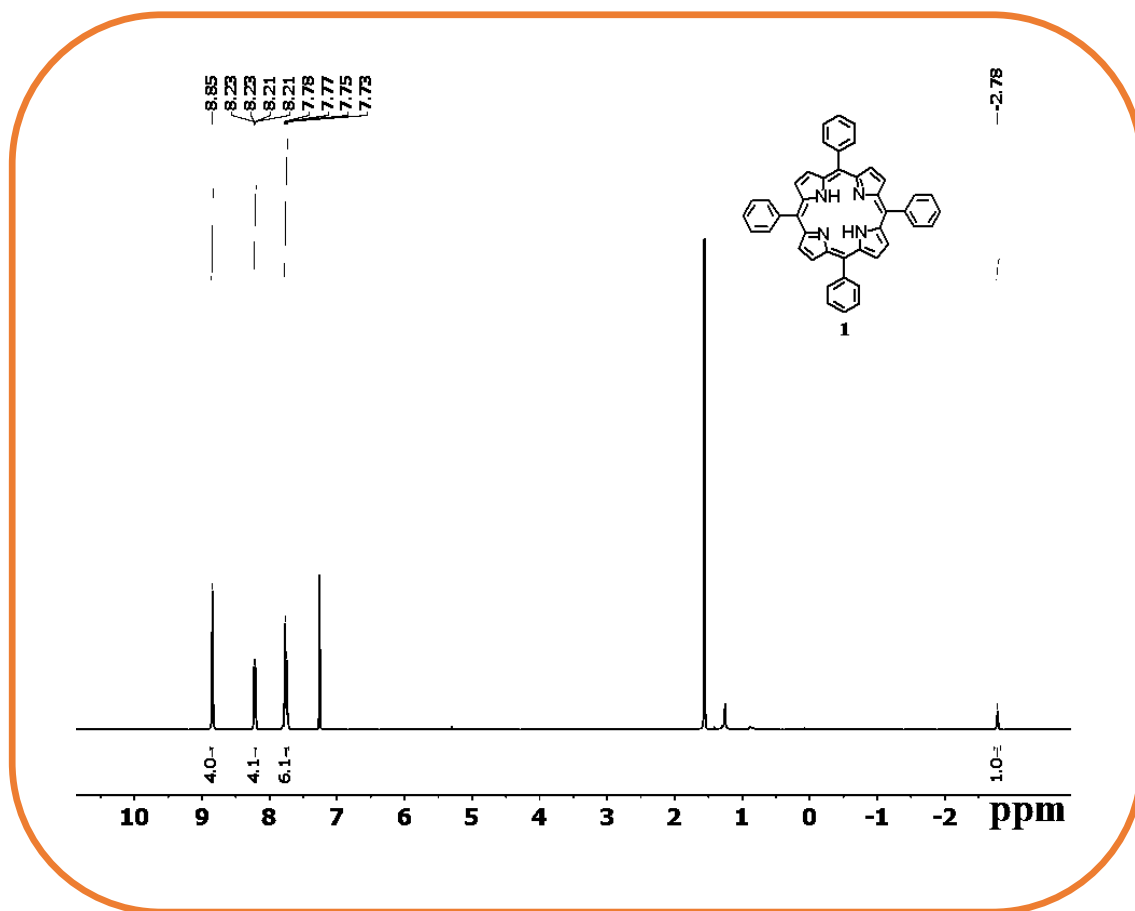
### 4.5.3 Syntheses

#### Synthesis of 5,10,15,20-Tetraphenylporphyrin, **1**

204  $\mu$ l (2 mmol) of benzaldehyde and 140  $\mu$ l (2 mmol) of pyrrole were added in a 100 ml MeOH and 50 ml water (2:1) mixture, followed by the addition of 10 ml HCl. The reaction mixture was stirred at RT for 2 hours. The reaction mixture was filtered with Whatman filter paper, and the precipitate was dissolved in 15 ml of DMF solution and was refluxed for another 1.5 hours. This solution was finally transferred to a beaker and was stirred overnight. Then the solution was evaporated to dryness. The crude product was purified using column chromatography through silica gel (100-200 mesh) or purified via crystallization.

#### For 5,10,15,20-Tetraphenylporphyrin, **1**

Yield: 21% (61 mg). Anal. Calcd (found) for  $C_{44}H_{30}N_4$  (**1**): C, 85.97 (85.88); H, 4.92 (4.83); N, 9.11 (9.17).  $^1H$  NMR (400 MHz, Chloroform-*d*)  $\delta$  8.85 (s, 8H), 8.25 – 8.19 (m, 8H), 7.79 – 7.72 (m, 12H), -2.78 (s, 2H) (Figure 4.2). Other analytical data are consistent with the previously reported authentic compounds.<sup>37</sup>



**Figure 4.2**  $^1\text{H}$  NMR spectrum of 5,10,15,20-Tetraphenylporphyrin, **1** in  $\text{CDCl}_3$ .

#### Gram-scale synthesis of 5,10,15,20-Tetraphenylporphyrin, **1**

1.02 ml (10 mmol) of benzaldehyde and 694  $\mu\text{l}$  (10 mmol) of pyrrole were added in a 500 ml MeOH and 250 ml water (2:1) mixture, followed by the addition of 20 ml HCl. The reaction mixture was stirred at RT for 2 hours. The reaction mixture was filtered with Whatman filter paper, and the precipitate was dissolved in 100 ml of DMF solution. This DMF solution was refluxed for another 1.5 hours. This solution was finally transferred to a beaker and was stirred overnight. Then the solution was evaporated to dryness. The crude product was purified by using column chromatography through silica gel (100–200 mesh), or it can be purified via crystallization also. Yield: 17% (261 mg).

---

**Synthesis of 5,10,15,20-Tetrakis(4-methoxyphenyl)porphyrin, 2**

243  $\mu$ l (2 mmol) of 4-methoxybenzaldehyde and 140  $\mu$ l (2 mmol) of pyrrole were added in a 100 ml MeOH and 50 ml water (2:1) mixture, followed by the addition of 10 ml HCl. The reaction mixture was stirred at RT for 2 hours. The reaction mixture was filtered with Whatman filter paper, and the precipitate was dissolved in 15 ml of DMF solution. This DMF solution was refluxed for another 1.5 hours. This solution was finally transferred to a beaker and was stirred overnight. Then the solution was evaporated to dryness. The crude product was purified using column chromatography through silica gel (100-200 mesh) or purified via crystallization.

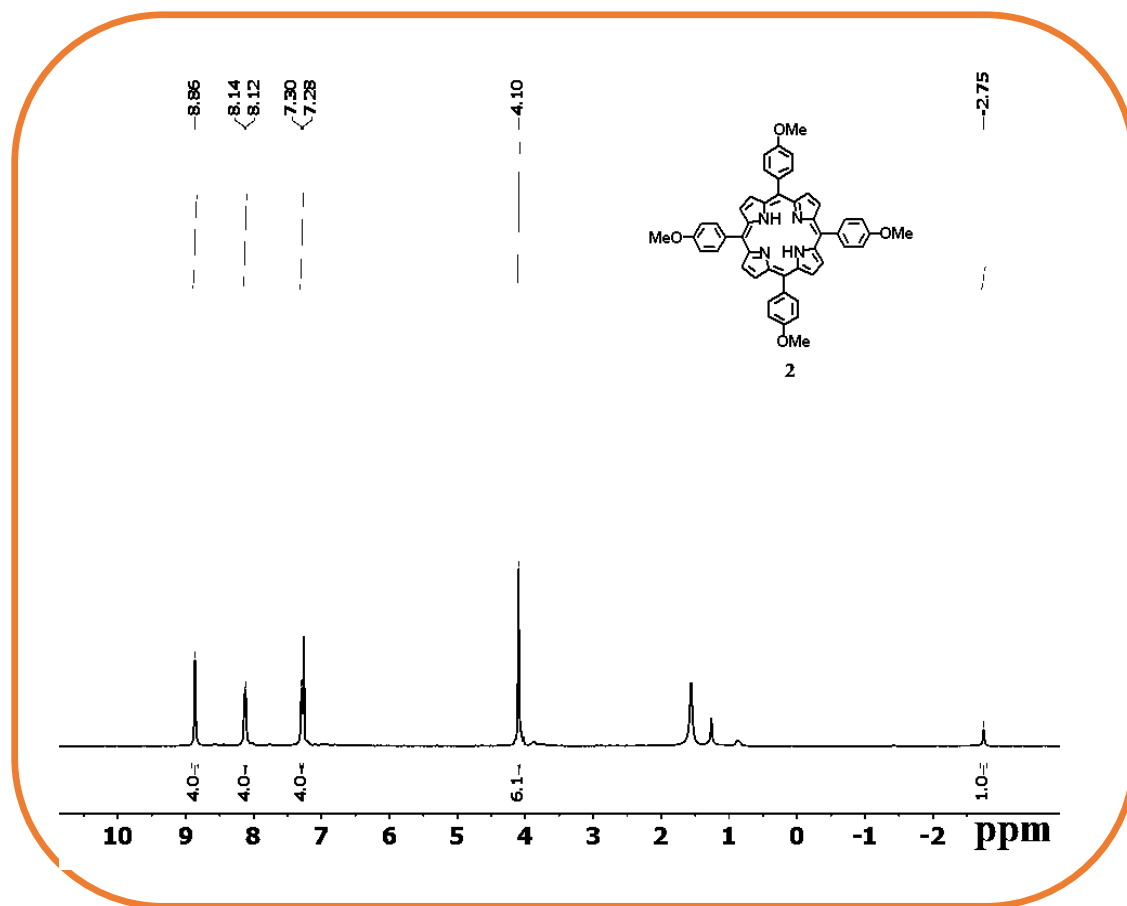
**For 5,10,15,20-Tetrakis(4-methoxyphenyl)porphyrin, 2**

Yield: 29 % (105 mg). Anal. Calcd (found) for  $C_{48}H_{38}N_4O_4$  (**2**): C, 78.45 (78.55); H, 5.21 (5.32); N, 7.62 (7.77).  $^1H$  NMR (400 MHz, Chloroform-*d*)  $\delta$  8.86 (s, 8H), 8.13 (d,  $J$  = 8.0 Hz, 8H), 7.29 (d,  $J$  = 8.0 Hz, 8H), 4.10 (s, 12H), -2.75 (s, 2H) (Figure 4.3). Other analytical data are consistent with the previously reported authentic compounds.<sup>37</sup>

**Gram-scale synthesis of 5,10,15,20-Tetrakis(4-methoxyphenyl)porphyrin, 2**

1.2 ml (10 mmol) of 4-methoxybenzaldehyde and 694  $\mu$ l (10 mmol) of pyrrole were added to a 500 ml MeOH and 250 ml water (2:1) mixture, followed by the addition of 20 ml HCl. The reaction mixture was stirred at RT for 2 hours. The reaction mixture was filtered with Whatman filter paper, and the precipitate was dissolved in 100 ml of DMF solution. This DMF solution was refluxed for another 1.5 hours. This solution was finally transferred to a beaker and was stirred overnight. Then the solution was evaporated to dryness. The crude product was purified using column chromatography through silica gel (100-200 mesh) or purified via crystallization. Yield: 24% (441 mg).





**Figure 4.3**  $^1\text{H}$  NMR spectrum of 5,10,15,20-Tetrakis(4-methoxyphenyl)porphyrin, **2** in  $\text{CDCl}_3$ .

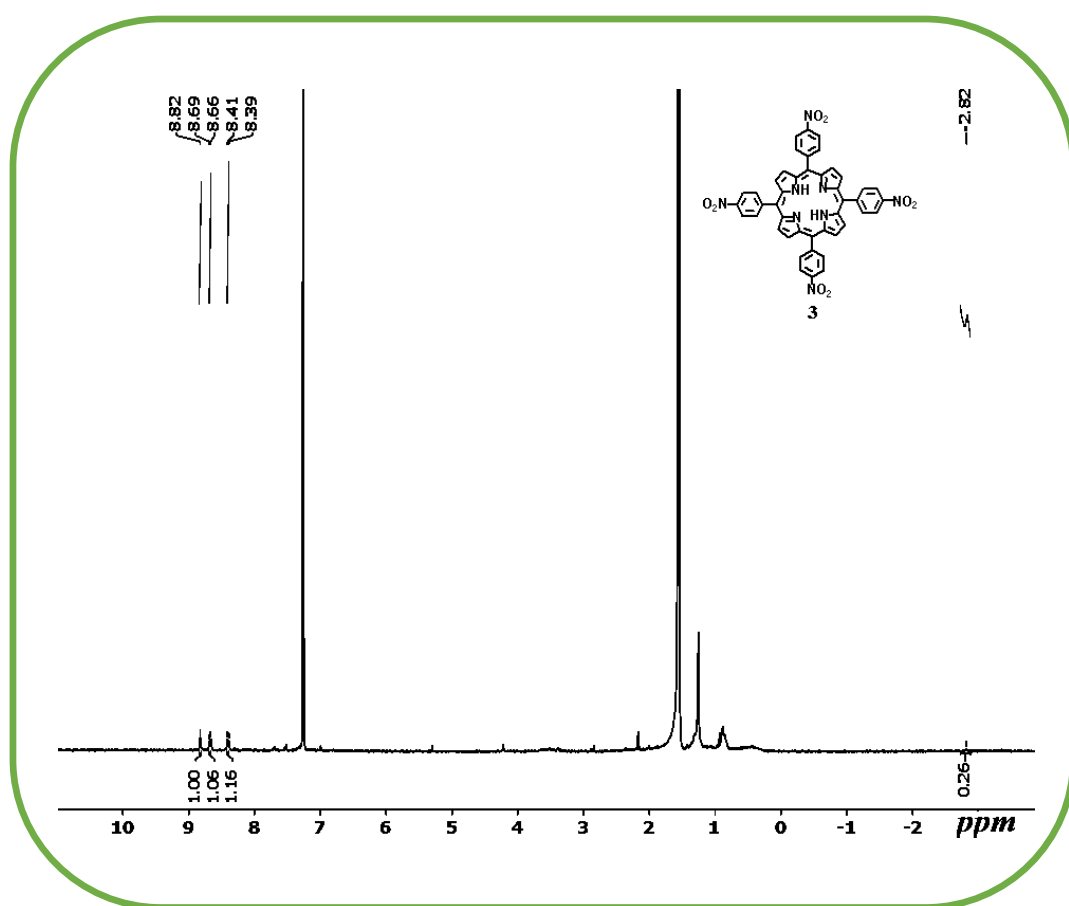
### Synthesis of 5,10,15,20-Tetrakis(4-nitrophenyl)porphyrin, **3**

302 mg (2 mmol) of 4-nitrobenzaldehyde and 140  $\mu\text{l}$  (2 mmol) of pyrrole were added in a 100 ml MeOH and 50 ml water (2:1) mixture, followed by the addition of 10 ml HCl. The reaction mixture was stirred at RT for 2 hours. The reaction mixture was filtered with Whatman filter paper, and the precipitate was dissolved in 15 ml of DMF solution. This DMF solution was refluxed for another 1.5 hours. This solution was finally transferred to a beaker and was stirred overnight. Then the solution was evaporated to dryness. The crude product was purified using column chromatography through silica gel (100-200 mesh) or purified via crystallization.

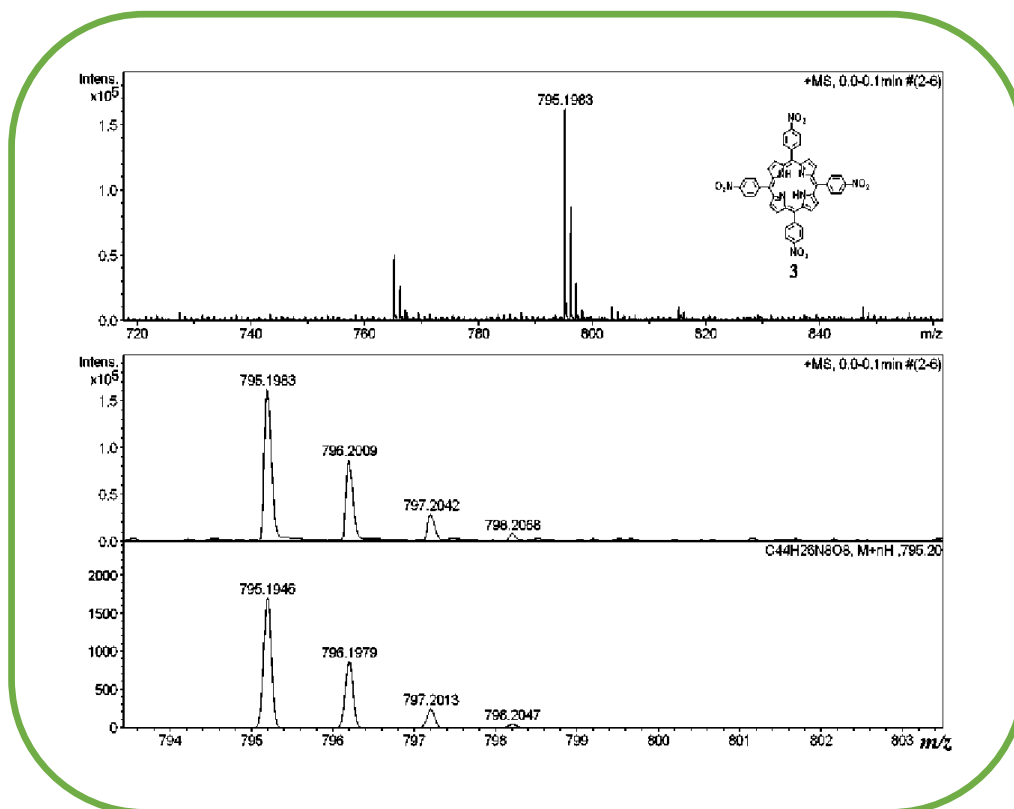
---

**For 5,10,15,20-Tetrakis(4-nitrophenyl)porphyrin, **3****

Yield: 28% (109 mg). Anal. Calcd (found) for  $C_{44}H_{26}N_8O_8$  (**3**): C, 66.50 (66.62); H, 3.30 (3.39); N, 14.10 (14.01).  $^1H$  NMR (400 MHz, Chloroform-*d*)  $\delta$  8.82 (m, 8H), 8.68 (m, 8H), 8.40 (m, 8H), -2.82 (s, 2H) (Figure 4.4).  $m/z$ :  $[3+H]^+$  Calcd for  $C_{44}H_{27}N_8O_8$  795.1946; Found 795.1983 (Figure 4.5). Other analytical data are consistent with the previously reported authentic compounds.<sup>38</sup>



**Figure 4.4**  $^1H$  NMR spectrum of 5,10,15,20-Tetrakis(4-nitrophenyl)porphyrin, **3** in  $CDCl_3$ .



**Figure 4.5** ESI-MS spectrum of 5,10,15,20-Tetrakis(4-nitrophenyl)porphyrin, **3** in CH<sub>3</sub>CN shows the measured spectrum with isotopic distribution pattern.

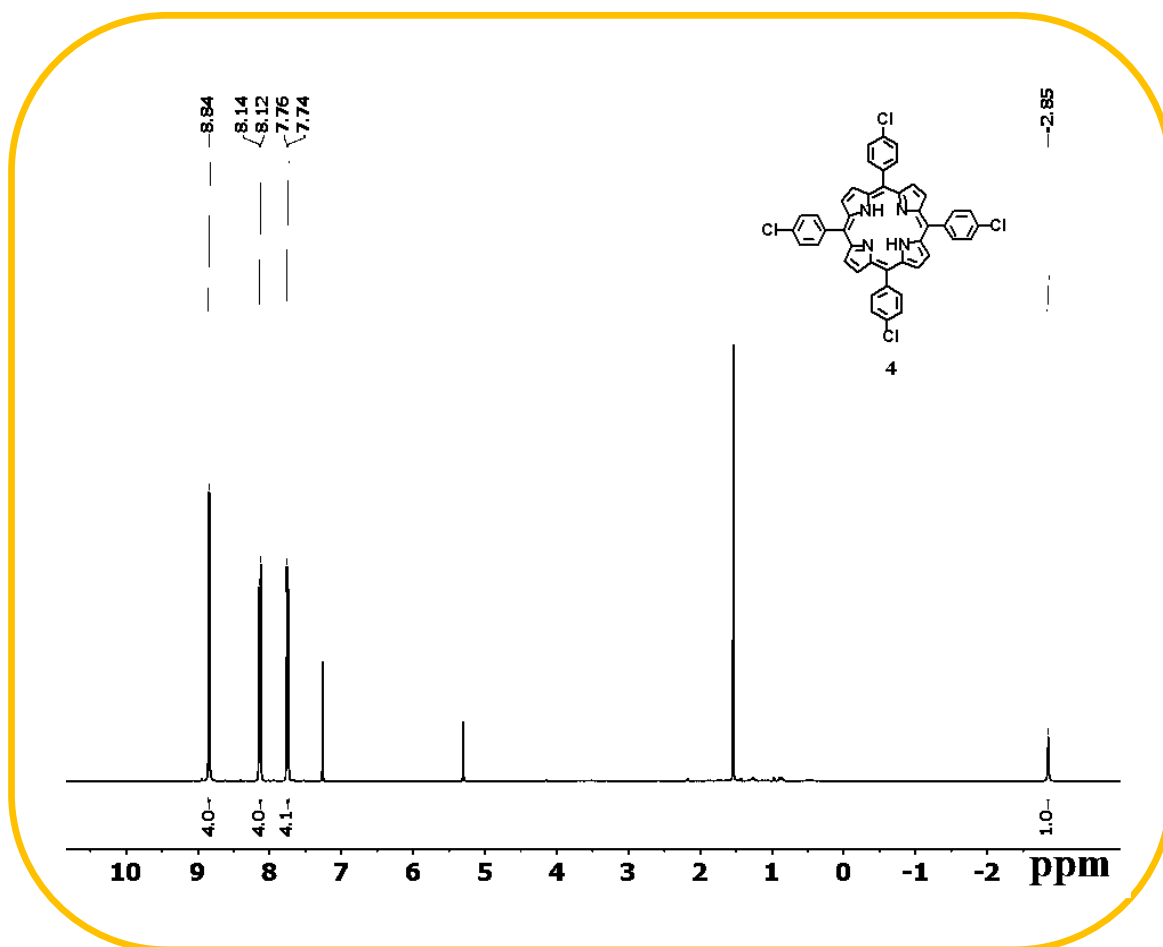
#### Synthesis of 5,10,15,20-Tetrakis(4-chlorophenyl)porphyrin, **4**

281 mg (2 mmol) of 4-chlorobenzaldehyde and 140  $\mu$ l (2 mmol) of pyrrole were added in a 100 ml MeOH and 50 ml water (2:1) mixture, followed by the addition of 10 ml HCl. The reaction mixture was stirred at RT for 2 hours. The reaction mixture was filtered with Whatman filter paper, and the precipitate was dissolved in 15 ml of DMF solution. This DMF solution was refluxed for another 1.5 hours. This solution was finally transferred to a beaker and was stirred overnight. Then the solution was evaporated to dryness. The crude product was purified by using column chromatography through silica gel (100-200 mesh).

---

#### For 5,10,15,20-Tetrakis(4-chlorophenyl)porphyrin, **4**

Yield: 20% (76 mg). Anal. Calcd (found) for  $C_{44}H_{26}Cl_4N_4$  (**4**): C, 70.23 (70.13); H, 3.48 (3.38); N, 7.45 (7.58).  $^1H$  NMR (400 MHz, Chloroform-*d*)  $\delta$  8.84 (s, 8H), 8.16 – 8.12 (d, 8H), 7.78 – 7.72 (d, 8H), -2.85 (s, 2H) (Figure 4.6). Other analytical data are consistent with the previously reported authentic compounds.<sup>39</sup>



**Figure 4.6**  $^1H$  NMR spectrum of 5,10,15,20-Tetrakis(4-chlorophenyl)porphyrin, **4** in  $CDCl_3$ .

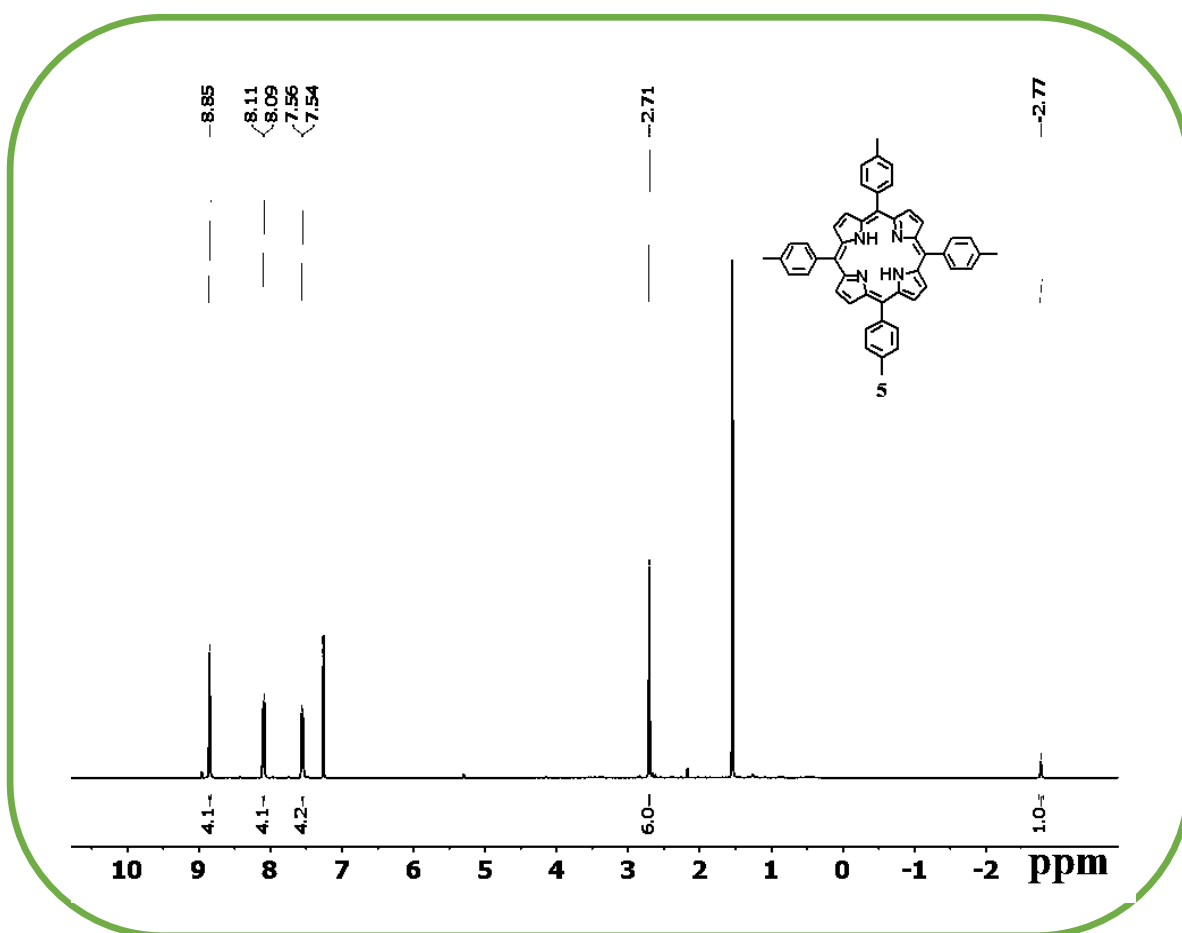
#### Synthesis of 5,10,15,20-Tetrakis(4-methylphenyl)porphyrin, **5**

236  $\mu$ l (2 mmol) of *p*-tolualdehyde and 140  $\mu$ l (2 mmol) of pyrrole were added in a 100 ml MeOH and 50 ml water (2:1) mixture, followed by the addition of 10 ml HCl. The reaction mixture was stirred at RT for 2 hours. The reaction mixture was filtered

with Whatman filter paper, and the precipitate was dissolved in 15 ml of DMF solution. This DMF solution was refluxed for another 1.5 hours. This solution was finally transferred to a beaker and was stirred overnight. Then the solution was evaporated to dryness. The crude product was purified using column chromatography through silica gel (100-200 mesh) or purified via crystallization.

**For 5,10,15,20-Tetrakis(4-methylphenyl)porphyrin, **5****

Yield: 20% (66 mg). Anal. Calcd (found) for  $C_{48}H_{38}N_4$  (**5**): C, 85.94 (85.85); H, 5.71 (5.62); N, 8.35 (8.47).  $^1H$  NMR (400 MHz, Chloroform-*d*)  $\delta$  8.85 (s, 8H), 8.12 – 8.08 (m, 8H), 7.55 (d,  $J = 7.7$  Hz, 8H), 2.71 (s, 12H), -2.77 (s, 2H) (Figure 4.7). Other analytical data are consistent with the previously reported authentic compounds.<sup>39</sup>



**Figure 4.7**  $^1H$  NMR spectrum of 5,10,15,20-Tetrakis(4-methylphenyl)porphyrin, **5** in  $CDCl_3$ .

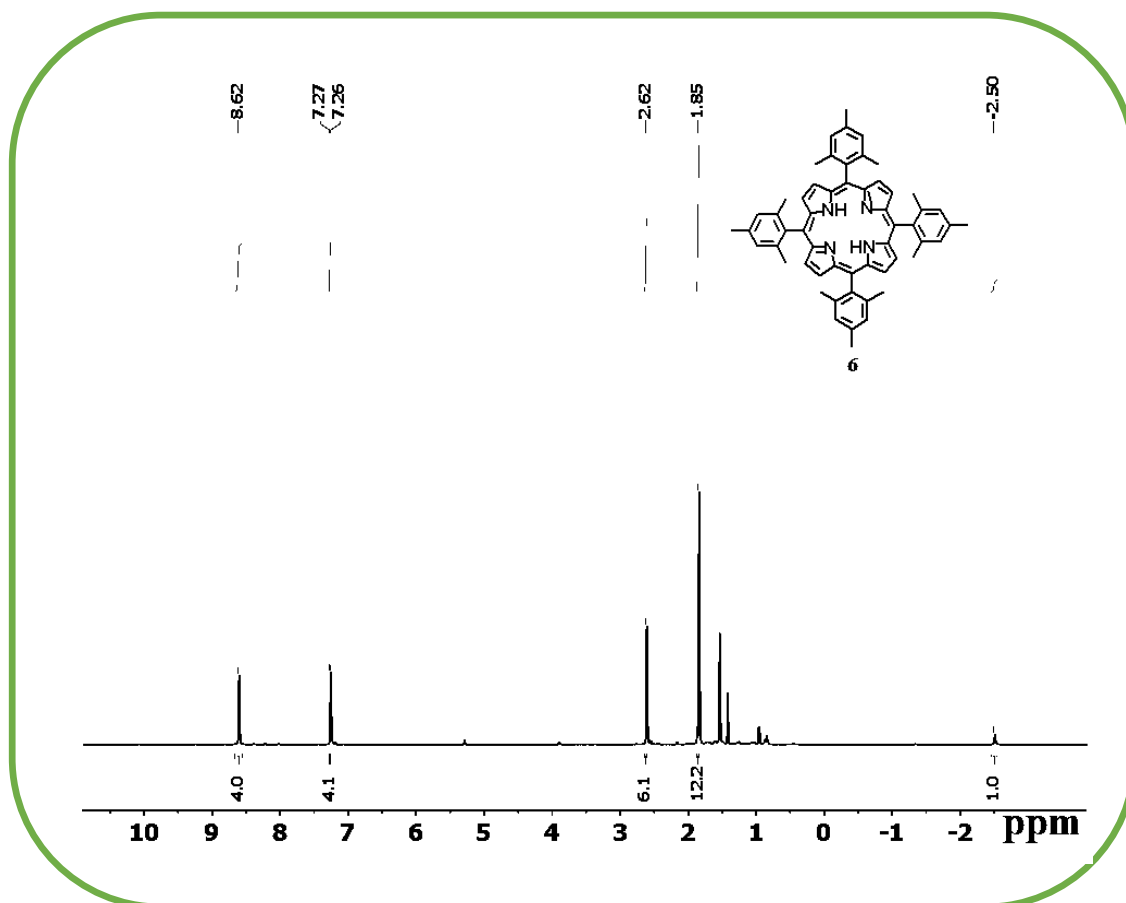
---

### Synthesis of 5,10,15,20-Tetrakis(2,4,6-trimethylphenyl)porphyrin, **6**

296 mg (2 mmol) of 2,4,6-trimethylbenzaldehyde and 140  $\mu$ l (2 mmol) of pyrrole were added in a 100 ml MeOH and 50 ml water (2:1) mixture, followed by the addition of 10 ml HCl. The reaction mixture was stirred at RT for 2 hours. The reaction mixture was filtered with Whatman filter paper, and the precipitate was dissolved in 15 ml of DMF solution. This DMF solution was refluxed for another 1.5 hours. This solution was finally transferred to a beaker and was stirred overnight. Then the solution was evaporated to dryness. The crude product was purified by using column chromatography through silica gel (100-200 mesh).

### For 5,10,15,20-Tetrakis(2,4,6-trimethylphenyl)porphyrin, **6**

Yield: 20% (78 mg). Anal. Calcd (found) for C<sub>56</sub>H<sub>54</sub>N<sub>4</sub> (**6**): C, 85.89 (85.78); H, 6.95 (6.87); N, 7.15 (7.27). <sup>1</sup>H NMR (400 MHz, Chloroform-*d*)  $\delta$  8.62 (s, 8H), 7.26 (s, 8H), 2.62 (s, 12H), 1.85 (s, 24H), -2.50 (s, 2H) (Figure 4.8). Other analytical data are consistent with the previously reported authentic compounds.<sup>40</sup>



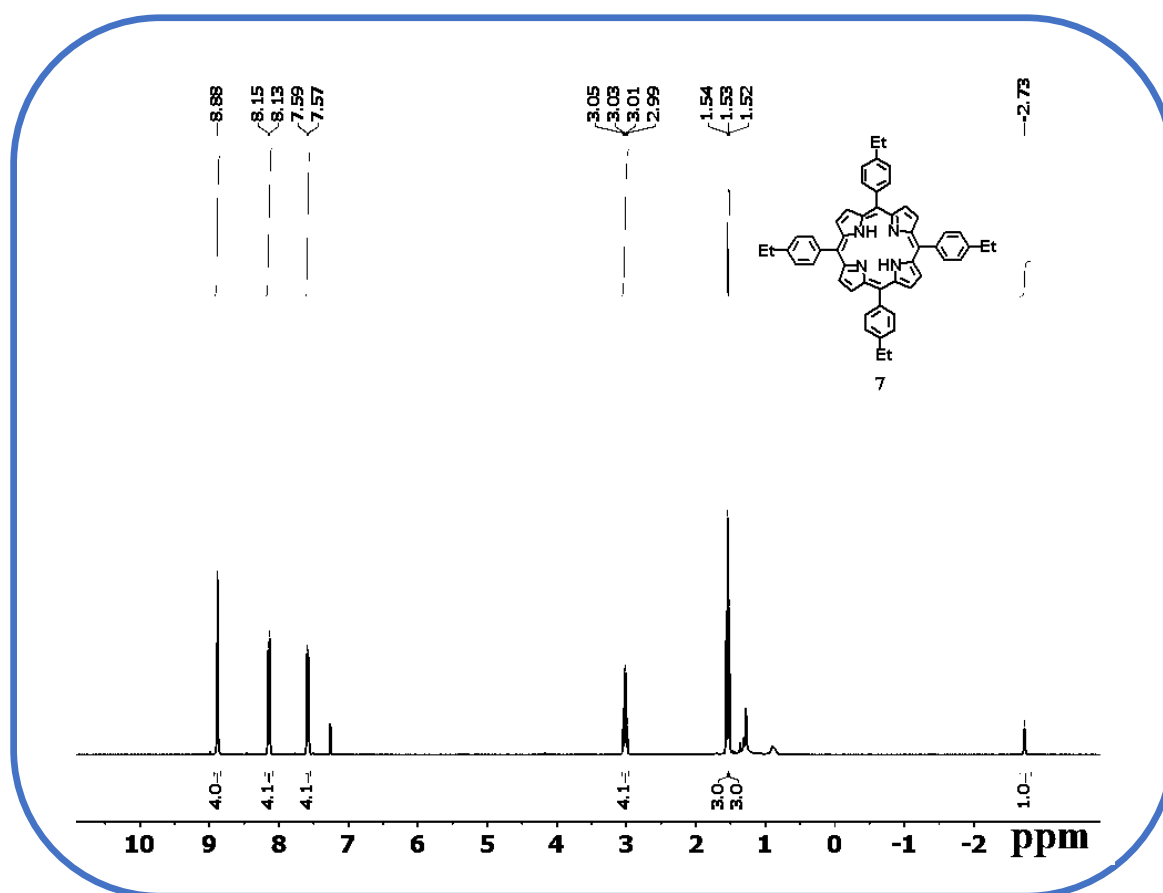
**Figure 4.8**  $^1\text{H}$  NMR spectrum of 5,10,15,20-Tetrakis(2,4,6-trimethylphenyl)porphyrin, **6** in  $\text{CDCl}_3$ .

#### Synthesis of 5,10,15,20-Tetrakis(4-ethylphenyl)porphyrin, **7**

268  $\mu\text{l}$  (2 mmol) of 4-ethylbenzaldehyde and 140  $\mu\text{l}$  (2 mmol) of pyrrole were added in a 100 ml MeOH and 50 ml water (2:1) mixture, followed by the addition of 10 ml HCl. The reaction mixture was stirred at RT for 2 hours. The reaction mixture was filtered with Whatman filter paper, and the precipitate was dissolved in 15 ml of DMF solution. This DMF solution was refluxed for another 1.5 hours. This solution was finally transferred to a beaker and was stirred overnight. Then the solution was evaporated to dryness. The crude product was purified using column chromatography through silica gel (100-200 mesh) or purified via crystallization.

### For 5,10,15,20-Tetrakis(4-ethylphenyl)porphyrin, **7**

Yield: 17% (60 mg). Anal. Calcd (found) for  $C_{52}H_{46}N_4$  (**7**): C, 85.91 (85.98); H, 6.38 (6.33); N, 7.71 (7.62).  $^1H$  NMR (400 MHz, Chloroform-*d*)  $\delta$  8.88 (s, 8H), 8.18 – 8.10 (d,  $J = 7.9$  Hz, 8H), 7.58 (d,  $J = 7.9$  Hz, 8H), 3.02 (q,  $J = 7.6$  Hz, 8H), 1.55 – 1.51 (m, 12H), -2.73 (s, 2H) (Figure 4.9). Other analytical data are consistent with the previously reported authentic compounds.<sup>41</sup>



**Figure 4.9**  $^1H$  NMR spectrum of 5,10,15,20-Tetrakis-(4-ethylphenyl)porphyrin, **7** in  $CDCl_3$ .

### Synthesis of 5,10,15,20-Tetrakis(4-cyanophenyl)porphyrin, **8**

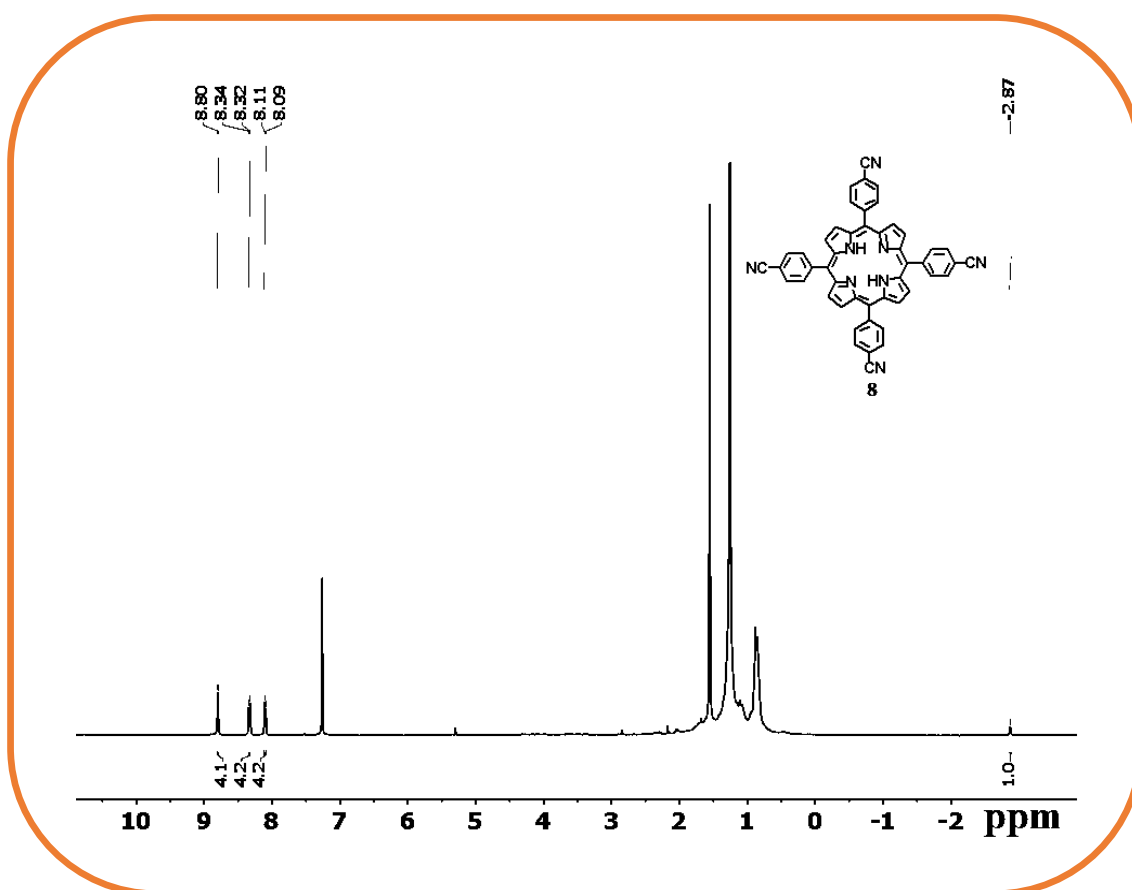
262 mg (2 mmol) of 4-cyanobenzaldehyde and 140  $\mu$ l (2 mmol) of pyrrole were added in a 100 ml MeOH and 50 ml water (2:1) mixture, followed by the addition of 10 ml HCl. The reaction mixture was stirred at RT for 2 hours. The reaction mixture was



filtered with Whatman filter paper, and the precipitate was dissolved in 15 ml of DMF solution. This DMF solution was refluxed for another 1.5 hours. This solution was finally transferred to a beaker and was stirred overnight. Then the solution was evaporated to dryness. The crude product was purified by using column chromatography through silica gel (100-200 mesh).

**For 5,10,15,20-Tetrakis(4-cyanophenyl)porphyrin, **8****

Yield: 12% (44 mg). Anal. Calcd (found) for  $C_{48}H_{26}N_8$  (**5**): C, 80.66 (80.50); H, 3.67 (3.53); N, 15.68 (15.77).  $^1H$  NMR (400 MHz, Chloroform-*d*)  $\delta$  8.80 (s, 8H), 8.33 (d,  $J = 7.8$  Hz, 8H), 8.10 (d,  $J = 7.9$  Hz, 8H), -2.88 (s, 2H) (Figure 4.10). Other analytical data are consistent with the previously reported authentic compounds.<sup>38</sup>



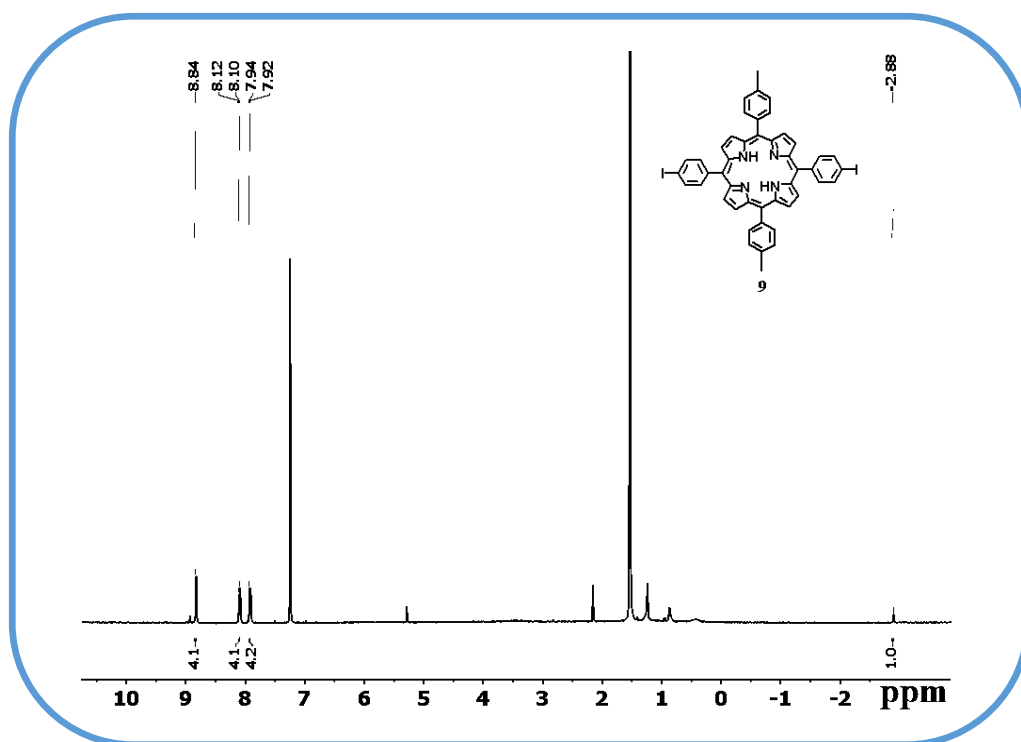
**Figure 4.10**  $^1H$  NMR spectrum of 5,10,15,20-Tetrakis(4-cyanophenyl)porphyrin, **8** in  $CDCl_3$ .

### Synthesis of 5,10,15,20-Tetrakis(4-iodophenyl)porphyrin, **9**

464 mg (2 mmol) of 4-iodobenzaldehyde and 140  $\mu$ l (2 mmol) of pyrrole were added in a 100 ml MeOH and 50 ml water (2:1) mixture, followed by the addition of 10 ml HCl. The reaction mixture was stirred at RT for 2 hours. The reaction mixture was filtered with Whatman filter paper, and the precipitate was dissolved in 15 ml of DMF solution. This DMF solution was refluxed for another 1.5 hours. This solution was finally transferred to a beaker and was stirred overnight. Then the solution was evaporated to dryness. The crude product was purified by using column chromatography through silica gel (100-200 mesh).

### For 5,10,15,20-Tetrakis(4-iodophenyl)porphyrin, **9**

Yield: 12% (63 mg). Anal. Calcd (found) for  $C_{44}H_{26}I_4N_4$  (**9**): C, 47.26 (47.39); H, 2.34 (2.43); N, 5.01 (5.17).  $^1H$  NMR (400 MHz, Chloroform-*d*)  $\delta$  8.84 (s, 8H), 8.11 (d,  $J$  = 8.0 Hz, 8H), 7.93 (d,  $J$  = 8.0 Hz, 8H), -2.88 (s, 2H) (Figure 4.11). Other analytical data are consistent with the previously reported authentic compounds.<sup>42</sup>



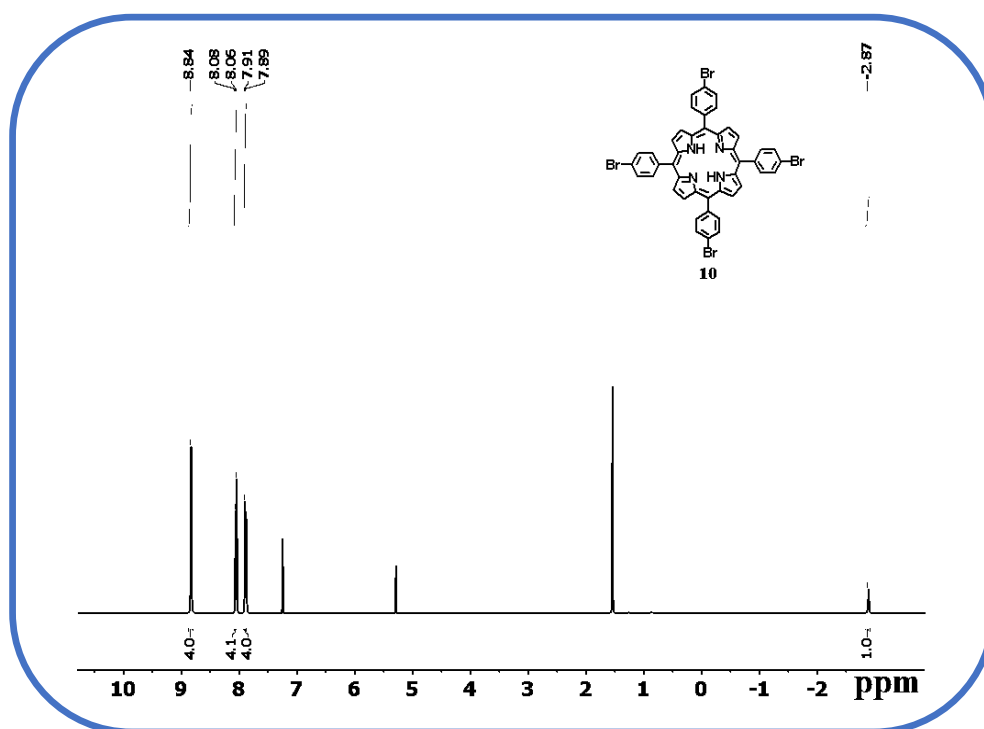
**Figure 4.11**  $^1H$  NMR spectrum of 5,10,15,20-Tetrakis(4-iodophenyl)porphyrin, **9** in  $CDCl_3$ .

### Synthesis of 5,10,15,20-Tetrakis(4-bromophenyl)porphyrin, **10**

370 mg (2 mmol) of 4-bromobenzaldehyde and 140  $\mu$ l (2 mmol) of pyrrole were added in a 100 ml MeOH and 50 ml water (2:1) mixture, followed by the addition of 10 ml HCl. The reaction mixture was stirred at RT for 2 hours. The reaction mixture was filtered with Whatman filter paper, and the precipitate was dissolved in 15 ml of DMF solution. This DMF solution was refluxed for another 1.5 hours. This solution was finally transferred to a beaker and was stirred overnight. Then the solution was evaporated to dryness. The crude product was purified by using column chromatography through silica gel (100-200 mesh).

#### For 5,10,15,20-Tetrakis(4-bromophenyl)porphyrin, **10**

Yield: 9% (40 mg). Anal. Calcd (found) for  $C_{44}H_{26}Br_4N_4$  (**10**): C, 56.81 (56.95); H, 2.82 (2.93); N, 6.02 (6.17).  $^1H$  NMR (400 MHz, Chloroform- $d$ )  $\delta$  8.84 (s, 8H), 8.07 (d,  $J$  = 8.1 Hz, 8H), 7.90 (dd,  $J$  = 8.2, 1.4 Hz, 8H), -2.87 (s, 2H) (Figure 4.12). Other analytical data are consistent with the previously reported authentic compounds.<sup>43</sup>



**Figure 4.12**  $^1H$  NMR spectrum of 5,10,15,20-Tetrakis(4-bromophenyl)porphyrin, **10** in  $CDCl_3$ .

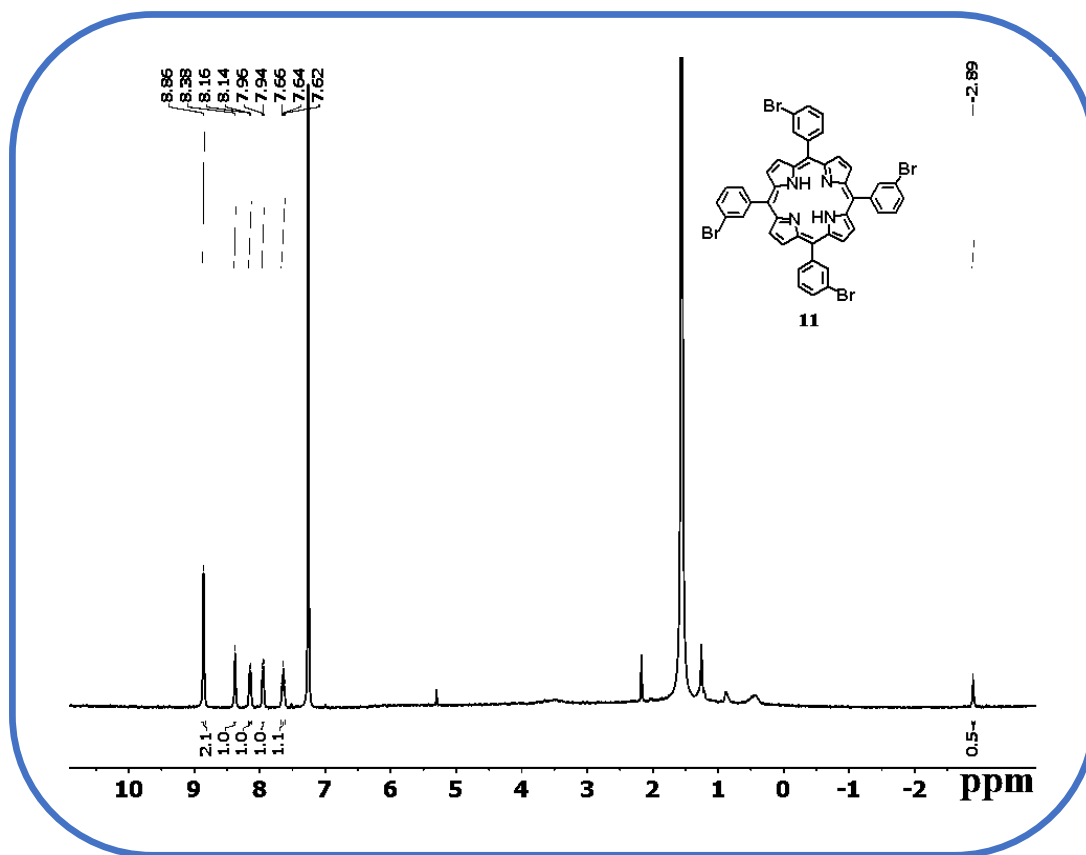
---

**Synthesis of 5,10,15,20-Tetrakis(3-bromophenyl)porphyrin, 11**

233  $\mu$ l (2 mmol) of 3-bromobenzaldehyde and 140  $\mu$ l (2 mmol) of pyrrole were added in a 100 ml MeOH and 50 ml water (2:1) mixture, followed by the addition of 10 ml HCl. The reaction mixture was stirred at RT for 2 hours. The reaction mixture was filtered with Whatman filter paper, and the precipitate was dissolved in 15 ml of DMF solution. This DMF solution was refluxed for another 1.5 hours. This solution was finally transferred to a beaker and was stirred overnight. Then the solution was evaporated to dryness. The crude product was purified by using column chromatography through silica gel (100-200 mesh).

**For 5,10,15,20-Tetrakis(3-bromophenyl)porphyrin, 11**

Yield: 7% (30 mg). Anal. Calcd (found) for  $C_{44}H_{26}Br_4N_4$  (**11**): C, 56.81 (56.70); H, 2.82 (2.73); N, 6.02 (6.14).  $^1H$  NMR (400 MHz, Chloroform-*d*)  $\delta$  8.86 (s, 8H), 8.38 (s, 4H), 8.15 (d,  $J = 7.5$  Hz, 4H), 7.95 (d,  $J = 8.1$  Hz, 4H), 7.64 (t,  $J = 7.9$  Hz, 4H), -2.89 (s, 2H) (Figure 4.13). Other analytical data are consistent with the previously reported authentic compounds.<sup>44</sup>



**Figure 4.13**  $^1\text{H}$  NMR spectrum of 5,10,15,20-Tetrakis(3-bromophenyl)porphyrin, **11** in  $\text{CDCl}_3$ .

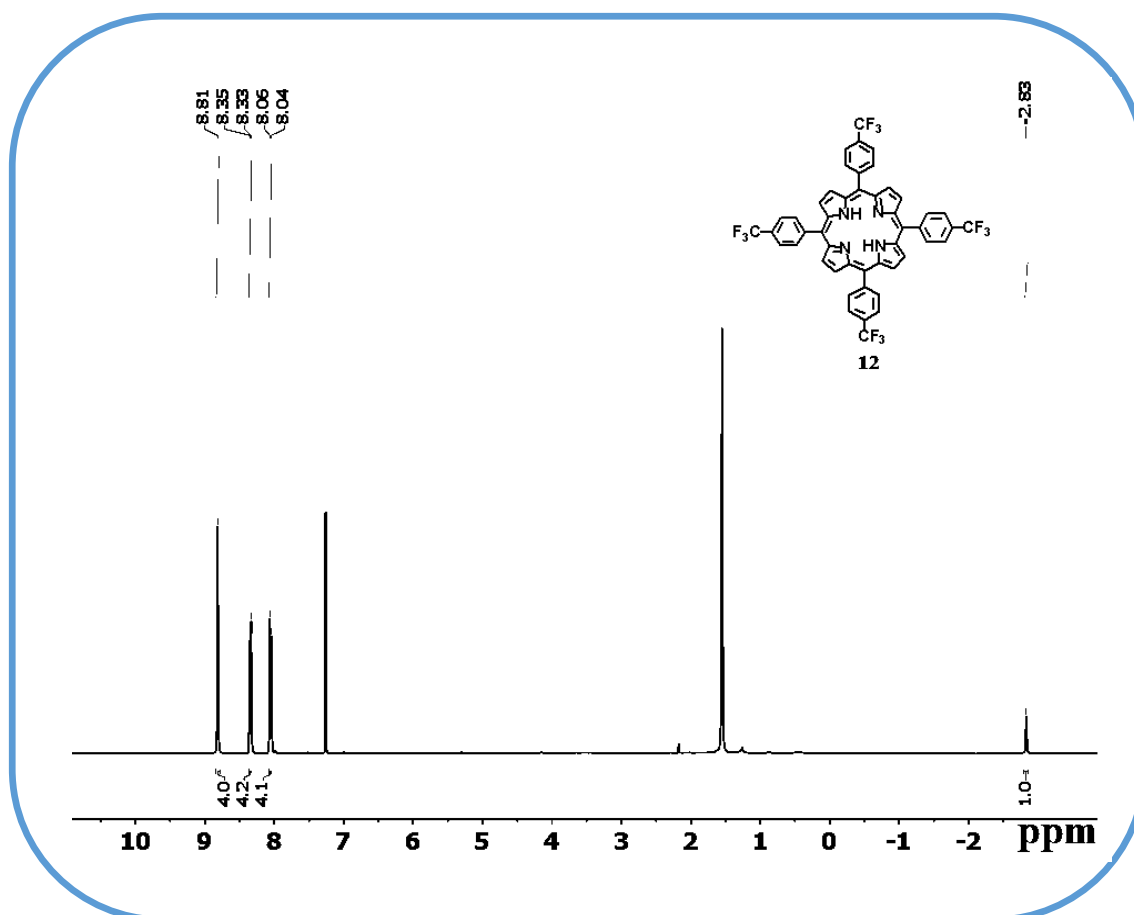
#### Synthesis of 5,10,15,20-(Tetra-4-trifluoromethylphenyl)porphyrin, **12**

273  $\mu\text{l}$  (2 mmol) of 4-(trifluoromethyl)benzaldehyde and 140  $\mu\text{l}$  (2 mmol) of pyrrole were added in a 100 ml MeOH and 50 ml water (2:1) mixture, followed by the addition of 10 ml HCl. The reaction mixture was stirred at RT for 2 hours. The reaction mixture was filtered with Whatman filter paper, and the precipitate was dissolved in 15 ml of DMF solution. This DMF solution was refluxed for another 1.5 hours. This solution was finally transferred to a beaker and was stirred overnight. Then the solution was evaporated to dryness. The crude product was purified by using column chromatography through silica gel (100-200 mesh).

---

**For 5,10,15,20-(Tetra-4-trifluoromethylphenyl)porphyrin, 12**

Yield: 4% (15 mg). Anal. Calcd (found) for  $C_{48}H_{26}F_{12}N_4$  (**12**): C, 65.02 (64.91); H, 2.96 (2.85); N, 6.32 (6.21).  $^1H$  NMR (400 MHz, Chloroform-*d*)  $\delta$  8.81 (s, 8H), 8.34 (d,  $J = 7.9$  Hz, 8H), 8.05 (d,  $J = 8.0$  Hz, 8H), -2.83 (s, 2H) (Figure 4.14). Other analytical data are consistent with the previously reported authentic compounds.<sup>45</sup>



**Figure 4.14**  $^1H$  NMR spectrum of 5,10,15,20-(tetra-4-trifluoromethylphenyl)porphyrin, **12** in  $CDCl_3$ .

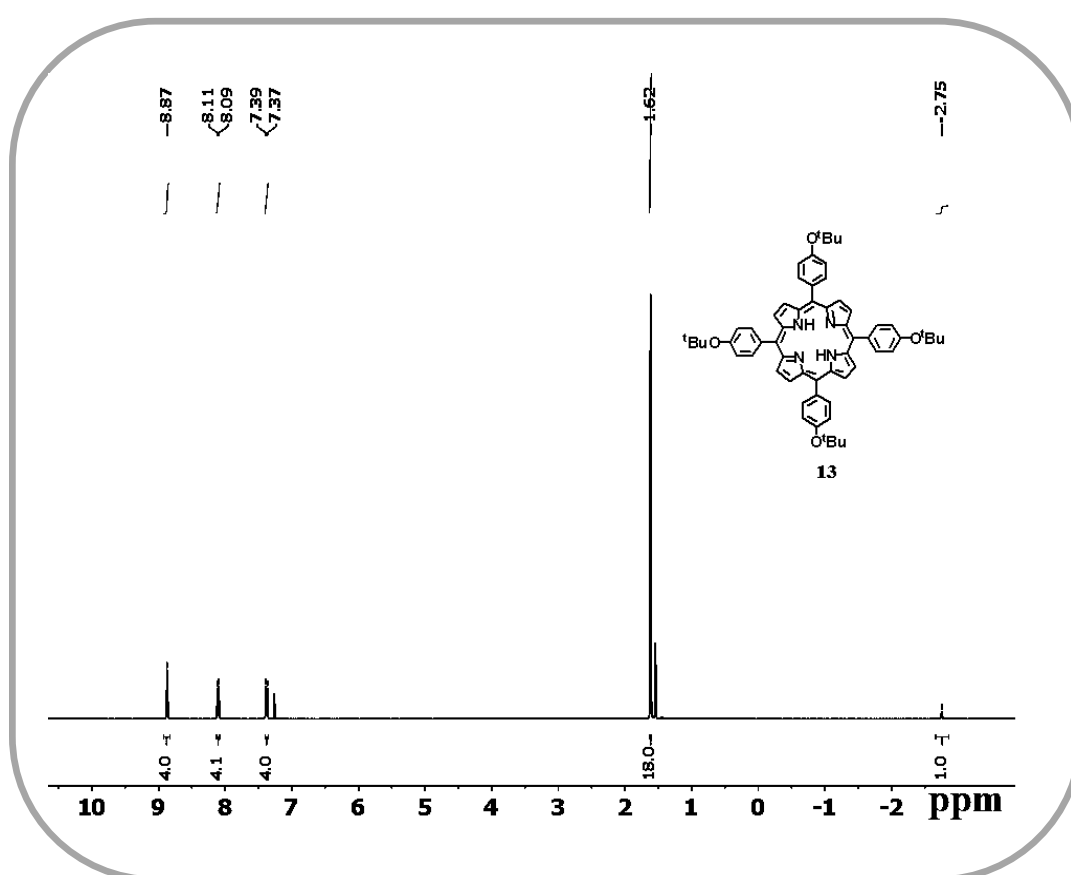
**Synthesis of 5,10,15,20-Tetrakis(4-butoxyphenyl)porphyrin, 13**

348  $\mu$ l (2 mmol) of 4-(*tert*-butoxy)benzaldehyde and 140  $\mu$ l (2 mmol) of pyrrole were added in a 100 ml MeOH and 50 ml water mixture followed by the addition of 10 ml HCl. The reaction mixture was stirred at RT for 2 hours. The reaction mixture

was filtered with Whatman filter paper and the precipitate was dissolved in 15 ml of DMF solution. This DMF solution was refluxed for another 1.5 hours. This solution was finally transferred to a beaker and was stirred overnight. Then the solution was evaporated to dryness. The crude product was purified by using column chromatography through silica gel (100-200 mesh).

**For 5,10,15,20-Tetrakis(4-butoxyphenyl)porphyrin, 13**

Yield: 12% (51 mg). Anal. Calcd (found) for  $C_{60}H_{62}N_4O_4$  (**13**): C, 79.79 (79.68); H, 6.92 (6.99); N, 6.20 (6.13).  $^1H$  NMR (400 MHz, Chloroform-*d*)  $\delta$  8.87 (s, 8H), 8.15 – 8.04 (d, 8H), 7.40 – 7.36 (m, 8H), 1.62 (s, 36H), -2.75 (s, 2H) (Figure 4.15). Other analytical data are consistent with the previously reported authentic compounds.<sup>38</sup>



**Figure 4.15**  $^1H$  NMR spectrum of 5,10,15,20-Tetrakis(4-butoxyphenyl)porphyrin, **13** in  $CDCl_3$ .

---

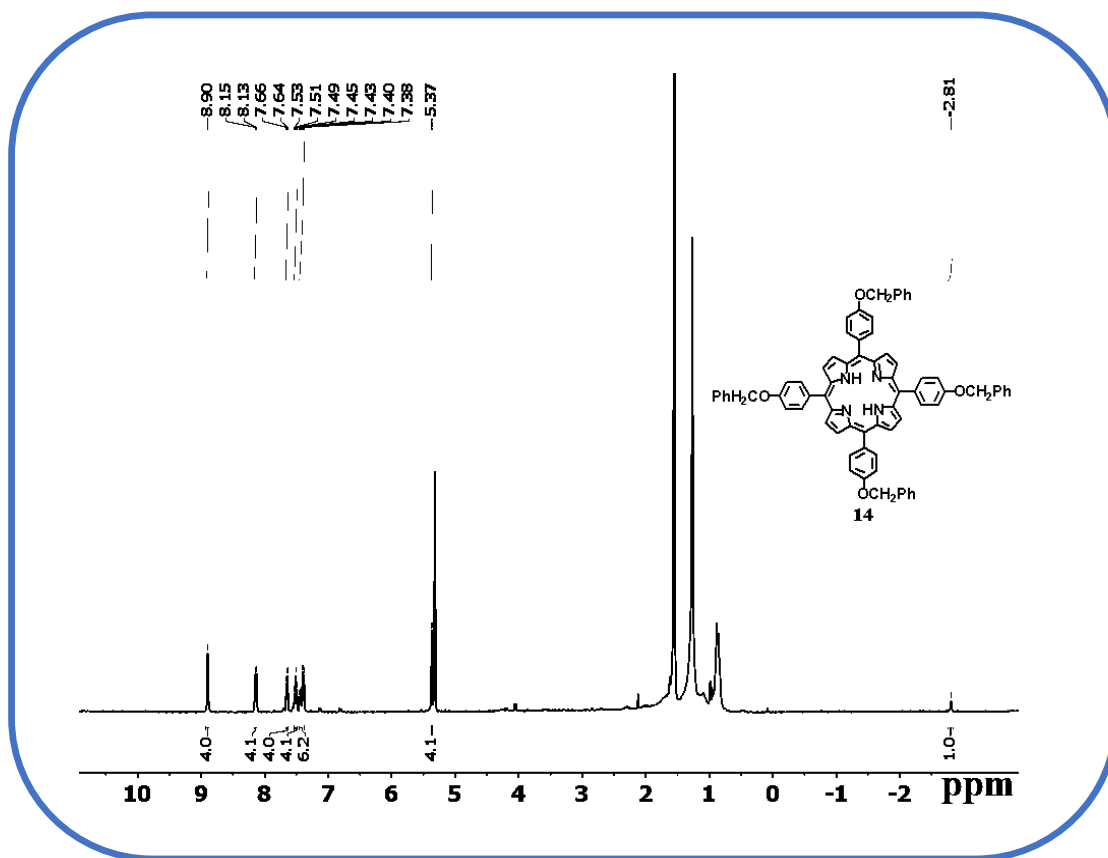
**Synthesis of 5,10,15,20-Tetrakis[4-(benzyloxy)phenyl]porphyrin, 14**

424 mg (2 mmol) of 4-(benzyloxy)benzaldehyde and 140  $\mu$ l (2 mmol) of pyrrole were added in a 100 ml MeOH and 50 ml water (2:1) mixture followed by the addition of 10 ml HCl. The reaction mixture was stirred at RT for 2 hours. The reaction mixture was filtered with Whatman filter paper and the precipitate was dissolved in 15 ml of DMF solution. This DMF solution was refluxed for another 1.5 hours. This solution was finally transferred to a beaker and was stirred overnight. Then the solution was evaporated to dryness. The crude product was purified by using column chromatography through silica gel (100-200 mesh).

**For 5,10,15,20-Tetrakis[4-(benzyloxy)phenyl]porphyrin, 14**

Yield: 16% (80 mg). Anal. Calcd (found) for  $C_{72}H_{54}N_4O_4$  (**14**): C, 83.21 (83.16); H, 5.24 (5.32); N, 5.39 (5.48).  $^1H$  NMR (400 MHz, Methylene Chloride- $d_2$ )  $\delta$  8.90 (s, 8H), 8.14 (d,  $J = 8.1$  Hz, 8H), 7.65 (d,  $J = 7.4$  Hz, 8H), 7.51 (t,  $J = 7.5$  Hz, 8H), 7.41 (m, 12H), 5.37 (s, 8H), -2.81 (s, 2H) (Figure 4.16). Other analytical data are consistent with the previously reported authentic compounds.<sup>46</sup>





**Figure 4.16**  $^1\text{H}$  NMR spectrum of 5,10,15,20-Tetrakis[4-(benzyloxy)phenyl]porphyrin, **14** in  $\text{CD}_2\text{Cl}_2$ .

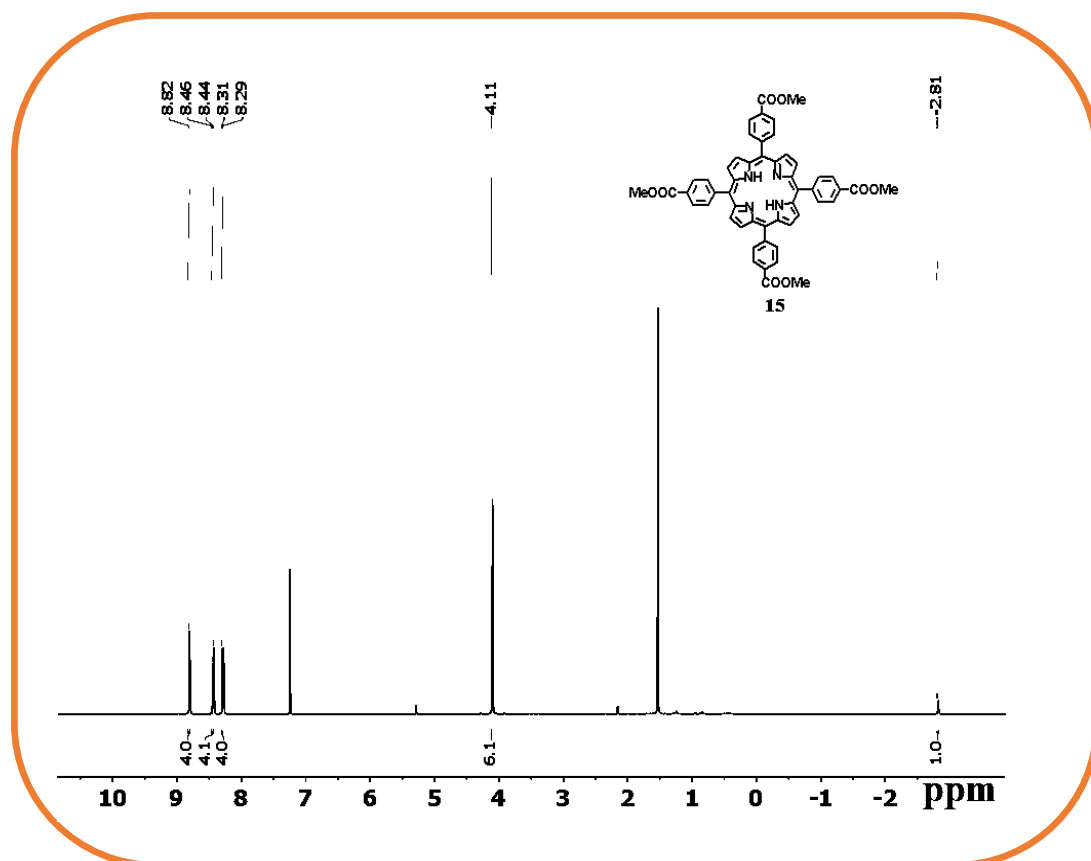
#### Synthesis of 5,10,15,20-Tetrakis(4-methoxycarbonylphenyl)porphyrin, **15**

328 mg (2 mmol) of methyl 4-formylbenzoate and 140  $\mu\text{l}$  (2 mmol) of pyrrole were added in a 100 ml MeOH and 50 ml water (2:1) mixture, followed by the addition of 10 ml HCl. The reaction mixture was stirred at RT for 2 hours. The reaction mixture was filtered with Whatman filter paper, and the precipitate was dissolved in 15 ml of DMF solution. This DMF solution was refluxed for another 1.5 hours. This solution was finally transferred to a beaker and was stirred overnight. Then the solution was evaporated to dryness. The crude product was purified by using column chromatography through silica gel (100-200 mesh).

---

### For 5,10,15,20-Tetrakis(4-methoxycarbonylphenyl)porphyrin, **15**

Yield: 10 % (39 mg). Anal. Calcd (found) for  $C_{52}H_{38}N_4O_8$  (**15**): C, 73.75 (73.65); H, 4.52 (4.63); N, 6.62 (6.77).  $^1H$  NMR (400 MHz, Chloroform-*d*)  $\delta$  8.82 (s, 8H), 8.47 – 8.43 (d, 8H), 8.32 – 8.27 (d, 8H), 4.11 (s, 12H), -2.81 (s, 2H) (Figure 4.17). Other analytical data are consistent with the previously reported authentic compounds.<sup>47</sup>



**Figure 4.17**  $^1H$  NMR spectrum of **15** in  $CDCl_3$ .

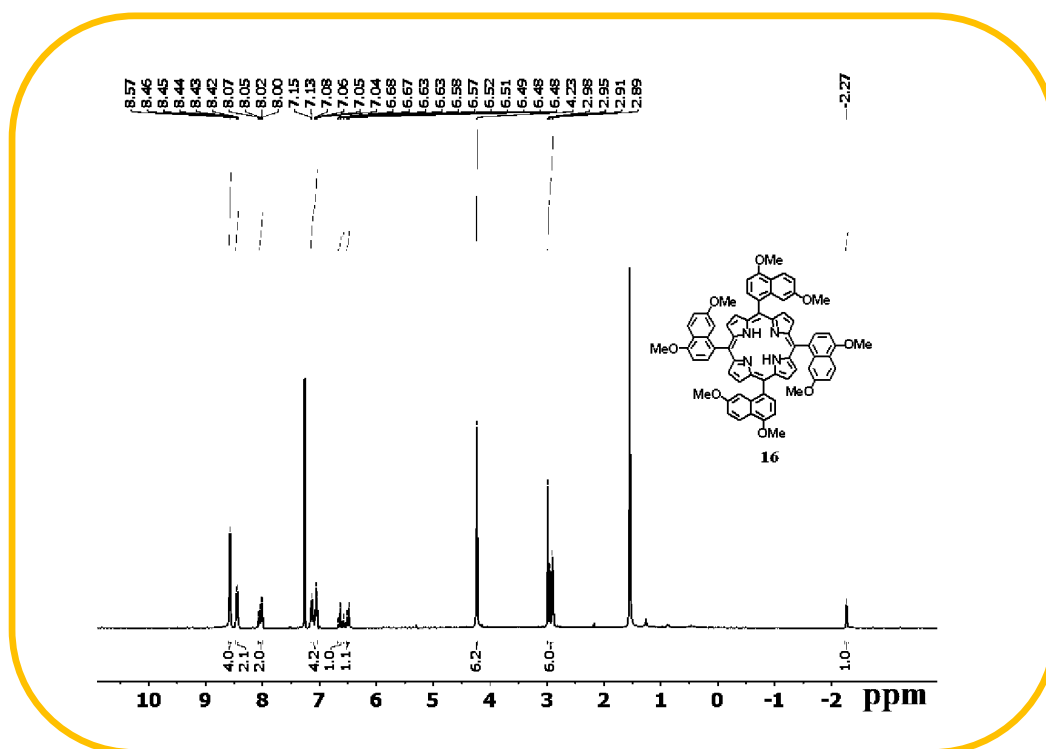
### Synthesis of 5,10,15,20-Tetrakis(4,7-dimethoxynaphthalen-1-yl)porphyrin, **16**

432 mg (2 mmol) of 4,7-dimethoxy-1-naphthaldehyde and 140  $\mu$ l (2 mmol) of pyrrole were added in a 100 ml MeOH and 50 ml water (2:1) mixture followed by the addition of 10 ml HCl. The reaction mixture was stirred at RT for 2 hours. The reaction mixture was filtered with Whatman filter paper and the precipitate was dissolved in 15 ml of DMF solution. This DMF solution was refluxed for another 1.5 hours. This solution

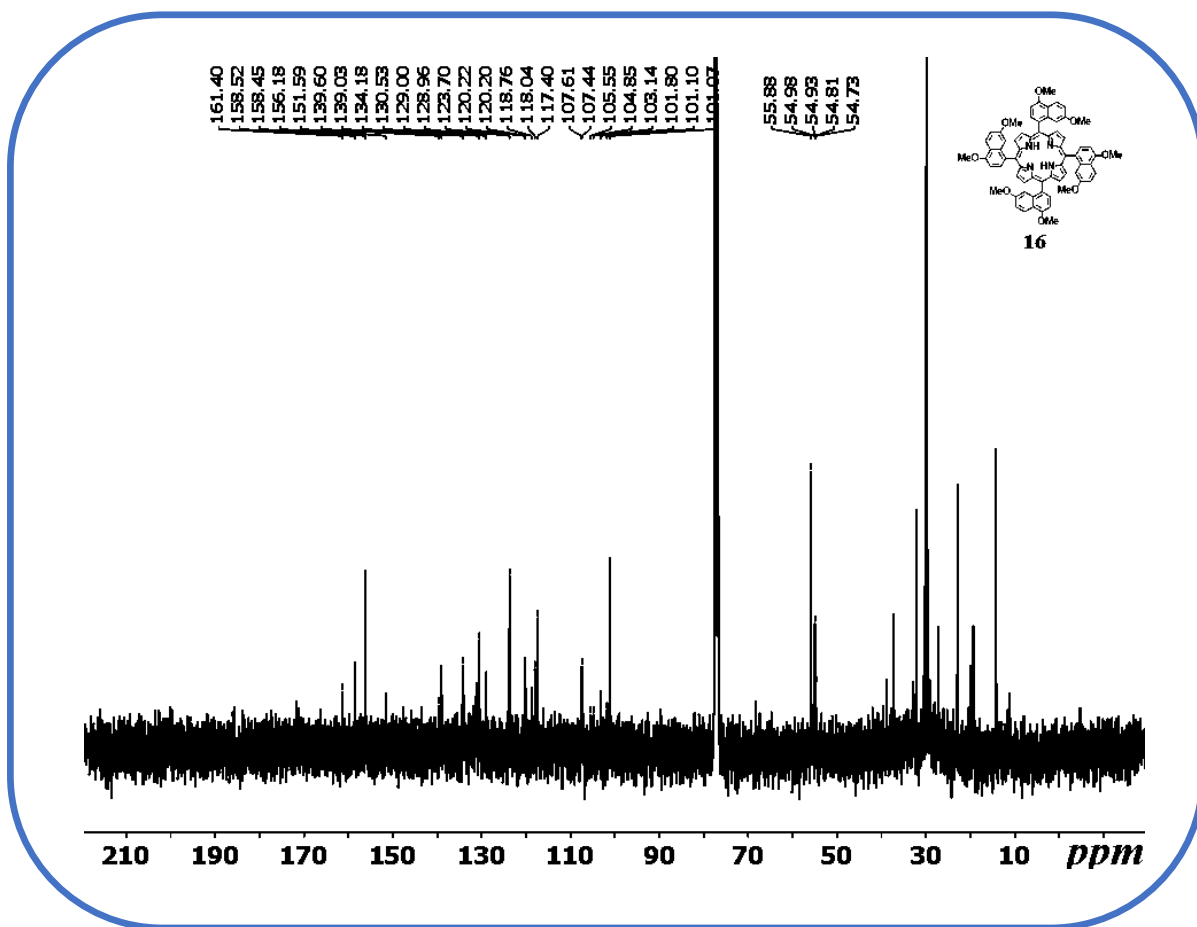
was finally transferred to a beaker and was stirred overnight. Then the solution was evaporated to dryness. The crude product was purified by using column chromatography through silica gel (100-200 mesh).

**For 5,10,15,20-Tetrakis(4,7-dimethoxynaphthalen-1-yl)porphyrin, **16****

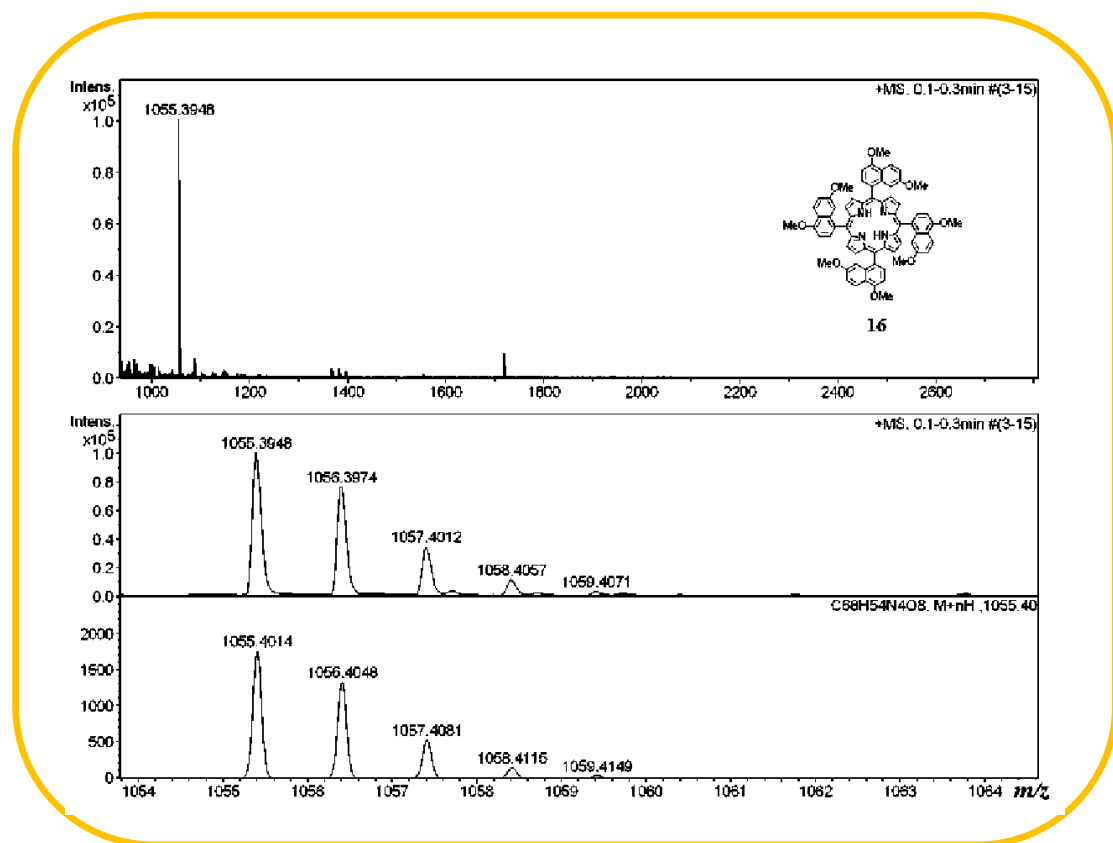
Yield: 17% (89 mg). Anal. Calcd (found) for  $C_{68}H_{54}N_4O_8$  (**16**): C, 77.40 (77.52); H, 5.16 (5.30); N, 5.31 (5.18).  $^1H$  NMR (400 MHz, Chloroform-*d*)  $\delta$  8.58 (d,  $J = 5.7$  Hz, 8H), 8.44 (td,  $J = 7.0, 3.4$  Hz, 4H), 8.08 – 7.99 (m, 4H), 7.17 – 7.03 (m, 8H), 6.60 (dd,  $J = 22.7, 2.5$  Hz, 2H), 6.55 – 6.45 (m, 2H), 4.23 (d,  $J = 2.0$  Hz, 12H), 3.00 – 2.89 (m, 12H), -2.27 (s, 2H) (Figure 4.18).  $^{13}C$  { $^1H$ } NMR (101 MHz,  $CDCl_3$ )  $\delta$  161.4, 158.5, 158.5, 156.2, 151.6, 139.6, 139.0, 134.2, 130.5, 129.0, 128.9, 123.7, 120.2, 120.2, 118.8, 118.0, 117.4, 107.6, 107.4, 105.6, 104.8, 103.1, 101.8, 101.1, 101.0, 55.9, 55.0, 54.9, 54.8, 54.7 (Figure 4.19).  $m/z$ : [**16**+H] $^+$  Calcd for  $C_{68}H_{55}N_4O_8$  1055.4014; Found 1055.3948 (Figure 4.20).



**Figure 4.18**  $^1H$  NMR spectrum of 5,10,15,20-Tetrakis(4,7-dimethoxynaphthalen-1-yl)porphyrin, **16** in  $CDCl_3$ .



**Figure 4.19**  $^{13}\text{C}\{^1\text{H}\}$ NMR (101 MHz) spectrum of 5,10,15,20-Tetrakis(4,7-dimethoxynaphthalen-1-yl)porphyrin, **16** in  $\text{CDCl}_3$ .



**Figure 4.20** ESI-MS spectrum of 5,10,15,20-Tetrakis(4,7-dimethoxynaphthalen-1-yl)porphyrin, **16** in CH<sub>3</sub>CN shows the measured spectrum with isotopic distribution pattern.

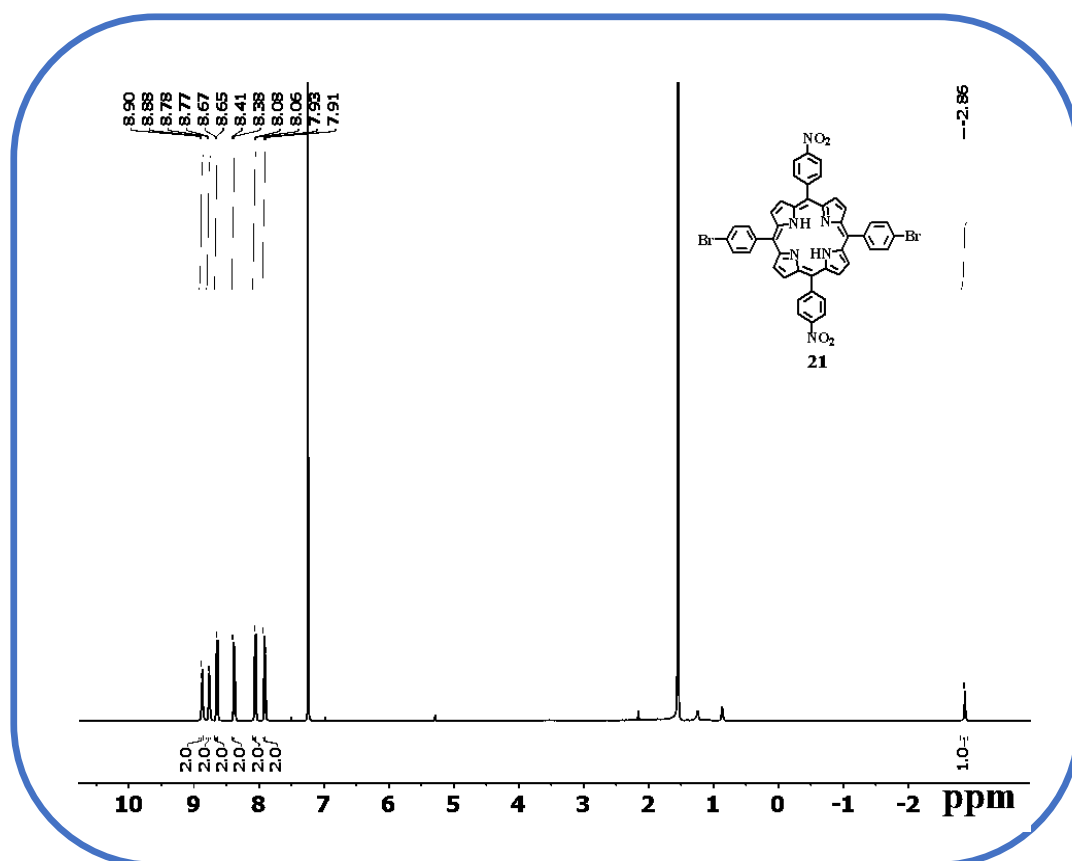
#### Synthesis of 5,15-Bis(4-bromophenyl)- 10,20-bis(4-nitrophenyl)porphyrin, **21**

301 mg (1 mmol) of 5-(4-bromophenyl)dipyrromethane and 151 mg (1 mmol) of 4-nitrobenzaldehyde were added in a 100 ml MeOH and 50 ml water (2:1) mixture, followed by the addition of 10 ml HCl. The reaction mixture was stirred at RT for 2 hours. The reaction mixture was filtered with Whatman filter paper, and the precipitate was dissolved in 15 ml of DMF solution. This DMF solution was refluxed for another 1.5 hours. This solution was finally transferred to a beaker and was stirred overnight. Then the solution was evaporated to dryness. The crude product was purified using column chromatography through silica gel (100-200 mesh) or purified via crystallization.

---

**For 5,15-Bis(4-bromophenyl)- 10,20-bis(4-nitrophenyl)porphyrin, 21**

Yield: 40 % (170 mg). Anal. Calcd (found) for  $C_{44}H_{26}Br_2N_6O_4$  (**21**): C, 61.27 (61.38); H, 3.04 (3.17); N, 9.74 (9.87).  $^1H$  NMR (400 MHz, Chloroform-*d*)  $\delta$  8.89 (d,  $J = 4.8$  Hz, 4H), 8.78 (d,  $J = 4.9$  Hz, 4H), 8.68 – 8.64 (m, 4H), 8.41 – 8.37 (m, 4H), 8.09 – 8.05 (m, 4H), 7.95 – 7.91 (m, 4H), -2.86 (s, 2H) (Figure 4.21). Other analytical data are consistent with the previously reported authentic compounds.<sup>48</sup>



**Figure 4.21**  $^1H$  NMR spectrum of 5,15-Bis(4-bromophenyl)-10,20-bis(4-nitrophenyl)porphyrin, **21** in  $CDCl_3$ .

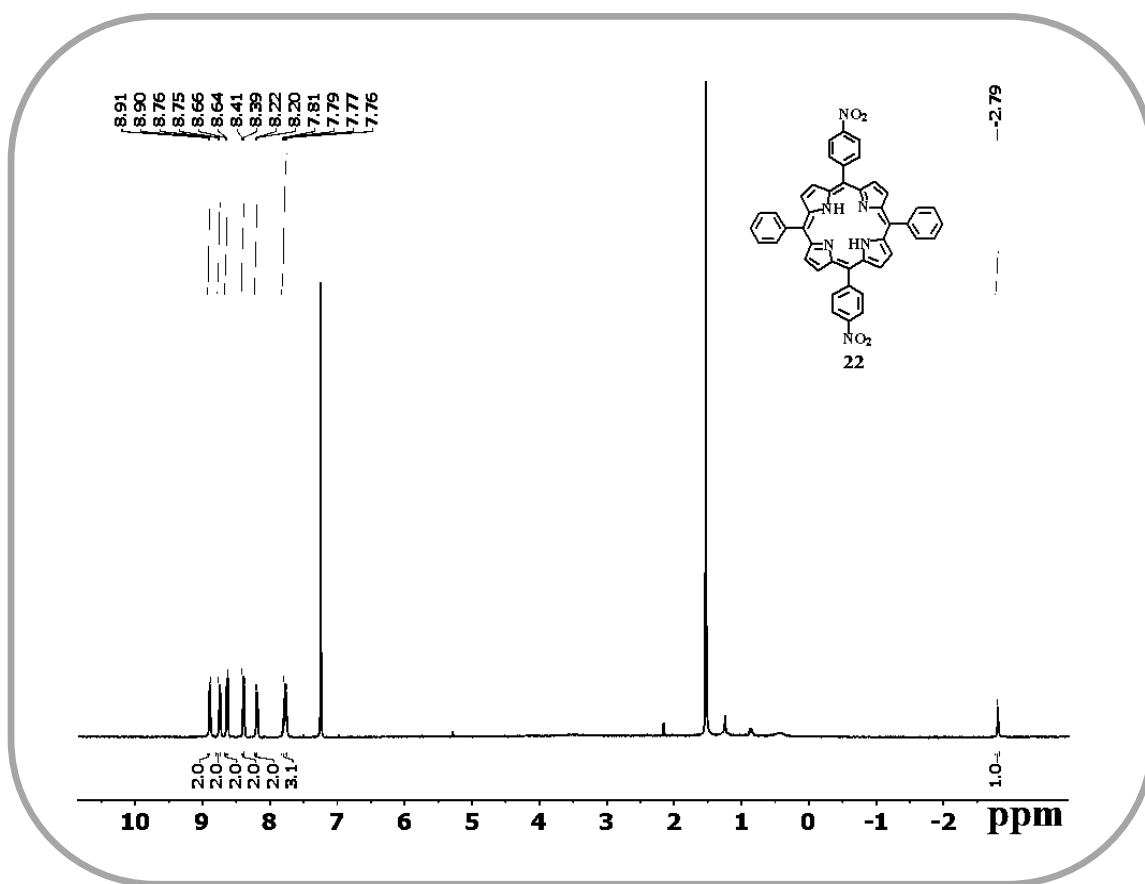
**Synthesis of 5,15-Bis(4-nitrophenyl)-10,20-diphenylporphyrin, 22**

222 mg (1mmol) of 5-phenyldipyrromethane and 151 mg (1mmol) of 4-nitrobenzaldehyde were added in a 100 ml MeOH and 50 ml water (2:1) mixture, followed by the addition of 10 ml HCl. The reaction mixture was stirred at RT for 2 hours. The reaction mixture was filtered with Whatman filter paper, and the precipitate

was dissolved in 15 ml of DMF solution. This DMF solution was refluxed for another 1.5 hours. This solution was finally transferred to a beaker and was stirred overnight. Then the solution was evaporated to dryness. The crude product was purified using column chromatography through silica gel (100-200 mesh) or purified via crystallization.

**For 5,15-Bis(4-nitrophenyl)-10,20-diphenylporphyrin, **22****

Yield: 31% (108 mg). Anal. Calcd (found) for  $C_{44}H_{28}N_6O_4$  (**22**): C, 74.99 (75.11); H, 4.00 (4.16); N, 11.93 (11.82).  $^1H$  NMR (400 MHz, Chloroform-*d*)  $\delta$  8.91 (d,  $J = 4.8$  Hz, 4H), 8.76 (d,  $J = 4.8$  Hz, 4H), 8.65 (d,  $J = 8.3$  Hz, 4H), 8.40 (d,  $J = 8.3$  Hz, 4H), 8.21 (d,  $J = 7.0$  Hz, 4H), 7.79 (m, 6H), -2.79 (s, 2H) (Figure 4.22). Other analytical data are consistent with the previously reported authentic compounds.<sup>48</sup>



**Figure 4.22**  $^1H$  NMR spectrum of 5,15-Bis(4-nitrophenyl)-10,20-diphenylporphyrin, **22** in  $CDCl_3$ .

---

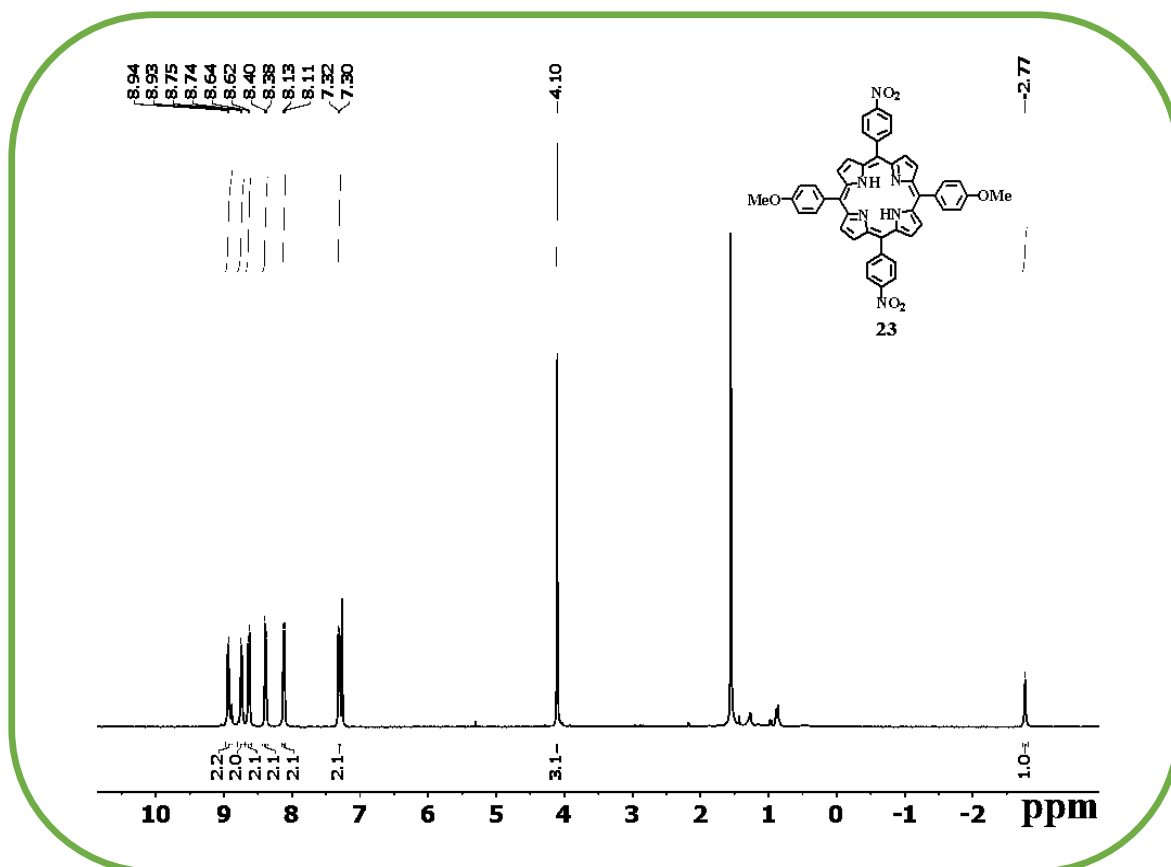
**Synthesis of 5,15-Bis(4-methoxyphenyl)-10,20-bis(4-nitrophenyl)porphyrin, 23**

252 mg (1 mmol) of 5-(4-methoxyphenyl)dipyrromethane and 151 mg (1 mmol) of 4-nitrobenzaldehyde were added in a 100 ml MeOH and 50 ml water (2:1) mixture, followed by the addition of 10 ml HCl. The reaction mixture was stirred at RT for 2 hours. The reaction mixture was filtered with Whatman filter paper, and the precipitate was dissolved in 15 ml of DMF solution. This DMF solution was refluxed for another 1.5 hours. This solution was finally transferred to a beaker and was stirred overnight. Then the solution was evaporated to dryness. The crude product was purified using column chromatography through silica gel (100-200 mesh) or purified via crystallization.

**For 5,15-Bis(4-methoxyphenyl)-10,20-bis(4-nitrophenyl)porphyrin, 23**

Yield: 30% (114 mg). Anal. Calcd (found) for  $C_{46}H_{32}N_6O_6$  (**23**): C, 72.24 (72.13); H, 4.22 (4.10); N, 10.99 (11.14).  $^1H$  NMR (400 MHz, Chloroform-*d*)  $\delta$  8.94 (d,  $J = 4.8$  Hz, 4H), 8.74 (d,  $J = 4.8$  Hz, 4H), 8.66 – 8.61 (m, 4H), 8.39 (d,  $J = 8.3$  Hz, 4H), 8.14 – 8.09 (m, 4H), 7.34 – 7.29 (m, 4H), 4.10 (s, 6H), -2.77 (s, 2H) (Figure 4.23). Other analytical data are consistent with the previously reported authentic compounds.<sup>49</sup>





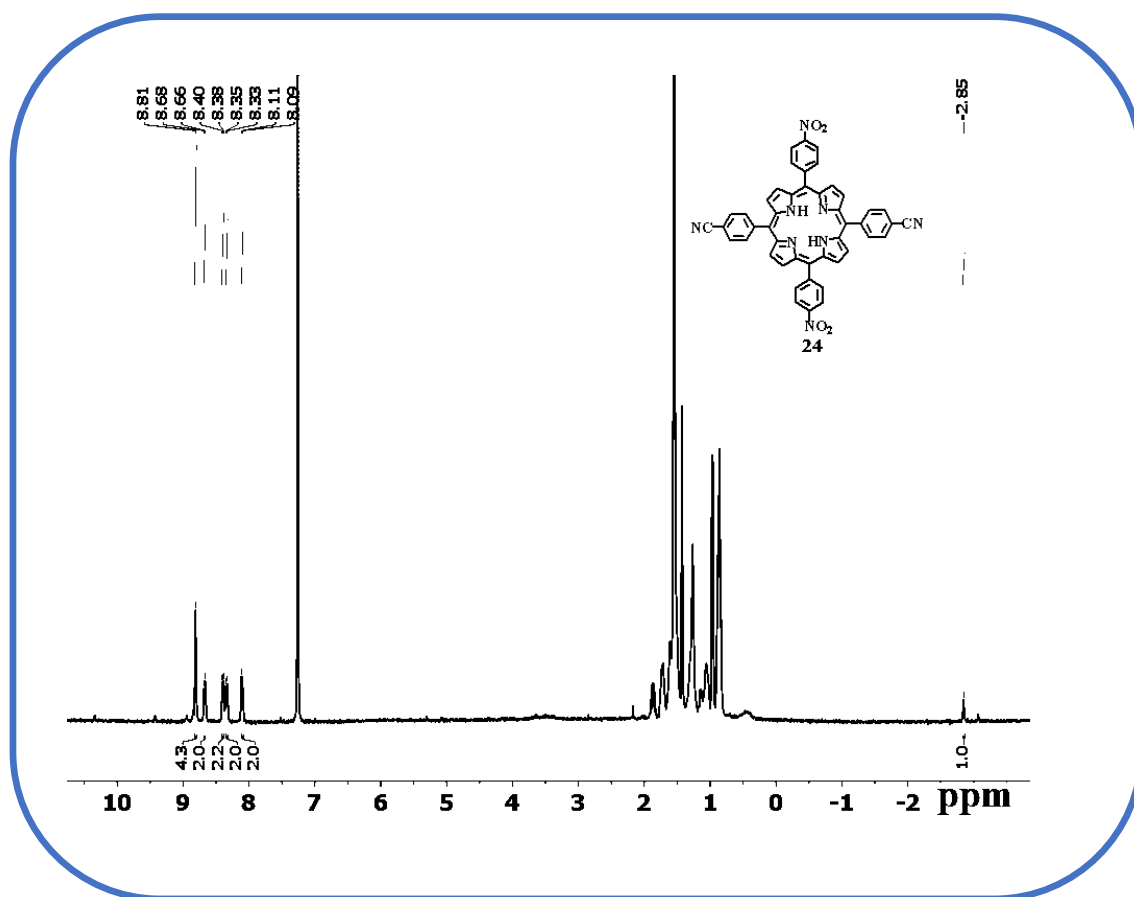
**Figure 4.23**  $^1\text{H}$  NMR spectrum of 5,15-Bis(4-methoxyphenyl)-10,20-bis(4-nitrophenyl)porphyrin, **23** in  $\text{CDCl}_3$ .

#### Synthesis of 5,15-bis(4-cyanophenyl)-10,20-bis(4-nitrophenyl)porphyrin, **24**

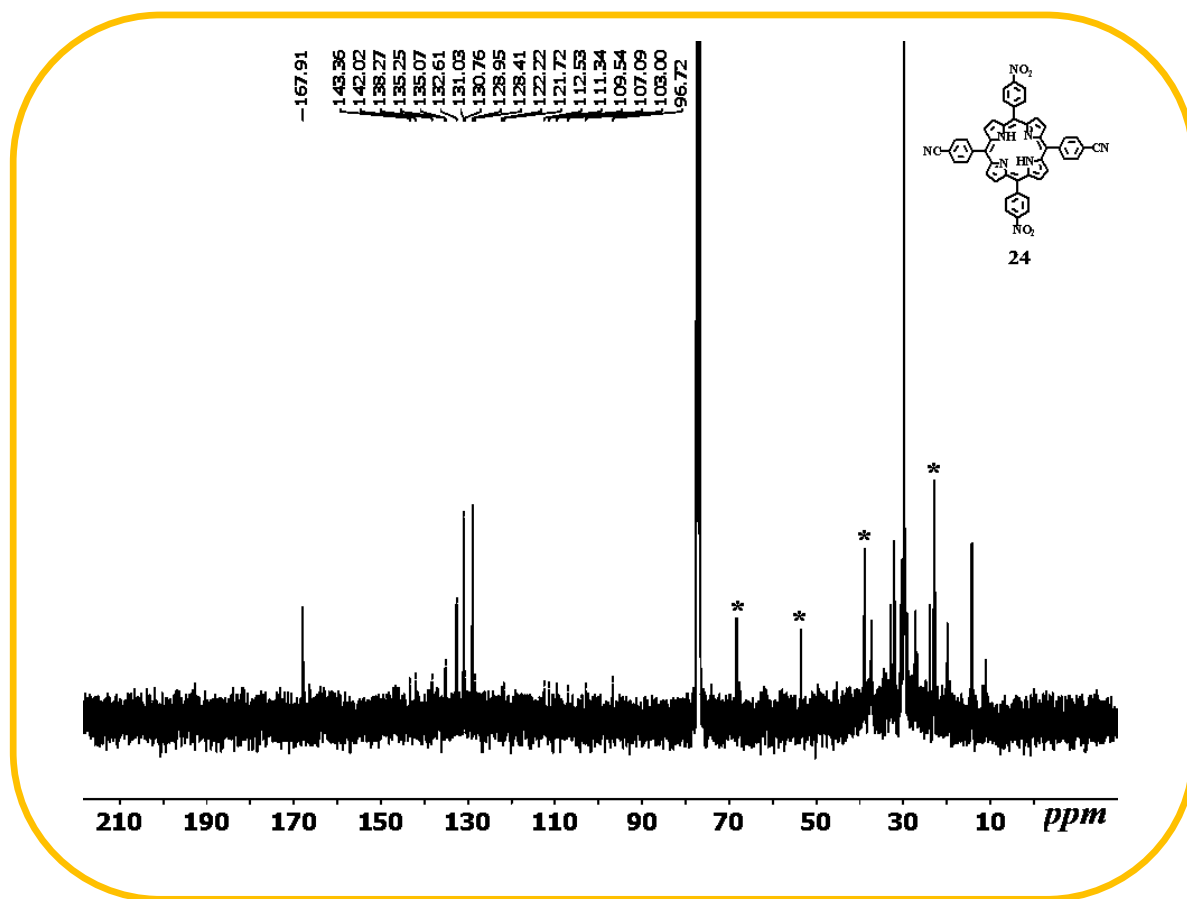
247 mg (1 mmol) of 5-(4-cyanophenyl)dipyrromethane and 151 mg (1 mmol) of 4-nitrobenzaldehyde were added in a 100 ml MeOH and 50 ml water (2:1) mixture, followed by the addition of 10 ml HCl. The reaction mixture was stirred at RT for 2 hours. The reaction mixture was filtered with Whatman filter paper, and the precipitate was dissolved in 15 ml of DMF solution. This DMF solution was refluxed for another 1.5 hours. This solution was finally transferred to a beaker and was stirred overnight. Then the solution was evaporated to dryness. The crude product was purified using column chromatography through silica gel (100-200 mesh) or purified via crystallization.

**For 5,15-bis(4-cyanophenyl)-10,20-bis(4-nitrophenyl)porphyrin, **24****

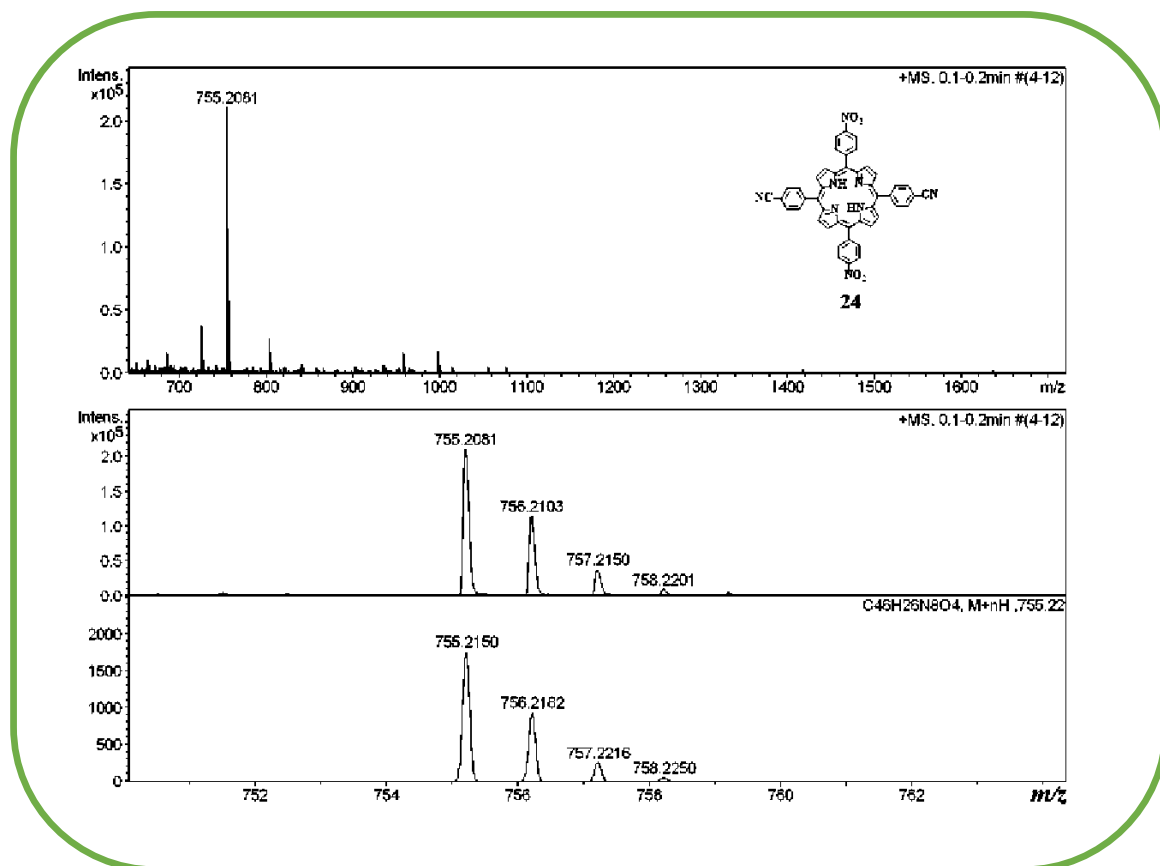
Yield: 23% (85 mg). Anal. Calcd (found) for  $C_{46}H_{26}N_8O_4$  (**24**): C, 73.20 (73.34); H, 3.47 (3.31); N, 14.85 (14.73).  $^1H$  NMR (400 MHz, Chloroform-*d*)  $\delta$  8.81 (s, 8H), 8.67 (d,  $J = 8.2$  Hz, 4H), 8.39 (d,  $J = 8.4$  Hz, 4H), 8.34 (d,  $J = 7.8$  Hz, 4H), 8.10 (d,  $J = 7.7$  Hz, 4H), -2.85 (s, 2H) (Figure 4.24).  $^{13}C$  { $^1H$ } NMR (101 MHz,  $CDCl_3$ )  $\delta$  167.9, 143.4, 142.0, 138.3, 135.3, 135.1, 132.6, 131.0, 130.8, 128.9, 128.4, 122.2, 121.7, 112.5, 111.3, 109.5, 107.1, 103.0, 96.7 (Figure 4.25).  $m/z$ : [**24**+H] $^+$  Calcd for  $C_{46}H_{27}N_8O_4$  755.2150; Found 755.2081 (Figure 4.26).



**Figure 4.24**  $^1H$  NMR spectrum of 5,15-bis(4-cyanophenyl)-10,20-bis(4-nitrophenyl)porphyrin, **24** in  $CDCl_3$ .



**Figure 4.25**  $^{13}\text{C}$  { $^1\text{H}$ } NMR (101 MHz) spectrum of 5,15-bis(4-cyanophenyl)-10,20-bis(4-nitrophenyl)porphyrin, **24** in  $\text{CDCl}_3$ .



**Figure 4.26** ESI-MS spectrum of 5,15-bis(4-cyanophenyl)-10,20-bis(4-nitrophenyl)porphyrin, **24** in CH<sub>3</sub>CN shows the measured spectrum with isotopic distribution pattern.

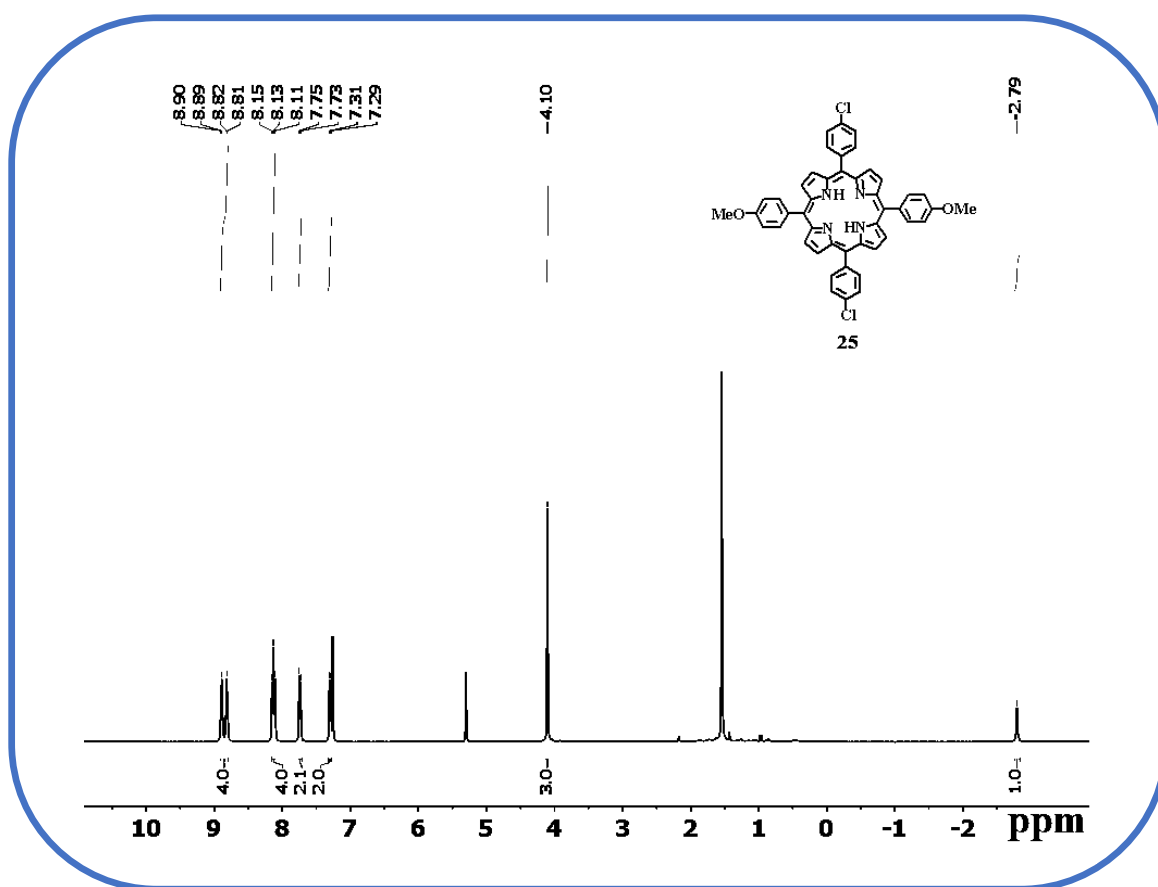
#### Synthesis of 5,15-Bis(4-methoxyphenyl)-10,20-(4-chlorophenyl)porphyrin, **25**

252 mg (1 mmol) of 5-(4-methoxyphenyl)dipyrromethane and 141 mg (1 mmol) of 4-chlorobenzaldehyde were added in a 100 ml MeOH and 50 ml water (2:1) mixture, followed by the addition of 10 ml HCl. The reaction mixture was stirred at RT for 2 hours. The reaction mixture was filtered with Whatman filter paper, and the precipitate was dissolved in 15 ml of DMF solution. This DMF solution was refluxed for another 1.5 hours. This solution was finally transferred to a beaker and was stirred overnight. Then the solution was evaporated to dryness. The crude product was purified by using column chromatography through silica gel (100-200 mesh).

---

**For 5,15-Bis(4-methoxyphenyl)-10,20-(4-chlorophenyl)porphyrin, 25**

Yield: 19% (69 mg). Anal. Calcd (found) for  $C_{46}H_{32}Cl_2N_4O_2$  (**25**): C, 74.29 (74.42); H, 4.34 (4.45); N, 7.53 (7.67).  $^1H$  NMR (400 MHz, Chloroform-*d*)  $\delta$  8.91 – 8.79 (m, 8H), 8.18 – 8.10 (m, 8H), 7.76 – 7.71 (m, 4H), 7.30 (d,  $J = 8.2$  Hz, 4H), 4.10 (s, 6H), -2.79 (s, 2H) (Figure 4.27). Other analytical data are consistent with the previously reported authentic compounds.<sup>50</sup>



**Figure 4.27**  $^1H$  NMR spectrum of **25** in  $CDCl_3$ .

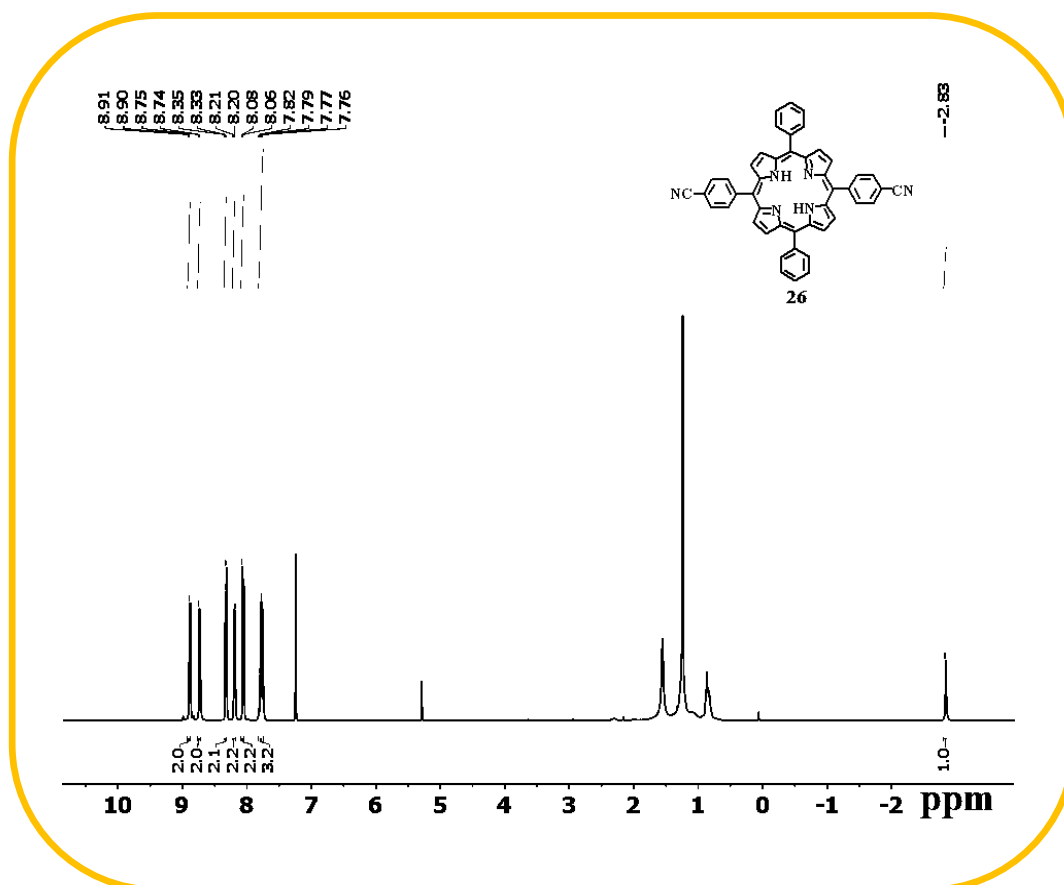
**Synthesis of 5,15-Bis(4-cyanophenyl)-10,20-diphenylporphyrin, 26**

247 mg (1 mmol) of 5-(4-cyanophenyl)dipyrromethane and 102  $\mu$ l (1 mmol) of benzaldehyde were added in a 100 ml MeOH and 50 ml water (2:1) mixture followed by the addition of 10 ml HCl. The reaction mixture was stirred at RT for 2 hours. The reaction mixture was filtered with Whatman filter paper and the precipitate was dissolved

in 15 ml of DMF solution. This DMF solution was refluxed for another 1.5 hours. This solution was finally transferred to a beaker and was stirred overnight. Then the solution was evaporated to dryness. The crude product was purified by using column chromatography through silica gel (100-200 mesh).

**For 5,15-Bis(4-cyanophenyl)-10,20-diphenylporphyrin, 26**

Yield: 17% (57 mg). Anal. Calcd (found) for  $C_{46}H_{28}N_6$  (**26**): C, 83.11 (83.02); H, 4.25 (4.37); N, 12.64 (12.52).  $^1H$  NMR (400 MHz, Chloroform-*d*)  $\delta$  8.90 (d,  $J = 4.8$  Hz, 4H), 8.75 (d,  $J = 4.8$  Hz, 4H), 8.37 – 8.31 (d, 4H), 8.23 – 8.17 (d, 4H), 8.10 – 8.05 (d, 4H), 7.79 (m, 6H), -2.83 (s, 2H) (Figure 4.28). Other analytical data are consistent with the previously reported authentic compounds.<sup>37</sup>



**Figure 4.28**  $^1H$  NMR spectrum of **26** in  $CDCl_3$ .

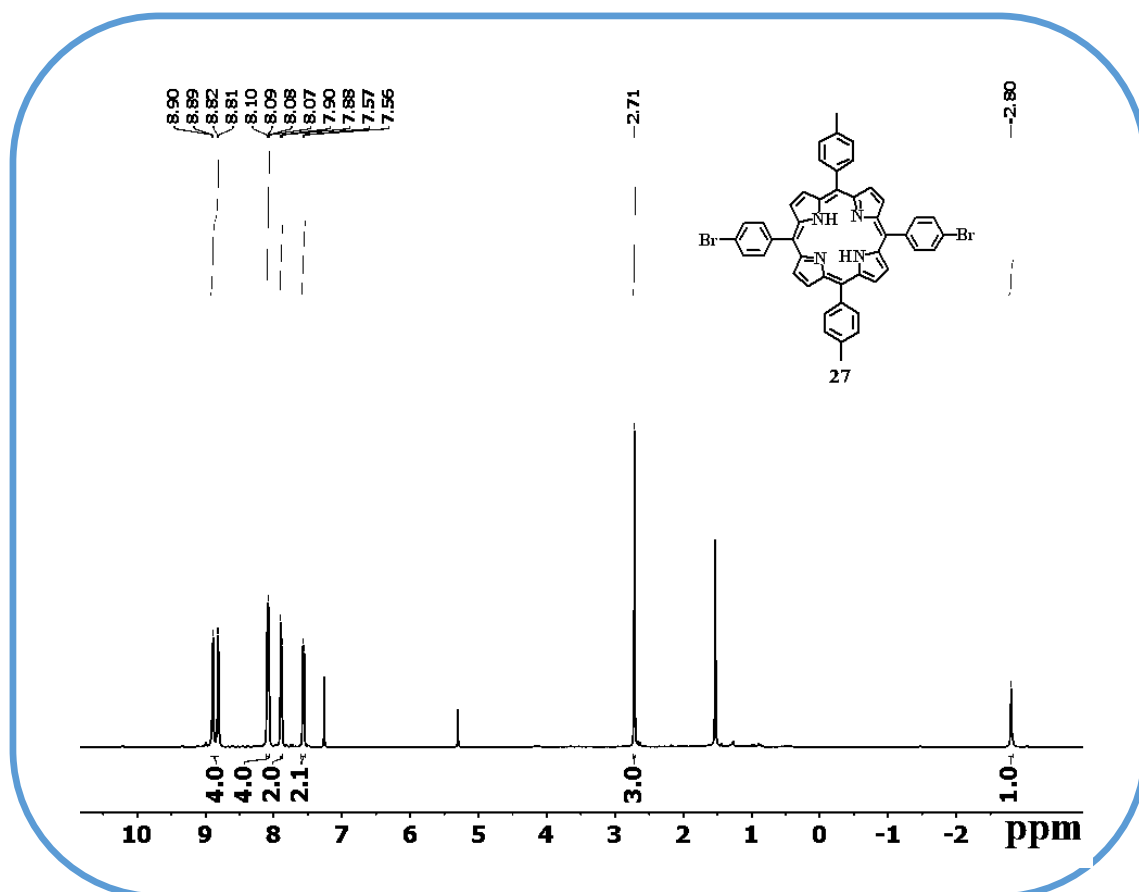
---

### **Synthesis of 5,15-Bis(4-bromophenyl)-10,20-(4-methylphenyl)porphyrin, 27**

301 mg (1 mmol) of 5-(4-bromophenyl)dipyrromethane and 117  $\mu$ l (1 mmol) of *p*-tolualdehyde were added in a 100 ml MeOH and 50 ml water (2:1) mixture, followed by the addition of 10 ml HCl. The reaction mixture was stirred at RT for 2 hours. The reaction mixture was filtered with Whatman filter paper, and the precipitate was dissolved in 15 ml of DMF solution. This DMF solution was refluxed for another 1.5 hours. This solution was finally transferred to a beaker and was stirred overnight. Then the solution was evaporated to dryness. The crude product was purified by using column chromatography through silica gel (100-200 mesh).

### **For 5,15-Bis(4-bromophenyl)-10,20-(4-methylphenyl)porphyrin, 27**

Yield: 13% (51 mg). Anal. Calcd (found) for  $C_{46}H_{32}Br_2N_4$  (**27**): C, 69.01 (69.14); H, 4.03 (4.17); N, 7.00 (6.88).  $^1H$  NMR (400 MHz, Chloroform-*d*)  $\delta$  8.85 (dd,  $J = 32.6, 4.8$  Hz, 8H), 8.08 (m, 8H), 7.91 – 7.87 (m, 4H), 7.56 (d,  $J = 7.6$  Hz, 4H), 2.71 (s, 6H), -2.80 (s, 2H) (Figure 4.29). Other analytical data are consistent with the previously reported authentic compounds.<sup>51</sup>



**Figure 4.29**  $^1\text{H}$  NMR spectrum of 5,15-Bis(4-bromophenyl)-10,20-(4-methylphenyl)porphyrin, **27** in  $\text{CDCl}_3$ .

#### Synthesis of 5,15-bis(4-cyanophenyl)-10,20-bis(4-methoxyphenyl)porphyrin, **28**

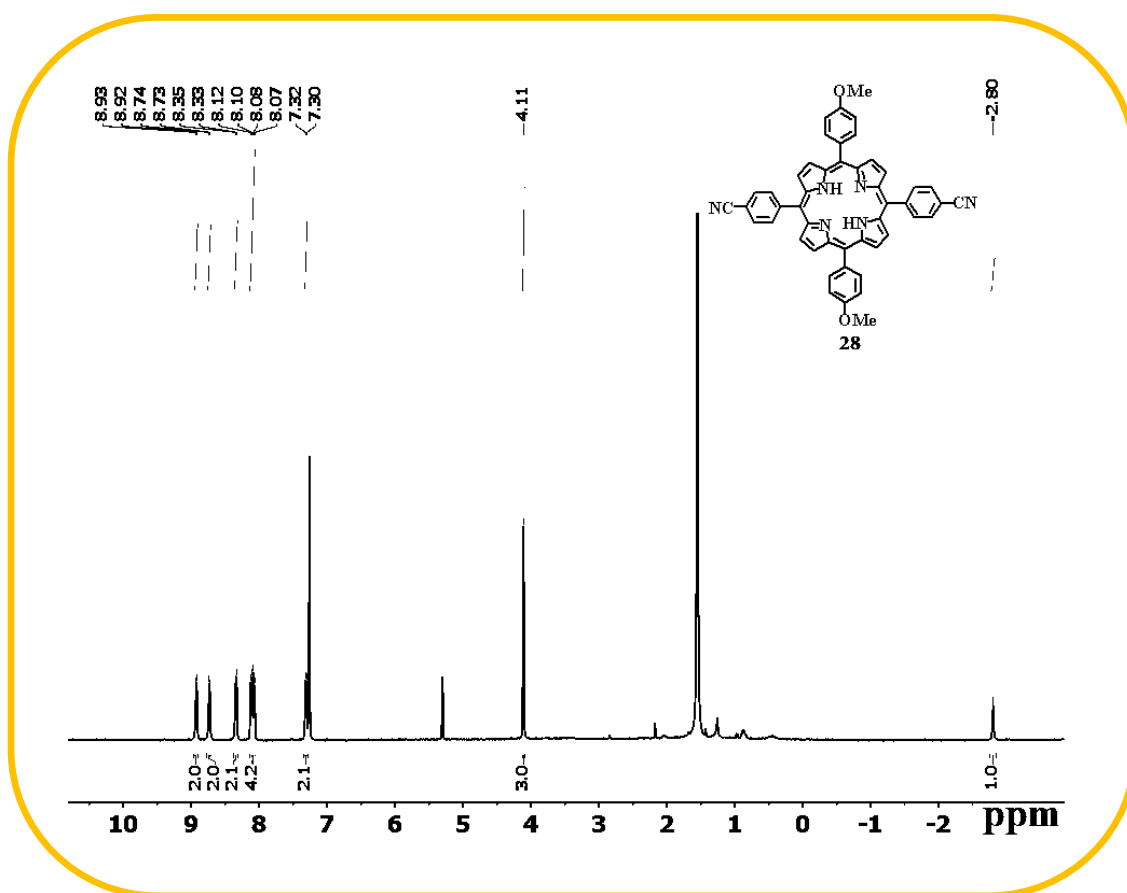
247 mg (1 mmol) of 5-(4-cyanophenyl)dipyrromethane and 122  $\mu\text{l}$  (1 mmol) of 4-methoxybenzaldehyde were added in a 100 ml MeOH and 50 ml water (2:1) mixture, followed by the addition of 10 ml HCl. The reaction mixture was stirred at RT for 2 hours. The reaction mixture was filtered with Whatman filter paper, and the precipitate was dissolved in 15 ml of DMF solution. This DMF solution was refluxed for another 1.5 hours. This solution was finally transferred to a beaker and was stirred overnight. Then the solution was evaporated to dryness. The crude product was purified by using column chromatography through silica gel (100-200 mesh).



---

**For 5,15-bis(4-cyanophenyl)-10,20-bis(4-methoxyphenyl)porphyrin, 28**

Yield: 13% (45 mg). Anal. Calcd (found) for C<sub>48</sub>H<sub>32</sub>N<sub>6</sub>O<sub>2</sub> (**28**): C, 79.54 (79.46); H, 4.45 (4.56); N, 11.59 (11.67). <sup>1</sup>H NMR (400 MHz, Chloroform-*d*) δ 8.92 (d, *J* = 4.8 Hz, 4H), 8.73 (d, *J* = 4.8 Hz, 4H), 8.34 (d, *J* = 7.8 Hz, 4H), 8.09 (m, 8H), 7.31 (d, *J* = 8.2 Hz, 4H), 4.11 (s, 6H), -2.80 (s, 2H) (Figure 4.30). Other analytical data are consistent with the previously reported authentic compounds.<sup>37</sup>



**Figure 4.30** <sup>1</sup>H NMR spectrum of 5,15-bis(4-cyanophenyl)-10,20-bis(4-methoxyphenyl)porphyrin, **28** in CDCl<sub>3</sub>.

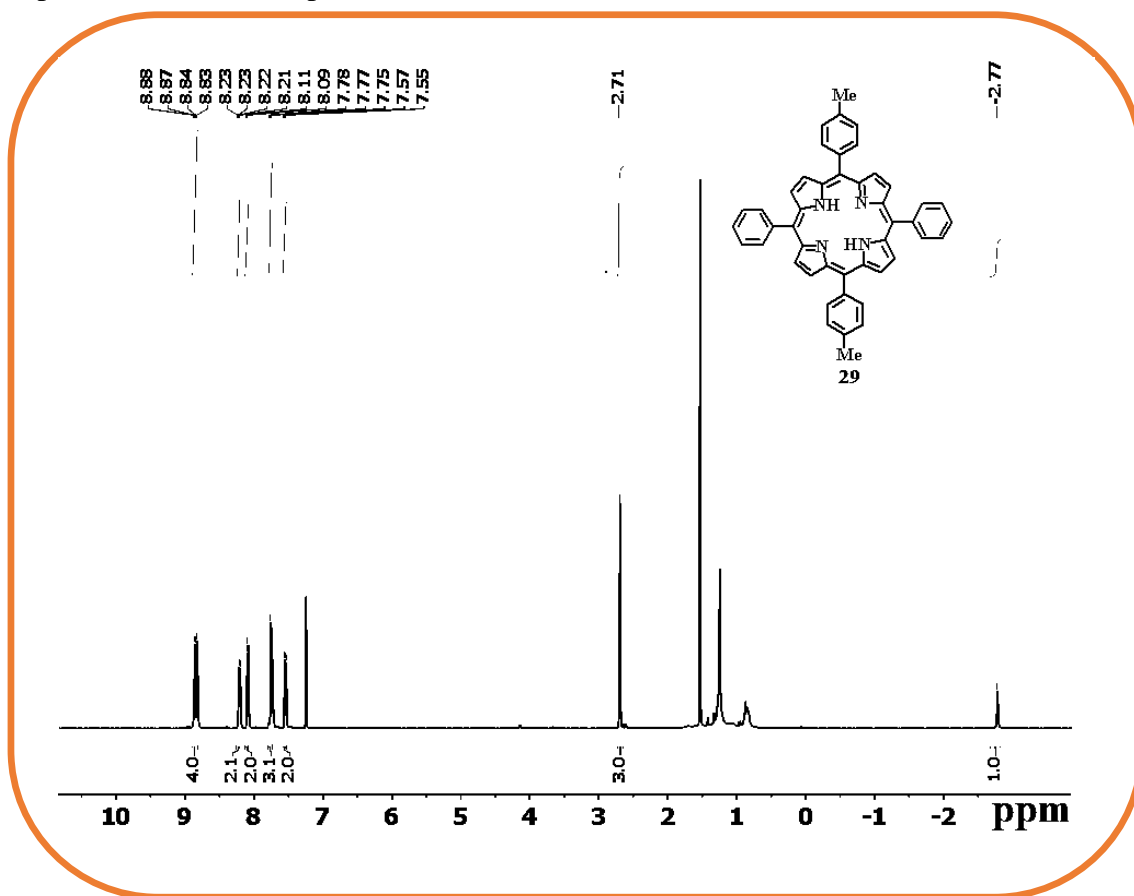
**Synthesis of 5,15-Bis(4-methylphenyl)-10,20-diphenylporphyrin, 29**

222 mg (1 mmol) of 5-phenyldipyrromethane and 117 μl (1 mmol) of *p*-tolualdehyde were added in a 100 ml MeOH and 50 ml water (2:1) mixture, followed by the addition

of 10 ml HCl. The reaction mixture was stirred at RT for 2 hours. The reaction mixture was filtered with Whatman filter paper, and the precipitate was dissolved in 15 ml of DMF solution. This DMF solution was refluxed for another 1.5 hours. This solution was finally transferred to a beaker and was stirred overnight. Then the solution was evaporated to dryness. The crude product was purified by using column chromatography through silica gel (100-200 mesh).

**For 5,15-Bis(4-methylphenyl)-10,20-diphenylporphyrin, **29****

Yield: 11% (34 mg). Anal. Calcd (found) for C<sub>46</sub>H<sub>34</sub>N<sub>4</sub> (**29**): C, 85.95 (85.81); H, 5.33 (5.43); N, 8.72 (8.64). <sup>1</sup>H NMR (400 MHz, Chloroform-*d*) δ 8.89 – 8.82 (m, 8H), 8.24 – 8.20 (m, 4H), 8.12 – 8.09 (m, 4H), 7.79 – 7.74 (m, 6H), 7.56 (d, *J* = 7.7 Hz, 4H), 2.71 (s, 6H), -2.77 (s, 2H) (Figure 4.31). Other analytical data are consistent with the previously reported authentic compounds.<sup>52</sup>



**Figure 4.31** <sup>1</sup>H NMR spectrum of **29** in CDCl<sub>3</sub>.

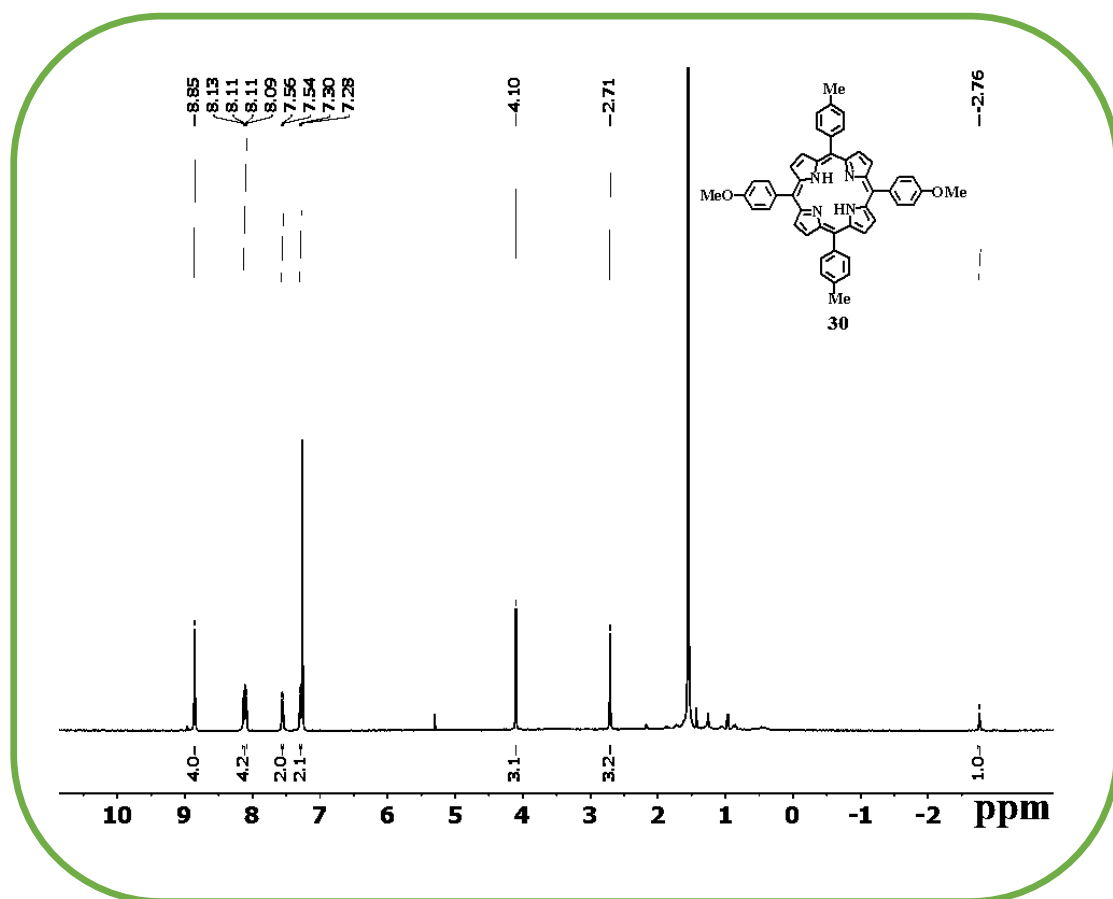
---

**Synthesis of 5,15-Bis(4-methoxyphenyl)-10,20-(4-methylphenyl)porphyrin, 30**

252 mg (1 mmol) of 5-(4-methoxyphenyl)dipyrromethane and 117  $\mu$ l (1 mmol) of *p*-tolualdehyde were added in a 100 ml MeOH and 50 ml water (2:1) mixture, followed by the addition of 10 ml HCl. The reaction mixture was stirred at RT for 2 hours. The reaction mixture was filtered with Whatman filter paper, and the precipitate was dissolved in 15 ml of DMF solution. This DMF solution was refluxed for another 1.5 hours. This solution was finally transferred to a beaker and was stirred overnight. Then the solution was evaporated to dryness. The crude product was purified using column chromatography through silica gel (100-200 mesh) or purified via crystallization.

**For 5,15-Bis(4-methoxyphenyl)-10,20-(4-methylphenyl)porphyrin, 30**

Yield: 9% (30 mg). Anal. Calcd (found) for  $C_{48}H_{38}N_4O_2$  (**30**): C, 82.03 (82.14); H, 5.45 (5.34); N, 7.97 (7.88).  $^1\text{H}$  NMR (400 MHz, Chloroform-*d*)  $\delta$  8.85 (s, 8H), 8.11 (m, 8H), 7.55 (d,  $J = 7.6$  Hz, 4H), 7.29 (d,  $J = 8.5$  Hz, 4H), 4.10 (s, 6H), 2.71 (s, 6H), -2.76 (s, 2H) (Figure 4.32). Other analytical data are consistent with the previously reported authentic compounds.<sup>52</sup>



**Figure 4.32**  $^1\text{H}$  NMR spectrum of 5,15-Bis(4-methoxyphenyl)-10,20-(4-methylphenyl)porphyrin, **30** in  $\text{CDCl}_3$ .

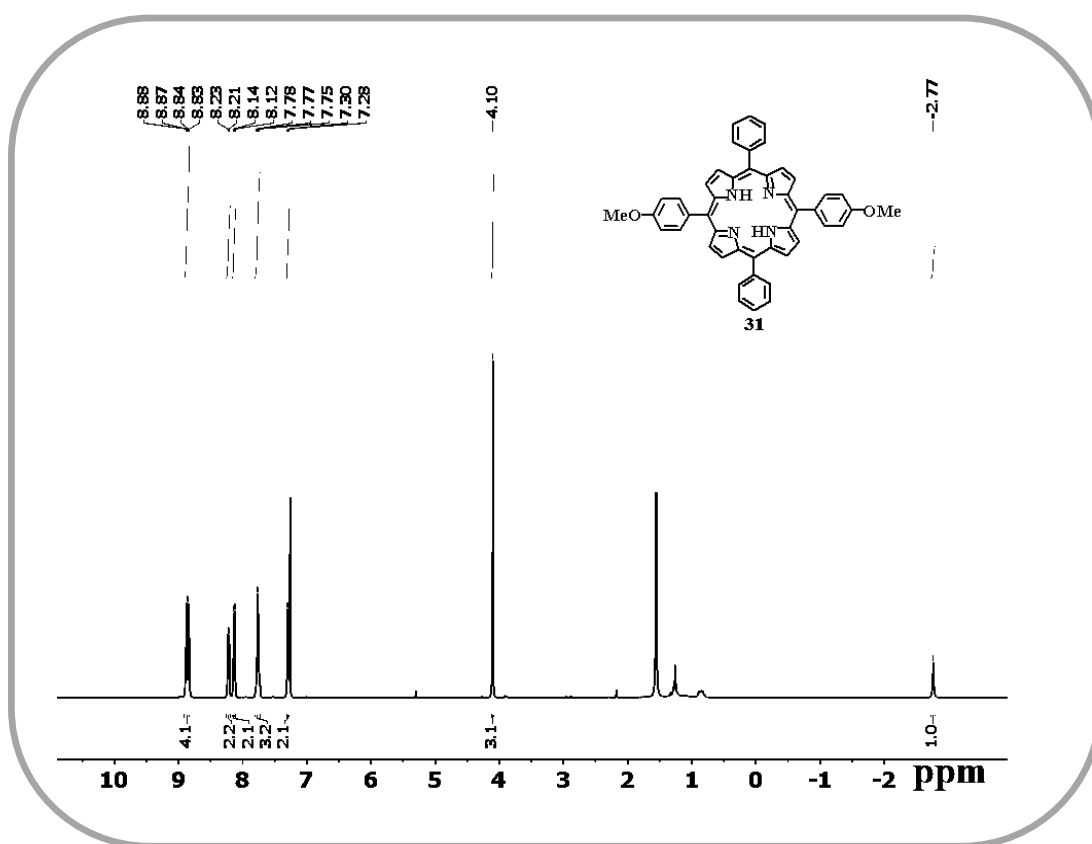
#### Synthesis of 5,15-Bis(4-methoxyphenyl)-10,20-diphenylporphyrin, **31**

252 mg (1 mmol) of 5-(4-methoxyphenyl)dipyrromethane and 102  $\mu\text{l}$  (1 mmol) of benzaldehyde were added in a 100 ml MeOH and 50 ml water (2:1) mixture, followed by the addition of 10 ml HCl. The reaction mixture was stirred at RT for 2 hours. The reaction mixture was filtered with Whatman filter paper, and the precipitate was dissolved in 15 ml of DMF solution. This DMF solution was refluxed for another 1.5 hours. This solution was finally transferred to a beaker and was stirred overnight. Then the solution was evaporated to dryness. The crude product was purified by using column chromatography through silica gel (100-200 mesh).

---

**For 5,15-Bis(4-methoxyphenyl)-10,20-diphenylporphyrin, 31**

Yield: 9% (31 mg). Anal. Calcd (found) for  $C_{46}H_{34}N_4O_2$  (**31**): C, 81.88 (81.99); H, 5.08 (4.97); N, 8.30 (8.45).  $^1H$  NMR (400 MHz, Chloroform-*d*)  $\delta$  8.91 – 8.82 (m, 8H), 8.24 – 8.20 (m, 4H), 8.16 – 8.11 (m, 4H), 7.77 (m, 6H), 7.31 – 7.27 (m, 4H), 4.10 (s, 6H), -2.76 (s, 2H) (Figure 4.33). Other analytical data are consistent with the previously reported authentic compounds.<sup>52</sup>



**Figure 4.33**  $^1H$  NMR spectrum of 5,15-Bis(4-methoxyphenyl)-10,20-diphenylporphyrin, **31** in  $CDCl_3$ .

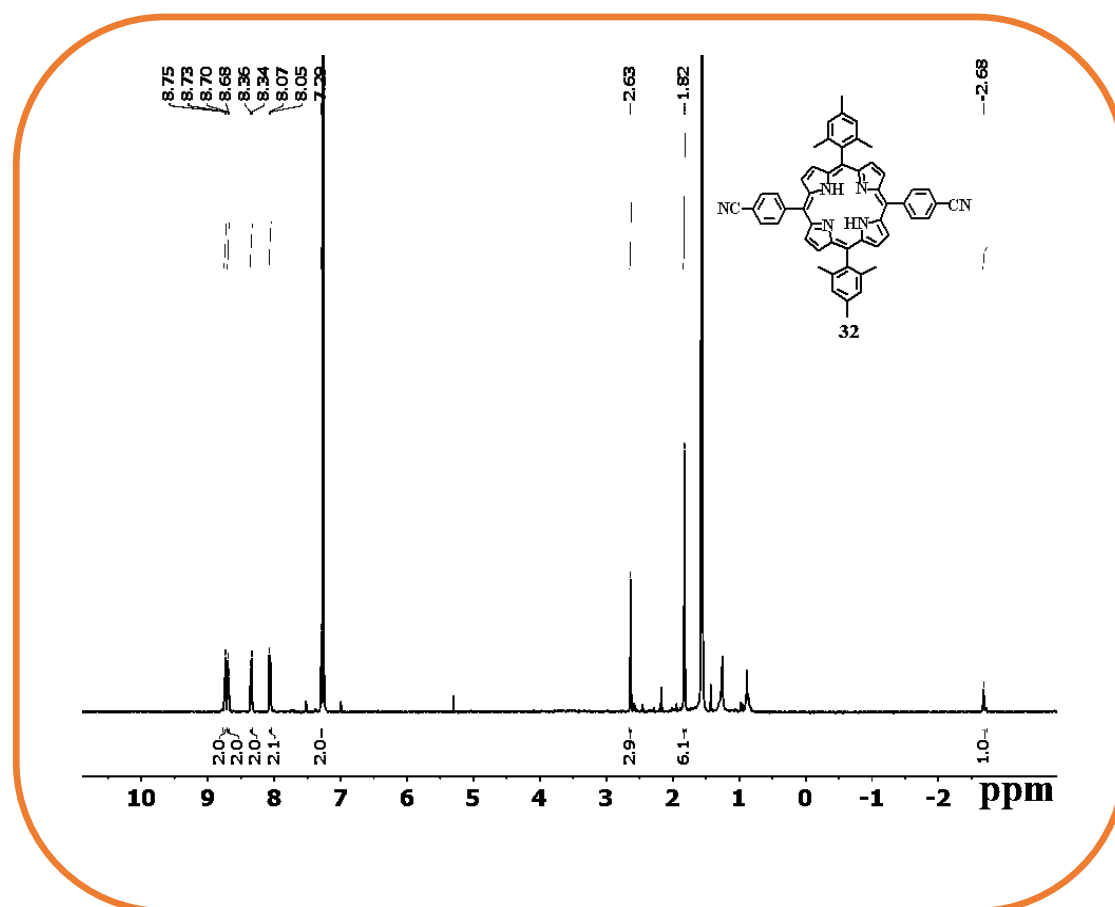
**Synthesis of 5,15-bis(4-cyanophenyl)-10,20-bis(2,4,6-trimethylphenyl)porphyrin, 32**

247 mg (1 mmol) of 5-(4-cyanophenyl)dipyrromethane and 148  $\mu$ l (1 mmol) of mesitaldehyde were added to a 100 ml MeOH and 50 ml water (2:1) mixture, followed by the addition of 10 ml HCl. The reaction mixture was stirred at RT for 2 hours. The

reaction mixture was filtered with Whatman filter paper, and the precipitate was dissolved in 15 ml of DMF solution. This DMF solution was refluxed for another 1.5 hours. This solution was finally transferred to a beaker and was stirred overnight. Then the solution was evaporated to dryness. The crude product was purified by using column chromatography through silica gel (100-200 mesh).

**For 5,15-bis(4-cyanophenyl)-10,20-bis(2,4,6-trimethylphenyl)porphyrin, **32****

Yield: 5% (20 mg). Anal. Calcd (found) for  $C_{52}H_{40}N_6$  (**32**): C, 83.39 (83.27); H, 5.38 (5.26); N, 11.22 (11.31).  $^1H$  NMR (400 MHz, Chloroform-*d*)  $\delta$  8.74 (d,  $J = 4.8$  Hz, 4H), 8.69 (d,  $J = 4.8$  Hz, 4H), 8.35 (d,  $J = 8.0$  Hz, 4H), 8.06 (d,  $J = 8.1$  Hz, 4H), 7.29 (s, 4H), 2.63 (s, 6H), 1.82 (s, 12H), -2.68 (s, 2H) (Figure 4.34). Other analytical data are consistent with the previously reported authentic compounds.<sup>53</sup>



**Figure 4.34**  $^1H$  NMR spectrum of 5,15-bis(4-cyanophenyl)-10,20-bis(2,4,6-trimethylphenyl)porphyrin, **32** in  $CDCl_3$ .

---

## References

- (1) Weissbluth, M., In *Molecular Biology Biochemistry and Biophysics*; Springer: Heidelberg, **1974**, *15*, 10-26.
- (2) Moore, M. R. A., In *Tetrapyrroles: Birth, Life and Death*; Warren, M. J.; Smith, A. G., Eds.; Springer: New York, **2009**, 1-28.
- (3) Ptaszek, M.; Yao, Z.; Savithri, D.; Boyle, P. D.; Lindsey, J. S., *Tetrahedron* **2007**, *63*, 12629-12638.
- (4) Murphy, M. J.; Siegel, L. M.; Tove, S. R.; Kamin, H., *Proc. Natl. Acad. Sci. U. S. A.* **1974**, *71*, 612-616.
- (5) Chang, C.; Barkigia, K.; Hanson, L.; Fajer, J., *J. Am. Chem. Soc.* **1986**, *108*, 1352-1354.
- (6) Zimmer, M.; Crabtree, R. H., *J. Am. Chem. Soc.* **1990**, *112*, 1062-1066.
- (7) Naruta, Y.; Tani, F.; Ishihara, N.; Maruyama, K., *J. Am. Chem. Soc.* **1991**, *113*, 6865-6872.
- (8) Yamaguchi, S.; Katoh, T.; Shinokubo, H.; Osuka, A., *J. Am. Chem. Soc.* **2007**, *129*, 6392-6393.
- (9) Akamine, K.; Morita, K.; Sakai, K.; Ozawa, H., *ACS Appl. Energy Mater.* **2020**, *3*, 4860-4866.
- (10) Kuttassery, F.; Mathew, S.; Remello, S. N.; Thomas, A.; Sano, K.; Ohsaki, Y.; Nabetani, Y.; Tachibana, H.; Inoue, H., *Coord. Chem. Rev.* **2018**, *377*, 64-72.
- (11) Jurow, M.; Schuckman, A. E.; Batteas, J. D.; Drain, C. M., *Coord. Chem. Rev.* **2010**, *254*, 2297-2310.
- (12) Mathew, S.; Yella, A.; Gao, P.; Humphry-Baker, R.; Curchod, B. F.; Ashari-Astani, N.; Tavernelli, I.; Rothlisberger, U.; Nazeeruddin, M. K.; Grätzel, M., *Nat. Chem.* **2014**, *6*, 242-247.

- 
- (13) Dhamija, A.; Mondal, P.; Saha, B.; Rath, S. P., *Dalton Trans.* **2020**, 49, 10679-10700.
- (14) Nobukuni, H.; Kamimura, T.; Uno, H.; Shimazaki, Y.; Naruta, Y.; Tani, F., *Bull. Chem. Soc. Jpn.* **2011**, 84, 1321-1328.
- (15) Araki, K.; Engelmann, F. M.; Mayer, I.; Toma, H. E.; Baptista, M. S.; Maeda, H.; Osuka, A.; Furuta, H., *Chem. Lett.* **2003**, 32, 244-245.
- (16) Pushpan, S.; Venkatraman, S.; Anand, V.; Sankar, J.; Parmeswaran, D.; Ganesan, S.; Chandrashekar, T., *Curr. Med. Chem. Anti-Cancer Agents* **2002**, 2, 187-207.
- (17) Groves, J. T., *J. Inorg. Biochem.* **2006**, 100, 434-447.
- (18) Yamasumi, K.; Notsuka, Y.; Yamaoka, Y.; Mori, S.; Ishida, M.; Furuta, H., *Chem. Eur. J.* **2020**, 26, 13590-13594.
- (19) Fukuzumi, S.; Guldi, D. M. In *Electron Transfer in Chemistry*, Balzani, V., Ed.; Wiley-VCH: Weinheim, 2001, Vol. 2, pp 270-337.
- (20) Kadish, K. M.; Smith, K. M.; Guillard, R. *The Porphyrin Handbook*; Academic Press: New York, 2003; Vols. 1-20.
- (21) Meunier, B., *Chem. Rev.* **1992**, 92, 1411-1456.
- (22) Fleischer, E. B., *Acc. Chem. Res.* **1970**, 3, 105-112.
- (23) Nakano, A.; Osuka, A.; Yamazaki, I.; Yamazaki, T.; Nishimura, Y., *Angew. Chem. Int. Ed.* **1998**, 37, 3023-3027.
- (24) Osuka, A.; Mataga, N.; Okada, T., *Pure Appl. Chem.* **1997**, 69, 797-802.
- (25) Furuta, H.; Asano, T.; Ogawa, T., *J. Am. Chem. Soc.* **1994**, 116, 767-768.
- (26) Sessler, J. L.; Burrell, A. K., *Macrocycles* **1992**, 177-273.
- (27) Lemon, C. M.; Brothers, P. J.; Boitrel, B., *Dalton Trans.* **2011**, 40, 6591-6609.
- (28) Patra, B.; Sobottka, S.; Mondal, S.; Sarkar, B.; Kar, S., *Chem. Commun.* **2018**, 54, 9945-9948.
-



- 
- (29) Fischer H.; Gleim W., *Justus Liebigs Ann. Chem.* **1936**, 521, 157-160.
- (30) Vicente, M. G. H.; Smith, K. M., *Curr. Org. Chem.* **2000**, 4, 139-174.
- (31) Rothmund, P., *J. Am. Chem. Soc.* **1936**, 58, 625-627.
- (32) Adler, A. D.; Longo, F. R.; Finarelli, J. D.; Goldmacher, J.; Assour, J.; Korsakoff, L., *J. Org. Chem.* **1967**, 32, 476-476.
- (1) Geier III, G. R.; Lindsey, J. S., *J. Chem. Soc., Perkin Trans 2* **2001**, 677-686.
- (2) Littler, B. J.; Ciringh, Y.; Lindsey, J. S., *J. Org. Chem.* **1999**, 64, 2864-2872.
- (3) Koszarna, B.; Gryko, D. T., *J. Org. Chem.* **2006**, 71, 3707-3717.
- (4) Arsenault, G.; Bullock, E.; MacDonald, S., *J. Am. Chem. Soc.* **1960**, 82, 4384-4389.
- (5) Mondal, S.; Sahu, K.; Patra, B.; Jena, S.; Biswal, H. S.; Kar, S., *Dalton Trans.* **2020**, 49, 1424-1432.
- (6) Okada, S.; Segawa, H., *J. Am. Chem. Soc.* **2003**, 125, 2792-2796.
- (7) Slomp, A. M.; Barreira, S. M.; Carrenho, L. Z.; Vandresen, C. C.; Zattoni, I. F.; Ló, S. M.; Dallagnol, J. C.; Ducatti, D. R.; Orsato, A.; Duarte, M. E. R., *Bioorg. Med. Chem. Lett.* **2017**, 27, 156-161.
- (8) Lindsey, J. S.; Wagner, R. W., *J. Org. Chem.* **1989**, 54, 828-836.
- (9) Campbell, W. M.; Jolley, K. W.; Wagner, P.; Wagner, K.; Walsh, P. J.; Gordon, K. C.; Schmidt-Mende, L.; Nazeeruddin, M. K.; Wang, Q.; Grätzel, M., *J. Phys. Chem. C* **2007**, 111, 11760-11762.
- (10) Lin, Q.; Bu, X.; Kong, A.; Mao, C.; Bu, F.; Feng, P *Adv. Mater.* **2015**, 27, 3431-3436.
- (11) Tan, Z.; Su, H.; Guo, Y.; Liu, H.; Liao, B.; Amin, A. M.; Liu, Q., *Polymers* **2020**, 12, 719.
-

- 
- (12) Liu, F.; Duan, L.; Wang, Y.-L.; Zhang, Q.; Wang, J.-Y., *Synth. Commun.* **2009**, *39*, 3990-3998.
- (13) Sobotta, L.; Sniechowska, J.; Ziental, D.; Dlugaszewska, J.; Potrzebowski, M. J., *Dyes and Pigments* **2019**, *160*, 292-300.
- (14) Lindsey, J. S.; Schreiman, I. C.; Hsu, H. C.; Kearney, P. C.; Marguerettaz, A. M., *J. Org. Chem.* **1987**, *52*, 827-836.
- (15) Asano, N.; Uemura, S.; Kinugawa, T.; Akasaka, H.; Mizutani, T., *J. Org. Chem.* **2007**, *72*, 5320-5326.
- (16) Acharya, R.; Paudel, L.; Joseph, J.; McCarthy, C. E.; Dudipala, V. R.; Modarelli, J. M.; Modarelli, D. A., *J. Org. Chem.* **2012**, *77*, 6043-6050.
- (17) Frixa, C.; Mahon, M. F.; Thompson, A. S.; Threadgill, M. D., *Org. Biomol. Chem.* **2003**, *1*, 306-317.
- (18) Xie, Y.; Zhang, F.; Liu, P.; Hao, F.; Luo, H., a., *Can. J. Chem.* **2014**, *92*, 49-53.
- (19) Nielsen, C. B.; Krebs, F. C., *Tetrahedron Lett.* **2005**, *46*, 5935-5939.
- (20) Shi, B.; Boyle, R. W., *J. Chem. Soc., Perkin Trans 1* **2002**, 1397-1400.
- (21) Kulikov, O. V.; Schmidt, I.; Muresan, A. Z.; Lee, M. A.-P.; Bocian, D. F.; Lindsey, J. S., *J. Porphyr. Phthalocyanines* **2007**, *11*, 699-712.

# CHAPTER 5

---

## The Reaction of NOBF<sub>4</sub> with the Sb(III)-corroles: Oxidative addition of Fluoride at the Antimony and Regioselective Nitration of Corroles

---

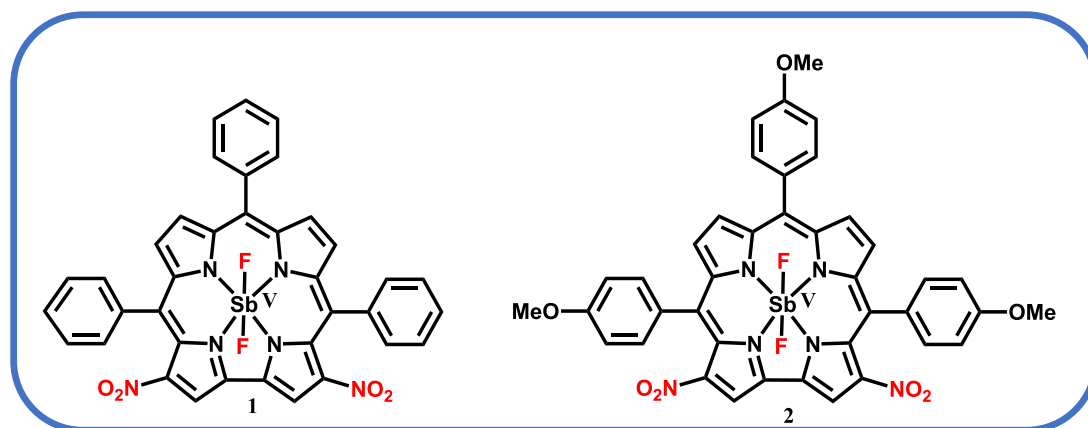
- 5.1 Introduction
- 5.2 Results and Discussions
  - 5.2.1 Synthesis and characterization
  - 5.2.2 Crystal Structure
  - 5.2.3 UV-vis and emission spectroscopy
  - 5.2.4 Redox properties
- 5.3 Catalytic Applicability
- 5.4 Conclusion
- 5.5 Experimental Section
  - 5.5.1 Materials
  - 5.5.2 Physical Measurements
  - 5.5.3 Crystal Structure Determination
  - 5.5.4 Syntheses
    - 5.5.4.1 Synthesis of [*trans*-difluoro(3,17-dinitro-5,10,15-triphenylcorrolato)antimony(V)], 1
    - 5.5.4.2 For [*trans*-difluoro(3,17-dinitro-5,10,15triphenylcorrolato)antimony(V)],
    - 5.5.4.3 Synthesis of {5,10,15-tris(4-methoxyphenyl)corrolato}antimony (III), 2A
    - 5.5.4.4 For {5,10,15-tris(4-methoxyphenyl)corrolato}antimony (III), 2A
    - 5.5.4.5 Synthesis of [*trans*-difluoro(3,17-dinitro-5,10,15-tris(4-methoxyphenyl)corrolato)antimony(V)], 2
    - 5.5.4.6 For [*trans*-difluoro(3,17-dinitro-5,10,15-tris(4-methoxyphenyl)corrolato)antimony(V)], 2

---

## 5.1 Introduction

Metallo-porphyrinoids constitute the most important class of naturally occurring and also artificially obtained photosensitizers.<sup>1-3</sup> Metallo-porphyrinoids can also participate in multiple electron transfer reactions due to the involvement of judiciously chosen central metal ions and the equatorially bound porphyrinoid ligands.<sup>4-5</sup> High valent metalloporphyrinoid complexes bearing  $\text{Sn}^{\text{IV}}$ ,  $\text{Sb}^{\text{V}}$ ,  $\text{As}^{\text{V}}$ , and  $\text{P}^{\text{V}}$  centers have the propensity to bind axial ligands covalently and they differ largely from their transition metalloporphyrinoid counterparts.<sup>6-9</sup> The axial ligands can bind and activate a series of substrates.<sup>10</sup> Antimony porphyrinoid complexes are the ideal choice for photocatalytic multiple electron transfer reactions due to their excellent photostability which arises due to the highly reversible shuttling of  $s^2$ (low valent) to  $s^0$ (high valent) electronic configuration.<sup>11-18</sup> Although antimony is the main group element, still, Sb-porphyrin complexes can efficiently replace various transition metal complexes in catalytic oxidation reactions and have the propensity to fulfill as a spectroscopic and functional model of the cytochrome P450 family of metalloenzymes.<sup>19-22</sup> Antimony is an ideal choice for two-electron transfer reactions due to the availability of thermodynamically stable Sb(III) and Sb(V) oxidation states. Antimony porphyrin complexes are traditionally used in visible-light-driven photo-catalysis reactions<sup>11-23</sup> and in recent times analogous antimony corrole complexes are gaining a lot of research interest.<sup>24-32</sup> Corrole, a contracted porphyrin analog having an  $18\pi$  electron aromatic system, has different photophysical properties than porphyrin. It is a tri-anionic chelating ligand and can stabilize Sb(III) and Sb(V) oxidation states easily.<sup>33-58</sup> Although sparsely reported, but still various researchers have discovered intriguing properties of different antimony corrole complexes.<sup>24-32</sup> Kadish *et al.* have described the facile access of antimony octaethylcorroles in different oxidation states ( $\text{Sb}^{\text{III}}$ ,  $\text{Sb}^{\text{IV}}$ , and  $\text{Sb}^{\text{V}}$ ).<sup>30</sup> Gross *et al.* have

demonstrated that antimony corroles can promote photocatalytic oxygenation of various organic molecules under aerobic conditions.<sup>24</sup> Photo-elimination of axial halide ligands in antimony corroles has been demonstrated by Nocera *et al.*<sup>26</sup> The bromide to bromine conversion was demonstrated by Gross *et al.* while using a difluoroantimony(V) corrole complex under visible light illumination.<sup>32</sup> We have also reported the synthesis and characterization of antimony corroles (Sb<sup>III</sup> and Sb<sup>V</sup>) in two different oxidation states.<sup>27</sup> It was also observed that a corrolato Sb(III) species reacts with oxygen donors like PhIO in the air resulting in the generation of oxo-corrolato Sb(V) species. Herein, we have observed that corrolato Sb(III) complexes react with NOBF<sub>4</sub> (a nitric oxide precursor) in air and generated *trans*-difluoro- corrolato Sb(V) species along with dinitration of corrole ring (Scheme 5.1).



**Scheme 5.1** Structures of the [*trans*-difluoro(3,17-dinitro-5,10,15 triphenylcorrolato)antimony(V)], **1**; [*trans*-difluoro(3,17-dinitro-5,10,15-tris(4-methoxyphenyl)corrolato)antimony(V)], **2**.

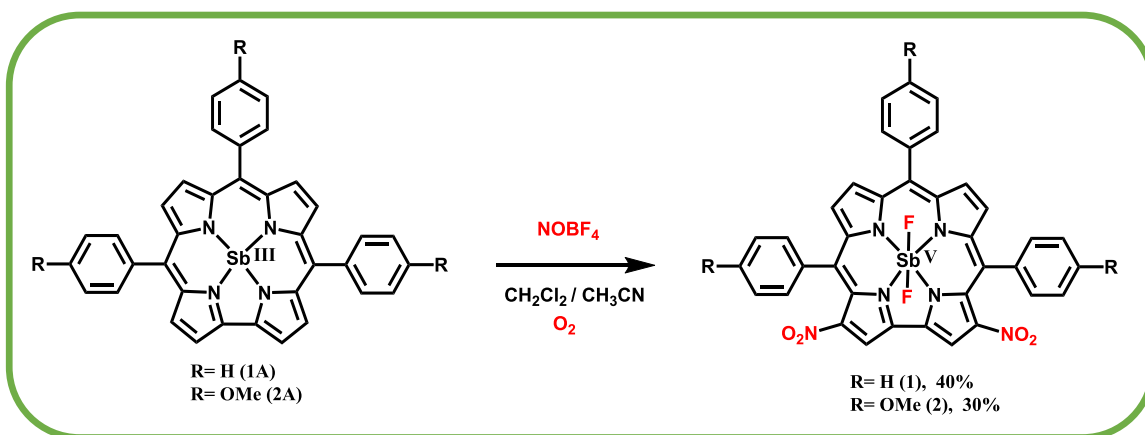
We have also proposed a putative *trans*- dinitrosyl (corrolato)antimony(V) species as a reaction intermediate. This metastable intermediate is subsequently converted into a *trans*- dinitro (corrolato)antimony(V) species, which ultimately leads to the transfer of the nitro groups to the  $\beta$ -positions (3 and 17) of corrole. This *trans*-difluoro-3,17-dinitro-corrolato Sb(V) species is capable of oxidizing

triphenylphosphine, 9,10-dihydroanthracene, and thioanisole, and the process is catalytic in presence of air and light at ambient temperature with a moderate to good turnover number.

## 5.2 Results and Discussion

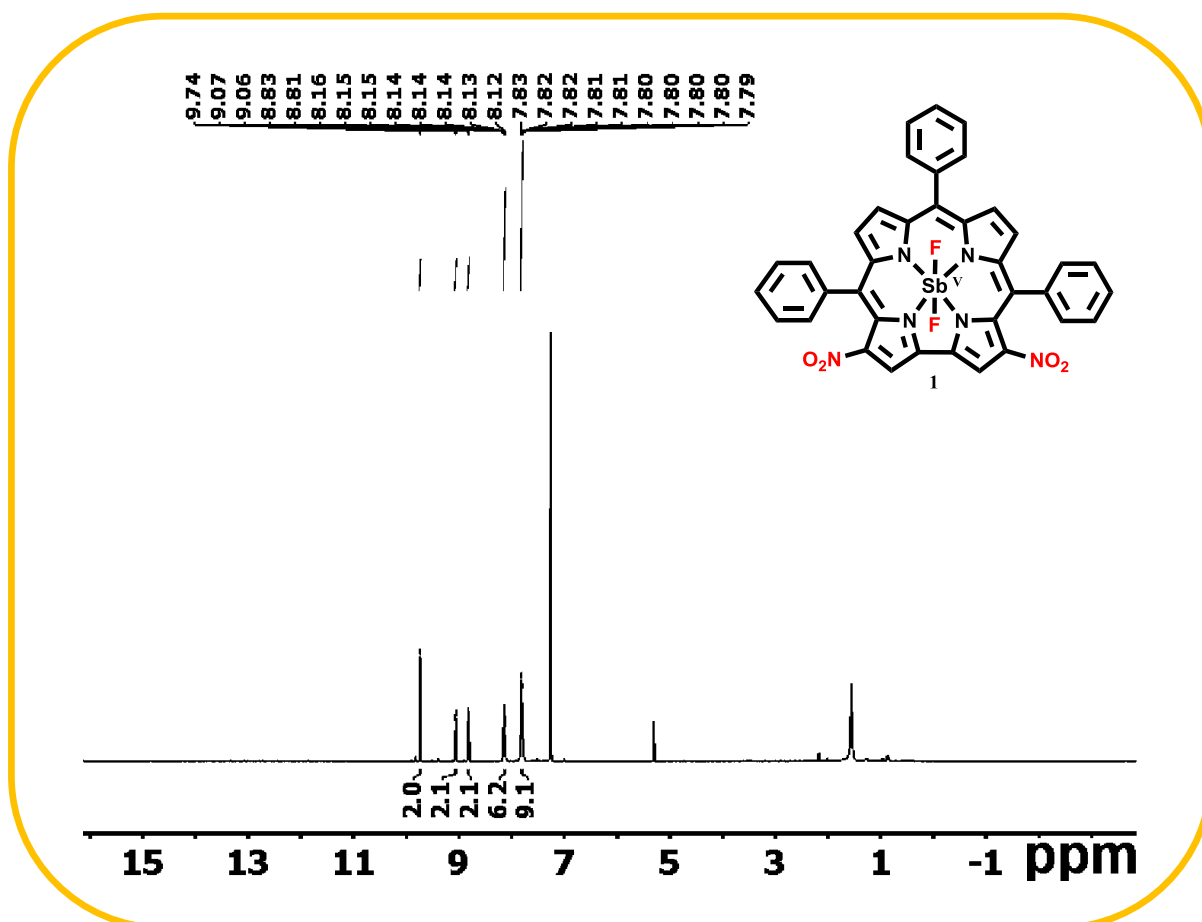
### 5.2.1 Synthesis and characterization

The synthesis of *trans*-difluoro(corrolato)antimony(V) derivatives (**1** and **2**) was achieved by serendipity. While attempting to synthesize nitrosyl derivatives of antimony corroles, we have treated the respective corrolato-Sb(III) complexes with the nitrosating agent, NOBF<sub>4</sub>. In a typical reaction, the corresponding corrolato-Sb(III) complexes were reacted with excess NOBF<sub>4</sub> in a CH<sub>2</sub>Cl<sub>2</sub>–CH<sub>3</sub>CN mixture. This reaction resulted in the immediate formation of *trans*-difluoro(corrolato)antimony(V) derivatives in good yields (Scheme 5.2). Purity and composition of the *trans*-difluoro(corrolato)antimony(V) derivatives (**1** and **2**) were established by their satisfactory elemental analyses, ESI-MS, NMR, UV-vis, emission, cyclic voltammogram, FT-IR, and single-crystal XRD analysis.



**Scheme 5.2** Synthetic application of [*trans*-difluoro(corrolato)antimony(V)] complexes: [*trans*-difluoro(3,17-dinitro-5,10,15-triphenylcorrolato)antimony(V)], **1**; [*trans*-difluoro(3,17-dinitro-5,10,15-tris(4-methoxyphenyl)corrolato)antimony(V)], **2**.

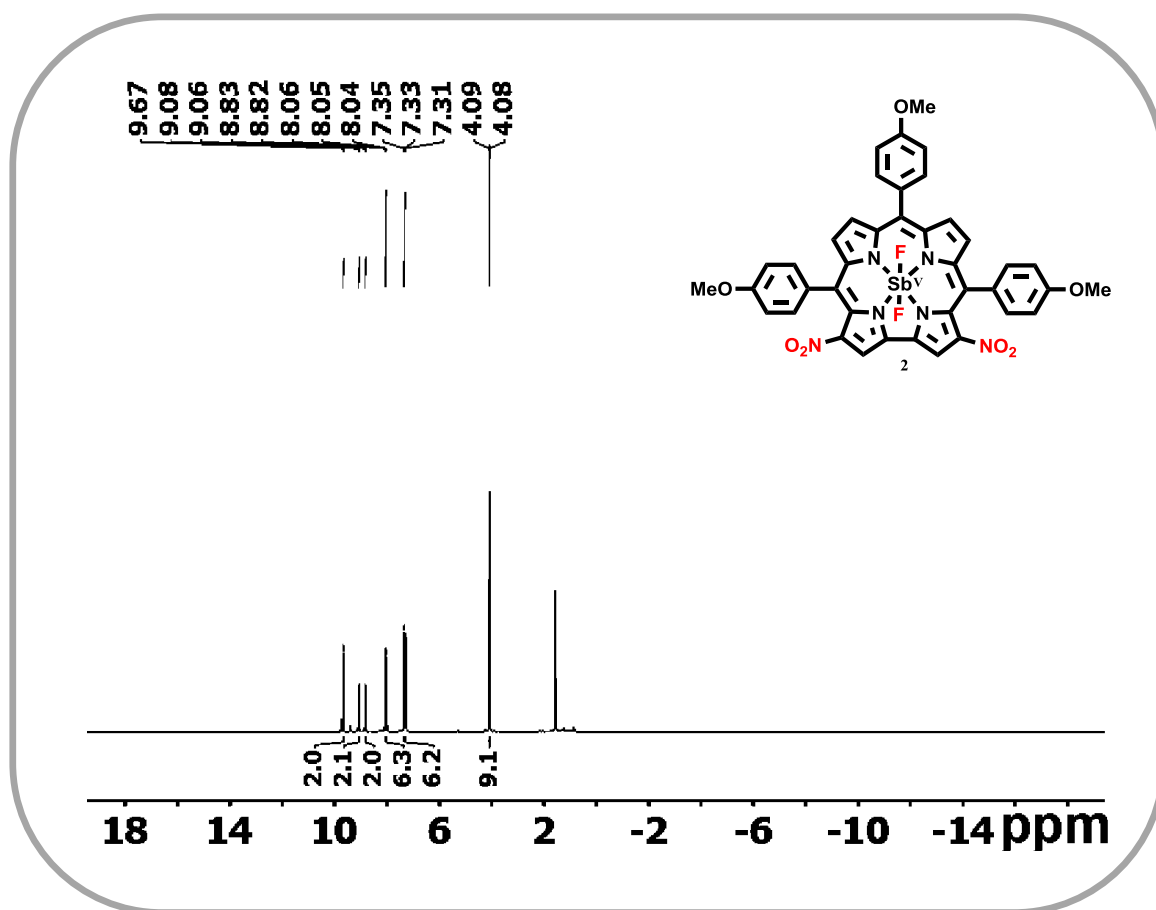
In the native state, the *trans*-difluoro(corrolato)antimony(V) derivatives (**1** and **2**) are diamagnetic in nature as is evident from the  $^1\text{H}$  NMR spectra of both these complexes (Figures 5.1 and 5.2).



**Figure 5.1**  $^1\text{H}$  NMR spectrum of **1** in  $\text{CDCl}_3$ .

In the  $^1\text{H}$  NMR spectra, both the complexes exhibited sharp signals with the normal chemical shift. Compound **1** exhibited twenty-one partially overlapping aromatic protons in the region,  $\delta$  9.74–7.79 ppm. Compound **2** exhibited eighteen partially overlapping aromatic protons in the region,  $\delta$  9.67–7.33 ppm. The nine methoxy protons appeared in the region of,  $\delta$  4.08 ppm for **2**. While comparing the  $^1\text{H}$  NMR shifts with the starting antimony(III) corroles (**1A** and **2A**), it was observed that the peaks of the

*trans*-difluoro(corrolato)antimony(V) derivatives (**1** and **2**) shifted to the downfield region.<sup>27</sup>

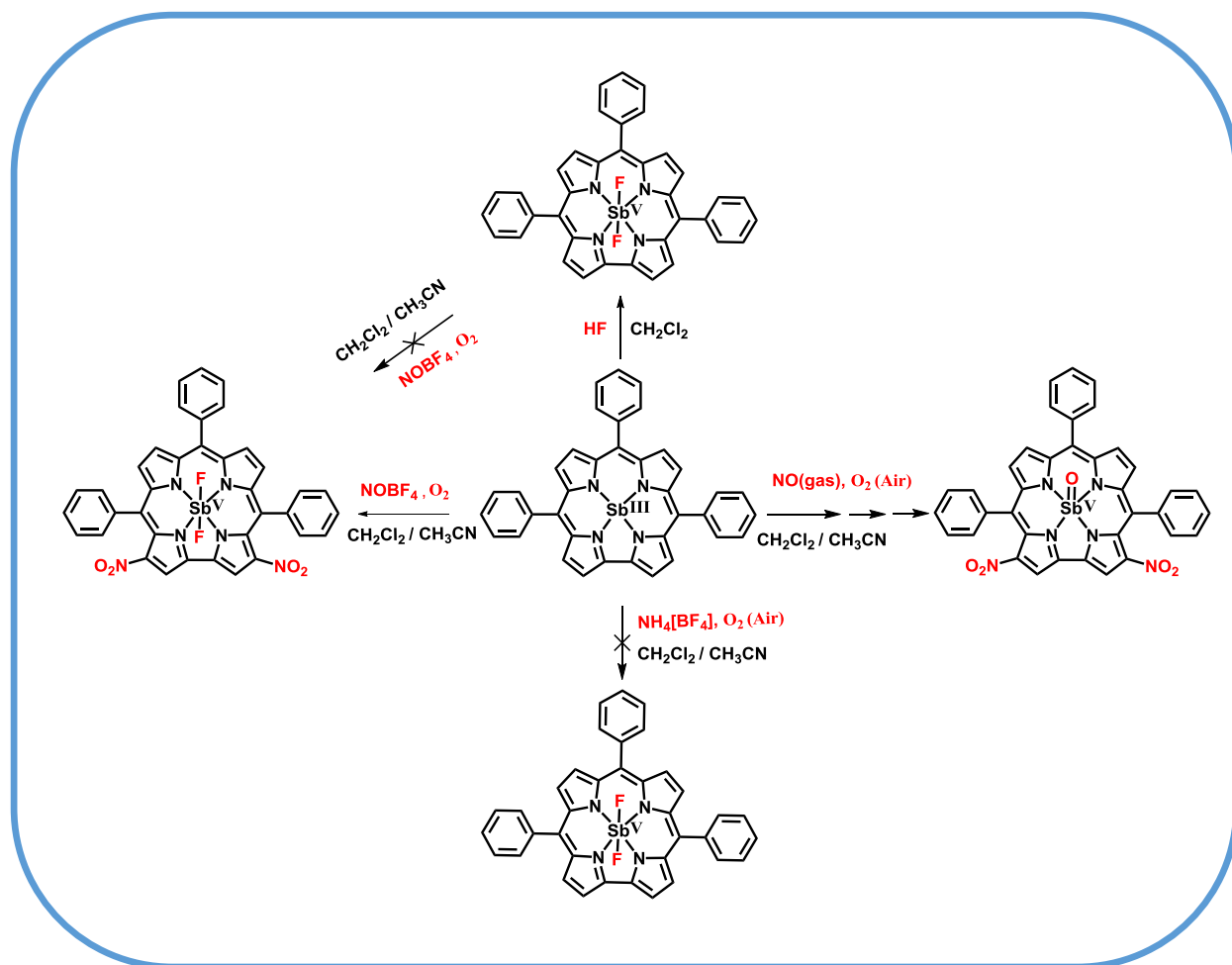


**Figure 5.2** <sup>1</sup>H NMR spectrum of **2** in CDCl<sub>3</sub>.

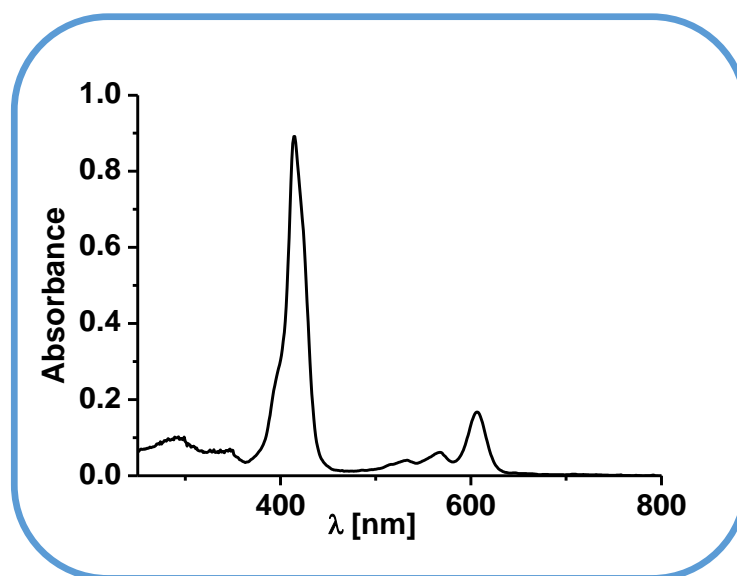
<sup>13</sup>C NMR spectrum of **2** displays methoxy group signals at values of ~ 55.8 ppm. From the conductivity data in acetonitrile solution, it appears that both compounds **1** and **2** are non-conducting. Thus, there is no dissociable counter ion in these compounds. It is assumed that this reaction occurs *via* the multi-step pathway leading to the formation of the complexes [*trans*- difluoro(3,17-dinitro–5,10,15 triphenylcorrolato)antimony(V)], **1** and [*trans*-difluoro(3,17-dinitro–5,10,15-tris(4-methoxyphenyl)corrolato)antimony (V)], **2**. The reagent NOBF<sub>4</sub> in a CH<sub>2</sub>Cl<sub>2</sub>–CH<sub>3</sub>CN mixture in presence of air is completely inert, thus a transformation of NO<sup>+</sup> (in the reagent) to the nitro groups (in the product) is highly improbable without the involvement of a reactive intermediate species. It is also



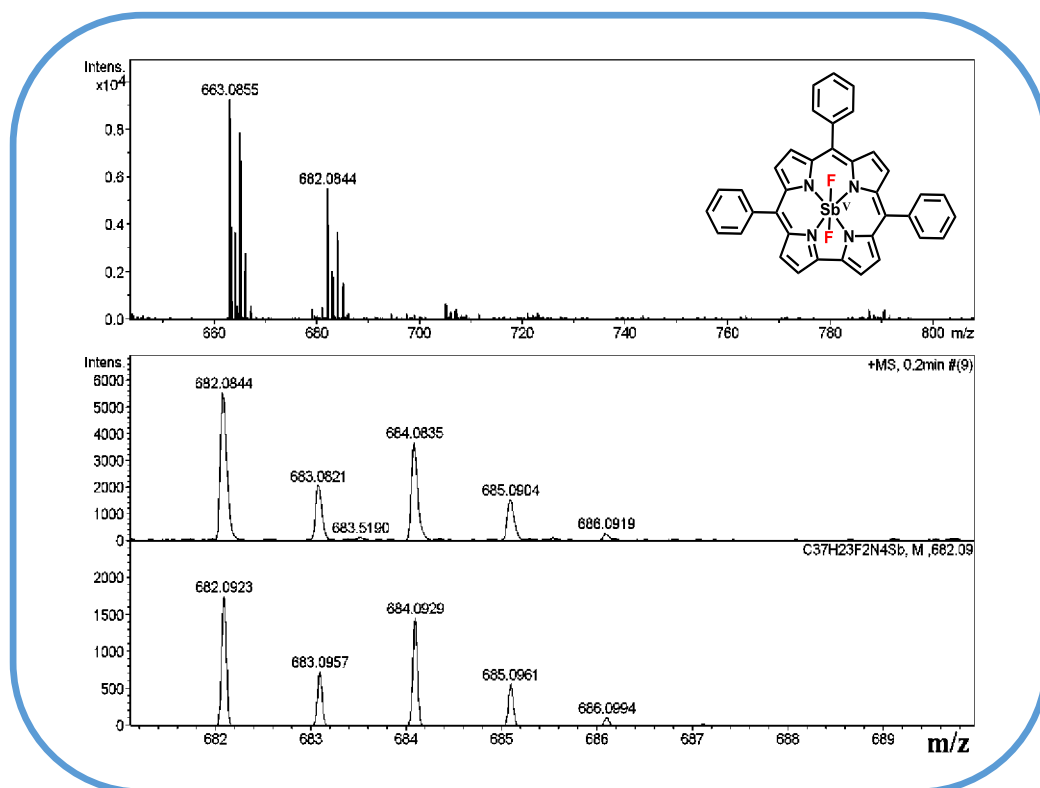
highly unlikely that the nitroso group is inserted directly into the corrole periphery via nuclear substitution and then subsequently transformed into the nitro groups. Treating the FB corroles with  $\text{NOBF}_4$  in a similar reaction condition does not afford the insertion of nitro groups into the corrole periphery which further supports this hypothesis. Thus it is assumed that the corrole chelated  $\text{Sb(III)}$  ion plays a key role. In order to prove the role of the metal center, we have synthesized *trans*-difluoro(5,10,15-triphenylcorrolato)antimony(V) complex (Scheme 5.3, Figures 5.3-5.4).



**Scheme 5.3** Chemical reactivity of (corrolato)antimony(III) complex, **1A**.

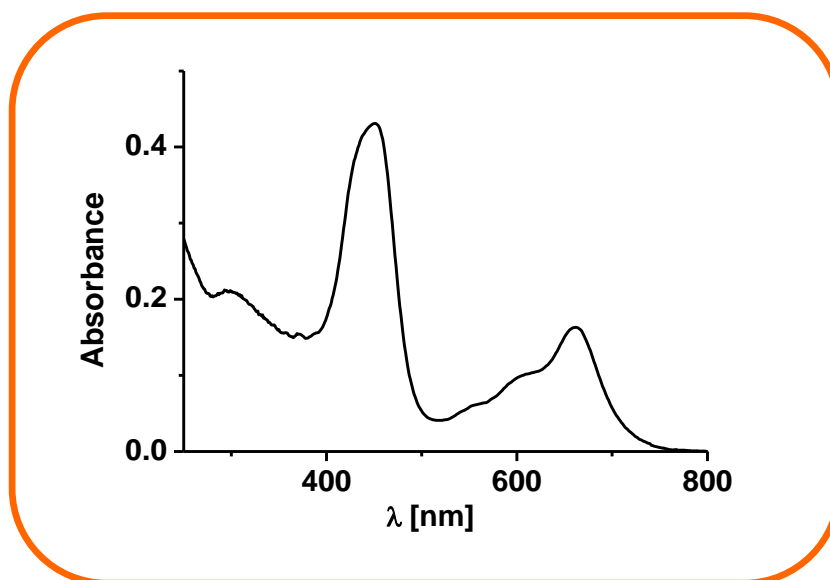


**Figure 5.3** Electronic absorption spectrum of (5,10,15-triphenylcorrolato)(*trans*-difluoro)antimony(V) in dichloromethane.

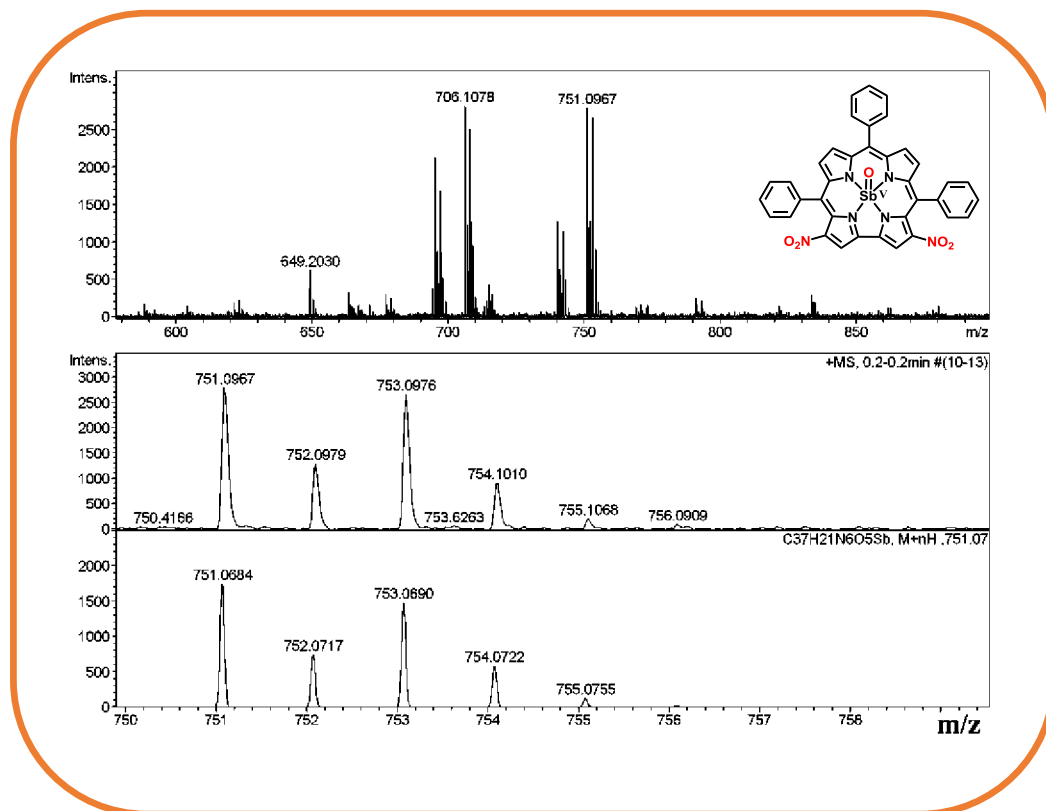


**Figure 5.4** ESI- MS spectrum of (5,10,15-triphenylcorrolato)(*trans*-difluoro)antimony(V) in  $\text{CH}_3\text{CN}$  shows the measured spectrum with isotopic distribution pattern.

While treating this complex with  $\text{NOBF}_4$  in a  $\text{CH}_2\text{Cl}_2$ - $\text{CH}_3\text{CN}$  mixture in presence of air does not yield the desired compound; [*trans*- difluoro(3,17-dinitro-5,10,15 triphenylcorrolato)antimony(V)], **1**. It appears that blocking both axial positions hinders the formation of nitrosyl chelated Sb(III/V) complexes (Scheme 5.3). While treating the Sb(III) corrole with NO gas in a  $\text{CH}_2\text{Cl}_2$ - $\text{CH}_3\text{CN}$  mixture in presence of air resulted in the formation of the compound; [oxo(3,17-dinitro-5,10,15 triphenylcorrolato)antimony(V)] (Scheme 5.3, Figures 5.5-5.6). If at all, Sb(V)-oxo-corrole is generated in the 1st step of the reaction, as it is penta-coordinated, thus, it can still accommodate one more axial ligand and thus the insertion of the nitro group in the corrole periphery will be unhindered.

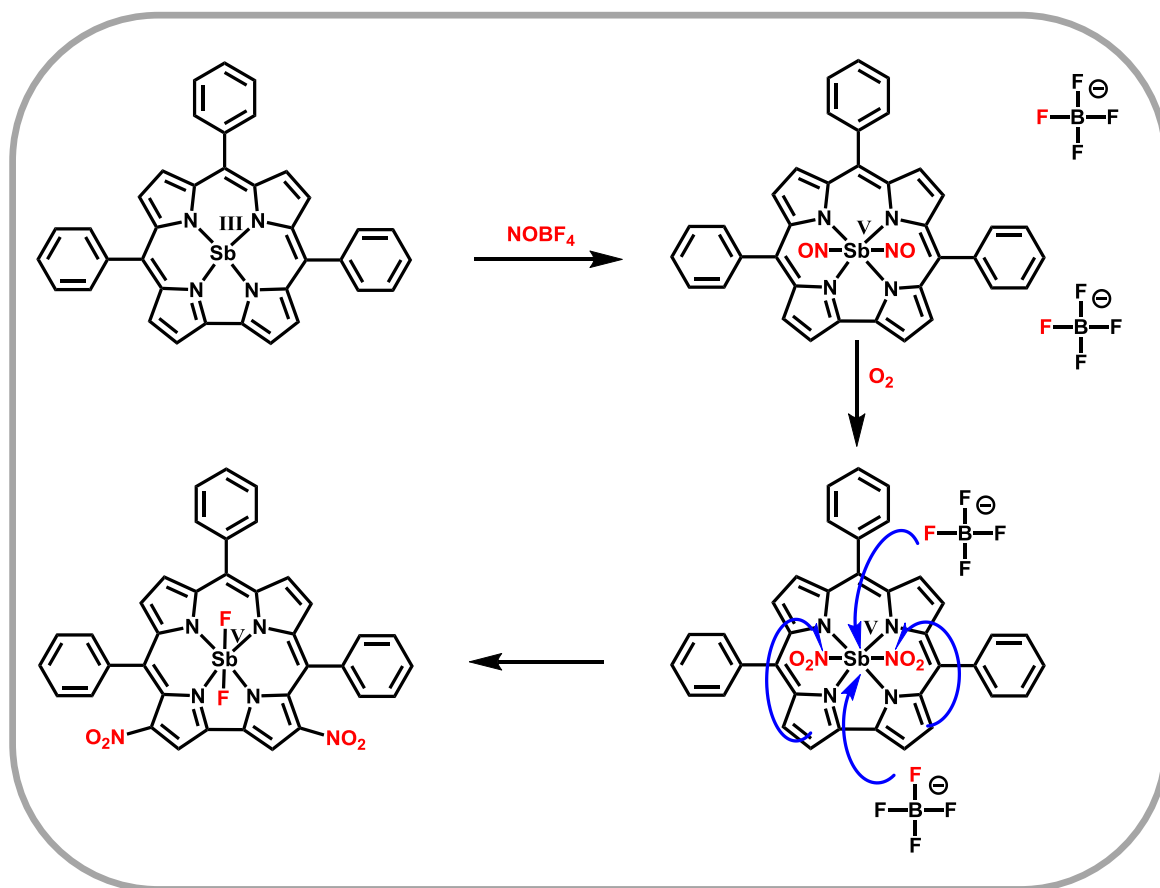


**Figure 5.5** Electronic absorption spectrum of (3,17-dinitro-5,10,15-triphenyl corrolato)(oxo)antimony(V) in  $\text{CH}_2\text{Cl}_2$ - $\text{CH}_3\text{CN}$  mixture.



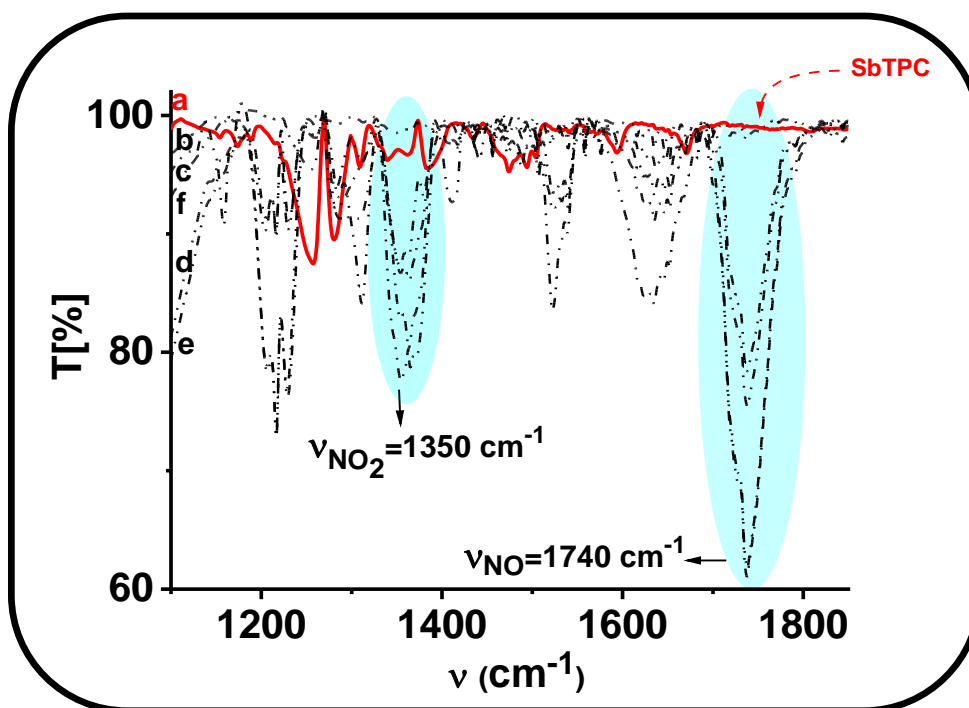
**Figure 5.6** ESI- MS spectrum of (3,17-dinitro-5,10,15-triphenylcorrolato)(oxo)antimony(V) in  $\text{CH}_3\text{CN}$  shows the measured spectrum with isotopic distribution pattern.

It is also observed that fluoride insertion does not occur into the axial positions while treating the Sb(III) corroles with  $\text{NH}_4[\text{BF}_4]$  alone (Scheme 5.3). In this context, Kochi *et al.* has studied earlier the mechanism of the oxidative aromatic nitration reaction of arenes by using nitrosonium salts.<sup>59</sup> A mechanism of this reaction has been proposed based on these observations and also based on the earlier hypothesis of Kochi *et al.* They have demonstrated that while anthracene was treated with  $\text{NOPF}_6$ , it resulted in the formation of anthracene radical cation and nitric oxide in  $\text{CH}_2\text{Cl}_2$  solvent. In analogy with that, we have proposed the formation of [*trans*- dinitrosyl (5,10,15-triphenylcorrolato)antimony(V)] compound as an intermediate while reacting antimony(III) corroles with excess  $\text{NOBF}_4$  in a  $\text{CH}_2\text{Cl}_2$ – $\text{CH}_3\text{CN}$  mixture (Scheme 5.4).



**Scheme 5.4** Probable mechanism for the formation of [*trans*-difluoro(3,17-dinitro-5,10,15-triphenylcorrolato)antimony(V)], **1** complex by the addition of  $\text{NOBF}_4$  into the (corrolato)antimony(III) precursors in  $\text{CH}_2\text{Cl}_2\text{-CH}_3\text{CN}$  mixture in the air ( $\text{O}_2$ ).

In the present case, metal-based oxidation is highly plausible as opposed to the ligand-based oxidation of anthracene. The intermediate species have been established via *in situ* FT-IR spectra. This [*trans*-dinitrosyl (5,10,15-triphenylcorrolato)antimony(V)] species is highly susceptible to oxidation in presence of air and thus can generate [*trans*-dinitro (5,10,15-triphenylcorrolato)antimony(V)] species. The FT-IR spectra of the reaction mixture have characteristic stretching frequencies at  $1740\text{ cm}^{-1}$  and at  $1350\text{ cm}^{-1}$  and are assigned as  $\nu_{\text{NO}}$  and  $\nu_{\text{NO}_2}$  respectively (Figure 5.7).



**Figure 5.7** Solution FT-IR spectra of (a) (5,10,15-triphenylcorrolato)antimony(III) in a  $\text{CH}_2\text{Cl}_2$ – $\text{CH}_3\text{CN}$  mixture. (b) (5,10,15-triphenylcorrolato)antimony(III) complex was treated with excess  $\text{NOBF}_4$  in a  $\text{CH}_2\text{Cl}_2$ – $\text{CH}_3\text{CN}$  mixture at  $0^\circ\text{C}$  after 3 minutes (c) (5,10,15-triphenylcorrolato)antimony(III) complex was treated with excess  $\text{NOBF}_4$  in a  $\text{CH}_2\text{Cl}_2$ – $\text{CH}_3\text{CN}$  mixture at  $0^\circ\text{C}$  after 15 minutes (d) (5,10,15-triphenylcorrolato)antimony(III) complex was treated with excess  $\text{NOBF}_4$  in a  $\text{CH}_2\text{Cl}_2$ – $\text{CH}_3\text{CN}$  mixture at  $0^\circ\text{C}$  after 25 minutes (e) (5,10,15-triphenylcorrolato)antimony(III) complex was treated with excess  $\text{NOBF}_4$  in a  $\text{CH}_2\text{Cl}_2$ – $\text{CH}_3\text{CN}$  mixture at  $0^\circ\text{C}$  after 35 minutes. (f) (5,10,15-triphenylcorrolato)antimony(III) complex was treated with excess  $\text{NOBF}_4$  in a  $\text{CH}_2\text{Cl}_2$ – $\text{CH}_3\text{CN}$  mixture at RT after 60 minutes.

Although, no previous report is available to compare these data, however, these data fall in the range of typically encountered metal nitrosyl and metal nitro stretching

---

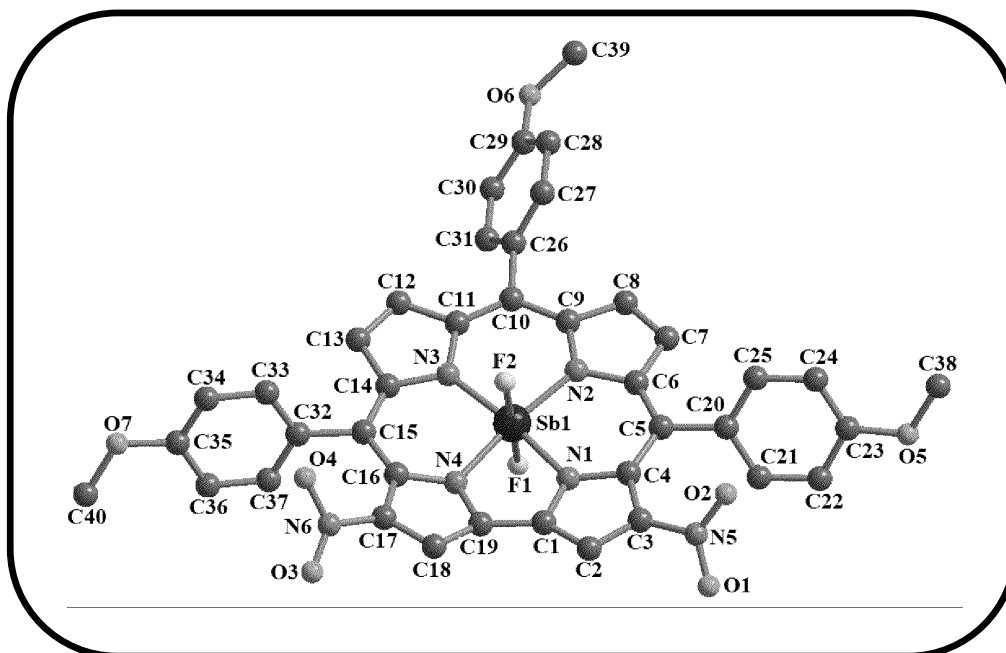
frequencies.<sup>60, 61</sup> This [*trans*- dinitro (5,10,15–triphenylcorrolato)antimony(V)] species can transfer the nitro group in the  $\beta$ -positions (3 and 17) of the corrole periphery in the antimony(V) corrole complexes.

This mechanism of this selective substitution in the corrole periphery has been demonstrated well.<sup>62</sup> Paolesse et al. has observed earlier the nitration of iron corrolates and the exclusive formation of regioselective di-substituted (3- and 17- positions) iron nitrosyl corrolates.<sup>63</sup> In analogy with that, as all these antimony corrole complexes are diamagnetic and no signal of radical character was detected, thus the lability of the axial ligands is probably responsible for these kinds of reactions.<sup>63</sup> The oxidation of the nitrite ion probably generates  $\cdot\text{NO}_2$  radical and which subsequently couples with the antimony corrole. This generated nitrocorrolatoantimony radical intermediate is subsequently oxidized and deprotonated and resulted in the formation of nitrocorrolatoantimony derivatives. Subsequently, the fluoride ion is inserted into the axial positions of antimony(V)corrole via nucleophilic attack of fluoride ion from  $\text{BF}_4^-$ .<sup>64</sup>

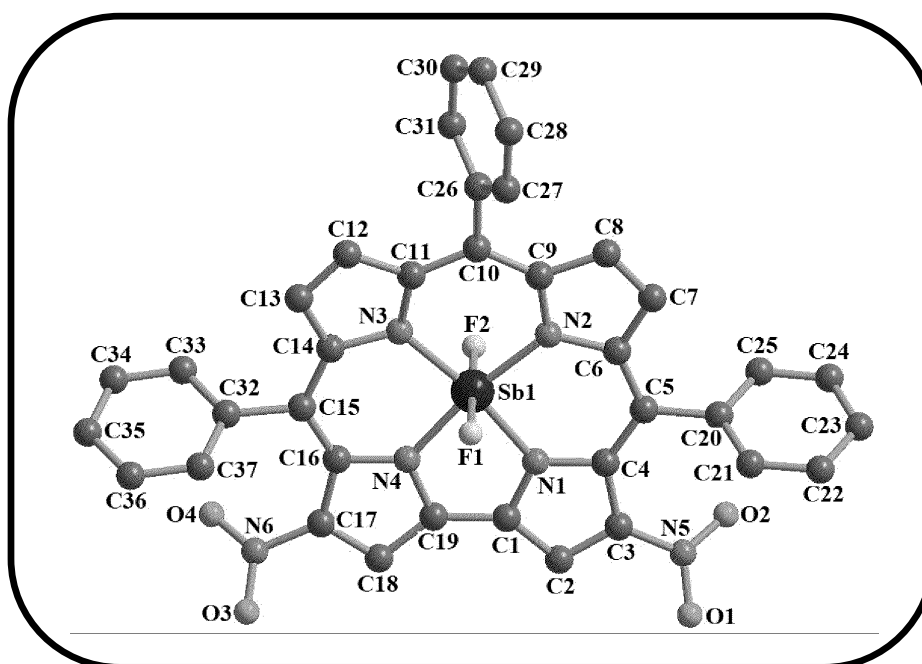
### 5.2.2 Crystal Structure

The crystal structures of **1** and **2** are shown in Figure 5.8 and Figure 5.9 respectively. As both the molecules have furnished similar structures, thus one of them will be described in detail (Figure 5.8). Important crystallographic parameters for **1** and **2** are summarized in Table 5.1. The crystal structure of **2** is triclinic in nature and each unit cell has two molecules of **2**. The bite angles of N1-Sb-N2, N2-Sb-N3, N3-Sb-N4, and N4-Sb-N1 for **2** are 92.3(4) °, 95.9(3) °, 91.6(3) °, and 80.2(3) °, respectively. The Sb-N bond distances of **2** are 1.997(8) Å for Sb-N1, 1.972(9) Å for Sb-N2, 1.968(8) Å for Sb-N3, and 1.984(8) Å for Sb-N4. While comparing the Sb–N bond distances with the previously reported antimony(III) corroles<sup>27</sup> and antimony(V) corroles,<sup>24,26,29</sup> it was observed that the Sb–N bond distances of the *trans*- difluoro(3,17-dinitro-

corrolato)antimony(V) derivatives (**1** and **2**) matches nicely with the earlier reported antimony(V) corroles.



**Figure 5.8** Single-crystal X-ray structure of **2**. Hydrogen atoms are omitted for clarity.



**Figure 5.9** Single-crystal X-ray structure of **1**. Hydrogen atoms are omitted for clarity.



**Table 5.1** Crystallographic data of **1** and **2**.

compound code	<b>1</b>	<b>2</b>
molecular formula	2(C <sub>37</sub> H <sub>21</sub> F <sub>2</sub> N <sub>6</sub> O <sub>4</sub> Sb),3(C <sub>2</sub> H <sub>3</sub> N)	C <sub>40</sub> H <sub>27</sub> F <sub>2</sub> N <sub>6</sub> O <sub>7</sub> Sb
Fw	834.95	863.45
Radiation	Cu K $\alpha$	Cu K $\alpha$
crystal symmetry	Triclinic	Triclinic
space group	P-1	P-1
<i>a</i> (Å)	12.9295(4)	7.6617(8)
<i>b</i> (Å)	13.5750(4)	16.0045(15)
<i>c</i> (Å)	21.8179(7)	16.1004(18)
<i>a</i> (deg)	103.476(3)	63.977(10)
<i>β</i> (deg)	97.404(2)	88.495(9)
<i>γ</i> (deg)	105.665(2)	83.425(8)
<i>V</i> (Å <sup>3</sup> )	3509.7(2)	1761.8(4)
<i>Z</i>	4	2
<i>μ</i> (mm <sup>-1</sup> )	6.796	6.843
<i>T</i> (K)	100	100
<i>D</i> <sub>calcd</sub> (g cm <sup>-3</sup> )	1.580	1.628
2 $\theta$ range (deg)	3.57 to 68.25	5.22 to 66.58
<i>e</i> data ( <i>R</i> <sub>int</sub> )	12580 (0.105)	5906 (0.103)
<i>R</i> 1 ( <i>I</i> > 2 $\sigma$ ( <i>I</i> ))	0.0564	0.1025
WR2 (all data)	0.1465	0.2388
GOF	1.012	1.063
$\Delta\rho_{\max}$ , $\Delta\rho_{\min}$ (e Å <sup>-3</sup> )	1.38, -1.59	3.58,-1.82

The reported Sb–N bond distances for (5,10,15-trisphenylcorrolato)antimony(III) are in the range of 2.127–2.114 Å,<sup>27</sup> whereas the Sb–N bond distances for (5,10,15-trispentafluorophenylcorrolato)(*trans*-difluoro)antimony(V) are in the range of 1.979–1.971 Å.<sup>24</sup> The central antimony atom deviates by 0.030 Å from the mean N4

corrole plane for **2**. Literature report suggests that the deviation of Sb(III) atom from the mean N4 corrole plane in a structurally characterized Sb(III)corrole is  $\sim 0.960 \text{ \AA}$ .<sup>27</sup> While in the literature reported Sb(V) corrole, this deviation of antimony atom from the mean N4 corrole plane is  $0.022 \text{ \AA}$ .<sup>26</sup> The Sb-F bond distances of **2** are  $1.920(6) \text{ \AA}$  for Sb-F1 and  $1.913(6) \text{ \AA}$  for Sb-F2. The Sb-F bond distances in the structurally characterized (5,10,15-trispentafluorophenylcorrolato)(*trans*-difluoro)antimony(V) are  $1.940(1) \text{ \AA}$  for Sb-F1 and  $1.932(1) \text{ \AA}$  for Sb-F2.<sup>24</sup> The F1-Sb1-F2 angle for **2** is  $179.3(3)^\circ$  and is comparable with the literature reported values of F1-Sb1-F2 angle of  $177.3(1)^\circ$ .

### 5.2.3 UV-vis and emission spectroscopy

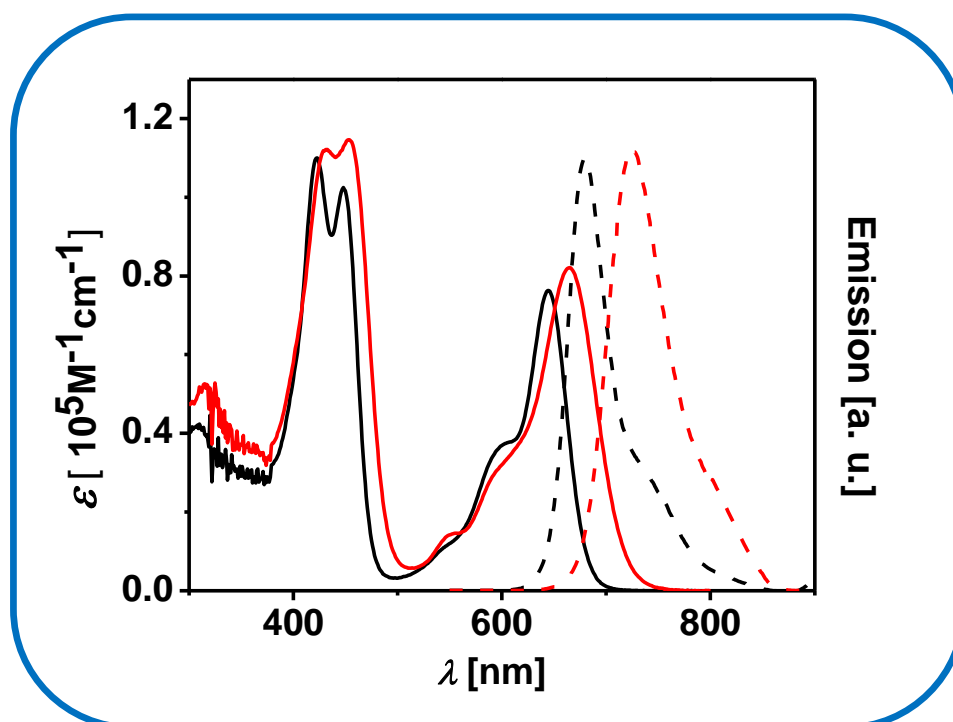
The electronic absorption and emission spectra of **1** and **2** are shown in Figure 5.10. Both the complexes showed similar absorption and emission profiles. The Soret band of complexes **1** and **2** split into two distinct bands and appears in the range of 423-454 nm. Three Q-bands are also observed for both the complexes (**1** and **2**) in the range of 543-665 nm. The molar absorption coefficient of the Soret bands in **1** and **2** are in the range of  $1.0\text{--}1.15 \times 10^5 \text{ M}^{-1}\text{cm}^{-1}$ , and the molar absorption coefficient of the lowest energy Q-type bands in **1** and **2** are in the range of  $7.5\text{--}8.5 \times 10^4 \text{ M}^{-1}\text{cm}^{-1}$  (Table 5.2).

**Table 5.2** UV-Vis data for **1** and **2**.

Compound	UV-vis. Data (In dichloromethane)
	$\lambda_{\text{max}} / \text{nm} (\epsilon / \text{M}^{-1}\text{cm}^{-1})$
<b>1</b>	423(110000), 448(103000), 543(11300), 590(34900), 645(76900)
<b>2</b>	431(112000), 454(115000), 548(14500), 593(30600), 665(82900).

Interestingly, out of these three Q bands in complexes **1** and **2**, the lowest energy band is very intense. The absorption profile of complexes **1** and **2**, can be easily compared with the previously reported 5,10,15-triphenylcorrolatoantimony(III) and (oxo)(5,10,15-

triphenylcorrolato)antimony(V) complexes.<sup>27</sup> Previously reported 5,10,15-triphenylcorrolatoantimony(III) complex exhibited split Soret bands at 440-459 nm due to its low symmetric nature. While the (oxo)(5,10,15-triphenylcorrolato) antimony(V) complex exhibited an unsplit Soret band at 408 nm. The 5,10,15-triphenylcorrolatoantimony(III) exhibited four Q-bands and (oxo)(5,10,15-triphenylcorrolato) antimony(V) complex exhibited three Q-bands.



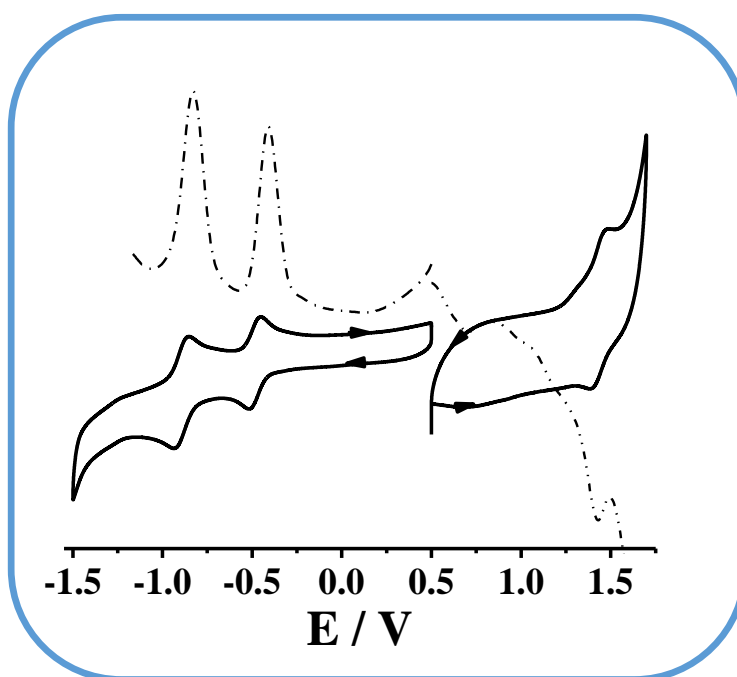
**Figure 5.10** Steady-state absorption (solid lines) and emission (dashed lines) spectra of **1** (black line) ( $\lambda_{\text{exc}}=424$  nm) and **2** (red line) ( $\lambda_{\text{exc}}=430$  nm) in aerated dichloromethane.

The emission spectra of complexes **1** and **2** are shown in Figure 5.10 . Complex **1** displayed strong emission at 679 nm and a shoulder at 755 nm in  $\text{CH}_2\text{Cl}_2$  (excited at the Soret band). Complex **2** displayed strong emission at 725 nm and a shoulder at 809 nm in  $\text{CH}_2\text{Cl}_2$  (excited at the Soret band). These observed emissions can be conveniently assigned as fluorescence due to the appearance of smaller Stokes shifts with reference to the Q-type bands.

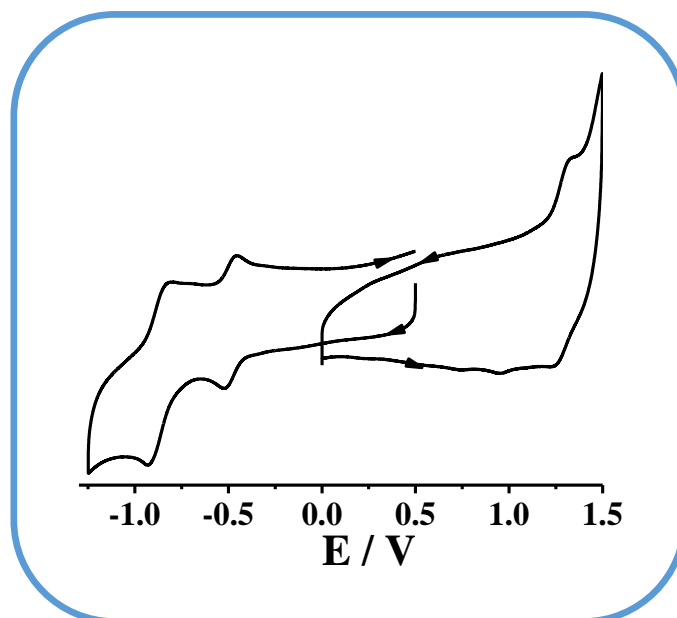
---

#### 5.2.4 Redox properties

The redox properties of complexes **1** and **2** were investigated in  $\text{CH}_2\text{Cl}_2/0.1 \text{ M TBAP}$  by using cyclic voltammetric and differential pulse voltammogram techniques (Figures 5.11-5.12, Table 5.3). Complexes **1** and **2** exhibited two successive one-electron reversible reductive couples and one reversible oxidative couple *versus* Ag-AgCl reference electrode. The first reduction was observed at  $E_{298}^0, \text{ V } (\Delta E_p, \text{ mV}): -0.48 (80)$ , and the second reduction process was observed at  $E_{298}^0, \text{ V } (\Delta E_p, \text{ mV}): -0.89(80)$  for **1**.



**Figure 5.11** Cyclic voltammograms and differential pulse voltammogram of **1** in  $\text{CH}_2\text{Cl}_2$ . The potentials are vs. Ag/AgCl.



**Figure 5.12** Cyclic voltammograms of **2** in CH<sub>2</sub>Cl<sub>2</sub>. The potentials are vs. Ag/AgCl.

They also showed one reversible oxidative couple  $E^0_{298}$ , V ( $\Delta E_p$ , mV): +1.44 (80) versus Ag-AgCl. The first reduction was observed at  $E^0_{298}$ , V ( $\Delta E_p$ , mV): -0.48 (80), and the second reduction process was observed at  $E^0_{298}$ , V ( $\Delta E_p$ , mV): -0.88(80) for **2**. They also showed one reversible oxidative couple  $E^0_{298}$ , V ( $\Delta E_p$ , mV): +1.30 (80) versus Ag-AgCl.

**Table 5.3** Electrochemical data for **1** and **2**.

Compound	Electrochemical data <sup>a,b</sup>	
	Oxidation $E^0$ , V ( $\Delta E_p$ , mV)	Reduction $E^0$ , V ( $\Delta E_p$ , mV)
<b>1</b>	+1.44 (80)	-0.48 (80), -0.89(80)
<b>2</b>	+1.30 (80)	-0.48 (80), -0.88 (80)

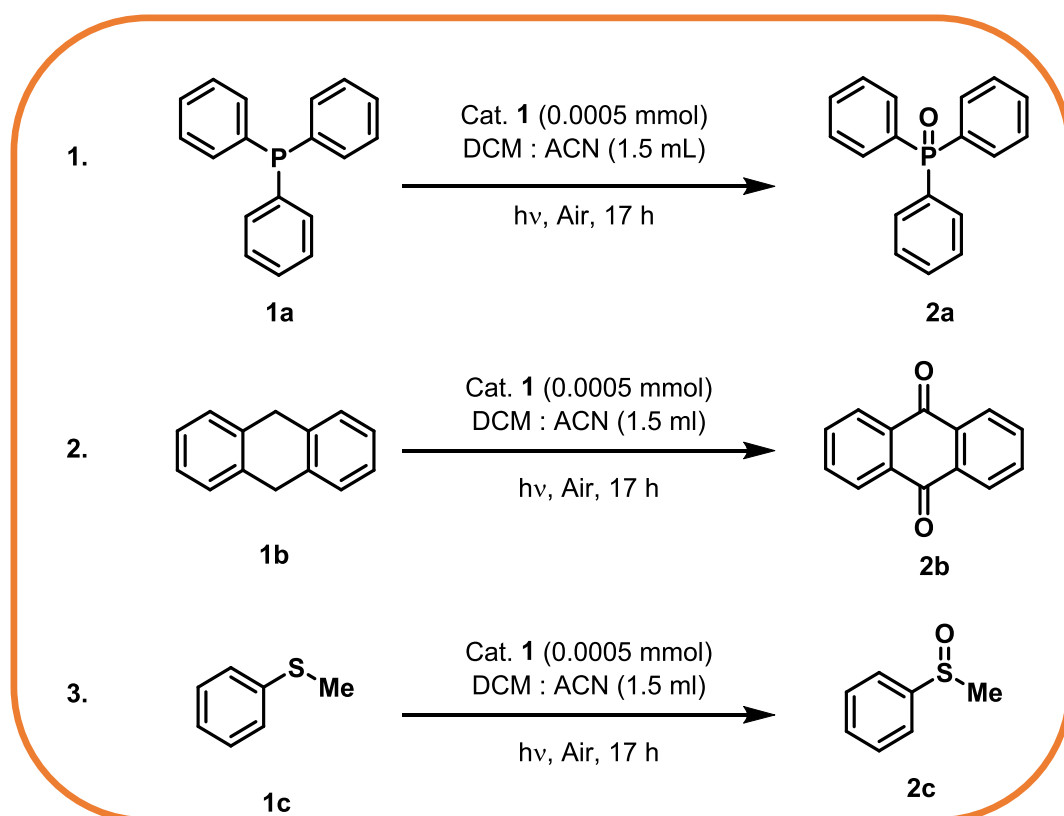
<sup>a</sup>In dichloromethane.

<sup>b</sup>The potentials are vs. Ag/AgCl

### 5.3 Catalytic Applicability:

Initially, the catalytic efficacy of synthesized complexes (**1** and **2**) was studied for the oxidation of triphenylphosphine as our model substrate under photochemical conditions (Table 5.4).

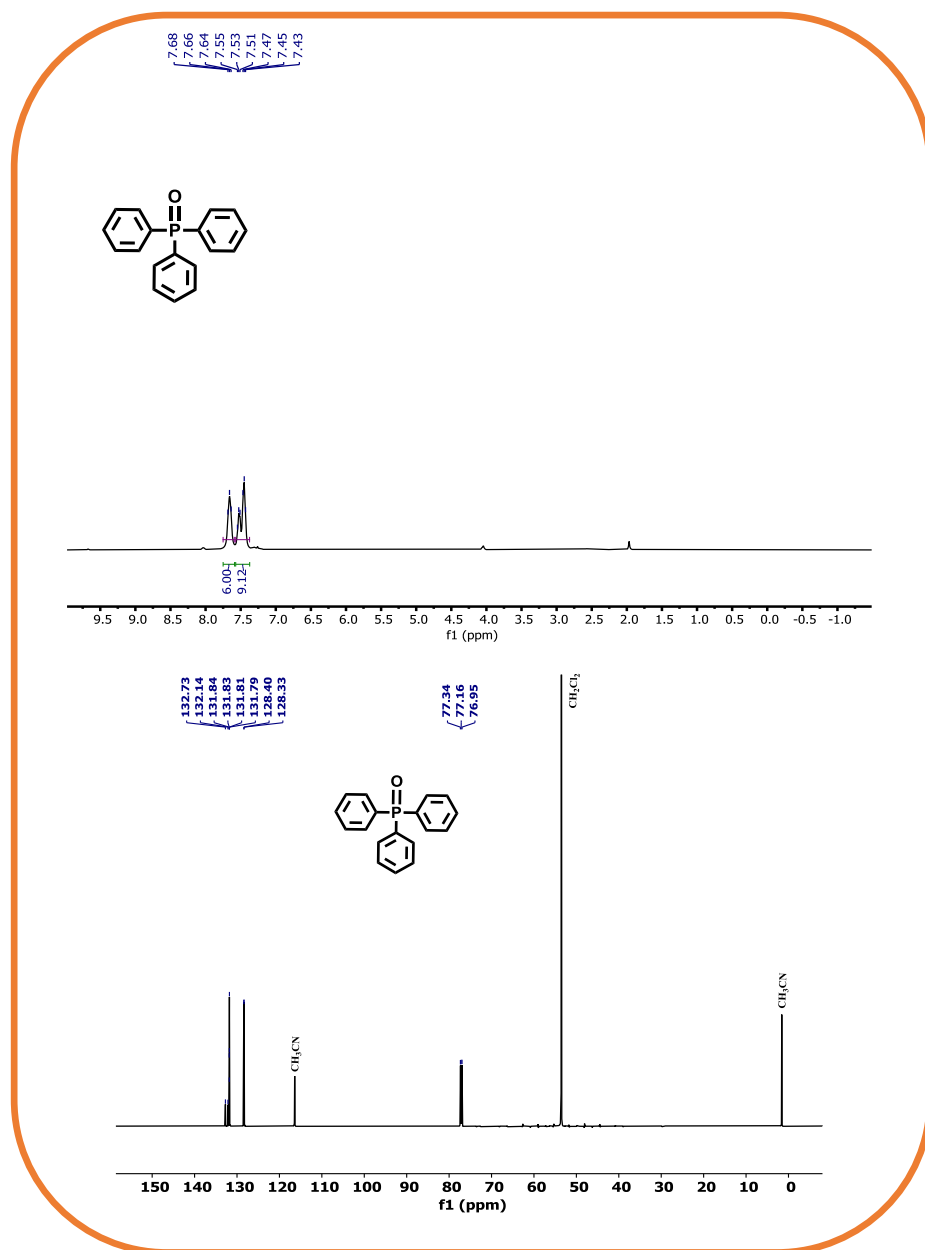
**Table 5.4** Catalytic oxidation reactions using [*trans*-difluoro(3,17-dinitro-corrolato)antimony(V)] complexes



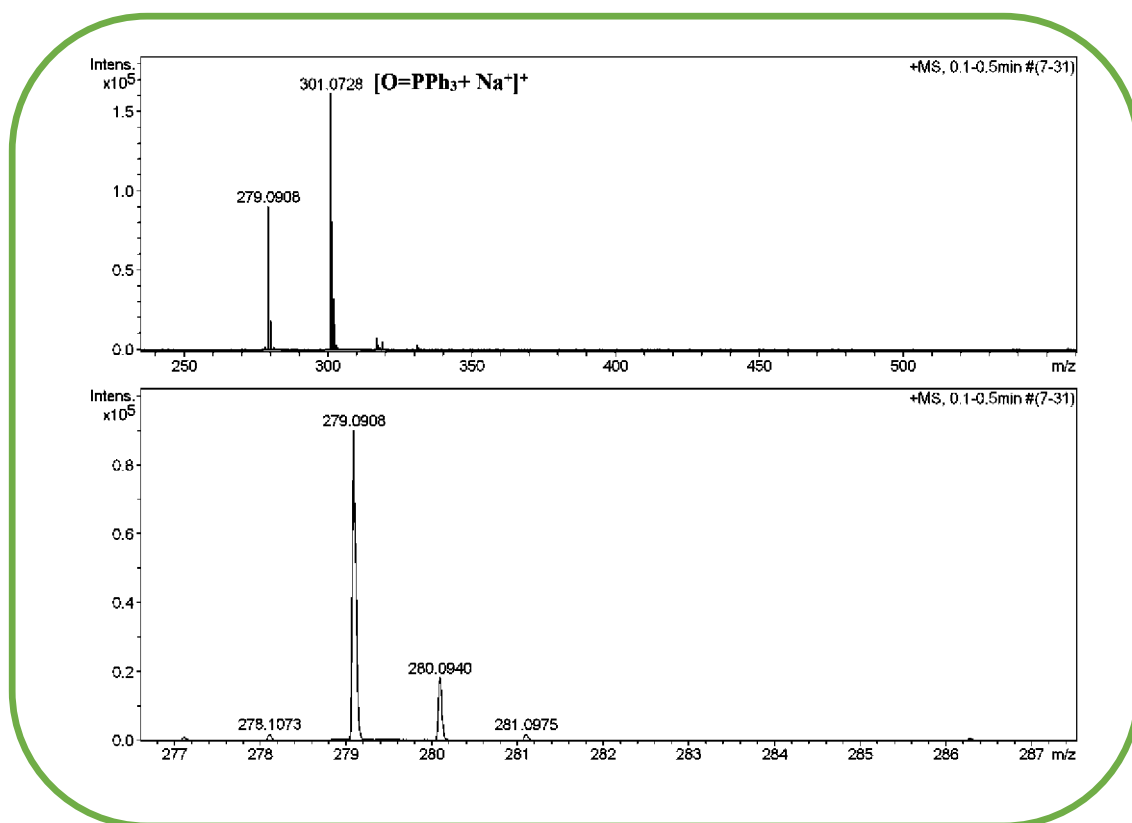
Product	Isolated Yield (%)	TON
2a	96	5000
2b	75	1500
2c	56	1120

Reaction condition: substrate for **1a** (2.6 mmol) and for **1b** and **1c** (1 mmol each), cat. **1** (0.0005 mmol), mixed solvent (DCM: ACN = 1:1), CFL (20 W), air, 17 h

To our delight, we have successfully obtained the desired oxidized product, triphenylphosphine oxide (**2a**) in an excellent yield of around 96% with TON  $\approx$  5000 (Figure 5.13-5.14).



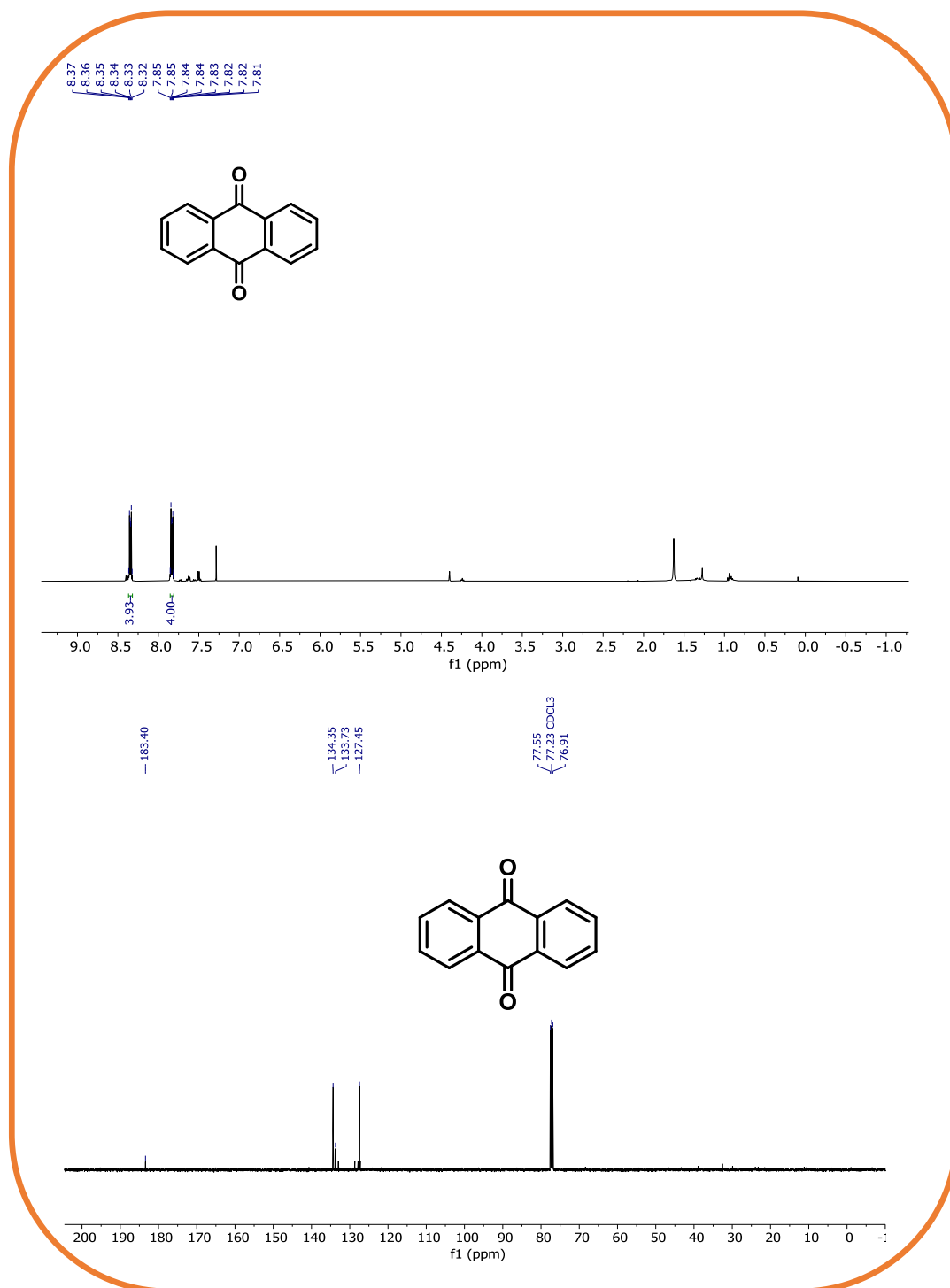
**Figure 5.13**  $^1\text{H}$  (top) and  $^{13}\text{C}$  (bottom) of compound **2a** in  $\text{CDCl}_3$ .



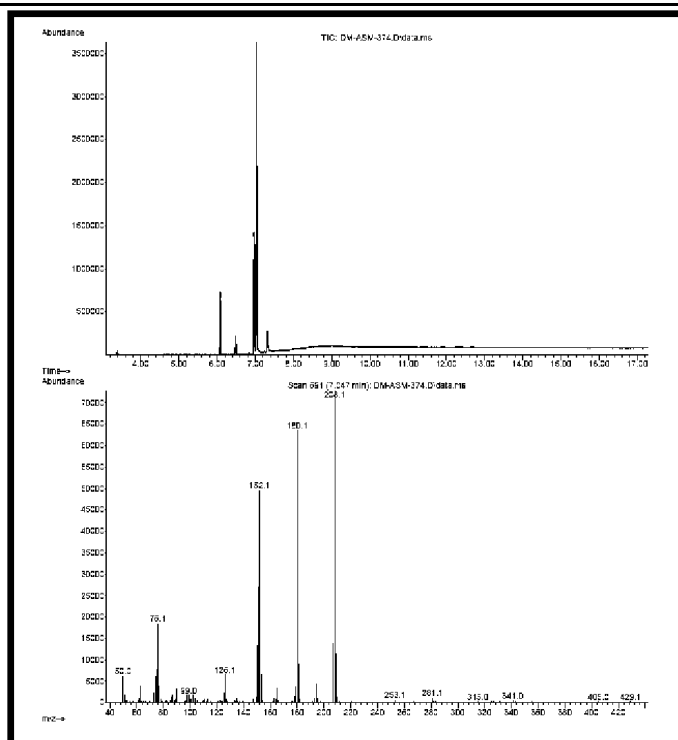
**Figure 5.14** ESI-MS data of compound **2a** in  $\text{CH}_3\text{CN}$ .

Additionally, we were also able to get the benzylic oxidation product of **1b** having  $\text{TON} \approx 1500$  under a similar reaction condition (Figures 5.15-5.16). Further sulfoxidation of thioanisole has been performed with complex **1** to demonstrate its adaptability in the oxidation reaction (Figures 5.17-5.19). Interestingly, sulfoxidation product (**2c**) was formed with  $\text{TON} > 1100$ . We have investigated the role of the [*trans*-difluoro(corrolato)antimony(V)] complexes as a catalyst in oxygenation reaction under photo-redox conditions.

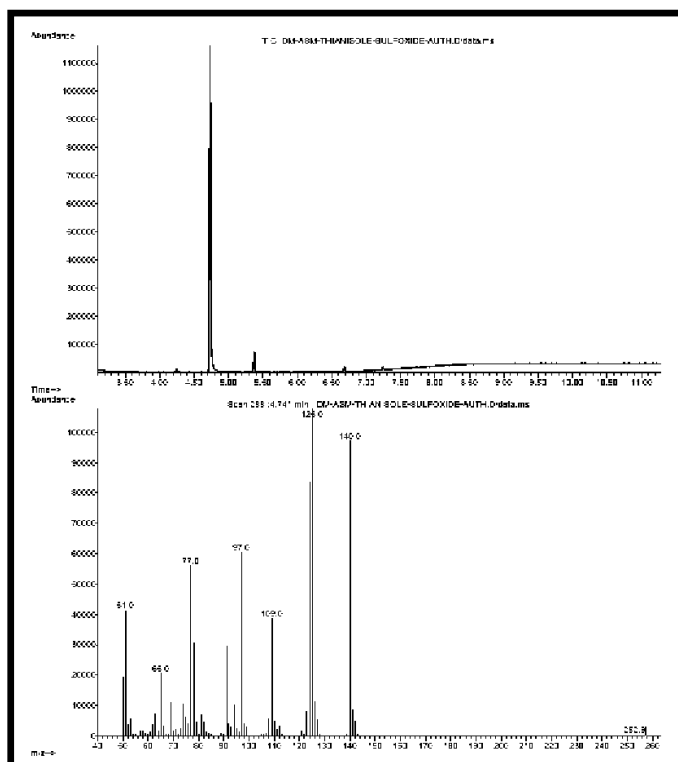




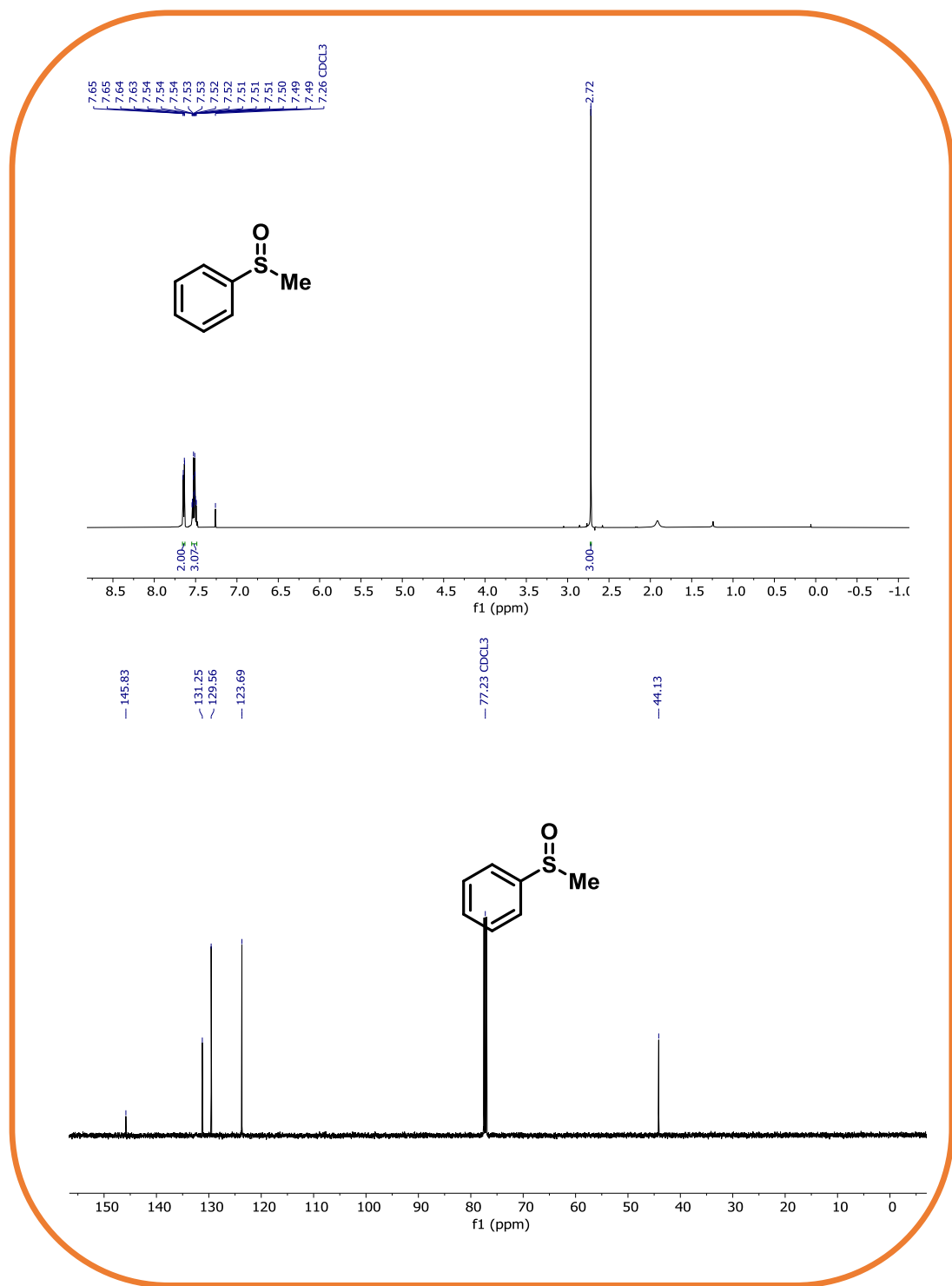
**Figure 5.15**  $^1\text{H}$  (top) and  $^{13}\text{C}$  (bottom) of compound **2b** in  $\text{CDCl}_3$ .



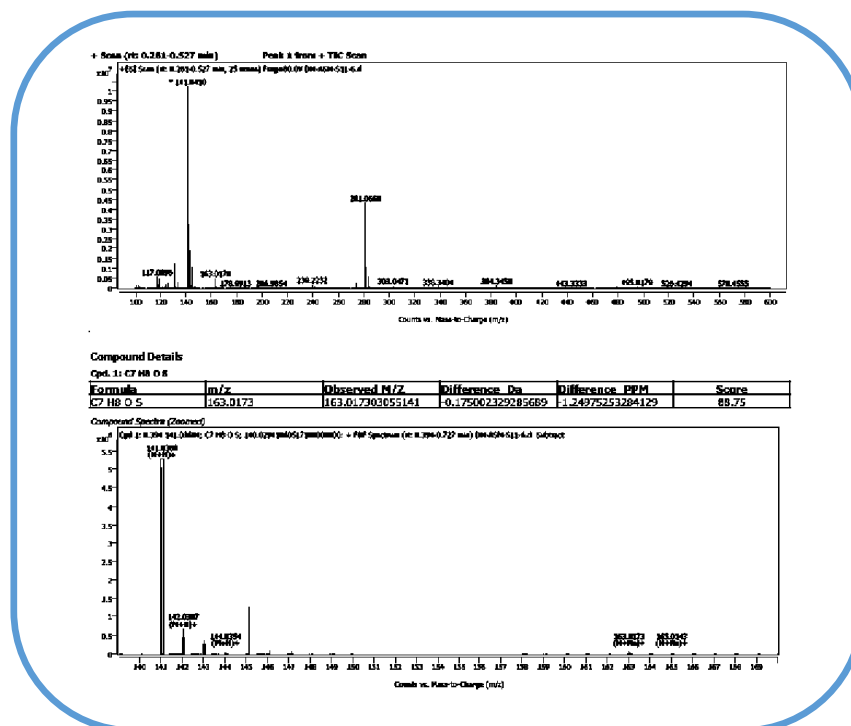
**Figure 5.16** Mass spectrum (GC-EIMS) of compound **2b** detected by GC of the reaction mixture.



**Figure 5.17** Mass spectrum (GC-EIMS) of compound **2c** detected by GC of the reaction mixture.



**Figure 5.18**  $^1\text{H}$  (top) and  $^{13}\text{C}$  (bottom) of compound **2c** in  $\text{CDCl}_3$ .

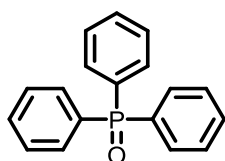


**Figure 5.19** HRMS data of compound **2c** in CH<sub>3</sub>CN.

## Characterization data of products

Triphenylphosphine oxide (**2a**):

White solid; isolated yield: 96%. <sup>1</sup>H NMR (400 MHz, Chloroform-*d*) δ 7.68-7.64 (m, 6H), 7.53-7.43 (m, 9H). <sup>13</sup>C NMR (176 MHz, CDCl<sub>3</sub>) δ 132.7,

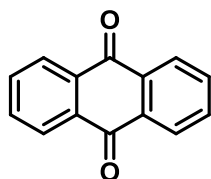


132.2, 131.8, 131.8, 131.8, 131.8, 128.5, 128.4. The electrospray mass spectrum in acetonitrile showed peaks centered at  $m/z$  =

301.07 correspond to  $[2a+Na]^+$  (301.08 calcd for C<sub>18</sub>H<sub>15</sub>NaOP).

Anthracene-9,10-dione (**2b**):

Eluent: ethyl acetate/petroleum ether (5:95 v/v); light yellow solid; isolated yield: 75%.

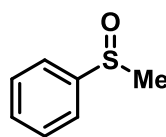


<sup>1</sup>H NMR (400 MHz, CDCl<sub>3</sub>) δ 8.35 (dd, *J* = 5.8, 3.3 Hz, 4H), 7.83 (dd, *J* = 5.8, 3.3 Hz, 4H). <sup>13</sup>C NMR (101 MHz, CDCl<sub>3</sub>) δ 183.40, 134.35, 133.73, 127.45.

---

(Methylsulfinyl)benzene (**2c**):

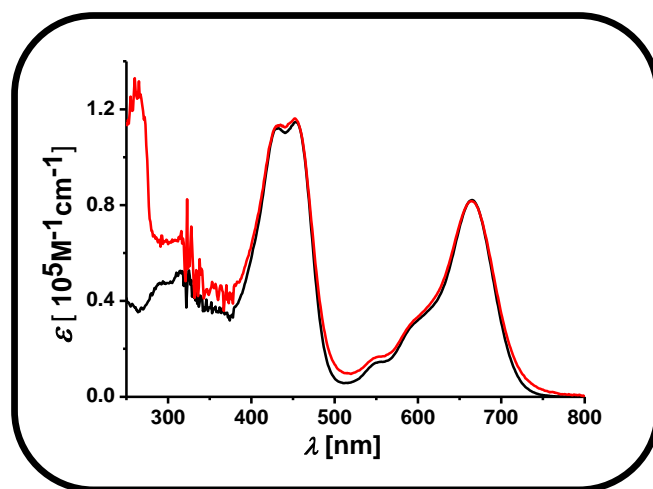
Eluent: ethyl acetate/petroleum ether (40:60 v/v); yellow liquid; isolated yield: 56%.  $^1\text{H}$



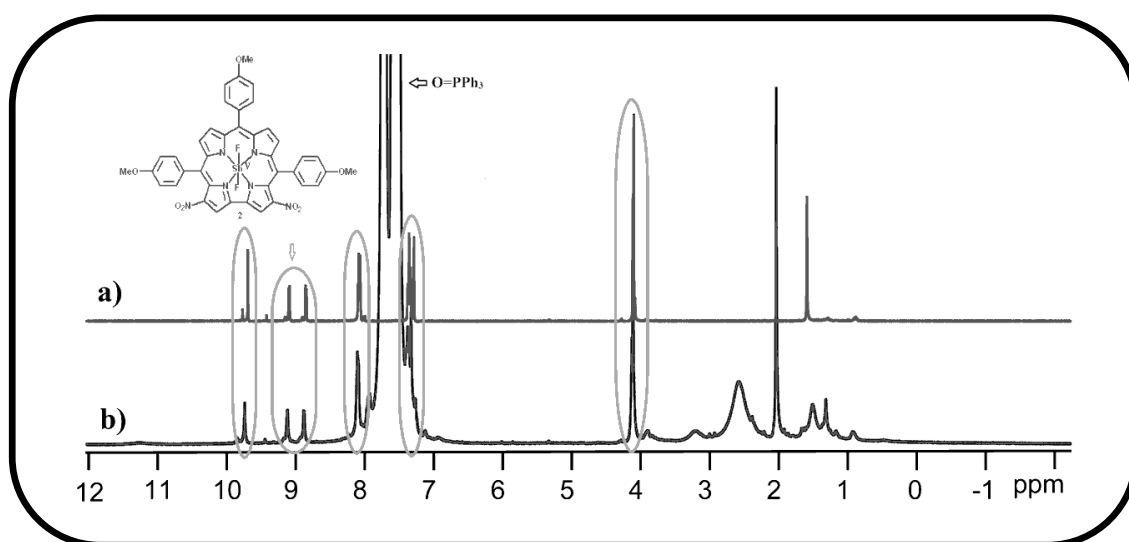
NMR (500 MHz,  $\text{CDCl}_3$ )  $\delta$  7.64 (dd,  $J = 8.1, 1.6$  Hz, 2H), 7.54 – 7.49 (m, 3H).  $^{13}\text{C}$  NMR (126 MHz,  $\text{CDCl}_3$ )  $\delta$  145.83, 131.25, 129.56, 123.69,

44.13. The electrospray mass spectrum in acetonitrile showed peaks centered at  $m/z = 163.0173$  correspond to  $[\text{2c} + \text{Na}^+]^+$  (163.0173 calcd for  $\text{C}_7\text{H}_8\text{NaOS}$ ).

In order to understand the fate of the catalyst, we have analyzed the reaction mixture at the end of the reaction. Column chromatography was performed on the crude reaction mixture. The starting catalyst was fully recovered with minimal decompositions and the identity of the catalyst was established via UV-vis and  $^1\text{H}$  NMR techniques (Figures 5.20-5.21). We did not detect traces of free base corrole from the reaction mixture and thus the demetallation process was ruled out. UV-vis spectra of the reaction mixture clearly demonstrate that the catalyst was intact throughout the reaction time. It is evident that these *trans*- difluoro(3,17-dinitro-corrolato)antimony(V) complexes are capable of oxidizing various substrates. Like the previous researchers, we have also observed an absolute selectivity of C-H activation instead of C=C bonds. However, we have not observed any hydroperoxides formation. Based on the previous literature, it is apparent that the catalytic cycle of the *trans*- difluoro(3,17-dinitro-corrolato)antimony(V) mediated oxygenation reaction probably involves singlet oxygen.<sup>24</sup>



**Figure 5.20** Electronic absorption spectrum of (a) pure **2** (—) in  $\text{CH}_2\text{Cl}_2$  at room temperature; (b) isolated compound (—) (in  $\text{CH}_2\text{Cl}_2$  at room temperature) obtained via the treatment of **2** (0.002 mmol) with  $\text{PPh}_3$  (10 mmol) in  $\text{CH}_2\text{Cl}_2$ - $\text{CH}_3\text{CN}$  mixture at RT for 17 h in air and light (20 W CFL bulb), followed by purification *via* column chromatography.



**Figure 5.21**  $^1\text{H}$  NMR spectrum of (a) pure **2** (—) in  $\text{CDCl}_3$  at room temperature; (b) crude reaction mixture (—) (in  $\text{CDCl}_3$  at room temperature) obtained via the treatment of **2** (0.002 mmol) with  $\text{PPh}_3$  (10 mmol) in  $\text{CH}_2\text{Cl}_2$ - $\text{CH}_3\text{CN}$  mixture at RT for 17 h in air and light (20 W CFL bulb).

---

## 5.4 Conclusion

In conclusion, we have structurally characterized *trans*-difluoro(3,17-dinitro-corrolato)antimony(V) species by reacting a corrolato Sb(III) complex with nitrosonium tetrafluoroborate in presence of air (O<sub>2</sub>) along with regioselective dinitration of corrole ring. A [*trans*-dinitrosyl(corrolato)antimony(V)] compound has been proposed as a possible reaction intermediate and its composition has been established via in situ FT-IR spectra. This species is subsequently converted into a [*trans*-dinitro(corrolato)antimony(V)] species and which can transfer the nitro group in the  $\beta$ -positions (3 and 17) of corrole periphery via a radical pathway. The Sb-N bond distances of the *trans*-difluoro(3,17-dinitro-corrolato)antimony(V) derivatives (**1** and **2**) match nicely with the earlier reported antimony(V) corroles. The central antimony atom deviates by 0.030 Å from the mean N4 corrole plane. The Sb-F bond distances of **2** are 1.920(6) Å and 1.913(6) Å for Sb-F1 and Sb-F2 respectively and the F1-Sb1-F2 angle is 179.3(3). The Soret band of these complexes split into two distinct bands and appears in the range of 423-454 nm. Three Q-bands are also observed for both the complexes in the range of 543-665 nm. The observed emissions can be conveniently assigned as fluorescence due to the appearance of smaller Stokes shifts with reference to the Q-type bands. The *trans*-difluoro(3,17-dinitro-corrolato)antimony(V) species exhibits two successive one-electron reversible reductive couples and one reversible oxidative couple versus Ag-AgCl reference electrode. The *trans*-difluoro(3,17-dinitro-corrolato)antimony(V) showed oxygenation reaction under photo-redox conditions in presence of air and light at ambient temperature.

---

## 5.5 Experimental Section

### 5.5.1 Materials

The precursor's pyrrole, chloranil, NOBF<sub>4</sub> and tetrabutylammonium perchlorate (TBAP) were purchased from Sigma-Aldrich, USA. SbCl<sub>3</sub> and pyridine were purchased from Merck, India. Benzaldehyde and 4-methoxy benzaldehyde were purchased from Merck, India. Other chemicals were of reagent grade. Hexane and CH<sub>2</sub>Cl<sub>2</sub> were distilled from KOH and CaH<sub>2</sub> respectively. 5,10,15-triphenylcorrole,<sup>55</sup> (5,10,15-triphenylcorrolato)antimony(III), **1A**<sup>27</sup> and 5,10,15-tris(4-methoxyphenyl)corrole<sup>55</sup> is synthesized by following earlier reported protocols.

### 5.5.2 Physical Measurements

UV-Vis spectral studies were performed on a Perkin-Elmer LAMBDA-750 spectrophotometer. The elemental analyses were carried out with a Euro EA elemental analyzer. Emission spectral studies were performed on a Perkin Elmer, LS 55 spectrophotometer using an optical cell of 1 cm path length. FT-IR spectra were recorded on a Perkin-Elmer spectrophotometer with samples prepared as KBr pellets. Solution FTIR spectra were recorded in a Nicolet iS5 FT-IR Spectrometer. The NMR measurements were carried out using a Bruker AVANCE 400 NMR spectrometer. Tetramethylsilane (TMS) is the internal standard. Electrospray mass spectra were recorded on a Bruker Micro TOF-QII mass spectrometer. Cyclic voltammetry measurements were carried out using a CS350 electrochemical test system (China). A glassy carbon working electrode, a platinum wire as an auxiliary electrode, and an Ag-AgCl reference electrode were used in a three-electrode configuration. Tetrabutylammonium perchlorate (TBAP) was the supporting electrolyte (0.1 M), and the concentration of the solution was 10<sup>-3</sup> M for the complex. The half-wave potential



---

$E_{298}^0$  was set equal to  $0.5 (E_{pa} + E_{pc})$ , where  $E_{pa}$  and  $E_{pc}$  are anodic and cathodic cyclic voltammetric peak potentials, respectively. The scan rate used was  $100 \text{ mV s}^{-1}$ .

### 5.5.3 Crystal Structure Determination

Single crystals of **1** were grown by slow diffusion of solution of **1** in acetonitrile into hexane, followed by slow evaporation under atmospheric conditions. Single crystals of **2** were grown by slow diffusion of solution of **2** in dichloromethane into hexane, followed by slow evaporation under atmospheric conditions. The crystal data of **1** and **2** were collected on a Rigaku Oxford diffractometer at 100 K. Selected data collection parameters and other crystallographic results are summarized in Table S1. All data were corrected for Lorentz polarization and absorption effects. The program package SHELXTL<sup>65</sup> was used for structure solution and full-matrix least-squares refinement on  $F^2$ . Hydrogen atoms were included in the refinement using the riding model. Contributions of H atoms for the water molecules were included but were not fixed. Disordered solvent molecules were taken out using the SQUEEZE command in PLATON.<sup>66</sup> CCDC 2145598 contains the supplementary crystallographic data for **1**. CCDC 2145599 contains the supplementary crystallographic data for **2**. These data can be obtained free of charge via [www.ccdc.cam.ac.uk/data\\_request/cif](http://www.ccdc.cam.ac.uk/data_request/cif).

### 5.5.4 Syntheses

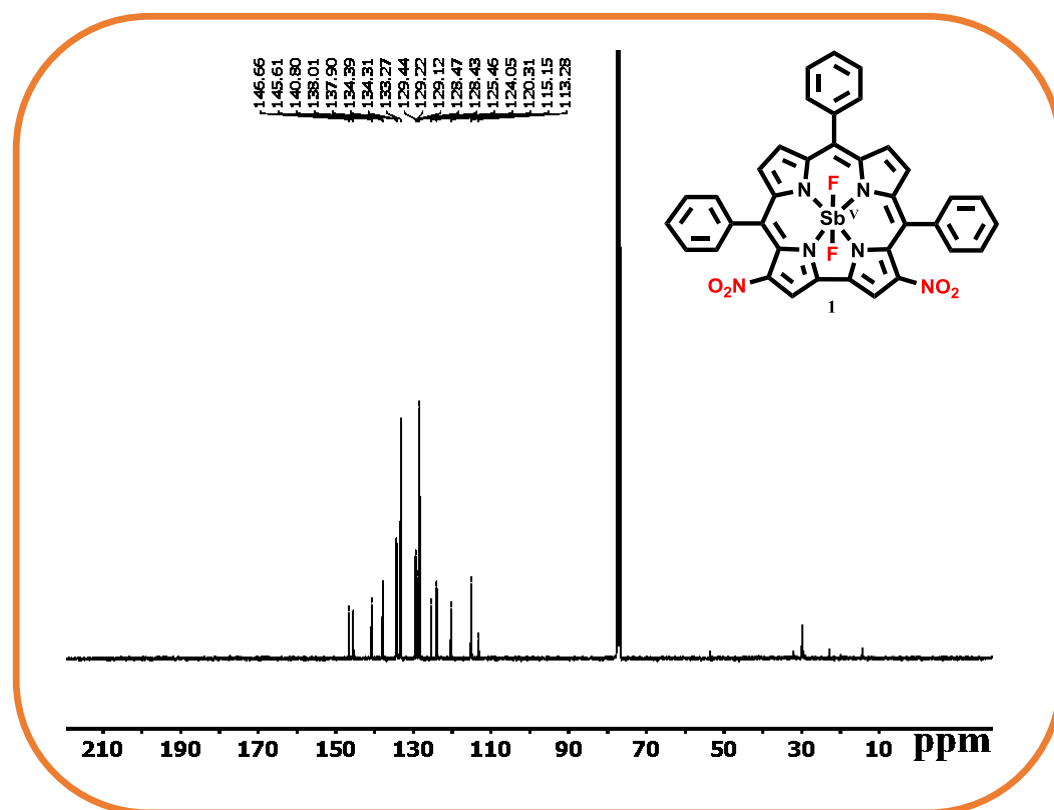
#### 5.5.4.1 Synthesis of [trans-difluoro(3,17-dinitro-5,10,15-triphenylcorrolato)antimony(V)], **1**:

**1** was prepared by reacting 50 mg (0.077 mmol) of (5,10,15-triphenylcorrolato)antimony(III), **1A** and excess of  $\text{NOBF}_4$  in a 20 mL solution of  $\text{CH}_2\text{Cl}_2$ – $\text{CH}_3\text{CN}$  (1:1) mixture. The solution was stirred for a few seconds till the color of the solution changed from yellowish green to sea green. Then the solution was immediately passed through a previously packed silica gel column using

CH<sub>2</sub>Cl<sub>2</sub>–CH<sub>3</sub>CN mixture (3:1) as eluent. The sea-green fraction containing **1** was further purified by recrystallization from CH<sub>2</sub>Cl<sub>2</sub>/hexane mixture to give 24 mg of pure **1**.

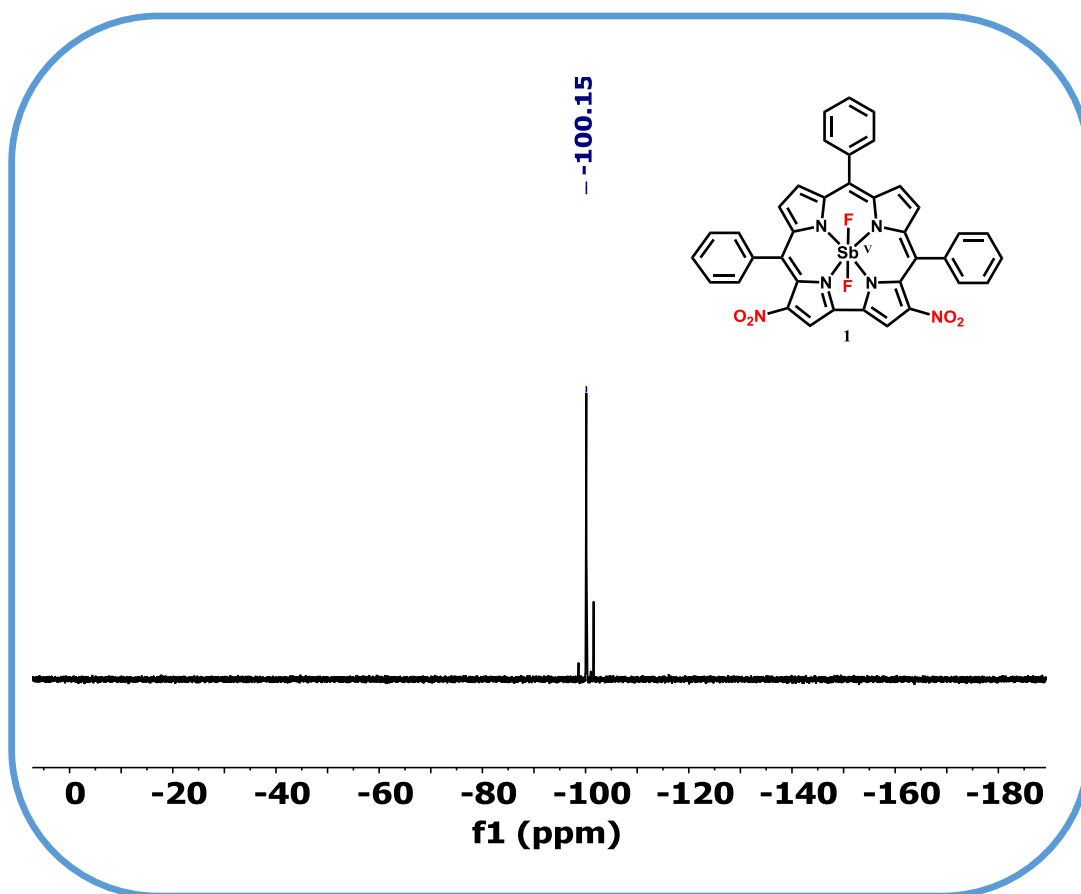
**5.5.4.2 For [trans-difluoro(3,17-dinitro-5,10,15 triphenylcorrolato)antimony(V)], **1**:**

Yield 24 mg, (0.031 mmol, 40%). Anal. Calcd (found) for C<sub>37</sub>H<sub>21</sub>F<sub>2</sub>N<sub>6</sub>O<sub>4</sub>Sb (**1**): C, 57.46 (57.61); H, 2.74 (2.92); N, 10.87 (10.76). UV-Vis (dichloromethane) λ<sub>max</sub>/nm (ε/M<sup>-1</sup>cm<sup>-1</sup>): 423(110000), 448(103000), 543(11300), 590(34900), 645(76900). <sup>1</sup>H NMR (400 MHz, Chloroform-*d*) δ 9.74 (s, 2H), 9.07 (d, *J* = 4.9 Hz, 2H), 8.82 (d, *J* = 5.0 Hz, 2H), 8.16–8.11 (m, 6H), 7.83–7.79 (m, 9H). <sup>13</sup>C NMR (101 MHz, CDCl<sub>3</sub>) δ 146.66, 145.61, 140.80, 138.01, 137.90, 134.39, 134.31, 133.27, 129.44, 129.22, 129.12, 128.47, 128.43, 125.46, 124.05, 120.31, 115.15, 113.28 (Figure 5.22).



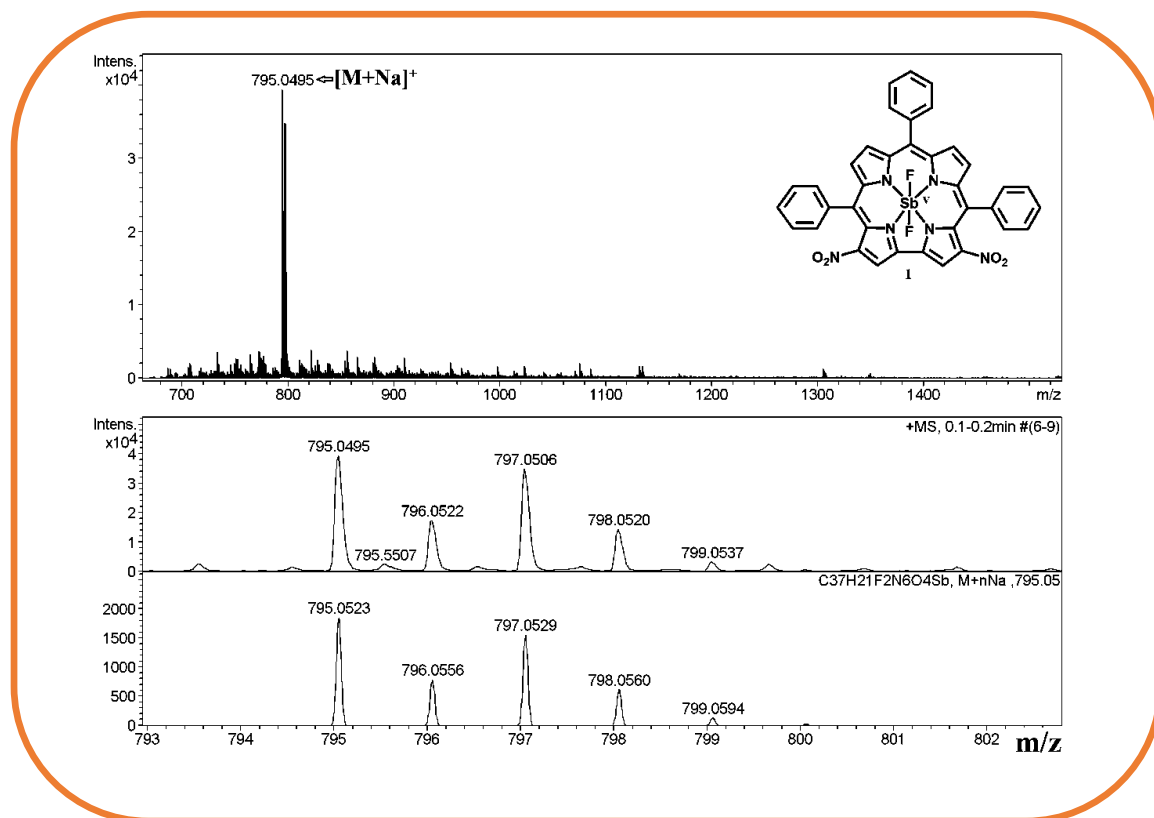
**Figure 5.22** <sup>13</sup>C NMR spectrum of **1** in CDCl<sub>3</sub>.

$^{19}\text{F}\{^1\text{H}\}$  NMR (377 MHz, Chloroform-*d*)  $\delta$  -100.1 (s, 2F) (Figure 5.23).

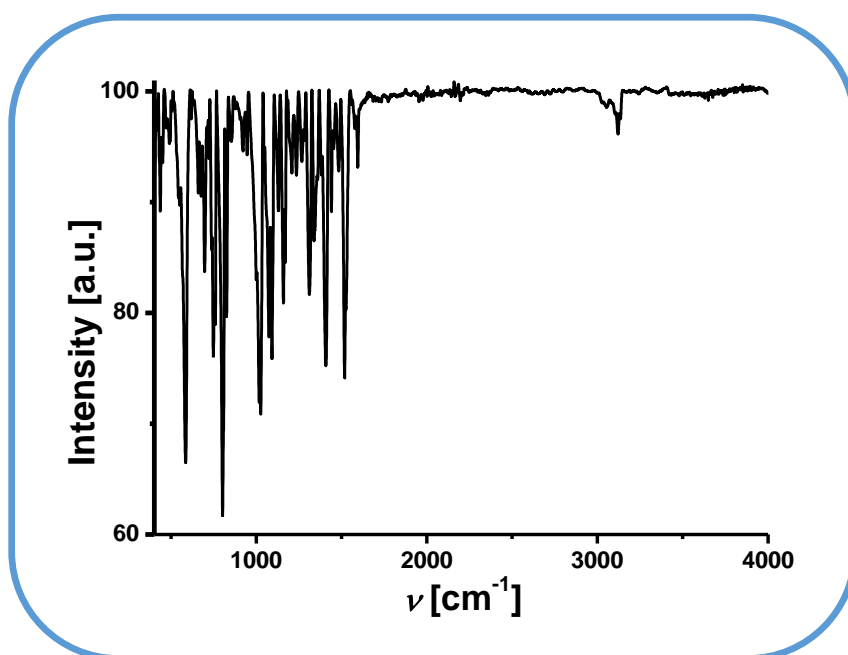


**Figure 5.23**  $^{19}\text{F}\{^1\text{H}\}$  NMR (377 MHz) spectrum of **1** in  $\text{CDCl}_3$ .

The electrospray mass spectrum in acetonitrile showed peaks centred at  $m/z = 795.0492$  correspond to  $[\text{M}+\text{Na}]^+$  (795.0528 calcd for  $\text{C}_{37}\text{H}_{21}\text{F}_2\text{N}_6\text{O}_4\text{SbNa}$ ) (Figure 5.24). **1** displayed strong emission at 679 nm and a shoulder at 755 nm in  $\text{CH}_2\text{Cl}_2$  (Excited at the Soret band).  $\Lambda_{\text{M}}$ , ( $\mu\text{S m}^2 \text{mol}^{-1}$ ) in acetonitrile at 298 K: 2.10. The FT-IR data of **1** is shown in Figure 5.25.



**Figure 5.24** ESI- MS spectrum of **1** in CH<sub>3</sub>CN shows the measured spectrum with isotopic distribution pattern.



**Figure 5.25** FT IR spectra of **1** as KBr Pellet.

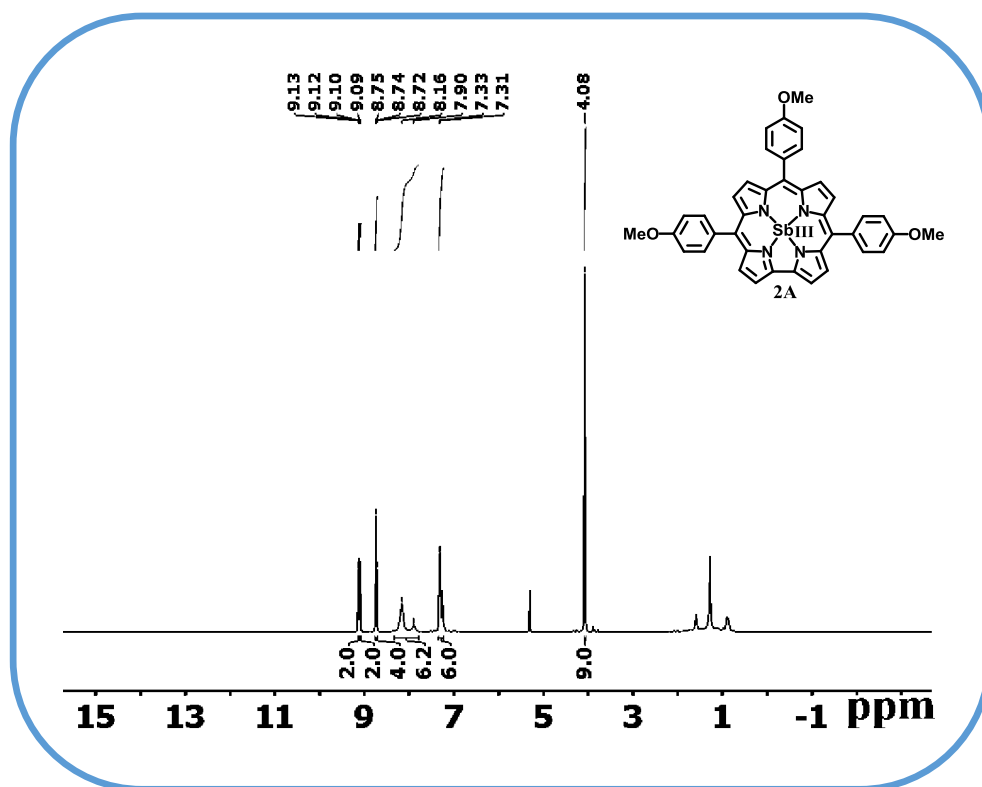
---

#### 5.5.4.3 Synthesis of {5,10,15-tris(4-methoxyphenyl)corrolato}antimony (III), **2A**:

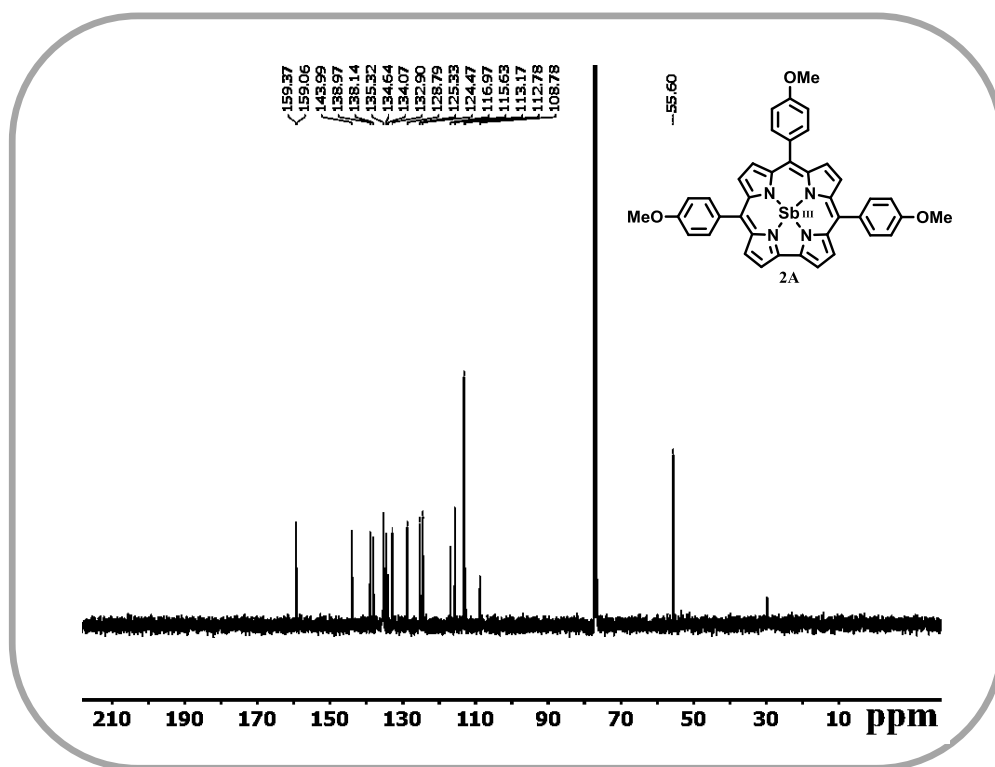
**2A** was prepared by a slight modification of a general procedure for the synthesis of Sb–corrole complex.<sup>16</sup> 100 mg (0.16 mmol) of 5,10,15-tris(4-methoxyphenyl)corrole, and 350 mg (1.5 mmol) of *antimony trichloride* were added to a 25 mL of pyridine solution. The solution was then heated to reflux at 100°C for half an hour. The solution was then evaporated to dryness by using a rotary evaporator. The residue was then purified by using silica gel column chromatography in CH<sub>2</sub>Cl<sub>2</sub>–acetonitrile mixture (5:1) as eluent. The yellowish green fraction containing antimony(III) corrole, **2A** was further purified by recrystallization to give 98 mg of pure **2A**.

#### 5.5.4.4 For {5,10,15-tris(4-methoxyphenyl)corrolato}antimony (III), **2A**:

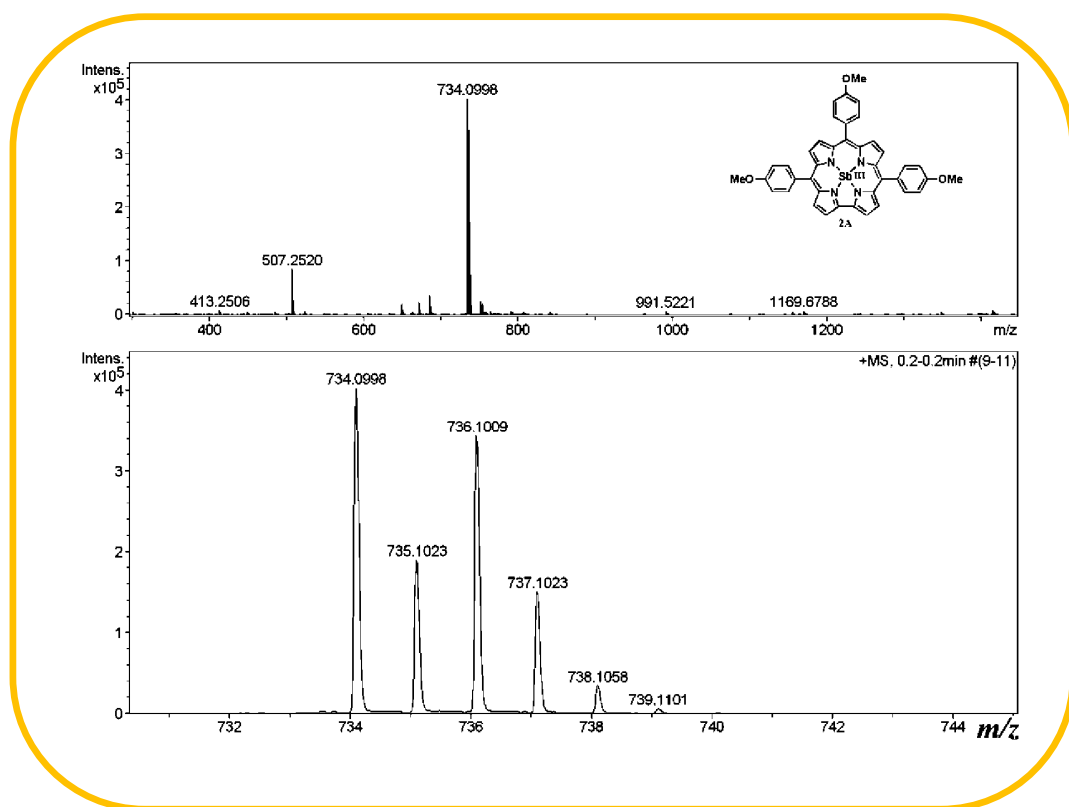
Yield 98 mg, (0.134 mmol, 84%). Anal. Calcd (found) for C<sub>40</sub>H<sub>29</sub>N<sub>4</sub>O<sub>3</sub>Sb (**2A**): C, 65.32 (65.44); H, 3.97 (3.81); N, 7.62 (7.75). <sup>1</sup>H NMR (400 MHz, Chloroform-*d*) δ 9.11 (dd, *J* = 12.1, 4.4 Hz, 4H), 8.74 (t, *J* = 4.8 Hz, 4H), 8.16 (bs, 5H), 7.89 (bs, 1H), 7.32 (d, *J* = 8.2 Hz, 6H), 4.07 (m, 9H) (Figure 5.26). <sup>13</sup>C NMR (101 MHz, CDCl<sub>3</sub>) δ 159.37, 159.06, 143.99, 138.97, 138.14, 135.32, 134.64, 134.07, 132.90, 128.79, 125.33, 124.47, 116.97, 115.63, 113.17, 112.78, 108.78, 55.60 (Figure 5.27). The electrospray mass spectrum in acetonitrile showed peaks centred at *m/z* = 734.0998 correspond to [**2A**]<sup>+</sup> (734.1278 calcd for C<sub>40</sub>H<sub>29</sub>N<sub>4</sub>O<sub>3</sub>Sb) (Figure 5.28).



**Figure 5.26** <sup>1</sup>H NMR spectrum of **2A** in CDCl<sub>3</sub>.



**Figure 5.27** <sup>13</sup>C NMR spectrum of **2A** in CDCl<sub>3</sub>.



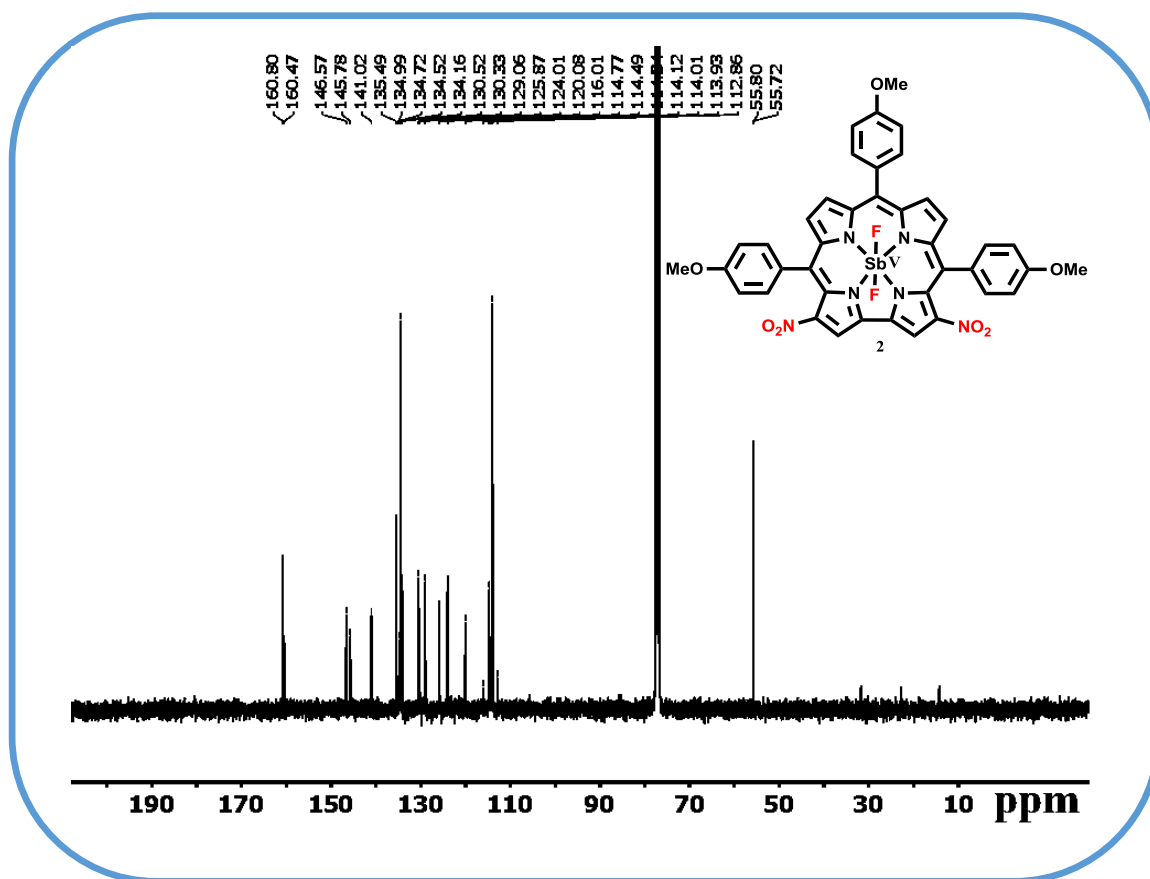
**Figure 5.28** ESI- MS spectrum of **2A** in CH<sub>3</sub>CN shows the measured spectrum with isotopic distribution pattern.

#### 5.5.4.5 Synthesis of [*trans*-difluoro(3,17-dinitro–5,10,15-tris(4-methoxyphenyl)corrolato)antimony(V)], **2**:

**2** was prepared by reacting 50 mg (0.068 mmol) of {5,10,15-tris(4-methoxyphenyl)corrolato}antimony(III), **2A** and excess of NOBF<sub>4</sub> in a 20 mL solution of CH<sub>2</sub>Cl<sub>2</sub>–CH<sub>3</sub>CN (1:1) mixture. The solution was stirred for a few seconds till the color of the solution changed from yellowish green to sea green. Then the solution was immediately passed through a previously packed silica gel column using CH<sub>2</sub>Cl<sub>2</sub>–CH<sub>3</sub>CN mixture (3:1) as eluent. The sea-green fraction containing **2** was further purified by recrystallization from CH<sub>2</sub>Cl<sub>2</sub>/hexane mixture to give 18 mg of pure **2**.

**5.5.4.6 For [trans-difluoro(3,17-dinitro-5,10,15-tris(4-methoxyphenyl)corrolato)antimony (V)], 2:**

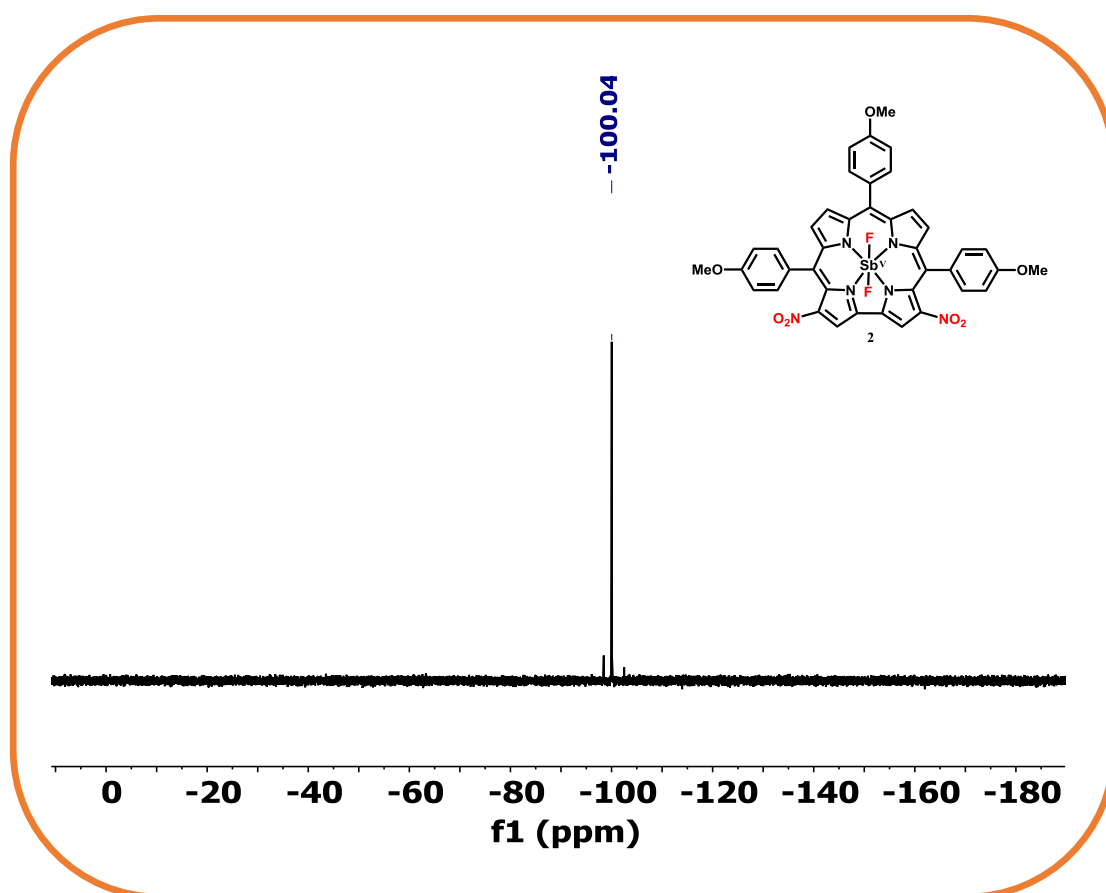
Yield 18 mg, (0.021 mmol, 30%). Anal. Calcd (found) for  $C_{40}H_{27}F_2N_6O_7Sb$  (**2**): C, 55.64 (55.78); H, 3.15 (3.31); N, 9.73 (9.90). UV-Vis (dichloromethane)  $\lambda_{max}/nm$  ( $\epsilon/M^{-1}cm^{-1}$ ): 431(112000), 454(115000), 548(14500), 593(30600), 665(82900).  $^1H$  NMR (400 MHz, Chloroform-*d*)  $\delta$  9.67 (s, 2H), 9.07 (d,  $J = 4.9$  Hz, 2H), 8.83 (d,  $J = 5.0$  Hz, 2H), 8.07 – 8.04 (m, 6H), 7.33 (m, 6H), 4.08 (m, 9H).  $^{13}C$  NMR (101 MHz,  $CDCl_3$ )  $\delta$  160.63 ( $J(CF) = 33.8$  Hz), 146.57, 145.78, 141.02, 135.49, 134.85 ( $J(CF) = 26.7$  Hz), 134.34 ( $J(CF) = 35.9$  Hz), 130.42 ( $J(CF) = 19.5$  Hz), 129.06, 125.87, 124.01, 120.08, 116.01, 114.77, 114.42 ( $J(CF) = 15.2$  Hz), 114.12, 114.01, 113.93, 112.86, 55.80, 55.72 (Figure 5.29).



**Figure 5.29**  $^{13}C$  NMR spectrum of **2** in  $CDCl_3$ .

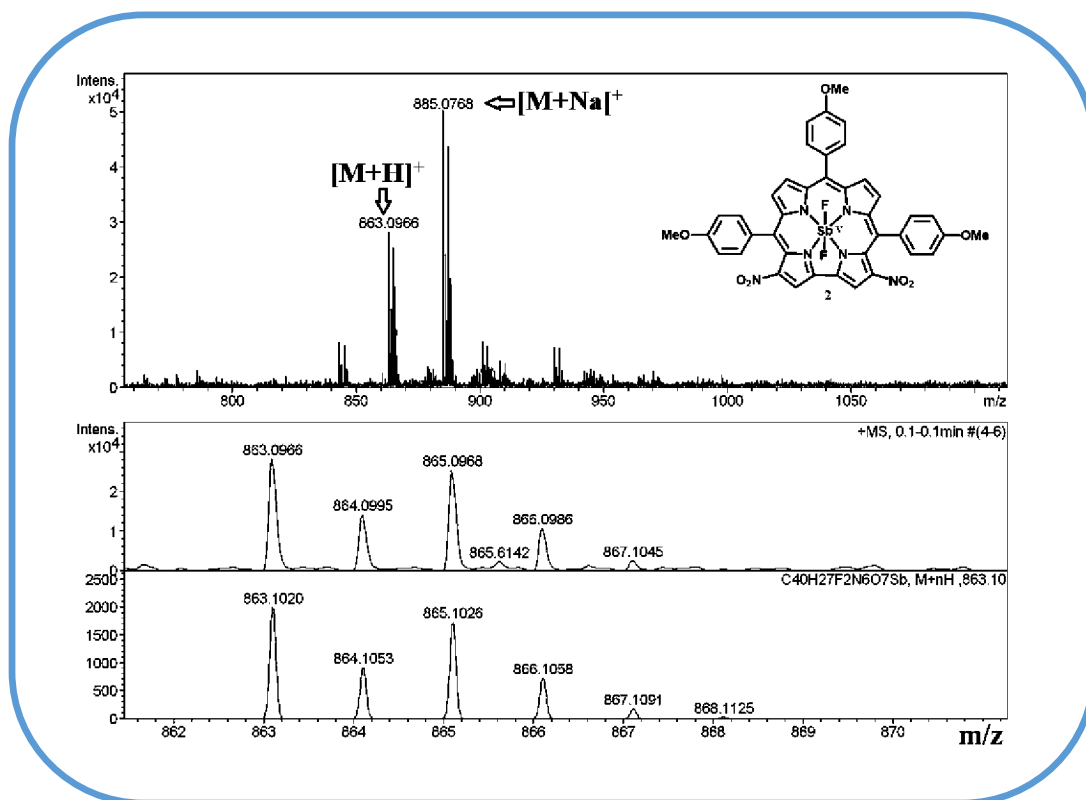


$^{19}\text{F}\{^1\text{H}\}$  NMR (377 MHz, Chloroform-*d*)  $\delta$  -100.0 (s, 2F) (Figure 5.30).

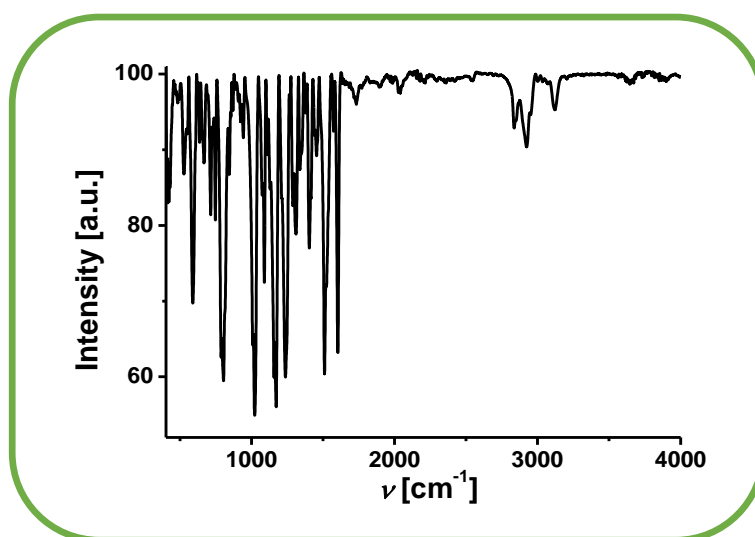


**Figure 5.30**  $^{19}\text{F}\{^1\text{H}\}$  NMR (377 MHz) spectrum of **2** in  $\text{CDCl}_3$ .

The electrospray mass spectrum in acetonitrile showed peaks centered at  $m/z = 885.0768$  correspond to  $[\text{M}+\text{Na}]^+$  (885.0845 calcd for  $\text{C}_{40}\text{H}_{27}\text{F}_2\text{N}_6\text{O}_7\text{SbNa}$ ) (Figure 5.31). **2** displayed strong emission at 725 nm and a shoulder at 809 nm in  $\text{CH}_2\text{Cl}_2$  (excited at the Soret band).  $A_{\text{M}}$ , ( $\mu\text{S m}^2 \text{mol}^{-1}$ ) in acetonitrile at 298 K: 1.85. The FT-IR data of **2** is shown in Figure 5.32.



**Figure 5.31** ESI- MS spectrum of **2** in CH<sub>3</sub>CN shows the measured spectrum with isotopic distribution pattern.



**Figure 5.32** FT IR spectra of **2** as KBr Pellet.

---

## References

- (1) Dąbrowski, J. M.; Pucelik, B.; Regiel-Futyr, A.; Brindell, M.; Mazuryk, O.; Kyzioł, A.; Stochel, G.; Macyk, W.; Arnaut, L. G., *Coord. Chem. Rev.* **2016**, 325, 67-101.
- (2) Berg, K.; Selbo, P.; Weyergang, A.; Dietze, A.; Prasmickaite, L.; Bonsted, A.; Engesaeter, B.; Angell-Petersen, E.; Warloe, T.; Frandsen, N., *J. Microsc.* **2005**, 218, 133-147.
- (3) Bonnett, R., *Chem. Soc. Rev.* **1995**, 24, 19-33.
- (4) Kadish, K.; Kelly, S., *Inorg. Chem.* **1979**, 18, 2968-2971.
- (5) Smith, K. M.; Kadish, K. M.; Guillard, R., *The porphyrin handbook*. Elsevier: 2000.
- (6) Sayer, P.; Gouterman, M.; Connell, C. R., *Acc. Chem. Res.* **1982**, 15, 73-79.
- (7) Arnold, D. P.; Blok, J., *Coord. Chem. Rev.* **2004**, 248, 299-319.
- (8) Matano, Y.; Imahori, H., *Acc. Chem. Res.* **2009**, 42, 1193-1204.
- (9) Satoh, W.; Nadano, R.; Yamamoto, Y.; Akiba, K.-y., *Chem. Commun.* **1996**, 2451-2452.
- (10) Scheidt, W. R., *The porphyrins* **1978**, 3, 463-511.
- (11) Capaldo, L.; Ertl, M.; Fagnoni, M.; Knör, G. n.; Ravelli, D., *ACS catalysis* **2020**, 10, 9057-9064.
- (12) Knoer, G.; Vogler, A., *Inorg. Chem.* **1994**, 33, 314-318.
- (13) Knör, G., *Coord. Chem. Rev.* **1998**, 171, 61-70.
- (14) Jiang, J.; Materna, K. L.; Hedström, S.; Yang, K. R.; Crabtree, R. H.; Batista, V. S.; Brudvig, G. W., *Angew. Chem. Int. Ed.* **2017**, 56, 9111-9115.

- 
- (15) Shiragami, T.; Matsumoto, J.; Inoue, H.; Yasuda, M., *Journal of Photochemistry and Photobiology C: Photochemistry Reviews* **2005**, *6*, 227-248.
- (16) Matsumoto, J.; Shiragami, T.; Hirakawa, K.; Yasuda, M., *International Journal of Photoenergy* **2015**, 2015.
- (17) Brothers, P. J., *Advances in Organometallic Chemistry* **2001**, *48*, 289-342.
- (18) Shiragami, T.; Kubomura, K.; Ishibashi, D.; Inoue, H., *J. Am. Chem. Soc.* **1996**, *118*, 6311-6312.
- (19) Knör, G., *Inorg. Chem. Commun.* **2000**, *3*, 505-507.
- (20) Feiters, M. C.; Rowan, A. E.; Nolte, R. J., *Chem. Soc. Rev.* **2000**, *29*, 375-384.
- (21) Satoh, W.; Masumoto, S.; Yamamoto, Y.; Akiba, K. y., *Heteroatom Chemistry: An International Journal of Main Group Elements* **2001**, *12*, 431-443.
- (22) a) Akiba, K.-y.; Onzuka, Y.; Itagaki, M.; Hirota, H.; Yamamoto, Y., *Organometallics* **1994**, *13*, 2800-2803.
- b) Sanghun, K.; Ryosuke, M.; Masahiko, H.; *J. Org. Chem.* **2019**, *84*, 2997-3003.
- c) Takahiro, O.; Takayuki, K.; Yukihiro, A.; Keiji, M; Yasushi, I; *Eur. J. Org. Chem.* **2019**, 2019, 1791-1795.
- (23) Takagi, S.; Suzuki, M.; Shiragami, T.; Inoue, H., *J. Am. Chem. Soc.* **1997**, *119*, 8712-8713.
- (24) Luobeznova, I.; Raizman, M.; Goldberg, I.; Gross, Z., *Inorg. Chem.* **2006**, *45*, 386-394.
- (25) Wagnert, L.; Berg, A.; Stavitski, E.; Luobeznova, I.; Gross, Z.; Levanon, H., *J. Porphyr. Phthalocyanines* **2007**, *11*, 645-651.
- (26) Lemon, C. M.; Hwang, S. J.; Maher, A. G.; Powers, D. C.; Nocera, D. G., *Inorg. Chem.* **2018**, *57*, 5333-5342.
-

- 
- (27) Mondal, S.; Garai, A.; Naik, P. K.; Adha, J. K.; Kar, S., *Inorganica Chimica Acta* **2020**, *501*, 119300.
- (28) Zahn, C.; Stensitzki, T.; Gerecke, M.; Berg, A.; Mahammed, A.; Gross, Z.; Heyne, K., *Molecules* **2017**, *22*, 1174.
- (29) Lemon, C. M.; Maher, A. G.; Mazzotti, A. R.; Powers, D. C.; Gonzalez, M. I.; Nocera, D. G., *Chem. Commun.* **2020**, *56*, 5247-5250.
- (30) Kadish, K. M.; Erben, C.; Ou, Z.; Adamian, V. A.; Will, S.; Vogel, E., *Inorg. Chem.* **2000**, *39*, 3312-3319.
- (31) Lopes, S. M.; Pineiro, M.; Pinho e Melo, T. M., *Molecules* **2020**, *25*, 3450.
- (32) Mahammed, A.; Gross, Z., *Angewandte Chemie* **2015**, *127*, 12547-12550.
- (33) Patra, B.; Mondal, S.; Kar, S. Corroles, in: Scott, R. A.; Storr, T. (Eds.) *Encyclopedia of Inorganic and Bioinorganic Chemistry*, John Wiley & Sons, Ltd, Chichester, UK, **2020**, DOI: <https://doi.org/10.1002/9781119951438.eibc2729>.
- (34) Paolesse, R., Nardis, S., Stefanelli, M., Fronczek, F. R. and Vicente, M. G. H., *Angew. Chem. Int. Ed.* **2005**, *44*, 3047-3050.
- (35) Dogutan, D. K., McGuire Jr, R. and Nocera, D. G., *J. Am. Chem. Soc.* **2011**, *133*, 9178-9180.
- (36) Autret, M., Will, S., Caemelbecke, E. V., Lex, J., Gisselbrecht, J.-P., Gross, M., Vogel, E. and Kadish, K. M., *J. Am. Chem. Soc.* **1994**, *116*, 9141-9149.
- (37) Liu, H.-Y., Yam, F., Xie, Y.-T., Li, X.-Y. and Chang, C. K., *J. Am. Chem. Soc.* **2009**, *131*, 12890-12891.
- (38) Brizet, B., Desbois, N., Bonnot, A., Langlois, A., Dubois, A., Barbe, J.-M., Gros, C. P., Goze, C., Denat, F. and Harvey, P. D., *Inorg. Chem.* **2014**, *53*, 3392-3403.
- (39) Aviv, I. and Gross, Z., *Chem. Commun.*, **2007**, 1987-1999.
-

- 
- (40) Thomas, K. E., Vazquez-Lima, H., Fang, Y., Song, Y., Gagnon, K. J., Beavers, C. M., Kadish, K. M. and Ghosh, A., *Chem. Eur. J.* **2015**, *21*, 16839-16847.
- (41) Mondal, S., Naik, P. K., Adha, J. K. and Kar, S., *Coord. Chem. Rev.* **2019**, *400*, 213043.
- (42) Nardis, S., Mandoj, F., Stefanelli, M. and Paolesse, R., *Coord. Chem. Rev.* **2019**, *388*, 360-405.
- (43) Aviv-Harel, I. and Gross, Z., *Chem. Eur. J.*, **2009**, *15*, 8382-8394.
- (44) Ghosh, A., *Chem. Rev.* **2017**, *117*, 3798-3881.
- (45) Orłowski, R., Gryko, D. and Gryko, D. T., *Chem. Rev.* **2017**, *117*, 3102–3137.
- (46) Fang, Y., Ou, Z. and Kadish, K. M., *Chem. Rev.* **2017**, *117*, 3377–3419.
- (47) Fujino, K., Hirata, Y., Kawabe, Y., Morimoto, T., Srinivasan, A., Toganoh, M., Miseki, Y., Kudo, A. and Furuta, H., *Angew. Chem. Int. Ed.* **2011**, *50*, 6855– 6859.
- (48) Hiroto, S., Furukawa, K., Shinokubo; H. and Osuka, A., *J. Am. Chem. Soc.* **2006**, *128*, 12380-12381.
- (49) Sinha, W.; Sommer, M. G.; Deibel, N.; Ehret, F.; Bauer, M.; Sarkar, B.; Kar, S., *Angew. Chem. Int. Ed.* **2015**, *54*, 13769-13774.
- (50) Sinha, W.; Sommer, M. G.; Deibel, N.; Ehret, F.; Sarkar, B.; Kar, S., *Chem. Eur. J.* **2014**, *20*, 15920-15932.
- (51) Sinha, W.; Sommer, M. G.; Van der Meer, M.; Plebst, S.; Sarkar, B.; Kar, S., *Dalton Trans.* **2016**, *45*, 2914-2923.
- (52) Patra, B.; Sobottka, S.; Sinha, W.; Sarkar, B.; Kar, S., *Chem. Eur. J.* **2017**, *23*, 13858-13863.
- (53) Sinha, W.; Sommer, M. G.; Hettmanczyk, L.; Patra, B.; Filippou, V.; Sarkar, B.; Kar, S., *Chem. Eur. J.* **2017**, *23*, 2396-2404.
-

- 
- (54) Patra, B.; Sobottka, S.; Mondal, S.; Sarkar, B.; Kar, S., *Chem. Commun.* **2018**, 54, 9945-9948.
- (55) Koszarna, B.; Gryko, D. T., *J. Org. Chem.* **2006**, 71, 3707-3717.
- (56) Gross, Z.; Galili, N.; Simkhovich, L.; Saltsman, I.; Botoshnsky, M.; Blaser, D.; Boese, R.; Goldberg, I., *Org. Lett.* **1999**, 1, 599-602.
- (57) Mahammed, A. and Gross, Z., *Coord. Chem. Rev.* **2019**, 379, 121-132.
- (58) Lemon, C.M., *Pure Appl. Chem.* **2020**, 1.
- (59) Kim, E.; Kochi, J., *J. Org. Chem.* **1989**, 54, 1692-1702.
- (60) Enemark, J.; Feltham, R., *Coord. Chem. Rev.* **1974**, 13, 339-406.
- (61) Nakamoto, K.; Fujita, J.; Murata, H., *J. Am. Chem. Soc.* **1958**, 80, 4817-4823.
- (62) Saltsman, I.; Mahammed, A.; Goldberg, I.; Tkachenko, E.; Botoshansky, M.; Gross, Z., *J. Am. Chem. Soc.* **2002**, 124, 7411-7420.
- (63) Stefanelli, M.; Nardis, S.; Tortora, L.; Fronczek, F. R.; Smith, K. M.; Licoccia, S.; Paolesse, R., *Chem. Commun.* **2011**, 47, 4255-4257.
- (64) Kitamura, Y.; Matsumura, M.; Murata, Y.; Yamada, M.; Kakusawa, N.; Tanaka, M.; Okabe, H.; Naka, H.; Obata, T.; Yasuike, S., *J. Fluor. Chem.* **2017**, 199, 1-6.
- (65) Sheldrick, G. M., *Acta Crystallogr., Sect. A: Found. Crystallogr.* **2008**, 64, 112-122.
- (66) Van der Sluis, P. V.; Spek, A. L., *Acta Crystallogr., Sect. A: Found. Crystallogr.* **1990**, 46, 194-201.
-